Isolation and characterization of nanocelluloses
from wheat straw and
their application in agricultural water-saving materials

Qi LIU

Dissertation originale présentée en vue de l'obtention du grade de docteur en sciences agronomiques et ingénierie biologique

Promoteurs: Prof. Dorothée GOFFIN, Prof. Aurore RICHEL, Prof. Jiqing SONG

Année civile: 2017

Isolation and characterization of nanocelluloses from wheat straw and their application in agricultural water-saving materials

Qi LIU

Dissertation originale présentée en vue de l'obtention du grade de docteur en sciences agronomiques et ingénierie biologique

Promoteurs: Prof. Dorothée GOFFIN, Prof. Aurore RICHEL, Prof. Jiqing SONG

Année civile: 2017

Abstract

Humans have been cultivating land for approximately 12,000 years. As such, most countries worldwide have considered crop waste as a global issue linked with environmental protection, economic development, and healthy living. Many varieties of straw are produced all over China in massive quantities (more than 900 million tons per year). Although banned by the government, stubble burning is widely applied by Chinese farmers as an easy and cheap way to remove stalks after harvests. However, this practice significantly contributes to China's carbon dioxide emissions and health risks associated with the thick mists it produces. As a renewable biomass resource, straw can be used to make new marketable materials, but its full potential has yet to be realized. Thus, future studies should be directed toward the isolation and rational use of agricultural waste. In addition to the pollution caused by agricultural waste, water shortage, particularly in northern and northwestern China, severely hinders agricultural production. This region accounts for half of the total surface of China but has less than 20% of the total national available water resources. Despite the severity of the water shortage in this region, the efficiency of irrigation water use is only 40%. Many strategies have been applied to promote a water-saving agriculture. One such strategy is the use of water-saving materials, such as plastic mulching films and superabsorbent polymers. However, these two materials are non-biodegradable, and their mechanical properties are unsatisfactory.

A systematic analysis of the literature revealed that agricultural waste is a cheap and promising source of raw materials that could be used to obtain cellulose and nanocelluloses. Nanocelluloses can be used for the industrial production of super-strong but lightweight nanocomposite materials.

The first step involved the isolation of cellulose, cellulose nanocrystallines (CNCs), and cellulose nanofibers (CNFs) from wheat straw. First, four CNCs were isolated from four commercial microcrystalline celluloses (MCCs) through sulfuric acid hydrolysis. The effects of the characteristics of the MCC on the morphology, structure, and properties of the resulting CNCs were assessed. The results revealed that both particle size and dispersity influenced the isolated CNCs. Second, cellulose was isolated from wheat straw through a microwave-assisted chemical treatment process that reduced chemical use. The reaction conditions and promoting effect of microwave on the resulting fibers were investigated. The results indicated that temperature played the most important role in cellulose isolation, and that microwave can reduce either the reaction time or the chemical use during the microwave-assisted alkali hydrolysis process.

High-purity (94%) CNFs were isolated from wheat straw through an environmentally friendly, multi-step treatment process that combined steam explosion, microwave-assisted hydrolysis, and microfluidization. Chemical identification and characterization were performed to study the effect of each treatment step and investigate the potential utilization of CNFs in nanocomposites. Chemical analysis showed that the cellulose content increased from 44.81% to 94.23%, whereas the hemicellulose and lignin contents significantly decreased from 33.41% and 8.75% to 5.54% and 1.68%, respectively. Long and loose 10–40 nm wide nanofiber

bundles and an entangled network of cellulose fibers with an average individual diameter of 5.42 nm were observed during this eco-friendly process.

In the last part of this study, nanocelluloses were introduced into superabsorbent polymers and mulching films used in agriculture to improve their performance. The effects of nanocelluloses on their structure, properties, and mechanical performance were investigated. First, superabsorbent polymers of acrylamide–acrylate copolymers and others with CNFs, CNCs, or MCC were synthesized. The swelling capacities in pure water and in various solutions, the capacities for repeated water absorption, the water-retaining capacities in soil, and the mechanical properties of the hydrogels were compared. The results revealed that the 3D structures of the acrylamide–acrylate–CNF and acrylamide–acrylate–CNC hydrogels were strengthened by the nanocellulose. These two polymers exhibited excellent capacities for repeated water absorption. By contrast, the biodegradable agricultural mulching film did not present satisfying mechanical and barrier properties as an alternative for ordinary polyethylene film. In this thesis, CNC was introduced into the film of poly (butyleneadipate-co-terephthalate) /polylactic acid composites. Poly(butyleneadipate-co-terephthalate)/polylactic acid/CNC films with various contents of CNC were prepared, characterized, and tested as for their properties. Compared with the film without CNC, poly (lactic acid) / poly (butylene-adipate-co-terephtalate)/3% CNC film showed an increased deformation by 188.80%. The barrier performance of the films increased with increasing CNC content. However, the tensile properties decreased when the CNC content exceeded 3%. Both the mechanical and barrier properties were promoted.

These results highlighted that (i) wheat straw is a cellulose-rich natural resource of CNF and CNC; (ii) microwave can reduce either the reaction time or the chemical use during the cellulose-isolation process; (iii) high-purity CNF could be obtained through an environmentally friendly method; and (iv) nanocellulose could improve the mechanical properties of both superabsorbent polymers and mulching films, and enhance their performances in agricultural applications.

In a broader perspective, microwave and other techniques should be further explored in the context of green isolation processes. Agricultural biomass natural fiber-based composites must be further investigated to maximize their applications. Approaches that could offer significant cost savings for the industrial production of nanocellulose and new nanocellulose-based materials should be developed further. We aim to promote the research interest for the isolation and application of agricultural-waste-based nanocellulose, which deserve further research and documentation. This thesis is only the beginning of a greater endeavor.

Résumé

L'apparition de l'agriculture remonte à quelque 12 000 ans. Et à mesure que celle-ci évoluait, la plupart des pays du monde n'ont cessé de voir dans la gestion des déchets créés par cette activité un problème général, lié à la fois à la protection de l'environnement, au développement économique et à la qualité de la vie. Partout en Chine, de la paille de multiples natures est produite en énormes quantités (plus de 900 millions de tonnes par an). Et c'est au brûlis que la plupart des fermiers chinois donnent la préférence pour s'en débarrasser, y voyant l'un des moyens les plus aisés et les moins chers de régler le problème, alors que le gouvernement a banni cette pratique. Et pourtant, cette technique contribue largement à accroître les émissions de dioxyde de carbone de la Chine et à aggraver les risques pour la santé que causent les brouillards épais qu'elle engendre. Or, la paille qui, en constituant une ressource de biomasse, peut être utilisée pour concevoir de nouveaux matériaux, commercialisables, n'est toujours pas exploitée comme elle le devrait. Il conviendrait dès lors de promouvoir des études sur l'isolation et l'utilisation rationnelle des résidus agricoles. En outre, au problème de la pollution engendrée par ces résidus, vient s'ajouter, en particulier dans le nord et le nord-ouest de la Chine, celui de la pénurie en eau, qui entrave considérablement la production agricole. Cette région, qui occupe la moitié de la surface totale du territoire chinois, ne détient que 20% des ressources en eau du pays. Et alors que la pénurie en eau est critique dans cette région, l'efficacité de l'utilisation de l'eau pour l'irrigation n'y est que de 40%. De nombreuses stratégies ont été déployées pour promouvoir une agriculture économe en eau. Dans ce contexte, des materiaux sont utilisés comme les films de paillage plastiques et les polymères superabsorbants. Cependant, ces deux matériaux ne sont quasiment pas biodégradables et leurs propriétés mécaniques laissent encore à désirer.

Une analyse systématique de la littérature a révélé que l'exploitation des déchets agricoles était considérée comme une source prometteuse, peu onéreuse, pour la production de matières premières utilisables pour obtenir de la cellulose et des nanocelluloses (cellulose nanocristalline et nanofibres de cellulose). Les nanocelluloses pourraient être utilisées pour produire à l'échelle industrielle des matériaux à la fois extrêmement résistants, et très légers.

La première partie du présent travail a consisté à isoler de la cellulose, de la cellulose nanocristalline et des nanofibres de cellulose à partir de paille de blé. D'abord, 4 celluloses nanocrystallines ont été isolées à partir de 4 celluloses microcristallines commerciales par hydrolyse sulfatée et l'accent a été mis sur les effets des caractéristiques de la cellulose microcristalline sur la morphologie, la structure et les propriétés de la cellulose nanocristalline obtenue. Les résultats de l'expérience montrent que la taille de la particule et sa dispersité exercent une influence sur les celluloses microcristallines isolées. Ensuite, de la cellulose a été isolée à partir de paille de blé par traitement chimique assisté aux micro-ondes, celles-ci servant à réduire le recours à la chimie. Les conditions de réaction et l'effet de promotion des micro-ondes sur les fibres obtenues ont fait l'objet de tests. Il en est résulté que la température jouait le rôle le plus important dans l'isolation de la cellulose et que les micro-ondes pouvaient

permettre de réduire à la fois le temps de réaction et le recours à la chimie au cours de l'hydrolyse alcaline assistée par micro-ondes.

Ensuite, des nanofibres de cellulose de pureté élevée (94%) ont été isolées à partir de paille de blé via une procédure de traitement à étapes multiples respectueuse de l'environnement combinant la steam explosion, l'hydrolyse assistée par micro-ondes et la microfluidisation. La détermination et la caractérisation chimiques ont été employées pour étudier l'effet de chacune des phases du traitement, ainsi que pour sonder le potentiel d'utilisation des nanofibres de cellulose dans les nanocomposites. L'analyse chimique a montré que la teneur en cellulose augmentait de 44,81% à 94,23%, alors que les teneurs en hémicellulose et lignine diminuaient nettement, passant de 33,41% et de 8,75% à 5,54% et 1,68% respectivement. Cette procédure écologique a permis d'observer des groupements longs et lâches de 10 à 40 nm de large de nanofibres, ainsi qu'un réseau enchevêtré de fibres de cellulose d'un diamètre individuel de 5,42 nm.

Au cours de la dernière partie de la recherche, les nanocelluloses ont été introduites dans des polymères superabsorbants et des films de paillage utilisés en agriculture afin d'obtenir des meilleures performances. Des tests ont été menés sur les effets des nanocelluloses sur leurs structures, leurs propriétés et leurs performances mécaniques. D'abord, des polymères superabsorbants de copolymères acrylamides–acrylates et d'autres contenant des nanofibres de cellulose, des celluloses nanocristallines ou des celluloses microcristallines ont été synthétisées. Une comparaison des capacités de gonflement en eau pure, dans diverses solutions, des capacités d'absorption de l'eau répétée, des capacités de rétention de l'eau dans le sol et des propriétés mécaniques des hydrogels a été réalisée. Les résultats ont montré que les structures en 3D de la nanofibre de cellulose acrylamide–acrylate et de l'hydrogel de cellulose nanocristalline–acrylamide-acrylate se trouvaient renforcées par la nanocellulose. Ces deux polymères ont par ailleurs révélé d'excellentes capacités d'absorption de l'eau répétée. Par ailleurs, le film agricole de paillage biodégradable, une alternative au film polyéthylène courant, ne donne pas suffisamment satisfaction en termes de propriétés mécaniques et de propriétés de barrière. Dans le cas présent, de la cellulose nanocristalline a été introduite dans le film de Poly (butyleneadipate-co-terephthalate)/composite d'acide polylactique. Des films de Poly (butyleneadipate-co-terephthalate)/composite d'acide polylactique/cellulose nanocristalline avec des teneurs variées en cellulose nanocristalline, ont été préparés, caractérisés et testés quant à leur propriétés. Les films PLA/PBAT/3% CNC ont révélé un accroissement de 188,0% de déformation en comparaison du film PLA/PBAT film. L'effet de barrière des films PLA/PBAT augmentait avec la teneur en CNC. Cependant, les propriétés de traction diminuaient lorsque la teneur en CNC était supérieure à 3%. Il y avait promotion des propriétés à la fois mécaniques et de barrière.

Ces résultats révèlent que (i) la paille de blé est une ressource naturelle riche en cellulose permettant d'obtenir et des nanofibres de cellulose et des celluloses nanocristallines, (ii) que les micro-ondes constituent une aide précieuse au cours de la procédure d'isolation de la cellulose

qui peut réduire à la fois temps de réaction et utilisation de produits chimiques, (iii) que des nanofibres de cellulose de pureté élevée pourraient être obtenues via une procédure combinée respectueuse de l'environnement et (iv) que les nanocelluloses pourraient améliorer les propriétés mécaniques à la fois des polymères superabsorbants et des films de paillage, ainsi que renforcer leurs performances dans les applications agricoles.

Dans une perspective plus large, les micro-ondes et d'autres techniques pourraient être explorées davantage dans le contexte d'une procédure d'isolation écologique. Les recherches futures sur les composites à base de fibres de la biomasse naturelle exigent d'explorer leur application à des domaines plus larges. Il conviendrait d'aller plus loin dans les approches visant à réduire significativement les coûts de la production industrielle de nanocellulose et des nouveaux matériaux à base de nanocellulose. Nous osons espérer éveiller l'intérêt des chercheurs pour l'isolation et l'utilisation de la nanocellulose issue des déchets agricoles, qui méritent d'être approfondies et pourraient être mieux utilisées et documentées. Le présent travail n'est que l'amorce d'un projet bien plus vaste.

Acknowledgements

Time flies! Four years study was long but going fast. The days that one after another in the lab, the days prepared the publications days and night; the days that participated in the lectures, the days that discussed together; the days I received guidance and strength from the supervisors and the days I obtained support and help from colleagues, will be never forgot.

Four years ago, I was very lucky to be one of the PhD students based on the ULg-CAAS cooperation program. I cherish the study opportunity all the time. And now, four years later, I am finishing my research work with improving the ability of doing scientific research. And my biggest gain during the study is that I worked in amazing groups and supported by those great people.

Therefore, this thesis represents dozens of people's work instead of only mine. Thanks all their supporting and help, their dedication and effort, their love and care, this thesis could be successfully completed. In Chinese, "6" means "everything will go well smoothly". So, I would like to express my faithful gratitude with **6** Chinese-style gestures of appreciation 🙏 to express all my THANKS.

🙏 I wish to express my deepest gratitude to my supervisors who accompanied me with their precious ideas, kind guidance and supervision during this thesis:

My promoter **Prof. Dorothée GOFFIN**, for giving me the freedom to think, seek and explore. I am very grateful to you for having always encourage me in my initiatives, discussion at the beginning of each step and supporting to my research plan.

My co-supervisor in Gembloux, **Prof. Aurore RICHEL** for offering me the amazing opportunity to work in Unit of Biological and Industrial Chemistry (CBI, now it's: Unit of Biomass and Green Technologies, BGT) for one year. I will never forget this wonderful time, which is one of the most unforgettable research experience during my life.

My co-supervisor in Beijing, **Prof. Jiqing SONG**, for your expertise and your valuable advice regarding the experimental work that we carried out in China, as well as the warm concern to my daily work and progress.

I am deeply indebted to all the members of my THESIS COMMITTEE MEMBERS, **Prof. Marie-Laure FAUCONNIER**, **Prof. Christophe BLECKER, Prof. Frank DELVIGNE, Prof. Magali DELEU, Prof. Nicolas JACQUET** and **Prof. Wenqing HE**, who devoted a lot of time and energy throughout my thesis preparation.

🙏 I am extremely grateful to all extensive support from my dear colleagues in the Gembloux Agro-Bio Tech, University of Liege (GABT-ULg).

I would like to thank the all **colleagues from CBI**: **Eric, Isabella, Caroline, Pilo, Quentin, Thomas, Thibaut… and anybody else** for giving helps in my research and personal life in Belgium. **Merci beaucoups!** Dear **Mario**, thank you for your valuable advice in

亲爱的**爸爸妈妈**，在我三十多年的成长道路上，你们永远是我最最强大的后盾，是我追求向上的动力，给我不断拼搏的勇气和力量。感谢你们对我付出的无私的爱与奉献、默默地支持与帮助。我爱你们！

亲爱的**公公婆婆**，感谢你们培养出如此优秀的儿子；感恩你们一直以来对我们的无私的爱和帮助，尤其感谢你们对我研究工作上的理解、支持，以及失落时候的安慰和鼓励。感谢你们呵护着我和我们小家庭的成长。我爱你们！

亲爱的**姐姐**，你是我从小到大人生路上最重要的伙伴，无论到哪里，你都是我永远的牵挂。

I'm really grateful. I want to thank everyone who helped me!

感恩所有给我爱与帮助的人。谢谢你们！

Table of content

List of figures

List of Tables

List of abbreviations

The following table describes various abbreviations used throughout the thesis. The page on which each one is defined or first used is also given.

Abbreviation	Meaning	Page
AFM	Atomic Force Microscopy	63
CNC	Cellulose Nanocrystalline	25
CNF(s)	Cellulose Nanofiber(s)	25
FTIR	Fourier Transform Infrared	44
MCC	Microcrystalline cellulose	26
MW	Microwave	27
MW-assisted	Microwave-assisted	27
PBAT	poly (butylene-adipate-co-terephtalate)	27
PLA	poly lactic acid	27
PT(s)	Pretreatment(s)	40
SAPs	Super Absorbent Polymers	26
SEM	Scanning Electron Microscope	44
TEM	Transmission Electron Microscope	39
TEMPO	2,2,6,6-tetramethylpiperidine-1-oxyl	40
TG(A)	Thermogravimetric Analysis	63
WS	Wheat Straw	26
XRD	X-Ray Diffraction	40

General introduction

1. General context

1.1 Agricultural waste disposal problematic

Production activities always results in different kinds of pollution from solid waste, wastewater, or gases. For thousands of years of planting, crop residues were incorporated into the soil or fed to livestock, and manure was returned to the land in amounts that could be absorbed and utilized. However, since farms have increasingly become highly mechanized and reliant on synthetic fertilizers and pesticides, the crop residues that were once recycled have largely become wastes. The disposal of these wastes has presented a continuing problem for farmers worldwide. The accumulation of this type of biomass in very huge quantities each year results not only in the deterioration of the environment but also in the loss of potentially valuable materials that can be processed to yield valuable added products.

In China, the crop yield is more than 700 million tons each year. Although banned by the government, burning is widely applied by Chinese farmers as an easy and cheap way to remove stalks after harvests. The burning of stalks in fields significantly contributes to China's carbon dioxide emissions and haze. Although agricultural residues can be safely disposed of because of their biodegradable nature, their vast quantities have prompted the need to utilize them in useful applications.
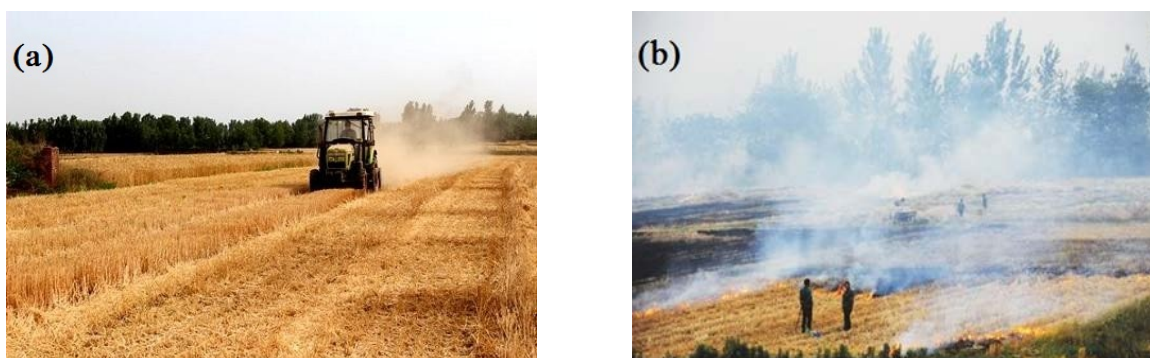
Figure 1. Wheat harvest (a) and smog (b) caused by straw burning

1.2 Agricultural wastes, a member of the "cellulose family"

Given that agricultural wastes are rich in natural cellulose, they represent one of the most energy-rich resources on the planet. These residues include renewable lignocellulosic materials, such as stalks, stems, straws, hulls, and cobs, all of which vary slightly in compositions. Cellulose and hemicellulose, which are the major constituents of these materials, can be considered alternative sources of renewable and sustainable materials that can be potentially used for different applications. Despite the enormous production of agricultural biomass, only a small fraction of the total biomass is utilized for different applications. Agricultural biomass

such as natural fibers has been successfully demonstrated as a potentially renewable and sustainable material for producing composite materials. Natural fibers offer excellent specific properties, and they exhibit promising potential as outstanding reinforcing fillers in the matrix that can be used as alternative materials for biocomposites, hybrid composites, and pulp and paper industries. Given their low cost and potential global sustainability, natural-fiber-based polymer composites are gaining increasing commercial use in different applications.

1.3 Nanocellulose as a green material

At present, researchers and manufacturers have focused on sustainable materials. "Green" generally refers to the materials, technologies, and products that exert less impact on the environment and/or are less detrimental to human health than their traditional equivalents. Cellulosic nanomaterials can satisfy nearly all of the requirements for being "green" because of its natural origin and biodegradability at the end of its life circle. Through further responsible and meticulous research and development, these nanomaterials could become a prospective candidate for sustainable materials in the 21st century.

The various forms of nanocellulose often refer to the cellulose nanofiber (CNF) and cellulose nanocrystalline (CNC) from plants, bacteria, and animals, leading to a wide array of global studies on the use of these nanomaterials in product applications. CNFs and CNCs are typically used as a reinforcing agent in composites due to their high strength properties, renewability, light weight, and high surface area. CNF- and CNC-based composites are applied in nearly every area in our society, including automotive, construction, structural applications, medicine, environmental protection, aerospace, sports, equipment, boats, office products, machinery, etc. Nanocellulose is one of the most popular reinforcing agents being investigated and produced.

1.4 Green process is essential for green materials

The term "green" was developed as a new measure not only for raw materials but also for technologies and products, suggesting that green products might be produced from sustainable raw materials and be manufactured in a more energy-conservative or environmentally friendly approach. Therefore, studies should also consider finding green or eco-friendly techniques for cellulose and nanocellulose preparation.

1.5 Water shortage, another limitation factor for agriculture in China

The water challenge in China is primarily driven by the intersection of demographics and climate. China suffers from a common problem faced by many countries: too much water in the "wrong" place and time. The agricultural development in China is limited by water availability, particularly in northern and western China. At present, agriculture uses for over 70% of the total exploited water. China having the world's largest population and second-largest national economy, water shortage could threaten global food security and prosperity. To ensure food security, China should promote water-saving agriculture, which is an integrated system

25

that should include rational utilization of agricultural water resources, water-saving irrigation, agronomic water-saving techniques, and agricultural management. Among these strategies, water-saving materials, including plastic mulching films and superabsorbent polymers (SAPs), occupy an important place.

1.6 Water-saving materials

Although plastic mulching films and SAPs play important roles in agricultural production, they are often considered unsustainable and not environmentally friendly. These polymers are non-biodegradable, and they damage the environment starting from their production to their disposal. In addition, the mechanical performance in practical agricultural production of these materials is generally unsatisfying. Therefore, to improve their roles in water-saving agriculture, their mechanical properties must be examined, and their environmental friendliness must be improved.

2. Objectives of the study

As mentioned, both the mechanical properties and environmental friendliness must be improved for practical use. Nanocellulose, which can be obtained from agricultural waste, can satisfy these requirements. In this study, wheat straw (WS), which is one of the most common agricultural wastes in northern China, was selected as the raw material for obtaining nanocellulose. The main objectives of this thesis were to: (i) isolate both CNC and CNF from wheat straw; (ii) use an environmentally friendly treatment process as much as possible; and (iii) investigate the effect of nanocellulose on the strength and performance of SAPs and mulching films.

3. Structure of this thesis

In this thesis, we considered the isolation of cellulose and nanocellulose, and their application in agricultural water-saving materials.

A systematic analysis of the literature on the nanocellulose isolated from agricultural waste and their application in various composites was completed prior to the experimental work.

Chapter I Isolation and Application of Nanocelluloses from Agricultural Biomass: A review

Through an analysis of the scientific literature, Chapter I (***Article 1***) clarified the concept of agricultural biomass as well as the source, distribution, and current situation of its applications. Then, the components of agricultural biomass, particularly fibers, were introduced. The most important part was the isolation and application of nanocelluloses, which could be used in various nanocomposite materials.

After the literature analyses, the three main parts of the work were conducted. First, CNC was isolated, and the effects of the size and dispersion of the microcrystalline cellulose (MCC) on

the resulting CNC were investigated.

Chapter II <u>Cellulose nanocrystalline isolation</u>

CNC was first isolated through a traditional sulfuric acid hydrolysis method, focusing on the effects of the size and dispersion of the MCC on the morphology, structure, and properties of the resulting CNC (***Article 2***).

CNF was isolated from wheat straw. Prior to the CNF isolation, cellulose was isolated from wheat straw. As stated, green or environmentally friendly treatments should be utilized for green materials processing. Therefore, in this study microwave (MW) was applied to reduce chemical use. In the following section, CNFs were isolated with a combined, environmentally friendly, and multi-step process.

Chapter III <u>Cellulose and cellulose nanofiber isolation from wheat straw</u>

The chemical isolation of cellulose from wheat straw was investigated by using a microwave-assisted (MW-assisted) process to reduce chemical use (***Article 3***). The reaction conditions and non-thermal effect of MW on the resulting fibers were investigated. Then, high-purity CNFs were isolated from wheat straw through an environmentally friendly, multi-step treatment process that combined steam explosion, microwave-assisted (MW-assisted) hydrolysis, and microfluidization (***Article 4***). The effects of each treatment on the morphology, structure, and properties of the processed fibers were examined.

The main purpose of the nanocellulose isolation from wheat straw was to investigate their effects on the properties of the two kinds of water-saving materials in agriculture, namely, mulching films and SAPs. Therefore, the obtained CNC and CNF were introduced into the two materials, and their effects were tested.

Chapter IV <u>Nanocellulose application in agricultural water-saving materials</u>

The application of CNCs and CNFs in agricultural water-saving materials such as SAPs and mulching film was investigated. First, acrylamide–acrylate-copolymer-based SAPs with CNC, CNF, and MCC were synthesized (***Article 5***). The swelling capacities in pure water and in various solutions, the capacities for repeated water absorption, the water-retaining capacities in the soil, and the mechanical properties of the hydrogels were compared. Second, CNC was added into the film of poly(butyleneadipate-co-terephthalate)/polylactic acid (PBAT/PLA) composites (***Article 6***). PBAT/PLA/CNC films with various contents of CNC were prepared, characterized, and tested for their properties. The tensile properties, puncture performance, and water vapor barrier properties were tested to evaluate the effects of CNC on the mechanical properties and barrier property.

Green isolation processes should be further explored. Future studies should broaden the application of nanocellulose. Approaches that can reduce the cost of nanocellulose production must be developed. All of these perspectives were discussed after a general conclusion was drawn for the entire thesis.

Chapter V <u>General conclusions and perspective</u>

After conclusions were drawn from the results of various analyses, a discussion of the perspectives was presented in a broader context. This last part highlighted that CNC and CNF could be isolated from wheat straw. In particular, high-purity CNF could be isolated through an environmentally friendly, multi-step combined process. In addition, the morphology, structure, and properties of the resulting CNC were affected by the size and dispersion of the MCC. Furthermore, the applications of CNC or/and CNF in acrylamide–acrylate copolymer SAPs and PBAT/PLA films improved several important properties of the two materials.

The structure and main milestones of the thesis are presented in Figure 2.

Note: *This present thesis is a compilation of articles independently published (or submitted or being prepared for publication). As such, repetitions may occur in the different chapters. I apologize for this to those reading the entire document.*

Chapter I (*Article 1*) Isolation and Application of Nanocelluloses from Agricultural Biomass. A review
- Source, distribution and components of agricultural biomass
- Isolation and application of nanocellulose

Literature Analyses

Chapter II (*Article 2*) Cellulose nanocrystalline (CNC) isolation.
- Four CNCs were isolated
- Effects of the size and dispersion of microcrystalline cellulose on the resulting CNC were investigated

Chapter III Cellulose and cellulose nanofiber isolation (CNF) from wheat straw.
- (*Article 3*) Cellulose isolation with the assistant of microwave
- (*Article 4*) CNFs were isolated with an environmentally friendly, multi-step process

Isolation of Nanocellulose

Chapter IV Nanocellulose application in agricultural water-saving materials.
- (*Article 5*) CNC and CNF were employed to improve the mechanical properties and water retention abilities of superabsorbent polymers
- (*Article 6*) CNC was used for improving the barriers of the PBAT/PLA film

Application of Nanocellulose

Chapter V General conclusions and perspective
- Conclusions on all the results of studies
- Simple perspectives on cellulose applications were given

Conclusions And Perspectives

Figure 2. Entire structure of the thesis and the relationship of the chapters

Chapter I An Overview Towards Isolation and Application of Agricultural Biomass Nanocelluloses

Article 1 Isolation and Application of Nanocelluloses from Agricultural Biomass. A review

Qi Liu [1,2,3], Wenqing He [1], Changrong Yan [1], Rui Guo [1], Jiqing Song *,[1], Aurore Richel*,[3], Dorothée Goffin *,[2,3]

[1]National Engineering Laboratory for Crop Efficient Water Use and Disaster Mitigation, Key Laboratory of Dryland Agriculture, Ministry of Agriculture and Key Laboratory for Prevention and Control of Residual Pollution in Agricultural Film, Ministry of Agriculture, Institute of Environment and Sustainable Development in Agriculture, Chinese Academy of Agricultural Sciences, No.12 Zhongguancun South Street, Beijing 100081, China

[2]TERRA Research Center and Laboratory of Gastronomical Science, Gembloux Agro-Bio Tech-University of Liège, Passage des Déportés 2B-5030 Gembloux, Belgium

[3]Unit of Biomass and Green Technologies, Gembloux Agro-Bio Tech-University of Liège, Passage des Déportés 2B-5030 Gembloux, Belgium

Abstract: This paper deals with the source, structure, properties, isolation methods and applications of cellulose nanocrystalline and cellulose nanofiber derived from agricultural biomass**.** Natural cellulose nanocrystalline and cellulose nanofibers have the special advantage of high specific strength and sustainability, which make them ideal candidates for reinforcement in various polymeric matrices. Agricultural nanocellulose is one of the main sources of cellulose, an eminent representative of nanomaterial. Extractions of cellulose from agriculture-based materials are discussed in detail. Various field of nanocellulose application and the advantages of these nanomaterials have also been generalized.

Keywords: Agricultural Biomass; Cellulose Nanocrystalline; Cellulose Nanofiber; Isolation; Application.

1. Introduction

The growing concepts of sustainability, new environmental regulations and high rate of depletion of petroleum resources have stimulated the search for green materials compatible with the environment. The waste disposal problems, especially the worldwide availability of natural fibers and other abundantly accessible agrowaste is responsible for the new interest in research in sustainable technology. Bioresources based on agricultural production have received much attention, because they can potentially serve as key components of biocomposites. Agricultural crop residues such as cereal straw, corn stalk, bagasse and grass, which are produced in billions of tones around the world, provide an abundant, inexpensive and renewable source of lignocellulosic biomass. The possibilities of using the fiber crop provide wide ranging opportunities in processing for developing new applications in automotive, aerospace, packaging, building, electronics and household. Among these researches and applications of such enormous amounts of agricultural residues, in recent years, considerable research has been done on the isolation of nanocellulose from the raw fibers to use them as fillers in biocomposites. Agricultural crop residues are one of the most valuable

sources of natural cellulose nanofibers. In agricultural fibers, the cellulose microfibrils are less tightly wound in the primary cell wall than in the secondary wall in wood, thus fibrillation to produce nanocellulose should be easier.

1.1 Resource of agricultural biomass

Biomass refers to the various organisms formed by photosynthesis. Biomass is a form of energy stored in the form of chemical energy in the form of chemical energy. Biomass for energy predominantly origins from three various sources: agriculture, forestry and waste streams. According to reports of The World Bioenergy Association about "Global biomass potential towards 2035"in March 2016, in the year 2012, the global supply of biomass was 56.2 EJ and World Bioenergy Association estimates that this can increase to 150 EJ by 2035. About 43% coming from agriculture (residues, by-products and energy crops), 52% from forests (wood fuel, forest residues and by-products of the forest industry) and 5% from waste streams.

Agricultural biomass energy resources include crop straw, livestock and poultry manure, agricultural products by-products and energy crops, etc. Straw is a general term for the stems, leaves, and panicles of mature crops. Usually refers to wheat, rice and corn other crops (usually coarse grains) in the remaining part of the grain after harvest. The potential biomass from animal waste includes primarily waste from intensive livestock operations, from poultry farms, pig farms, cattle farms and slaughterhouses. Livestock wastes include wet animal manure for biogas production and dry manure such as poultry litter that can be used in thermochemical conversion technologies. Agricultural products by-products mainly include rice husk, corn cob, bagasse, etc., mostly from grain processing plants, food processing plants, sugar mills and wineries. The number is huge, and the origin is relatively concentrated, so it is easy to collect and deal with. Energy crops are herbs and woody plants that are specially planted to provide energy raw materials. Sugarcane, sweet sorghum, cassava, sweet potato and other crops are suitable to produce fuel ethanol, and rapeseed is suitable to produce biodiesel.

Agricultural biomass resources have a wide range, a considerable number, and there are scattered. According to its use, agricultural biomass can be attributed to two types: traditional and modern. Traditional agricultural biomass refers mainly to the direct combustion of fuel wood, charcoal, straw and other crop wastes; modern agricultural biomass also including organic carriers (such as animal feces, energy plants, etc.) which is turned into fuel by using modern biomass conversion technology.

1.2 Distribution of agricultural biomass resources in the world

According to the United Nations Environment Program, crops grown in the world can provide about 2 billion tons of straw each year, and the annual output of crop straw in China is about 700 million tons, ranking first in the world, equivalent to 53 million tons of standard coal accounted for about 30% of the world's total straw. Agriculture in the US is developed, farms

and pastures occupy 40% of land area, arable land area accounted for more than 20% of the land area. In these lands, at least 55% of the land has the potential to develop agricultural biomass energy. At present the development of the first generation of biomass energy use of raw materials are mainly corn, sugar cane, oil crops. The United States is mainly for corn and soybean oil, the EU is for corn, wheat, barley, rapeseed oil, sugar beet and soybean oil, Brazil is for sugar cane and soybean oil, Canada is for corn and wheat, China and India are for corn, rice and wheat, Malaysia, Indonesia is for Palm oil. In 2005, the United States instead of Brazil jumped to the world's number one producer of fuel ethanol, which brought huge benefits to US economy. Brazil is the second largest producer of fuel ethanol. Unlike the United States, which uses maize, Brazil uses sugarcane fermentation to produce fuel ethanol [1]. According to "Global Bioenergy Statistics 2016", in 2015, 133 billion liters of biofuels were produced. 62% of all biofuel produced was in the form of bioethanol, 24% as biodiesel and the rest as advanced biofuels. 87% of all bioethanol produced was in Americas – USA and Brazil. Europe produced 43% of all biodiesel production.

1.3 Agricultural biomass resources in China

China is a big agricultural country and one of the most abundant straw resources in the world, producing more than 620 million tons of straw in 2002, and representing about 33–45% of energy consumption for livelihood in rural areas. Rice stalk, corn stalk, wheat stalk and other main grain crops straw and oil-bearing crop straw are two main types of straw resources in China. The total output of the crop straw was 622 million ton in 2002, and straw of rice, wheat and corn was 109, 121 and 243 million ton, respectively. The three kinds of straw were about 76.1% of the total crop straw resources. The most part of straw was corn, accounting for 39.12% of the total straw, North (Hebei and Inner mongolia) and Northeast (Liaoning, Jilin and Heilongjiang) and parts of East (Shandong) and Central South (Henan) of China were the main producing areas. The second was wheat, which accounted for 19.45% of the total straw and mainly came from East (Shandong, Jiangsu and Anhui), Central South (Henan) and North (Hebei) of China. The third was rice, accounting for 17.53% of the total straw and teeming in Central South (Hunan, Hubei, Guangdong and Guangxi), East (Jiangsu, Jiangxi, Zhejiang and Anhui) and Southwest (Sichuan) of China. Others were beans, tubers and oil-bearing crops, accounting for 5.42%, 2.96%, 9.34% [2].

China is abounding with straw, and the yield of straw has increased at a rate of 1.4% annually. From 1995 to 2005, China produces some 630 million tons of crop residues per year, 50% of which comes from east and central south of China. The amount of crop residues is 1.3 times of the total yield of crops, 2 times of the total fodder of grassland, which covers 41% of China's territory. Crop residues of corn, wheat and rice amounted to 239, 137 and 116 million tons, respectively, accounting for nearly 80% of the total crop residues.

China's plain regions are the main sources of crop residues, with four districts being involved, i.e., east, central south, northeast and central China. The detailed compositions of crop residues

in China were noted as follows. Corn, took up 38%, mainly from north east, east and north provinces; wheat took up 22%, mainly from central south, east and north China; rice took up 19%, mainly from central south, east and south west provinces. Others like beans, tubers and oil bearing plants were only 4.8%, 2.8% and 8.3%, respectively. However, most of these small parts of crop residues were often discarded with little usage purposes [3].

The main sources of livestock waste materials are cattle, pigs and chickens. The 6 provinces with the most abundant livestock and poultry manure are Henan, Shandong, Hebei, Sichuan, Hunan and Yunnan. In 2009, the discharged amount of the excrements in China was 330 million tons. The biogas producing potential of the excrements was 1.2×1011 m^3, and that in large- and medium-sized livestock and poultry breeding farms was responsible for 2.4×1010 m^3, corresponding to about 1.35×1010 m^3 of natural gas [4].

According to the formation components of energy carrier material, energy crops can be divided into three categories: 1. Starch and sugar crops, rich in starch and carbohydrates, used in the production of fuel ethanol. 2. Fat crops, rich in oil, through the lipid process to form fatty acid methylesters, that is, biodiesel. 3. Lignocellulosic crops, rich in cellulose, hemicellulose and lignin, can be used to produce heat, electricity, ethanol and biological gases through appropriate transformation [5]. "China Economic Flora" describes 2411 kinds of economic plants, including 468 kinds of fiber, 278 kinds of starch and sugar, 430 kinds of fats and oils. These three types of plants accounted for more than 40% of China's total economic plant species and all can be developed and utilized as energy plant [6].

1.4 Use of agricultural biomass

At present, the agricultural biomass resources utilization technology mainly includes agricultural biomass resources pellet fuel technology, crop straw power generation technology, rural biogas technology and biomass liquid fuel production technology [7].

There are six generic biomass processing technologies based on direct combustion (for power), anaerobic digestion (for methane-rich gas), fermentation (of sugars for alcohols), oil exaction (for biodiesel), pyrolysis (for biochar, gas and oils) and gasification (for carbon monoxide and hydrogen-rich syngas). These technologies can then be followed by an array of secondary treatments (stabilization, dewatering, upgrading, refining) depending on specific final products. Based on the research of Zeng et al. the present utilization of straw in biomass energy has been made in the following aspects. Direct combustion of biomass is the main and traditional way of the utilization of biomass energy [2]. Anaerobic digestion (or biogas technology) is a bioconversion technology widely adopted in China, especially in rural areas. Straw gasification is a technology used for extracting gaseous fuel from straw in gasifier. Many countries have been interested in this technology of generating clean renewable energy. Straw briquette technology refers to press the straw in which moisture content is about 10% into all kinds of shaped fuel such as bar-formed, pellet-formed and block-formed under certain pressure (heat or unheated). Biomass liquefaction includes biochemical conversion to produce ethanol and

thermos-chemical conversion to produce bio-oil. The main technology of straw liquefaction is hydrolytic liquefaction and pyrolytic liquefaction. In fact, hydrolytic liquefaction is the process of producing ethanol, which is fermented by microorganism from materials of high starch content such as steamed and saccharified corn or potato. Straw carbonization is the technology that puts briquette production of straw into furnace through pyrolysis (400℃) in the condition of isolation of oxygen, then gets molding charcoal [8].

Animal manure contains all 13 of the essential plant nutrients that are used by plants. These include nitrogen (N), phosphorous (P), potassium (K), calcium (Ca), magnesium (Mg), sulfur (S), manganese (Mn), copper (Cu), zinc (Zn), chlorine (Cl), boron (B), iron (Fe), and molybdenum (Mo). Using animal manure as a fertilizer for crops or trees may provide a portion, or all, of the plant requirements [9].

Utilizing livestock and poultry manure to generate electricity, plant mushroom, make pyrolytic products, make ethanol and so on need new methods and modern technology.

2. Agricultural biomass

Agricultural biomass is abundant worldwide, which can be considered as alternative source of renewable and sustainable materials which can be used as potential materials for different applications [10]. It is a huge source of renewable energy produced by means of photosynthesis, which can be stably stored in biomass in the form of chemical energy. It has basically no cost in energy storage compared with other renewable energy such as wind energy, solar energy. In addition, agricultural biomass has the potential to meet demands of chemical raw material in a sustainable manner through thermochemical or biochemical technologies [11]. The Agricultural biomass encompasses all organic plant matter as well as organic waste derived from plants life. The term is broad enough to include: bagasse, linen cotton，coconut shell, banana pods.

2.1 Agricultural biomass composition

In nature, cellulose, lignocellulose and lignin are major sources of plant biomass; therefore, their recycling is indispensable for the carbon cycle. Each polymer is degraded by a variety of microorganisms which produce a battery of enzymes that work synergistically. In the near future, processes that use lignocellulolytic enzymes or are based on microorganisms could lead to new, environmentally friendly technologies [12]. Cellulose and hemicellulose are macromolecules from different sugars; whereas lignin is an aromatic polymer synthesized from phenylpropanoid precursors [13]. The composition and percentages of these polymers vary from one plant species to another. Moreover, the composition within a single plant varies with age, stage of growth, and other conditions [14].

Cellulose and hemicellulose covered a wide range in composition due to distinct species, soil characteristics, climates, farm management and regions. While Lignin proved to be with less variance. Huang et al. established a rapid estimation of cellulose, hemicellulose, and lignin contents in rice straw by near infrared spectroscopy. A total of 172 samples from 17 provinces

of China were collected and scanned. The mean, range and standard deviation of the cellulose, hemicellulose and lignin contents measured by the reference Method are shown in Table 1 [19], which means are considered to lie within the normal ranges and agree with reported values. Jung et al. compared the lignin, cellulose, and hemicellulose contents in miscanthus, switchgrass, sorghum, and reed (from 14 accessions according to the collection site) in the leaves and stems [20].

Table 1 Cellulose, Hemicellulose and Lignin contents of the Samples Component [19].

Component	No. of Samples	Range /%	Mean/ %	SD/%
Cellulose	169	28.98-46.01	39.04	3.4899
Hemicellulose	171	13.77-31.09	20.91	2.8290
Lignin	169	3.53-10.53	5.71	1.3747

2.2 Agricultural biomass cellulose

Cellulose was first described by Anselme Payen in 1838 as a "resistant fibrous solid that remains behind after treatment of various plant tissues with acid and ammonia." In its simplest form, cellulose is composed of β-1, 4-linked glucan chains that can be arranged in diverse ways giving rise to different forms of cellulose. In nature, cellulose is produced in a hierarchical manner with the glucan chains associating with each other to form crystalline and non-crystalline regions that are assembled into higher-order structures such as the microfibril. Depending on how the glucan chains associate, different crystalline forms of cellulose may be observed within the same microfibril. In nature, cellulose is generally obtained as the cellulose I crystalline form in which the glucan chains are aligned parallel to each other. Two forms of the native crystalline polymer, cellulose, Iα and Iβ, have been shown to be present in differing amounts obtained from various sources. Other crystalline and non-crystalline forms of cellulose have also been identified, and many of these forms can be converted from one form to the other form by chemical or physical treatments.

The main sources of cellulose are plants. The content of cellulose in different raw materials is given as:

- bushes: 30%
- woods: 40-50%
- bast plants (flax, ramie, etc.): 65-70%
- cotton fibers: >90%

During biosynthesis, van der Waals and intermolecular hydrogen bonds between hydroxyl groups and oxygen atoms of adjacent molecules promote parallel stacking of multiple cellulose chains, which form elementary fibrils that further aggregate into larger microfibrils, which have a diameter of 5-50 nm and length of several microns. The hydrogen-bonding (intra- and inter chain) network makes cellulose a very stable polymer and imparts high axial stiffness to

cellulose fibrils, which are the main reinforcement phase for trees, plants, some marine creatures (tunicates), algae, and bacteria. There are regions within these cellulose fibrils where the cellulose chains are arranged in a highly ordered structure and regions that are disordered (amorphous-like). The structure and distribution of these crystalline and amorphous regions within cellulose fibrils have not been rectified yet. It is the crystalline regions contained within the cellulose "microfibrils" are extracted, resulting in cellulose nanocrystals.

Cellulose is located within the fiber walls of plants. One fiber is an elongated vegetable cell. Fibers of different plants have different dimensions and shapes. Fibers of bast plants and cotton are long, with lengths in the range of centimeters, whereas wood fibers are short, typically 1-3 mm in length. Cotton fibers are twisted, whereas fibers of wood, the tracheids, are generally untwisted and subject to flattening when delignified [21]. Fibers of the bast plants (ramie, flax, etc.) are straight and round. A hollow capillary is called the lumen, which extends through most of the length of the fiber. Cellulose fibers contain various defects or dislocations. These are cracks, pores, nodes, compression failures, thin places, and other sites of damage. These dislocations are weak points for mechanical forces and chemical attack. The width of various plant fibers is in the range of 15-30 μm, including the lumen.

2.3 Agricultural biomass nanocellulose

Cellulose is one of the most important natural polymers, an almost inexhaustible raw material, and a key source of sustainable materials on an industrial scale [22]. It could be obtained from different natural resources depending upon the applications [23-27]. Cellulose exists naturally as crystalline and amorphous configurations within plant, animal, and bacterial systems [28-31]. Its multi-functionality based on the chemical structure and hierarchical design is now newly being appreciated [32-34]. Moreover, cellulose is a high molecular and crystalline polymer with well-defined molecular and supramolecular structure. The crystalline domains in natural cellulose achieve irreducible packing, which is in the order of several nanometers in dimension [35]. Without question, plants ostensibly remain as a huge reservoir for the ultimate production of such "nanocrystalline" cellulose.

It is worth noting that there are two major structures of nanocellulose, namely cellulose nanofibers (CNFs) and cellulose nanocrystals (CNCs). CNFs can be isolated using mechanical processes such as high-pressure homogenization, grinding and refining, whereas CNCs have been extensively isolated by using acid hydrolysis treatments [36,37]. The typical sources of CNFs and CNCs are given in table 2.

Table 2.   Types of nanocellulose.

Type of nanocellulose	Synonyms	Typical sources	Average size

Cellulose nanocrystal (CNC)	Nanocrystalline cellulose (NCC), whiskers, rod like cellulose, microcrystals	Wood, cotton, hemp, flax, wheat straw, rice straw, mulberry bark, ramine, MCC, Avicel, tunicin, algae, bacteria, etc.	Diameter: 5-70 nm Length: 100-250 nm (from plant);100 nm-several micrometers (from cellulose of tunicate, algae, bacteria)
Nanofibrillated cellulose (NFC)	Nanofibrils, microfibrils, nanofibrillated cellulose, Microfibrillated cellulose	Wood, sugar beet, potato tuber, hemp, flax, etc.	Diameter: 5-60 nm Length: several micrometers

The cell wall in lignocellulosic fiber possesses basic structural units that are known as elementary fibrils. These elementary fibrils are about 2-20 nm in diameter and a few micrometers in length. These cellulose microfibrils can be considered CNFs, considering the definition of nanofiber size 100 nm in one dimension. The CNF bundles may have diameters within the range of 20-200 nm depending on the source from which they were derived, while the individual CNFs usually have diameters in the range of 3-20 nm [38], a few micrometers in length and very much alike (Figure 1 A-I).
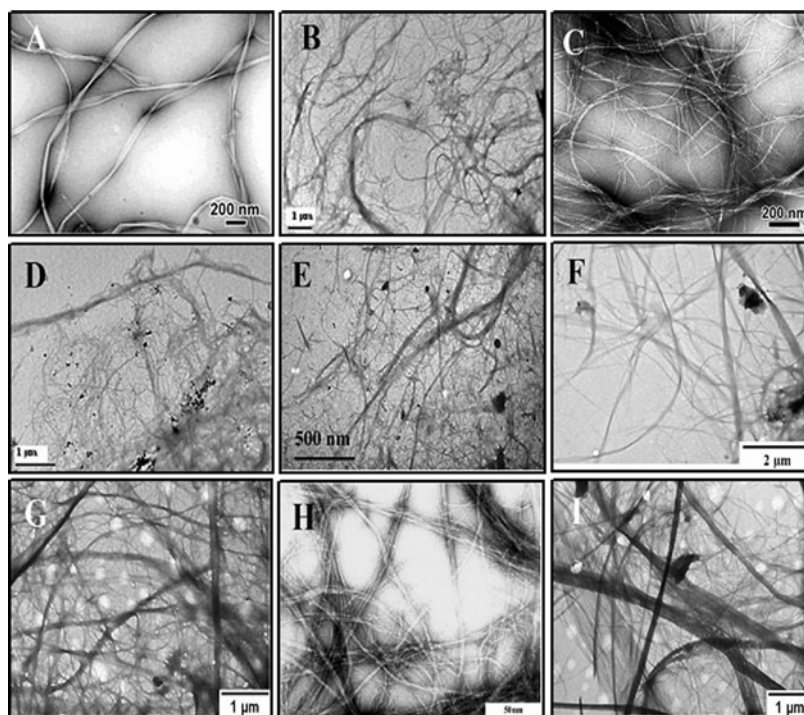
Figure 1. Transmission electron microscope (TEM) images of isolated cellulose nanofibers, obtained from A bacterial cellulose [39], B bagasse [40], C banana rachis [41], D rice straw [40], E hemp [42], F kenaf [43], G oil palm [44], H prickly pear fruits [45] and I rubber wood [44].
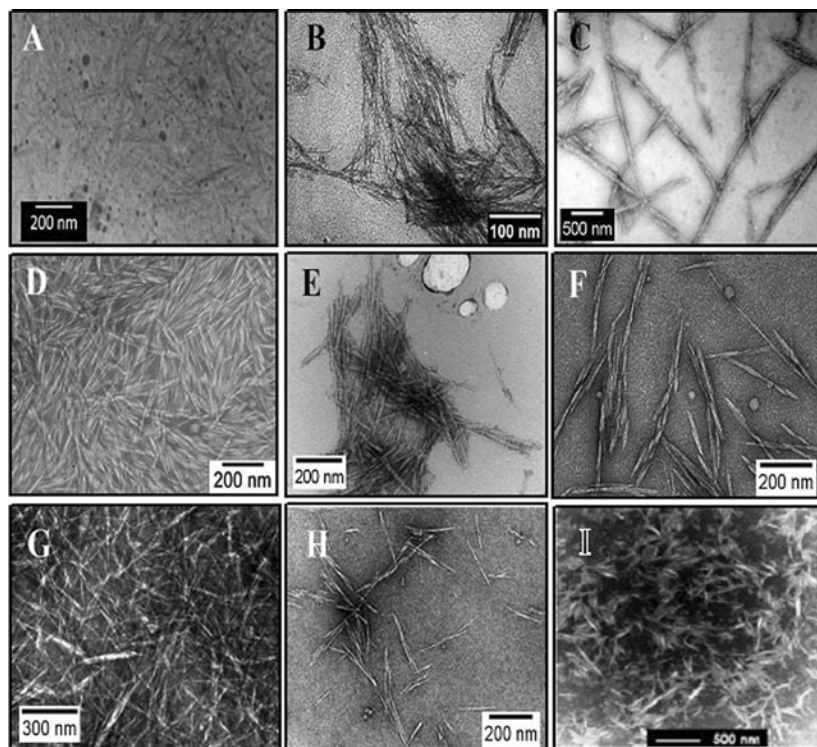
Figure 2. Transmission electron microscope (TEM) images of cellulose crystals obtained from A jute [46], B cotton linter [47], C bacterial cellulose [48], D rice straw [49], E soy hulls [50], F mengkuang leaves [51], G sugarcane bagasse [52], H bamboo [53] and I eucalyptus pulp [54].

On the other hand, the images of nanocrystals obtained from dilute suspensions of several plant sources showed a rod-like structure. Many researchers isolated CNCs from various sources, and they studied the size and morphology of the obtained nanocrystals by microscopies (Figure 2). The widths of CNFs and CNCs are shown in Table 3 based on diverse sources [60].

Table 3 Diameter of cellulose nanofibers (CNF) and nanocrystalline (CNC) from various source.

Source	Diameter (nm)	References
Cellulose nanofibers (CNF)		
Bacterial cellulose	40-70	[55]
Bagasse	5-15	[44]
Banana	3-5	[56]
Rice straw	4–13	[44]
Hemp	30-100	[42]
Kenaf	10-70	[43]
Oil palm	5-40	[44]
Prickly pear fruits	2-5	[45]
Rubber wood	10-90	[44]
Soy hull	20-120	[57]
Wheat straw	10-80	[57]
Cellulose nanocrystalline (CNC)		

Jute	3-10	[46]
Cotton linter	10-13	[47]
Bacterial cellulose	—	[57]
Rice straw	30.7	[49]
Soy hull	2.77 ± 0.67	[50]
Mengkuang leaves	5-25	[51]
Sugarcane bagasse	4 ± 2	[52]
Bamboo	8 ± 3	[53]
Eucalyptus wood	11 ± 4	[54]
Coconut husk	5.5 ± 1.4	[58]
Kenaf bast	2-5	[59]

In order to analyze the crystalline structure of lignocellulosic materials, X-ray diffraction (XRD) is generally used. It is widely realized that cellulose is partly crystalline and partly amorphous in molecular structure [61]. A number of parameters such as the source of cellulose, isolation process conditions and various pretreatments (PTs) determine the final crystallinity of nanocellulose in either crystal or fiber form. For instance, the crystallinity of flax, rutabaga and wood CNFs were calculated as 59, 64 and 54 %, respectively [62], whereas a crystallinity of 85.9, 76, 84.9, 94, 80.6 and 81.7 % was estimated for CNCs from sisal, rice husk, flax, cotton, corn stover and commercial MCC [63].

3. Nanocellulose isolation methods

The nanofibrillar domains, generally referred as nanocellulose, can be separated from each other by overcoming the extensive and strong inter-fibrillar hydrogen bonds with harsh caustic chemicals, specific enzymes and/or intense mechanical forces. Nanocellulose, either in rod-like cellulose nanocrystals (CNCs) or longer cellulose nanofibrils (CNFs), has generated significant interest due to its nanoscale dimensions and superior properties including extraordinary elastic modulus of 150 GPa [64], low axial thermal expansion coefficient of 10^{-7} K^{-1} [65] and high specific surface area [66,67].

Cellulose nanocrystals (CNCs) and nanofibrils (CNFs) have been isolated from pure rice straw cellulose via sulfuric acid hydrolysis, mechanical blending and 2,2,6,6-tetramethylpiperidine-1-oxyl (TEMPO)-mediated oxidation to 16.9%, 12% and 19.7% yields, respectively. Sulfuric acid hydrolysis produced highly crystalline (up to 90.7% CrI) rod-like (3.96-6.74 nm wide, 116.6-166 nm long) CNCs with similarly negative surface charges (-67 to -57 mV) and sulfate contents but decreasing yields and dimensions with longer hydrolysis time. Mechanical defibrillated CNFs were 82.5% crystalline and bimodally distributed in sizes (2.7 nm wide and 100-200 nm long; 8.5 nm wide and micrometers long). TEMPO mediated oxidation liberated the most uniform, finest (1.7 nm) and micrometer long, but least crystalline (64.4% CrI) CNFs. These nanocellulose self-assembled into submicron (153-440 nm wide) fibers of highly crystalline (up to 90.9% CrI) cellulose Iβ structure upon rapid freezing (-196 °C) and freeze-drying. The self-assembling behaviors were analyzed based on nanocellulose dimensions, specific surfaces and surface chemistries [68].

3.1 Isolation methods of CNC

The isolation of nanocrystalline cellulose is dependent of the cellulosic raw-material used and the process parameters. There is a vast type of lignocellulosic materials used for isolation of nanocrystalline cellulose, as garlic skin, oil palm, mulberry, sesame and rice husks [69-73]. The isolation process is usually performed in two stages. The first one may consist of successive mechanical and/or chemical treatments to remove complete or partially the non-cellulosic components. The second stage is a chemical treatment, generally acid hydrolysis, which the reaction parameters are acid specie, acid concentration, fiber/acid ratio, time and temperature [74].

Acid hydrolysis has been the primary method for isolating rod-like CNCs since early reports in the late 1940s [75]. Usually, cellulose nanocrystals (CNCs) are prepared by strong acid hydrolysis (e.g., 64% sulfuric acid) of cellulose to remove amorphous regions, to obtain needle-like morphologies with 10-20 nm in diameter and several hundred nanometers in length [76]. Wilson Pires Flauzino Neto et al. successfully isolated cellulose nanocrystals (CNC) from soy hulls. The Soy hulls was firstly purified by 2% NaOH and 1.7% $NaClO_2$, and then hydrolyzed at 40 °C with 64% H_2SO_4. The resulting nanocrystals presented a high crystallinity (73.5%), an average length of 122.66 ± 39.40 nm, a diameter of 2.77 ± 0.67 nm and an aspect ratio around 44 [77]. The nanocrystalline cellulose was isolated from corn husk by de Carvalho Mendes et al. The corn husk was firstly purified by H_2O_2 (24%) and NaOH (4%) (H_2O_2/NaOH ratio: 1:1) at 45 °C, for 2 h, with a fiber/solution ratio of 1:20, and then hydrolyzed at 45 °C with 60% H_2SO_4.

Ahmed et al isolated cellulose nanocrystals (CNC) from seed fibers of Ushar (*Calotropis procera*), the CNCs obtained by acid hydrolysis (64% sulfuric acid solution with fiber to acid ratio of 1:20 at 50 °C for 75 min with strong agitation) showed well-dispersed suspension and needle shape with the diameter of 14-24 nm and length of 140-260 mm (aspect ratio: about 10) with the yield of 79% [76]. Highly stable and dispersible nanocrystalline cellulose (NCC) was successfully isolated by R. Rohaizu et al from oil palm empty fruit bunch microcrystalline cellulose, with yields of 93% via a sono-assisted TEMPO-oxidation and a subsequent sonication process **[78]**.

Sulfuric acid hydrolysis has shown to produce relatively uniformly sized CNCs from a sole source under a fixed condition, however, widely varied dimensions of 3-70 nm widths and 35-3000 nm lengths have been reported from different cellulose sources and hydrolysis conditions [79,80]. Other acids such as hydrochloric acid, hydrobromic acid as well as mixed acetic and nitric acids are also capable of hydrolyzing cellulose into CNCs, without esterifying the surfaces as in the case with sulfuric acid while in higher yields [81-83]. Strong acids hydrolyze cellulose chains in the less ordered regions, producing CNCs with higher crystallinities than the original source but usually at low yields of less than 30% [84,85].

3.2 Isolation methods of CNF

In the literature, different cellulosic resources were used as sources for the generation of cellulose nanoparticles and several processes have been used to extract highly purified nanofibers from lignocellulosic fibers. Different raw materials used for production of cellulose nanofibers are soy hulls, pine-apple, corncob, cassava bagasse, hemp fibers, rice husk, sludge, etc [86-90]. The different processes adopted include mechanical treatments, chemical treatments, biological treatments, electrospinning methods, etc [91-794]. It is usually combined by chemical method and mechanical method, which can be classified three types according to the chemical treatment.

3.2.1 chemo-mechanical treatment

Depending on the source of raw material and disintegration process, nanofibrils with wide range of dimensionality are isolated [95]. Chen et al. individualized cellulose nanofibers from poplar wood in two distinct stages. Initially, wood fibers were subjected to a chemical process to eliminate lignin and hemicellulose. The obtained chemical-purified cellulose fibers were then mechanically separated into nanofibers using high-intensity ultrasonication [96]. At the same time, they isolated cellulose nanofibers (CNFs) from flax, bamboo, and wheat straw fibers though a chemical-ultrasonic treatment and made a comparative study. The study shows the CNFs isolated from bamboo, wood and wheat straw fibers have a uniform diameter of 10–40 nm, whereas the flax fibers were not uniformly nanofibrillated because of their initially high cellulose content [97]. Alemdar and Sain isolated cellulose nanofibers from the agricultural residues, soy hull and wheat straw by a chemi-mechanical technique to examine their potential as reinforcement in biocomposites applications [98].

3.2.2 TEMPO + mechanical treatment

CNFs can be produced by first pretreated with TEMPO-mediated oxidation (2, 2, 6, 6, -tetrame-thylpipelidine-1-oxyl radical), and then multipass high-pressure homogenization [99]. The native wood celluloses can be converted to individual nanofibers 3-4 nm wide that are at least several microns in length, i.e. with aspect ratios >100, by TEMPO (2,2,6,6-tetramethylpiperidine-1-oxyl radical)-mediated oxidation and successive mild disintegration in water [100]. More uniform CNFs with 1–5 nm diameters have been isolated through oxidation using nitroxyl radical 2,2,6,6-tetramethylpyperidine-1-oxyl (TEMPO) by Saito, Nishiyama, Putaux, Vignon, & Isogai. The TEMPO oxidized CNFs have been reported to have the same crystallinity as the starting materials and, when aided with mechanical means, over 90% yield [100,101]. Saito, Nishiyama, Putaux, Vignon, & Isogai. recently completely individualized cellulose nanofibers have been extracted from cotton stalks by Soni, Hassan & Mahmoud though 2,2,6,6-tetramethylpiperidine-1-oxyl radical (TEMPO)-mediated oxidation under moderate aqueous condition [102].

3.2.3 Enzyme hydrolysis + mechanical treatment

In previous decades the challenge associated with isolating CNF was the high energy demand required by mechanical disintegration process [103]. However, with discovering strong impact of

pretreatment methods, *e.g.*, enzymatic hydrolysis, which were aimed at facilitating the mechanical disintegration. CNF production methods usually comprise several operations, *e.g.*, successive refining, enzymatic hydrolysis, again refining and finally homogenization [104-106]. In nature, cellulose does not degrade by single enzymes. Instead aerobic fungi like Trichoderma-, Phanerochaete-, and Aspergillus-species degrade cellulose by excreting a mixture of independently acting, but cooperating hydrolytic enzymes [107]. Such a set of cellulases can contain seven or more different enzymes belonging to different protein families [108], but at least four functional types of cellulases can be recognized: A- and B-type cellulases are termed cellobiohydrolases, and are able to attack also highly crystalline cellulose, whereas C -and especially D-type cellulases, endoglucanases with a common name, generally require some disorder in the Structure in order to attack the cellulose [109]. The use of enzymes as a clean and environmentally friendly treatment prior to isolation of microfibrillated cellulose (MFC) has been also investigated with the aim to reduce energy and chemicals during the isolation process [110-114]. Hassan et al studied xylanase enzymes for isolation of MFC from date palm fruit stalks pulp using ultra-high friction grinding and showed the width of MFC isolated from untreated pulp was 21 ± 9 nm whereas that of MFC isolated from xylanase-treated pulps ranged from 81 ± 25 to 60 ± 20 nm. In addition, surface charge of MFC isolated from xylanase-pretreated fibers was lower than that of MFC isolated from untreated fibers. MFC films made from xylanase pretreated fibers showed higher density and tensile strength properties, lower water absorption and air permeability than those made from MFC isolated from untreated fibers [115].

4. Applications of CNC and CNF derived from agricultural biomass

Nanocellulose is of increasing interest for a range of applications relevant to the fields of material science and biomedical engineering due to its renewable nature, anisotropic shape, excellent mechanical properties, good biocompatibility, tailorable surface chemistry, and interesting optical properties.

4.1 Hydrogels

Hydrogels are polymeric materials with capability to swell and retain large amounts of water without dissolving in water (Thermal studies of plant carbohydrate polymer hydrogels). Hydrogels can be produced from both natural and synthetic polymers by physical or chemical crosslinking [116]. At present, numerous studies have been carried out to reinforce hydrogels by incorporating rigid, rod-like cellulose nanocrystals (CNCs), or cellulose nanofibers (CNFs) [117]. In recent years, polysaccharides have attracted much attention as biomedical intelligent hydrogels, because of their biodegradability, biocompatibility, readily available and cost-effective nature [118].

Among various kinds of nanofillers, cellulose nanocrystals (CNCs) as polysaccharides have gained importance for making hydrogels, because of good mechanical properties, biocompatibility, commercial availability, nontoxicity, and biodegradability [119].

The mechanical performance of bionanocomposite hydrogels was improved significantly as increased CNC content (from 2 to 10 wt%) [120]. Nanocomposite hydrogels with various amounts of CNCs were used to remove methylene blue dye from an aqueous solution [121]. Shok et al studied that cellulose nanocrystals extracted from rice husks as a reinforcing material in gelatin hydrogels for use in controlled drug delivery systems, they found that hydrogels showed increased crystallinity and storage moduli with CNC incorporation [122].

4.2 Aerogel

The use of cellulose aerogels as antibacterial materials has been investigated by applying a contact-active layer-by-layer modification to the aerogel surface. Studying the adsorption of multilayers of polyvinylamine and polyacrylic acid to aerogels comprising crosslinked cellulose nanofibrils and monitoring the subsequent bacterial adhesion revealed aerogel was adsorbed without noticeably affecting the aerogel structure. The antibacterial effect was tested by measuring the reduction of viable bacteria in solution when the aerogels were present. The results show that >99.9% of the bacteria adhered to the surface of the aerogels. Microscopy further showed adherence of bacteria to the surfaces of the modified aerogels. These results indicate that it is possible to create materials with three-dimensional cellulose structures that adsorb bacteria with very high efficiency utilizing the high specific surface area of the aerogels in combination with their open structure [123].

Monolithic cellulose nanofibrils (CNF) silica composite aerogels were successfully prepared by immersing CNF aerogels into a silica solution in a two-step sol-gel process (initial hydrolysis of tetraethyl orthosilicate followed by condensation of silica particles). Aerogels were characterized by scanning electron microscope (SEM), surface area test, bulk density and silica content analysis, fourier Transform Infrared (FTIR) spectroscopy, and compression test. The form of SiO_2 existing in the composite aerogel was the spherical individual particles coated on CNF fibrils. The pH value of condensation solution was found to have profound influence on the properties of the composite aerogels. By varying the pH value of condensation atmosphere from 8 to 12, the bulk densities of composite aerogels were able to be linearly increased from 0.059 g cm^{-3} to 0.29 g cm^{-3}, and the silica content in the matrix sharply jumped from 3 % to 79 %. The porosities of the aerogels remained very high, between 85 and 96%, and the surface area of the composite aerogel reached up to 700.1 m^2 g^{-1}. The compression properties of the composite aerogel improved greatly compared with those of the silica aerogel, about 8-30 times higher. Moreover, the compressive strength of the composite aerogel prepared in this work greatly exceeded the conventional insulation materials found in the recent commercial market, and without substantial increases in thermal conductivity [124].

4.3 Nanocellulose in medical applications

Nanocellulose is a promising biomaterial for medical applications owing to its good

biocompatibility and relatively low toxicity, as well as distinct geometry, surface chemistry, rheology, crystallinity and self-assembly behavior [125,126]. While it is generally accepted that BC is non-toxic, the issue of biotoxicity is less resolved for other nanoparticles of cellulose, such as CNCs and CNFs. The toxicity of these materials depends on particle size, surface chemistry, and process purity. Preliminary results indicate low dermal and oral toxicity, but are conflicting with regards to inhalation and cytotoxicity. The assembly and surface chemistry properties of nanocellulose are useful in scaffold design to enhance mechanical properties [127–132], cell adhesion, proliferation and differentiation [133,134], and cellular patterning [135,136]. With the possibility of diverse fabrication shapes, such as membrane-like structures having tailorable porosities and surface chemistries, BC and CNCs are inherently suitable for tissue engineering scaffolds, such as coatings, membranes and hydrogels, electrospun nanofibers, and all-cellulose nanocomposites [137-139].

Another hot topic is nanocellulose-based materials for drug delivery, in the form of membranes, tablet coatings [140-143], and in composite-bio polymer delivery systems [144,145]. These materials can be loaded with the drug of choice, and provide good drug stability as well as a controlled release profile [146,147]. In addition, CNC surface modification has been used to design novel carriers [148-150]; a particularly versatile modification of CNCs uses an aromatic linker to facilitate both binding and controlled release of amine-containing drugs. Furthermore, nanocellulose is a promising candidate for protein immobilization, preserving the structural integrity of the protein, and enhancing activity and long-term storage stability.

Fluorescent labeling of nanocellulose with a variety of fluorophores is of emerging interest in bio-imaging, targeting and sensing applications. Finally, CNC-based systems are also compelling as mechanically adaptive materials for intracortical microelectrode applications. The first report of this nature described CNC-based microprobes which exhibited switchable mechanical properties from wet to dry [151].

4.4 superabsorbent polymers

Wheat Straw is one of the best-known fiber crops, and can easily actuate a series of chemical reactions, such as esterification, etherification, and copolymerization since a large amount of hydroxyl groups exists on the molecular chain. This can be changed into hydrophobic groups by acetylation [152] or radical by oxidation [153]. Because of the low toxicity, good water absorbent capacity, excellent biocompatibility, and biodegradability, recently, there has been a lively interest in addition of lignocellulose or chemical modified cellulose into superabsorbent formulation, such as cellulose-grafted superabsorbent polymers with eco-friendly property and biodegradability, in the academic and industrial field [154-157], and has found new generations of superabsorbent hydrogels (SARs). New SARs are cheaper in price, and possess superior mechanical properties than nanocellulose-based counterparts.

However, researches on the formulation and preparation for superabsorbent hydrogel were based on a process of chemical modifying or digesting of pulverized wheat straw and CS, these

pretreatments resulted in black liquor that may be harm to environment. Few studies have formulated, and prepared superabsorbent hydrogel based on raw CS by utilizing nonchemical treatment in this field.

Gel can be produced from pure cellulose; however, it requires special solvents for dissolution [158]. Thus, the gel preparation from various water-soluble cellulose derivatives is easier. For gel synthesis, usually cellulose derivatives containing carboxymethyl, alkyl or hydroxyalkyl groups are used [159]. It should be noted that beside the substituent, the polymer properties, such as molecular weight and degree of substitution also affect the polymer solubility [160,161].

4.5 Environmental applications

The consumption of fossil fuels to produce energy and petrochemicals over the last 50 years has resulted in the rapid accumulation of green-house gases that is impacting the livelihood of many communities around the globe. There is thus a compelling motivation to seek alternative sources of energy and raw materials not derived from fossil fuels, but from renewable resources.

Currently, there is a growing market trend toward the formulation of products that can maintain the consumer perception of being natural and "green". This has motivated the production of bio-based nanoparticles for the formulation of Pickering emulsions for the food and cosmetic industries. Cellulose nanocrystals are ideal for this application, and they have been shown to be effective Pickering emulsifiers [163,164]. They can stabilize monodispersed oil (hexadecane) droplets of ~4 μm in water phase against coalescence for 4 months (Figure 3A). This is due to the partitioning of stable CNCs nanoparticles at the oil-water interface that significantly enhance the stability of oil droplets [165]. Further research suggested that cellulose nanocrystals with a charge density greater than 0.03 e/nm 2 could not efficiently stabilize oil droplets due to the strong electrostatic repulsions between the nanoparticles located at the oil-water interface [166]. In addition, neutral CNCs extracted by HCl hydrolysis performed better than sulfated CNCs at the oil/water interface [167].

4.6 Application in polymers

Polymer grafting has been investigated to modify CNCs by 'grafting-onto' and 'grafting-from' techniques. The grafted chains improve the association between polymer matrix and CNC filler, and facilitate stress-transfer to enhance the strength of nanocomposite materials. Moreover, polymer grafting may be used to impart unique properties to the modified CNCs [168-170].

Nanocellulose, including CNCs and CNFs, is extensively used as a filler in thermoplastic polymeric matrices to produce cost-effective, highly durable nanocomposite materials, with a 'greener' footprint. The native crystallinity, high strength, and moderate to high aspect ratio (ca. 10–1000 length/diameter; type dependent) of nanocellulose are relevant for stress transfer and load-bearing in thermoplastics, such as starch, polyvinyl alcohol [171], poly lactic acid (PLA) [172-174], polycarbonate [175], polyurethane [176], and polymethyl methacrylate. In order to

improve compatibility with hydrophobic matrices, it may be necessary to modify nanocellulose surfaces [177].

Hard templating using preformed mesoporous materials (also termed "nanocasting") has emerged as a versatile technique to prepare materials that cannot be accessed through conventional lyotropic template synthesis, e.g. due to hydrolytic instability of precursors. Cellulose nanocrystal dispersions can exhibit lyotropic chiral nematic behavior at relatively low concentrations, have lower viscosities and they form over shorter time scales when compared to several other cellulose derivatives, i.e. ethyl cellulose or hydropropylethyl cellulose. This has generated a strong interest in using evaporation-induced self-assembly protocols to prepare functional mesoporous materials with chiral nematic order. In the templating approach, successive loading of precursors permeates through a stable mesoporous support, often followed by calcination to construct an interconnected network to produce the desired product. The remaining active components can either be templating materials (CNCs) or functional materials introduced in the synthesizing steps. Many kinds of ordered mesoporous materials (e.g., carbon, metal oxides, and polymers) can be prepared through hard templating approaches.

4.7 Other nanocellulose composites

4.7.1 Nanocellulose photonics

Nanocellulose is of interest for photonic applications for reasons inherent to the material; first among these is the liquid crystalline behavior of CNCs which gives rise to iridescent films of defined optical character, secondly both CNCs and CNFs may form optically transparent stand-alone films. The versatility of these materials lies in the nature and surface chemistry of cellulose with relatively little effort, nanocellulose can be made compatible with both hydrophilic and hydrophobic components, used as a host for optically active nanoparticles, and modified to covalently incorporate optically relevant molecules.

CNCs can form chiral nematic, iridescent, colored films simply by evaporation of aqueous suspensions [178-180]. Over the past five years, CNC-templating had been used to access a stunningly diverse range of left-handed, chiral materials, such as mesoporous silica [181,182], organosilicon [183], cellulose [184], nanocrystalline titania [185], carbon [186], as well as polymer/CNC nanocomposites [187-189].

4.7.2 Nanocellulose films and foams

CNC films have been proposed for diverse applications, ranging from food packaging [190] to cellular orientation [191] and electronics. It was recently shown that ultrathin, aligned CNC films exhibit a large piezoelectric response and thus have potential in flexible electronic devices [192]. The combination of CNCs and conducting polymers is another approach to produce flexible, conductive films in which the CNC component enhances the mechanical properties of the conductive polymers, which are typically poor. Moreover, chiral nematic order can be

preserved in such films. The topic of conductive CNC films, as well as chiral mesoporous carbon films, which can be used as supercapacitor electrodes with near-ideal capacitor behavior, is discussed in depth in a recent review.

CNC foams and aerogels have not been investigated as intensively as films. Unlike cellulose fibers and nanofibers, it is difficult to form stable 3D structures from CNCs due to limited entanglement. In recent years, several different methods based upon physical interactions between CNCs have been utilized to prepare foams and aerogels, including freeze drying and solvent exchange/critical point drying. CNC properties, such as charge, size and concentration, play a significant role in the self-organization of the particles and thus in the architecture of the resulting foams. Recently, chemical-crosslinking/ critical point drying was used to produce all NC aerogels, which exhibited good mechanical and ape recovery properties, especially in water [193]. Further, the incorporation of capacitive nanoparticles within the aerogels resulted in supercapacitors with excellent capacitance retention at high charge-discharge rates [194].

Conclusions

Crop residues were incorporated into the soil or fed to livestock and the manure returned to the land in amounts that could be absorbed and utilized. Since farms have become highly mechanized and reliant on synthetic fertilizers and pesticides, the crop residues, which were once recycled, are now largely wastes whose disposal presents a continuing problem for the farmer. The agricultural residues consist of many and varied wastes from agriculture. The prospects and application of biotechnical principles facilitates these problems to be seen in a novel approach, as resources, which in many cases have tremendous potential.

The uniqueness, abundance, and potential low cost of cellulosic nanomaterials from agricultural waste will serve many industrial materials needs. Several areas should draw more concentrate efforts:

• Economically viable and environmentally preferable production of the various forms of cellulose nanomaterials

• Characterizing cellulosic nanomaterial morphology and properties

• Exploring new applications for using cellulosic nanomaterials and tailoring them to perform well in those applications

In our immediate future, we can envision automobiles and trucks made with cellulosic nanomaterials, wind turbines producing green power, ships crossing the oceans, and medicines and medical diagnostics. We hope the vision that we and others share will open the mind to the potential opportunities presented by this new material.

It is essential for national and international to cooperate, share resources and devote efforts to develop and commercialize uses of cellulose nanomaterials. Cellulosic nanomaterials will be on the list of materials of choice for the 21st Century.

Acknowledgments

Reference

[1] Che C, Yuan J. Developing trend of biomass energy sources in the world [J]. Natural Gas Industry, 2011, 31(1):104-106.

[2] Zeng X, Ma Y, Ma L. Utilization of straw in biomass energy in China [J]. Renewable & Sustainable Energy Reviews, 2007, 11(5):976-987.

[3] Liu H, Jiang G M, Zhuang H Y, et al. Distribution, utilization structure and potential of biomass resources in rural China: With special references of crop residues [J]. Renewable & Sustainable Energy Reviews, 2008, 12(5):1402-1418.

[4] Zhang T, Bu M D, Geng W. Pollution status and biogas-producing potential of livestock and poultry excrements in China [J]. Chinese Journal of Ecology, 2012.

[5] Bassam N E. Energy plant species: their use and impact on environment and development [M]// The World yearbook of robotics research and development /. Kogan Page, 1998:31-37.

[6] WANG Xian-pu. The features of plant resources in China and its rational utilization [J]. Guihaia, 1991, (2):171-176.

[7] Li M U. Research on the Development and Utilization of Agricultural Biomass Resource [J]. Agricultural Science & Technology & Equipment, 2015.

[8] Chastain J P, Camberato J J, Albrecht J E. Nutrient Content of Livestock and Poultry Manure [J]. Clemson University, 2001.

[9] Zhang Z D, Jing-Gui W U. Progress of the researches on resource utilization of livestock and poultry manure [J]. Guangdong Agricultural Sciences, 2010, 37(1):135-138.

[10] Hakeem, Khalid Rehman, Mohammad Jawaid, and Othman Y. Alothman, eds. Agricultural biomass based potential materials [M]. Berlin: Springer, 2015.

[11] Sharma S, Sheth P N. Air–steam biomass gasification: experiments, modeling and simulation [J]. Energy Conversion and Management, 2016, 110: 307-318.

[12] Pérez J, Munoz-Dorado J, de la Rubia T, et al. Biodegradation and biological treatments of cellulose, hemicellulose and lignin: an overview [J]. International Microbiology, 2002, 5(2): 53-63.

[13] Jeffries T W. Biodegradation of lignin and hemicelluloses [M]//Biochemistry of microbial degradation. Springer Netherlands, 1994: 233-277.

[14] Amari M, Abe A, Kawano S, et al. Near infrared reflectance spectra of fibrous constituents in forages and rice straw [J]. Bulletin of National Institute of Animal Industry (Japan), 1991.

[15] McLellan T M, Aber J D, Martin M E, et al. Determination of nitrogen, lignin, and cellulose content of decomposing leaf material by near infrared reflectance spectroscopy

[J]. Canadian Journal of Forest Research, 1991, 21(11): 1684-1688.

[16] Ono K, Hiraide M, Amari M. Determination of lignin, holocellulose, and organic solvent extractives in fresh leaf, litterfall, and organic material on forest floor using near-infrared reflectance spectroscopy [J]. Journal of Forest Research, 2003, 8(3): 191-198.

[17] Cozzolino D, Fassio A, Gimenez A. The use of near-infrared reflectance spectroscopy (NIRS) to predict the composition of whole maize plants [J]. Journal of the Science of Food and Agriculture, 2001, 81(1): 142-146.

[18] Bai Q L, Chen S J, Dong X L, et al. Prediction of NDF and ADF concentrations with near infrared reflectance spectroscopy (NIRS) [J]. Guang pu xue yu guang pu fen xi, 2004, 24(11): 1345-1347.

[19] Huang C, Han L, Liu X, et al. The rapid estimation of cellulose, hemicellulose, and lignin contents in rice straw by near infrared spectroscopy [J]. Energy Sources, Part A: Recovery, Utilization, and Environmental Effects, 2010, 33(2): 114-120.

[20] Jung S J, Kim S H, Chung I M. Comparison of lignin, cellulose, and hemicellulose contents for biofuels utilization among 4 types of lignocellulosic crops [J]. Biomass and Bioenergy, 2015, 83: 322-327.

[21] Ioelovich M. Cellulose as a nanostructured polymer: a short review [J]. BioResources, 2008, 3(4): 1403-1418.

[22] Klemm D, Kramer F, Moritz S, et al. Nanocelluloses: A new family of nature‐based materials [J]. Angewandte Chemie International Edition, 2011, 50(24): 5438-5466.

[23] Singha AS, Thakur VK (2009) Fabrication and characterization of H. sabdariffa fiber-reinforced green polymer composites [J]. Polym-Plast Technol Eng 48:482–487.

[24] Singha AS, Thakur VK (2009) Fabrication and characterization of S. cilliare fibre reinforced polymer composites [J]. Bull Mater Sci 32:49–58.

[25] Singha AS, Thakur VK (2009) Physical, chemical and mechanical properties of Hibiscus sabdariffa fiber/polymer composite [J]. Int J Polym Mater 58:217–228.

[26] Singha AS, Thakur VK (2009) Grewia optiva fiber reinforced novel, low cost polymer composites [J]. J Chem 6:71–76.

[27] Singha AS, Thakur VK (2009) Synthesis, characterization and analysis of Hibiscus Sabdariffa Fibre reinforced polymer matrix based composites [J]. Polym Polym Compos 17:189–194

[28] Thakur VK, Thakur MK, Gupta RK (2013) Development of functionalized cellulosic biopolymers by graft copolymerization [J]. Int J Biol Macromol 62:44–51.

[29] Thakur VK, Singha AS, Thakur MK (2013) Fabrication and Physico-Chemical Properties of High-Performance Pine Needles/Green Polymer Composites [J]. Int J Polym Mater Polym Biomater 62:226–230.

[30] Thakur VK, Singha AS, Thakur MK (2013) Ecofriendly biocomposites from natural fibers: mechanical and weathering study [J]. Int J Polym Anal Charact 18:64–72.

[31] Thakur VK, Thakur MK, Gupta RK (2013) Synthesis of lignocellulosic polymer with improved chemical resistance through free radical polymerization [J]. Int J Biol Macromol

61:121–126

[32] Thakur VK, Thakur MK (2014) Processing and characterization of natural cellulose fibers/thermoset polymer composites [J]. Carbohydr Polym 109:102–117.

[33] Thakur VK, Thakur MK, Gupta RK (2014) Review: raw natural fiber-based polymer composites [J]. Int J Polym Anal Charact 19:256–271.

[34] Thakur VK, Grewell D, Thunga M, Kessler MR (2014) Novel composites from eco-friendly soy flour/SBS triblock copolymer [J]. Macromol Mater Eng 299:953–958.

[34] Thakur VK, Thakur MK, Raghavan P, Kessler MR (2014) Progress in green polymer composites from lignin for multifunctional applications: a review [J]. ACS Sustain Chem Eng 2:1072–1092.

[35] Moon RJ, Marini A, Nairn J, Simonsen J, Youngblood J (2011) Cellulose nanomaterials review: structure, properties and nanocomposites [J]. Chem Soc Rev 40:3941–3994.

[36] Wang B, Sain M, Oksman K (2007) Study of structural morphology of hemp fiber from the micro to the nanoscale [J]. Appl Compos Mater 14:89–103.

[37] Habibi Y, Lucia LA, Rojas OJ (2010) Cellulose nanocrystals: chemistry, self-assembly, and applications [J]. Chem Rev 110:3479–3500.

[38] Sassi JF, Chanzy H (1995) Ultrastructural aspects of the acetylation of cellulose [J]. Cellulose 2:111–127.

[39] Castro C, Zuluaga R, Álvarez C, et al. Bacterial cellulose produced by a new acid-resistant strain of Gluconacetobacter genus [J]. Carbohydrate polymers, 2012, 89(4): 1033-1037.

[40] Hassan S F, Rosen R A. Resolving the ghost problem in nonlinear massive gravity [J]. Physical review letters, 2012, 108(4): 041101.

[41] Zuluaga R, Putaux J L, Cruz J, et al. Cellulose microfibrils from banana rachis: Effect of alkaline treatments on structural and morphological features [J]. Carbohydrate Polymers, 2009, 76(1): 51-59.

[42] Wang J, Agrawala M, Cohen M F. Soft scissors: an interactive tool for realtime high quality matting [C]//ACM Transactions on Graphics (TOG). ACM, 2007, 26(3): 9.

[43] Jonoobi M, Harun J, Mathew A P, et al. Mechanical properties of cellulose nanofiber (CNF) reinforced polylactic acid (PLA) prepared by twin screw extrusion [J]. Composites Science and Technology, 2010a, 70(12): 1742-1747.

[44] Jonoobi M, Harun J, Mathew A P, et al. Preparation of cellulose nanofibers with hydrophobic surface characteristics [J]. Cellulose, 2010b, 17(2): 299-307.

[45] Habibi Y, Mahrouz M, Vignon M R. Microfibrillated cellulose from the peel of prickly pear fruits [J]. Food Chemistry, 2009, 115(2): 423-429.

[46] Cao Y, Chan F, Chui Y H, et al. Characterization of flax fibres modified by alkaline, enzyme, and steam-heat treatments [J]. BioResources, 2012, 7(3): 4109-4121.

[47] Morais J M. Petróleo em águas profundas: uma história tecnológica da Petrobras na exploração e produção offshore [J]. 2013.

[48] Grunert M, Winter W T. Nanocomposites of cellulose acetate butyrate reinforced with cellulose nanocrystals [J]. Journal of Polymers and the Environment, 2002, 10(1): 27-30.

[49] Lu P, Hsieh Y L. Preparation and characterization of cellulose nanocrystals from rice straw [J]. Carbohydrate Polymers, 2012, 87(1): 564-573.

[50] Neto W P F, Silvério H A, Dantas N O, et al. Extraction and characterization of cellulose nanocrystals from agro-industrial residue–Soy hulls [J]. Industrial Crops and Products, 2013, 42: 480-488.

[51] Sheltami R M, Abdullah I, Ahmad I, et al. Extraction of cellulose nanocrystals from mengkuang leaves (Pandanus tectorius) [J]. Carbohydrate Polymers, 2012, 88(2): 772-779.

[52] de Morais Teixeira E, Bondancia T J, Teodoro K B R, et al. Sugarcane bagasse whiskers: extraction and characterizations [J]. Industrial Crops and Products, 2011, 33(1): 63-66.

[53] Brito B S L, Pereira F V, Putaux J L, et al. Preparation, morphology and structure of cellulose nanocrystals from bamboo fibers[J]. Cellulose, 2012, 19(5): 1527-1536.

[54] Tonoli G H D, Teixeira E M, Corrêa A C, et al. Cellulose micro/nanofibres from Eucalyptus kraft pulp: preparation and properties[J]. Carbohydrate polymers, 2012, 89(1): 80-88.

[55] Castro C, Zuluaga R, Álvarez C, et al. Bacterial cellulose produced by a new acid-resistant strain of Gluconacetobacter genus[J]. Carbohydrate polymers, 2012, 89(4): 1033-1037.

[56] Zuluaga R, Putaux J L, Cruz J, et al. Cellulose microfibrils from banana rachis: Effect of alkaline treatments on structural and morphological features [J]. Carbohydrate Polymers, 2009, 76(1): 51-59.

[57] Alemdar A, Sain M. Isolation and characterization of nanofibers from agricultural residues–Wheat straw and soy hulls [J]. Bioresource technology, 2008, 99(6): 1664-1671.

[58] Rosa M F, Medeiros E S, Malmonge J A, et al. Cellulose nanowhiskers from coconut husk fibers: Effect of preparation conditions on their thermal and morphological behavior [J]. Carbohydrate Polymers, 2010, 81(1): 83-92.

[59] Zaini L H, Jonoobi M, Tahir P M, et al. Isolation and characterization of cellulose whiskers from kenaf (Hibiscus cannabinus L.) bast fibers [J]. Journal of Biomaterials and Nanobiotechnology, 2013, 4(01): 37.

[60] Jonoobi M, Oladi R, Davoudpour Y, et al. Different preparation methods and properties of nanostructured cellulose from various natural resources and residues: a review [J]. Cellulose, 2015, 22(2): 935-969.

[61] Ciolacu D, Ciolacu F, Popa VI (2011) Amorphous cellulose-structure and characterization [J]. Cellul Chem Technol 45:13–21.

[62] Bhatnagar A, Sain M (2005) Processing of cellulose nanofiberre inforced composites [J]. J Reinf Plast Compos 24:1259–1268

[63] Luduen ˜a LN, Vecchio A, Stefani PM, Alvarez VA (2013) Extraction of cellulose nanowhiskers from natural fibers and agricultural byproducts [J]. Fibers Polym 14:1118–1127

[64] Iwamoto, S., Kai, W., Isogai, A., & Iwata, T. (2009). Elastic modulus of single cellulose microfibrils from tunicate measured by atomic force microscopy [J]. Biomacromolecules, 10(9): 2571-2576.

[65] Nishino, T., Matsuda, I., & Hirao, K. (2004). All-cellulose composite [J]. Macromolecules, 37(20): 7683-7687.

[66] Heath, L., & Thielemans, W. (2010). Cellulose nanowhisker aerogels [J]. Green Chemistry, 12(8):1448-1453.

[67] Saito, T., Uematsu, T., Kimura, S., Enomae, T., & Isogai, A. (2011). Self-aligned integration of native cellulose nanofibrils towards producing diverse bulk materials [J]. Soft Matter, 7(19): 8804-8809.

[68] Jiang, F., & Hsieh, Y. L. (2013). Chemically and mechanically isolated nanocellulose and their self-assembled structures [J]. Carbohydrate Polymers, 95(1): 32-40.

[69] Reddy, J. P., & Rhim, J. W. (2014). Isolation and characterization of cellulose nanocrystals from garlic skin [J]. Materials Letters, 129: 20-23.

[70] Haafiz, M. M., Hassan, A., Zakaria, Z., Inuwa, I. M., & Islam, M. S. (2013). Physicochemical characterization of cellulose nanowhiskers extracted from oil palm biomass microcrystalline cellulose [J]. Materials Letters, 113: 87-89.

[71] Purkait, B. S., Ray, D., Sengupta, S., Kar, T., Mohanty, A., & Misra, M. (2010). Isolation of cellulose nanoparticles from sesame husk [J]. Industrial & Engineering Chemistry Research, 50(2): 871-876.

[721] Li, R., Fei, J., Cai, Y., Li, Y., Feng, J., & Yao, J. (2009). Cellulose whiskers extracted from mulberry: A novel biomass production [J]. Carbohydrate Polymers, 76(1): 94-99.

[73] Johar, N., Ahmad, I., & Dufresne, A. (2012). Extraction, preparation and characterization of cellulose fibres and nanocrystals from rice husk [J]. Industrial Crops and Products, 37(1): 93-99.

[74] de Carvalho Mendes, C. A., Ferreira, N. M. S., Furtado, C. R. G., & de Sousa, A. M. F. (2015). Isolation and characterization of nanocrystalline cellulose from corn husk [J]. Materials Letters, 148: 26-29.

[75] Nickerson, R. F., & Habrle, J. A. (1947). Cellulose intercrystalline structure [J]. Industrial & Engineering Chemistry, 39(11): 1507-1512.

[76] Oun, A. A., & Rhim, J. W. (2016). Characterization of nanocelluloses isolated from Ushar (Calotropis procera) seed fiber: Effect of isolation method [J]. Materials Letters, 168: 46-150.

[77] Neto, W. P. F., Silvério, H. A., Dantas, N. O., & Pasquini, D. (2013). Extraction and characterization of cellulose nanocrystals from agro-industrial residue-soy hulls [J]. Industrial Crops and Products, 42: 480-488.

[78] Rohaizu, R., & Wanrosli, W. D. (2017). Sono-assisted TEMPO oxidation of oil palm lignocellulosic biomass for isolation of nanocrystalline cellulose [J]. Ultrasonics Sonochemistry, 34: 631-639.

[79] Beck-Candanedo, S., Roman, M., & Gray, D. G. (2005). Effect of reaction conditions on the properties and behavior of wood cellulose nanocrystal suspensions [J]. Biomacromolecules, 6(2): 1048-1054.

[80] Elazzouzi-Hafraoui, S., Nishiyama, Y., Putaux, J. L., Heux, L., Dubreuil, F., & Rochas, C.

(2007). The shape and size distribution of crystalline nanoparticles prepared by acid hydrolysis of native cellulose [J]. Biomacromolecules, 9(1): 57-65.

[81] Jiang, F., Esker, A. R., & Roman, M. (2010). Acid-catalyzed and solvolytic desulfation of H2SO4-hydrolyzed cellulose nanocrystals [J]. Langmuir, 26(23): 17919-17925.

[82] Sadeghifar, H., Filpponen, I., Clarke, S. P., Brougham, D. F., & Argyropoulos, D. S. (2011). Production of cellulose nanocrystals using hydrobromic acid and click reactions on their surface [J]. Journal of materials science, 46(22): 7344-7355.

[83] Zuluaga, R., Putaux, J. L., Restrepo, A., Mondragon, I., & Gañán, P. (2007). Cellulose microfibrils from banana farming residues: isolation and characterization [J]. Cellulose, 14(6): 585-592.

[84] Bondeson, D., Mathew, A., & Oksman, K. (2006). Optimization of the isolation of nanocrystals from microcrystalline cellulose by acid hydrolysis [J]. Cellulose, 13(2): 171-180.

[85] Lu, P., & Hsieh, Y. L. (2012). Preparation and characterization of cellulose nanocrystals from rice straw [J]. Carbohydrate Polymers, 87(1): 564-573.

[86] Costa, L. M. M., de Olyveira, G. M., Cherian, B. M., Leão, A. L., de Souza, S. F., & Ferreira, M. (2013). Bionanocomposites from electrospun PVA / pineapple nanofibers / Stryphnodendron adstringens bark extract for medical applications [J]. Industrial Crops and Products, 41: 198-202.

[87] Silvério, H. A., Neto, W. P. F., Dantas, N. O., & Pasquini, D. (2013). Extraction and characterization of cellulose nanocrystals from corncob for application as reinforcing agent in nanocomposites [J]. Industrial Crops and Products, 44: 427-436.

[88] Pasquini, D., de Morais Teixeira, E., da Silva Curvelo, A. A., Belgacem, M. N., & Dufresne, A. (2010). Extraction of cellulose whiskers from cassava bagasse and their applications as reinforcing agent in natural rubber [J]. Industrial Crops and products, 32(3): 486-490.

[89] Dai, D., Fan, M., & Collins, P. (2013). Fabrication of nanocelluloses from hemp fibers and their application for the reinforcement of hemp fibers [J]. Industrial Crops and Products, 44: 192-199.

[90] Jonoobi, M., Mathew, A. P., & Oksman, K. (2012). Producing low-cost cellulose nanofiber from sludge as new source of raw materials [J]. Industrial Crops and Products, 40: 232-238.

[91] Abe, K., & Yano, H. (2010). Comparison of the characteristics of cellulose microfibril aggregates isolated from fiber and parenchyma cells of Moso bamboo (Phyllostachys pubescens [J]. Cellulose, 17(2): 271-277.

[92] Liu, H., Liu, D., Yao, F., & Wu, Q. (2010). Fabrication and properties of transparent polymethylmethacrylate/cellulose nanocrystals composites [J]. Bioresource Technology, 101(14): 5685-5692.

[93] Henriksson, M., Henriksson, G., Berglund, L. A., & Lindström, T. (2007). An environmentally friendly method for enzyme-assisted preparation of microfibrillated

cellulose (MFC) nanofibers [J]. European Polymer Journal, 43(8): 3434-3441.

[94] Frenot, A., Henriksson, M. W., & Walkenström, P. (2007). Electrospinning of cellulose‐based nanofibers [J]. Journal of applied polymer science, 103(3): 1473-1482.

[95] Chirayil, C. J., Joy, J., Mathew, L., Mozetic, M., Koetz, J., & Thomas, S. (2014). Isolation and characterization of cellulose nanofibrils from Helicteres isora plant [J]. Industrial Crops and Products, 59: 27-34.

[96] Chen, W., Yu, H., Liu, Y., Chen, P., Zhang, M., & Hai, Y. (2011). Individualization of cellulose nanofibers from wood using high-intensity ultrasonication combined with chemical pretreatments [J]. Carbohydrate Polymers, 83(4): 1804-1811.

[97] Chen, W., Yu, H., Liu, Y., Hai, Y., Zhang, M., & Chen, P. (2011). Isolation and characterization of cellulose nanofibers from four plant cellulose fibers using a chemical-ultrasonic process [J]. Cellulose, 18(2): 433-442.

[98] Alemdar, A., & Sain, M. (2008). Isolation and characterization of nanofibers from agricultural residues–Wheat straw and soy hulls [J]. Bioresource technology, 99(6): 1664-1671.

[99] Li, N., Chen, W., Chen, G., & Tian, J. (2017). Rapid shape memory TEMPO-oxidized cellulose nanofibers/polyacrylamide/gelatin hydrogels with enhanced mechanical strength [J]. Carbohydrate Polymers, 171: 77-84.

[100] Isogai, A., Saito, T., & Fukuzumi, H. (2011). TEMPO-oxidized cellulose nanofibers [J]. Nanoscale, 3(1): 71-85.

[101] Saito, T., Kimura, S., Nishiyama, Y., & Isogai, A. (2007). Cellulose nanofibers prepared by TEMPO-mediated oxidation of native cellulose [J]. Biomacromolecules, 8(8),：2485-2491.

[102] Soni, B., & Mahmoud, B. (2015). Chemical isolation and characterization of different cellulose nanofibers from cotton stalks [J]. Carbohydrate polymers, 134：581-589.

[103] Nechyporchuk, O., Belgacem, M. N., & Bras, J. (2016). Production of cellulose nanofibrils: a review of recent advances [J]. Industrial Crops and Products, 93：22-25.

[104] Bardet, R., & Bras, J. (2014). Cellulose nanofibers and their use in paper industry [J]. Handbook of green materials: bionanomaterials: separation processes, characterization and properties, 1：207-232.

[105] Chauve, G., & Bras, J. (2014). Industrial point of view of nanocellulose materials and their possible applications [M]. Handbook of Green Materials. World Scientific, 233-252.

[106] Pääkkö, M., Ankerfors, M., Kosonen, H., Nykänen, A., Ahola, S., Österberg, M., & Lindström, T. (2007). Enzymatic hydrolysis combined with mechanical shearing and high-pressure homogenization for nanoscale cellulose fibrils and strong gels. Biomacromolecules, 8(6), 1934-1941.

[107] Rabinovich, M. L., Melnick, M. S., & Bolobova, A. V. (2002). The structure and mechanism of action of cellulolytic enzymes [J]. Biochemistry (Moscow), 67(8): 850-871.

[108] Henrissat, B. (1991). A classification of glycosyl hydrolases based on amino acid

sequence similarities [J]. Biochemical Journal, 280(2): 309-316.

[109] Johansson, G., Ståhlberg, J., Lindeberg, G., Engström, Å., & Pettersson, G. (1989). Isolated fungal cellulose terminal domains and a synthetic minimum analogue bind to cellulose [J]. FEBS letters, 243(2): 389-393.

[110] Janardhnan, S., & Sain, M. M. (2007). Isolation of cellulose microfibrils–an enzymatic approach [J]. Bioresources, 1(2): 176-188.

[111] Hassan, M. L., Mathew, A. P., Hassan, E. A., & Oksman, K. (2010). Effect of pretreatment of bagasse pulp on properties of isolated nanofibers and nanopaper sheets [J]. Wood and Fiber Science, 42(3): 362-376.

[112] Henriksson, M., Berglund, L. A., Isaksson, P., Lindstrom, T., & Nishino, T. (2008). Cellulose nanopaper structures of high toughness [J]. Biomacromolecules, 9(6): 1579-1585.

[113] Siddiqui, N., Mills, R. H., Gardner, D. J., & Bousfield, D. (2011). Production and characterization of cellulose nanofibers from wood pulp [J]. Journal of Adhesion Science and Technology, 25(6-7): 709-721.

[114] Janardhnan, S., & Sain, M. (2011). Bio-treatment of natural fibers in isolation of cellulose nanofibres: Impact of pre-refining of fibers on bio-treatment efficiency and nanofiber yield [J]. Journal of Polymers and the Environment, 19(3): 615-621.

[115] Hassan, M. L., Bras, J., Hassan, E. A., Silard, C., & Mauret, E. (2014). Enzyme-assisted isolation of microfibrillated cellulose from date palm fruit stalks [J]. Industrial Crops and Products, 55: 102-108.

[116] Ooi S Y, Ahmad I, Amin M C I M. Cellulose nanocrystals extracted from rice husks as a reinforcing material in gelatin hydrogels for use in controlled drug delivery systems [J]. Industrial Crops & Products, 2015, 93:227-234.

[117] Nan L, Wei C, Chen G, et al. Rapid shape memory TEMPO-oxidized cellulose nanofibers / polyacrylamide / gelatin hydrogels with enhanced mechanical strength [J]. Carbohydrate Polymers, 2017, 171:77.

[118] Shelke N B, James R, Laurencin C T, et al. Polysaccharide biomaterials for drug delivery and regenerative engineering [J]. Polymers for Advanced Technologies, 2014, 25(5):448–460.

[119] Kumar A, Rao K M, Kwon S E, et al. Xanthan gum/bioactive silica glass hybrid scaffolds reinforced with cellulose nanocrystals: Morphological, mechanical and in vitro cytocompatibility study [J]. Materials Letters, 2017, 193: 274-278.

[120] Rao K M, Kumar A, Han S S. Polysaccharide based bionanocomposite hydrogels reinforced with cellulose nanocrystals: drug release and biocompatibility analyses [J]. International Journal of Biological Macromolecules, 2017.

[121] Zhou C, Wu Q, Lei T, et al. Adsorption kinetic and equilibrium studies for methylene blue dye by partially hydrolyzed polyacrylamide/cellulose nanocrystal nanocomposite hydrogels [J]. Chemical Engineering Journal, 2014, 251(251):17-24.

[122] Ooi S Y, Ahmad I, Amin M C I M. Cellulose nanocrystals extracted from rice husks as a

reinforcing material in gelatin hydrogels for use in controlled drug delivery systems [J]. Industrial Crops & Products, 2015, 93:227-234.

[123] Henschen J, Illergård J, Larsson P A, et al. Contact-active antibacterial aerogels from cellulose nanofibrils [J]. Colloids & Surfaces B Biointerfaces, 2016, 146:415.

[124] Fu J, Wang S, He C, et al. Facilitated fabrication of high strength silica aerogels using cellulose nanofibrils as scaffold [J]. Carbohydrate Polymers, 2016, 147:89-96.

[125] Helenius G, Bäckdahl H, Bodin A, et al. In vivo biocompatibility of bacterial cellulose [J]. Journal of Neuroscience the Official Journal of the Society for Neuroscience, 2006, 76(2):431-438.

[126] Jia B, Li Y, Yang B, et al. Effect of microcrystal cellulose and cellulose whisker on biocompatibility of cellulose-based electrospun scaffolds [J]. Cellulose, 2013, 20(4):1911-1923.]

[127] Rui M A D, Gomes M E, Rui L R. The Potential of Cellulose Nanocrystals in Tissue Engineering Strategies [J]. Biomacromolecules, 2014, 15(7):2327-46.

[128] Jorfi M, Foster E J. Recent advances in nanocellulose for biomedical applications [J]. Journal of Applied Polymer Science, 2015, 132(14):41719.

[129] Hagiwara Y, Putra A, Kakugo A, et al. Ligament-like tough double-network hydrogel based on bacterial cellulose [J]. Cellulose, 2010, 17(1):93-101.

[130] He X, Xiao Q, Lu C, et al. Uniaxially aligned electrospun all-cellulose nanocomposite nanofibers reinforced with cellulose nanocrystals: scaffold for tissue engineering [J]. Biomacromolecules, 2014, 15(2): 618-27.

[131] Zhang C, Salick M R, Cordie T M, et al. Incorporation of poly(ethylene glycol) grafted cellulose nanocrystals in poly(lactic acid) electrospun nanocomposite fibers as potential scaffolds for bone tissue engineering [J]. Materials Science & Engineering C Materials for Biological Applications, 2015, 49(39): 463.

[132] Domingues R M, Silva M, Gershovich P, et al. Development of Injectable Hyaluronic Acid/Cellulose Nanocrystals Bionanocomposite Hydrogels for Tissue Engineering Applications [J]. Bioconjugate Chemistry, 2015, 26(8): 1571.

[133] Bodin A, Ahrenstedt L, Fink H, et al. Modification of nanocellulose with a xyloglucan-RGD conjugate enhances adhesion and proliferation of endothelial cells: implications for tissue engineering [J]. Biomacromolecules, 2007, 8(12): 3697-704.

[134] Muller D, Silva J P, Rambo C R, et al. Neuronal cells' behavior on polypyrrole coated bacterial nanocellulose three-dimensional (3D) scaffolds [J]. Journal of Biomaterials Science Polymer Edition, 2013, 24(11): 1368-1377.

[135] Dugan J M, Gough J E, Eichhorn S J. Directing the morphology and differentiation of skeletal muscle cells using oriented cellulose nanowhiskers [J]. Biomacromolecules, 2010, 11(9): 2498.

[136] Berti F V, Rambo C R, Dias P F, et al. Nanofiber density determines endothelial cell behavior on hydrogel matrix [J]. Mater Sci Eng C Mater Biol Appl, 2013, 33(8): 4684-91.

[137] Mai I, Oaki Y, Tanaka Y, et al. Fabrication of nanocellulose–hydroxyapatite composites

and their application as water-resistant transparent coatings [J]. Journal of Materials Chemistry B, 2015, 3(28): 5858-5863.

[138] Svensson A, Nicklasson E, Harrah T, et al. Bacterial cellulose as a potential scaffold for tissue engineering of cartilage [J]. Biomaterials, 2005, 26(4):419-431.

[139] Luo H, Xiong G, Hu D, et al. Characterization of TEMPO-oxidized bacterial cellulose scaffolds for tissue engineering applications [J]. Materials Chemistry & Physics, 2013, 143(1):373-379.

[140] Naseri N, Mathew A P, Girandon L, et al. Porous electrospun nanocomposite mats based on chitosan–cellulose nanocrystals for wound dressing: effect of surface characteristics of nanocrystals [J]. Cellulose, 2015, 22(1):521-534.

[141] Silva N H, Rodrigues A F, Almeida I F, et al. Bacterial cellulose membranes as transdermal delivery systems for diclofenac: in vitro dissolution and permeation studies [J]. Carbohydrate Polymers, 2014, 106(1):264.

[142] Moritz S, Wiegand C, Wesarg F, et al. Active wound dressings based on bacterial nanocellulose as drug delivery system for octenidine [J]. International Journal of Pharmaceutics, 2014, 471(1-2):45.

[143] Amin M C I M, Abadi A G, Ahmad N, et al. Bacterial Cellulose Film Coating as Drug Delivery System: Physicochemical, Thermal and Drug Release Properties [J]. Sains Malaysiana, 2012, 41(5):561-568.

[144] Zhang X, Huang J, Chang P R, et al. Structure and properties of polysaccharide nanocrystal-doped supramolecular hydrogels based on Cyclodextrin inclusion [J]. Polymer, 2010, 51(19):4398-4407.

[145] Lin N, Huang J, Chang P R, et al. Effect of polysaccharide nanocrystals on structure, properties, and drug release kinetics of alginate-based microspheres [J]. Colloids & Surfaces B Biointerfaces, 2011, 85(2):270-9.

[146] Jackson J K, Letchford K, Wasserman B Z, et al. The use of nanocrystalline cellulose for the binding and controlled release of drugs [J]. International Journal of Nanomedicine, 2011, 6(6):321-330.

[147] Carlsson D O, Hua K, Forsgren J, et al. Aspirin degradation in surface-charged TEMPO-oxidized mesoporous crystalline nanocellulose [J]. International Journal of Pharmaceutics, 2014, 461(1-2):74-81.

[148] Akhlaghi, Parinaz S, Kam C, et al. Surface modification of cellulose nanocrystal with chitosan; oligosaccharide for drug delivery applications [J]. Cellulose, 2013, 20(4):1747-1764.

[149] Lin N, Dufresne A. Supramolecular hydrogels from in situ host-guest inclusion between chemically modified cellulose nanocrystals and cyclodextrin [J]. Biomacromolecules, 2013, 14(3):871-80.

[150] Dash R, Ragauskas A J. Synthesis of a novel cellulose nanowhisker-based drug delivery system [J]. Rsc Advances, 2012, 2(8): 3403-3409.

[151] Harris J P, Capadona J R, Miller R H, et al. Mechanically adaptive intracortical implants

improve the proximity of neuronal cell bodies [J]. Journal of Neural Engineering, 2011, 8(6): 066011.

[152] D. Li, F.Z. Zhu, J.Y. Li, P. Na, and N. Wang, Ind. Eng.Chem. Res., 52, 516 (2013).

[153] L.J. Maschio, P.H.F. Pereirab, and M.L.C.P. da Silva, Carbohydr. Polym., 89, 992 (2012).

[154] Z.H. Ma, Q. Li, Q.Y. Yue, B.Y. Gao, X. Xu, and Q.Q.Zhong, Bioresour. Technol., 102, 2853 (2011).

[155] Z.X. Liu, Y.G. Miao, Z.Y. Wang, and G.H. Yin, Carbohydr.Polym., 77, 131 (2009).

[156] F. Lionetto, A. Sannino, A. Maffezzoli, Polymer, 46, 1796(2005).

[157] Q. Li, Z.H. Ma, Q.Y. Yue, B.Y. Gao, W.H. Li, X. Xu, Carbohydr. Polym., 94, 539 (2013).

[158] Saito H, Sakurai A, Sakakibara M, et al. Preparation and properties of transparent cellulose hydrogels [J]. Journal of Applied Polymer Science, 2010, 90(11):3020-3025.

[159] Chang C, Zhang L. Cellulose-based hydrogels: Present status and application prospects [J]. Carbohydrate Polymers, 2011, 84(1):40-53.

[160] Burchard W. Solubility and Solution Structure of Cellulose Derivatives [J]. Cellulose, 2003, 10(3):213-225.

[161] Fekete T, Borsa J, Takács E, et al. Synthesis of cellulose-based superabsorbent hydrogels by high-energy irradiation in the presence of crosslinking agent [J]. Radiation Physics & Chemistry, 2016, 118:114-119.)

[162] Kobashima K. Application of superabsorbent polymers gels to oil-water separation (use of superabsorbent polymer containing sheet) - Gels Handbook - Section 4 [J]. Gels Handbook, 2001:381–392.

[163] Schlesinger M, Giese M, Blusch L K, et al. Chiral nematic cellulose-gold nanoparticle composites from mesoporous photonic cellulose [J]. Chemical Communications, 2015, 51(3):530-3.

[164] Qi H, Shopsowitz K E, Hamad W Y, et al. Chiral nematic assemblies of silver nanoparticles in mesoporous silica thin films [J]. Journal of the American Chemical Society, 2011, 133(11):3728.

[165] Schlesinger M, Giese M, Blusch L K, et al. Chiral nematic cellulose-gold nanoparticle composites from mesoporous photonic cellulose [J]. Chemical Communications, 2015, 51(3):530-3.

[166] Qi H, Shopsowitz K E, Hamad W Y, et al. Chiral nematic assemblies of silver nanoparticles in mesoporous silica thin films [J]. Journal of the American Chemical Society, 2011, 133(11):3728.

[167] Abitbol T, Rivkin A, Cao Y, et al. Nanocellulose, a tiny fiber with huge applications [J]. Current Opinion in Biotechnology, 2016, 39:76-88.

[168] Hemraz U D, Campbell K A, Burdick J S, et al. Cationic poly(2-aminoethylmethacrylate) and poly(N-(2-aminoethylmethacrylamide) modified cellulose nanocrystals: synthesis, characterization, and cytotoxicity [J]. Biomacromolecules, 2015, 16(1):319-25.

[169] Rosilo H, Mckee J R, Kontturi E, et al. Cationic polymer brush-modified cellulose nanocrystals for high-affinity virus binding [J]. Nanoscale, 2014, 6(20):11871-81.

[170] Tang J, Song Y, Tanvir S, et al. Polyrhodanine Coated Cellulose Nanocrystals: A Sustainable Antimicrobial Agent [J]. Acs Sustainable Chemistry & Engineering, 2015, 3(8):1801.

[171] Ago M, Okajima K, Jakes J E, et al. Lignin-based electrospun nanofibers reinforced with cellulose nanocrystals [J]. Biomacromolecules, 2012, 13(3):918

[172] Li M, Liu W, Sun J, et al. Culturing Primary Human Osteoblasts on Electrospun Poly (lactic-co-glycolic acid) and Poly (lactic-co-glycolic acid) / Nanohydroxyapatite Scaffolds for Bone Tissue Engineering [J]. Applied Materials & Interfaces, 2013, 5(13):5921.

[173] Xu H, Xie L, Chen Y H, et al. Strong Shear Flow-Driven Simultaneous Formation of Classic Shish-Kebab, Hybrid Shish-Kebab, and Transcrystallinity in Poly (lactic acid) / Natural Fiber Biocomposites [J]. Acs Sustainable Chemistry & Engineering, 2013, 1(12):1619-1629.

[174] Goffin A L, Raquez J M, Duquesne E, et al. From interfacial ring-opening polymerization to melt processing of cellulose nanowhisker-filled polylactide-based nanocomposites [J]. Biomacromolecules, 2011, 12(7):2456.

[175] Khoshkava V, Kamal M R. Effect of surface energy on dispersion and mechanical properties of polymer/nanocrystalline cellulose nanocomposites [J]. Journal of Surgical Oncology, 2013, 14(9):3155-63.

[176] Floros M, Hojabri L, Abraham E, et al. Enhancement of thermal stability, strength and extensibility of lipid-based polyurethanes with cellulose-based nanofibers [J]. Polymer Degradation & Stability, 2012, 97(10):1970-1978.]

[177] Abitbol T, Rivkin A, Cao Y, et al. Nanocellulose, a tiny fiber with huge applications [J]. Current Opinion in Biotechnology, 2016, 39:76-88.

[178] Dumanli A G, Kooij H M V D, Kamita G, et al. DigitalColor in Cellulose Nanocrystal Films [J]. Acs Applied Materials & Interfaces, 2014, 6(15):12302.

[179] Mu X, Gray D G. Formation of chiral nematic films from cellulose nanocrystal suspensions is a two-stage process [J]. Langmuir the Acs Journal of Surfaces & Colloids, 2014, 30(31):9256.

[180] Mu X, Gray D G. Droplets of cellulose nanocrystal suspensions on drying give iridescent 3-D "coffee-stain" rings [J]. Cellulose, 2015, 22(2):1103-1107.

[181] Shopsowitz K E, Qi H, Hamad W Y, et al. Free-standing mesoporous silica films with tunable chiral nematic structures [J]. Nature, 2010, 468(7322):422.

[182] Shopsowitz K E, Kelly J A, Hamad W Y, et al. Biopolymer Templated Glass with a Twist: Controlling the Chirality, Porosity, and Photonic Properties of Silica with Cellulose Nanocrystals [J]. Advanced Functional Materials, 2014, 24(3):327-338.

[183] Shopsowitz K E, Hamad W Y, Maclachlan M J. Flexible and iridescent chiral nematic mesoporous organosilica films [J]. Journal of the American Chemical Society, 2012, 134(2):867-870.

[184] Giese M, Blusch L K, Khan M K, et al. Responsive mesoporous photonic cellulose films by supramolecular cotemplating.[J]. Angewandte Chemie, 2014, 53(34):8880-8884.

[185] Shopsowitz K E, Stahl A, Hamad W Y, et al. Hard Templating of Nanocrystalline Titanium Dioxide with Chiral Nematic Ordering [J]. Angewandte Chemie, 2012, 124(28):6992–6996.

[186] Shopsowitz K E, Hamad W Y, Maclachlan M J. Chiral nematic mesoporous carbon derived from nanocrystalline cellulose [J]. Angewandte Chemie, 2011, 50(46):10991-5.

[187] Khan M K, Bsoul A, Walus K, et al. Photonic patterns printed in chiral nematic mesoporous resins [J]. Angewandte Chemie, 2015, 54(14):4304.

[188] Khan M K, Giese M, Yu M, et al. Flexible mesoporous photonic resins with tunable chiral nematic structures [J]. Angewandte Chemie, 2013, 52(34):8921-8924.

[189] Khan M K, Hamad W Y, Maclachlan M J. Tunable Mesoporous Bilayer Photonic Resins with Chiral Nematic Structures and Actuator Properties [J]. Advanced Materials, 2014, 26(15):2323-8.

[190] Li, Fei, Piergiovanni, et al. Multi-functional coating of cellulose nanocrystals for flexible; packaging applications [J]. Cellulose, 2013, 20(5):2491-2504.

[191] Dugan J M, Collins R F, Gough J E, et al. Oriented surfaces of adsorbed cellulose nanowhiskers promote skeletal muscle myogenesis [J]. Acta Biomaterialia, 2013, 9(1):4707.

[192] Csoka L, Hoeger I C, Rojas O J, et al. Piezoelectric Effect of Cellulose Nanocrystals Thin Films [J]. Acs Macro Letters, 2012, 1(1):867-870.

[193] Yang X, Cranston E D. Chemically Cross-Linked Cellulose Nanocrystal Aerogels with Shape Recovery and Superabsorbent Properties [J]. Chemistry of Materials, 2014, 26(20):6016-6025.

[194] Yang X, Shi K, Zhitomirsky I, et al. Cellulose Nanocrystal Aerogels as Universal 3D Lightweight Substrates for Supercapacitor Materials [J]. Advanced Materials, 2015, 27(40):6104-6109.

Chapter II Cellulose nanocrystalline isolation

Introduction to Chapter II

As summarized in *Chapter 1*, cellulose nanocrystalline (CNC) could be isolated form raw cellulose fibers with varying method. And these have been studied for decades. After our systematic review of the publications in the scientific literature over the last decades, however, we found there was no significant difference among the separation technique. High concentration of sulfuric acid hydrolysis was almost essential in each study of CNC isolation, whatever other techniques it combined with.

CNC are normally isolated from microcrystalline cellulose (MCC), which could be obtained from abundant natural resources, such as cotton, wood, straw, weed, industrial and agricultural waste. Similar to the passion of CNC isolation studies, plenty of researches have been intensely devoted to "How to obtain MCC from the raw materials" and "What the other materials could be used for MCC production". However, there is very limited research about the effect of MCC itself on the morphology, structure and properties of the resulting CNC.

Therefore, the diversity of MCC make it necessary to explore more considerations regarding the influence of different morphology, particle size and dispensability of MCC. In *Chapter II (Article 2）*, we isolated four kinds of CNCs from four commercial MCCs via sulfuric acid hydrolysis and examined their morphology and particle size. Transmission Electron Microscope (TEM), Atomic Force Microscopy (AFM), Fourier Transform Infrared (FTIR), X-Ray Diffraction (XRD) and Thermogravimetric Analysis (TG(A)) were employed to characterize and compare the shape, size distribution, structure, crystallinity and thermal stability of each resulting CNC.

Article 2 Effect of size and dispersity of microcrystalline celluloses on size, structure, and stability of nanocrystalline celluloses extracted by acid hydrolysis

QI LIU

National Engineering Laboratory for Crop Efficient Water Use and Disaster Mitigation, and Key Laboratory of Dryland Agriculture, Ministry of Agriculture, Institute of Environment and Sustainable Development in Agriculture, Chinese Academy of Agricultural Sciences, Beijing, 100081, P.R. China.
Department of Agriculture, Bio-engineering and Chemistry, University of Liege-Gembloux Agro-Bio Tech, 5030, Belgium.
liuqi@caas.cn

WEIPING HAO

National Engineering Laboratory for Crop Efficient Water Use and Disaster Mitigation, and Key Laboratory of Dryland Agriculture, Ministry of Agriculture, Institute of Environment and Sustainable Development in Agriculture, Chinese Academy of Agricultural Sciences, Beijing, 100081, P.R. China.
haoweiping@caas.cn

YONGGUANG YANG

Department of Cancer and Cell Biology, University of Cincinnati College of Medicine, Cincinnat, Ohio, 45267, U.S.A.
yangy9@ucmail.uc.edu

AURORE RICHEL

Unit of Biological and Industrial Chemistry, University of Liege-Gembloux Agro-Bio Tech, 5030, Belgium.
a.richel@ulg.ac.be

CANBIN OUYANG

Department of Pesticide, Key Laboratory of Pesticide Chemistry and Application, Institute of Plant Protection, Chinese Academy of Agricultural Sciences, Beijing, 100193, P.R. China.
oycb@iccas.ac.cn

HUAN LIU

School of music and recording arts, Communication University of China, Beijing, 100024, P.R. China.
Guor219@163.com

RUI GUO

National Engineering Laboratory for Crop Efficient Water Use and Disaster Mitigation, and Key Laboratory of Dryland Agriculture, Ministry of Agriculture, Institute of Environment and Sustainable Development in Agriculture, Chinese Academy of Agricultural Sciences, Beijing, 100081, P.R. China.
guorui@caas.cn

XU XIA

National Engineering Laboratory for Crop Efficient Water Use and Disaster Mitigation, and Key Laboratory of Dryland Agriculture, Ministry of Agriculture, Institute of Environment and Sustainable Development in Agriculture, Chinese Academy of Agricultural Sciences, Beijing, 100081, P.R. China.

xiaxu@caas.cn

JING YANG

Construction Engineering Test Center, Central Research Institute of Building and Construction, CO., LTD.
MCC Group, Beijing, China, 100088, P.R. China.
yj001010@126.com

JIQING SONG*

National Engineering Laboratory for Crop Efficient Water Use and Disaster Mitigation, and Key Laboratory of
Dryland Agriculture, Ministry of Agriculture, Institute of Environment and Sustainable Development in
Agriculture, Chinese Academy of Agricultural Sciences, Beijing, 100081, P.R. China.
songjiqing@caas.cn

DOROTHÉE GOFFIN*

Department of Agriculture, Bio-engineering and Chemistry, University of Liege-Gembloux Agro-Bio Tech, 5030,
Belgium.
dorothee.goffin@ulg.ac.be

Abstract: Nanocrystalline celluloses (CNCs) were separated from four commercial microcrystalline celluloses (MCCs) by an acid hydrolysis–sonication treatment. Transmission electron microscope, atomic force microscopy, Fourier transform infrared spectrum, X-ray diffraction, and thermogravimetric analysis were conducted to investigate the CNCs. MCCs with different morphologies and particle sizes showed different aggregation degrees. The aggregation of MCCs followed the order MCC1 > MCC3 > MCC2 > MCC4, which is the same order of the heights of the resulting CNCs. The best uniformity and thermal stability were characterized for CNC3, which was produced by MCC3 with smallest original particle size and good dispersity among the four MCCs. This result suggests that both the original particle size and dispersity of MCCs had significant effects on separated CNCs.

Keywords: Microcrystalline cellulose, Acid hydrolysis, Nanocrystalline celluloses

1. Introduction

Cellulose is an important biopolymer and the most ubiquitous and abundant natural biomacromolecule produced by plants and microorganisms worldwide[1]. Cellulose fibers possess highly advantageous properties, such as low cost, biodegradability, renewability, high specific strength and modulus, low density, easy processability, and relatively reactive surface for grafting specific groups[2]. This material is widely used because of its biocompatibility, biological degradability, and sustainability. Microcrystalline celluloses (MCCs) represent novel commercial cellulose and exist as a fine, white, odorless, crystalline powder, which has been used for years in different industries, including cosmetics, food, pharmaceuticals, and plastics[3]. Numerous researchers have reported on the preparation and characterization of MCC particles isolated from various cellulosic sources[4, 5, 6].

Producing composite materials with nanocrystalline cellulose (CNC) reinforcement has been recently attracting increasing attention because of the extraordinary properties of the nanometric size effect for reinforcement. Stable CNC suspensions have been known for more than half a century to be prepared by submitting native cellulose to a harsh sulfuric acid hydrolysis and often followed by ultrasound treatments[7]. CNCs prepared from different types of raw cellulose materials are characterized by methods, such as transmission electron microscope (TEM), atomic force microscopy (AFM), and scanning electron microscope (SEM)[8,9]. Particles are generally elongated and flat, a few hundreds of nanometers long, 10 nm to 20 nm wide, and a few nanometer thick[10,11]. Several studies about preparation and characterization of CNCs from MCCs also exist[12, 13]. Compared with cellulose nanocrystalline extracted from industrial bio-residue, those isolated from MCCs by acid hydrolysis show higher surface charge and crystallinity, as well as lower aggregation and degradation temperature[12]. The high crystallinity of these nanoscale celluloses makes these materials a suitable reinforcement for biocomposites. In addition, Bondeson *et al.*[13] reported that obtaining cellulose nanocrystals/whiskers with a length between 200 and 400 nm and a width less than 10 nm is possible with a sulfuric acid concentration of 63.5% (w/w). The effects of hydrolysis conditions and surface charge density[14], ionic strength[15], and pH[16] on the phase separation behavior and structures of the products have been studied over the past two decades.

Although numerous studies about the effect of hydrolysis conditions and properties of the resulting CNCs have been conducted, comparative studies about acid hydrolysis of MCCs with different morphologies, particle sizes, and dispersibilities are few. In this study, we submitted four commercial MCCs to sulfuric acid hydrolysis and examined their morphology and particle size. The shape and size distribution of the resulting CNCs were determined by TEM and AFM. Fourier transform infrared (FTIR) spectrum and X-ray diffraction (XRD) experiments were used to describe material structure and crystallinity. Thermogravimetric analysis (TGA) was conducted to determine thermal stability.

2. Materials and methods

2.1 Materials

The four commercial MCCs used in this work were purchased from Ruibio-bio Company (Germany), Sigma-Aldrich Company (USA), Aladdin Industrial Corporation (China), and Xiya Regent Research Center (China). All other reagents and chemicals were of analytical grade. All experiments were performed with ultrapure water.

2.2 Preparation of the CNCs

MCCs were hydrolyzed according to the method described by Revol *et al.*[17]. All four samples were treated with 64% sulfuric acid at a temperature of 50 °C in a Pro Thermo Shaker NTS-3100 (Rikakikai Co., Ltd, Tokyo, Japan) and a speed of 120 r/min for 40 min. MCC

content was 5 wt.%. The bottles with suspension were placed in cold water to quench the reactions. The hydrolyzed samples were washed by centrifugation at 15,000 rpm and 8 °C for 15 min with a Heraeus centrifuge (Heraeus Co., Ltd, Germany). Centrifugation was repeated five times before the suspension was dialyzed against ultrapure water for several days to neutrality. The molecular weight cut-off of the dialysis bag ranged from 8000 Da to 14000 Da. The resulting suspension was then sonicated for 10 min with a JY99-IIDN Ultrasonic Processor (Saifu Experimental Instrument Co., Ltd, Ningbo, China) at an output power of 1100 W to obtain the CNCs. The entire treatment process was performed in an ice bath.

A portion of each resulting suspension was then freeze-dried with an FD-1 freeze dryer at −50 °C (Boyikang Experimental Instrument Co., Ltd, Beijing, China) to obtain the CNC powder. The resulting products were then collected.

2.3 Characterization

2.3.1 Morphology of MCCs

The cellulose fibers were observed by SEM using a Hitachi S-4800 field emission scanning electron microscope (Hitachi High Technologies America, Inc., USA). The original MCC cellulose fibers were directly used. The samples were coated with gold by an ion sputter coater and were observed under SEM operating at 5 kV.

2.3.2 Laser particle size analysis of MCCs

The particle size distributions of all the MCC samples were analyzed using a Malvern Mastersizer 2000 laser-diffraction particle size analyzer (Malvern Instruments Ltd., UK) with Malvern Mastersizer 2000 software. The samples were first measured directly in the original state of aggregation to obtain the mean volume diameter of the aggregated particle size. The primary particle size of the MCCs was achieved by sonication for 10 s. Aggregation degrees were calculated from the ratio of the aggregated particle size to the primary particle size.

2.3.3 Morphology and size of CNCs

The morphology of the fibers was characterized with both TEM and AFM.
2.3.3.1 TEM
Drops of 0.001 wt.% CNC suspensions were deposited on carbon-coated TEM grids. The samples were then negatively stained with 2% uranyl acetate prior to complete drying and observed under a JEM-1200EX transmission electron microscope (JEOL Ltd., Tokyo, Japan) operating at 80 kV. Images were recorded.
2.3.3.2 AFM
To accurately characterize surface topography and microfibril structure, we obtained surface imaging and particle height distribution using a Mutimode 8 atomic force microscope (Bruker Daltonics Inc., USA). Drops of dilute cellulose CNC suspensions were deposited onto freshly cleaved mica and allowed to dry. AFM observations were carried out operating in nitrogen

condition and using a ScanAsyst mode. ScanAsyst is based on the Bruker-exclusive PeakForce Tapping mode. Tapping mode is speculated to be more suitable than contact mode for imaging polymer surfaces because the AFM tip intermittently contacts the surface, leading to minimized destructive lateral forces that can produce surface artifacts. Therefore, all AFM images were recorded in tapping mode[19].

2.3.4 FTIR spectroscopy

FTIR spectroscopy was used to examine any change in the structure of the cellulose fibers after nanocrystallization treatment. A Thermo Scientific Nicolet iN10 (Thermo Electron Corp., USA) was employed to record the FTIR spectra of each sample. The dried samples were ground and then blended with KBr before pressing the mixture into ultrathin pellets. Spectral outputs were recorded in the transmittance mode as a function of wave number.

2.3.5 Powder XRD

Crystallinities of the MCC and CNC fibers were examined using a Bruker D8 Focus (Bruker AXS Inc., Madison, WI, USA) equipped with a high-power point focus Cu Kα target, graphite monochromator for elimination of Cu kβ lines, and a Hi-Star General Area Diffraction Detection System area detector for 2D images. High-resolution frames for accurate integration of the diffraction images were recorded. Scattered radiation was detected in the range of $2\theta = 10°$ to $30°$ at a scan rate of $4°/min$.

Crystallinity index (CI) was calculated from the heights of the 200 peaks (I_{200}, $2\theta = 22.6°$) and the intensity minimum between the 200 and 110 peaks (I_{am}, $2\theta = 18°$) with the Segal's method[20], as shown in Eq. (1). I_{200} represents both crystalline and amorphous material, whereas I_{am} represents the amorphous material.

$$C_I(\%) = \left(1 - \frac{I_{am}}{I_{200}}\right) \times 100 \tag{1}$$

2.3.6 Thermal analysis

TGA was performed to compare the degradation characteristics of MCCs with those of CNCs. The thermal stability of each sample was determined using a TGA/DSC 1 thermogravimetric analyzer (Mettler Toledo Corporation, Schwarzenbach, Switzerland) and analyzed by STAR software (Version 9.3). Runs were performed by weighing out 1 mg to 4 mg sample in a 70 μL aluminum cup. The cup was crimped, and a hole was pierced automatically by the instrument just prior to the analysis. The analysis was performed with a constant flux of 40 mL/ min of nitrogen to ensure that the change in weight is due to thermal degradation. The temperature of the sample was ramped at a constant rate of 10 °C/min, and weight loss or heat evolved was measured against increasing temperature.

3. Results and Discussion

3.1 Morphology of MCCs

The morphology of fiber or particle materials is usually observed by SEM[21, 22, 23]. The MCC particles were investigated with SEM to determine their shape, size, and surface morphology. Fig. 3 is a comparison of the SEM images of each MCC prior to hydrolysis. The micrographs show the different shapes of the four MCCs. Figure. 3(a) shows that MCC1 are ribbon-like in structure and are composed of long cellulose microfibrils. The microfibrils, which measured about 15 μm to 25 μm wide and 30 μm to 200 μm long, maintain the basic shape of cotton fiber. Figure. 3(b) indicates that the particles of MCC2 are non-uniformly sized at about 10 μm to 100 μm. Figure. 3(c) shows that MCC3 are more uniform and composed of smaller particles with diameters between 10 and 50 μm. Fig. 3(d) indicates that the cellulose particles of MCC4 are larger than those of MCC3 and smaller than those of MCC2. The MCCs show diverse shape and size, but these micro-sized cellulose fibers were reported to be composed of strong hydrogen bonding nanofibers[24], which enable isolation of nanoscale cellulose fibers from the MCCs.
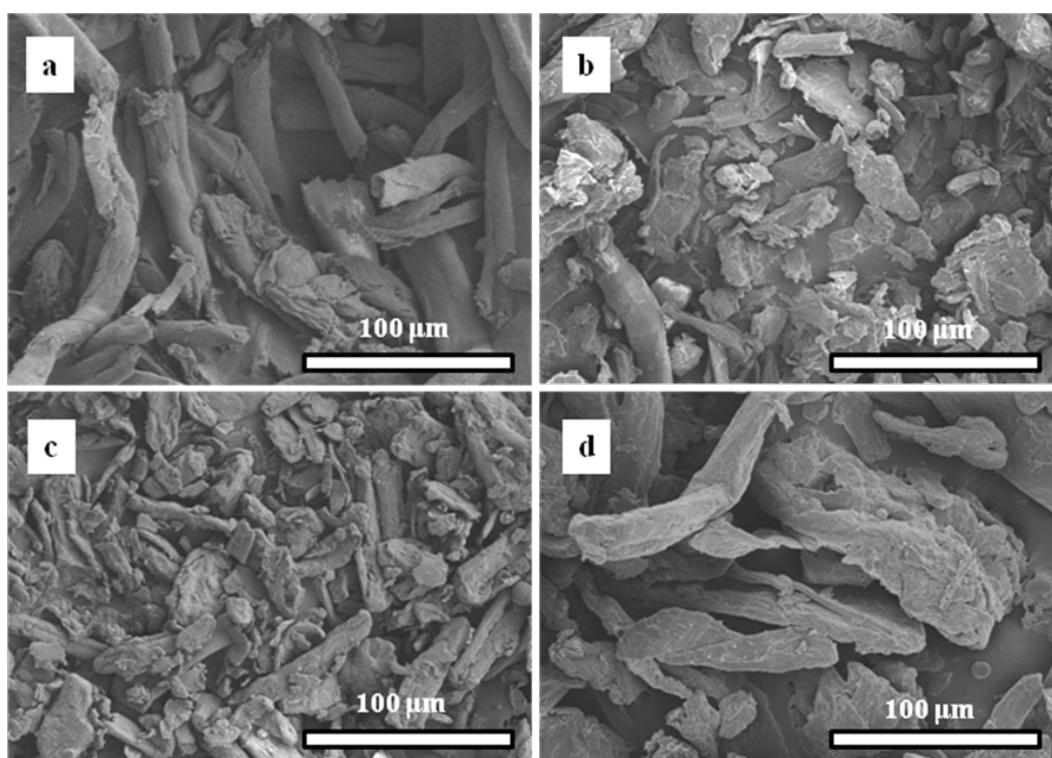
Figure 3. SEM micrographs of the MCCs: (a) MCC1, (b) MCC2, (c) MCC3, and (d) MCC4.

3.2 Laser particle size analysis

The size distribution of MCCs was investigated through comparing the mean volume diameter before and after sonication. The test results for each sample and the calculated aggregation degree are given in Table 4. Sonication of the original MCC samples for 10 s resulted in a significant reduction in particle size distribution of the MCC sample, especially for MCC1. The different MCCs had different aggregation degrees, which followed the order MCC1 > MCC3 > MCC2 > MCC4 as listed in Table 4. The strong aggregation showed by MCC1 may cause

incomplete reaction during hydrolysis when preparing CNCs. However, MCC4 exhibited similar particle size before and after the sonication treatment. This result may be beneficial for sulfuric acid to access the cellulose molecule because MCCs were used to prepare CNCs without any treatment.

Table 1 Particle size and aggregation degree of MCCs

	Mean volume diameter (μm)		Aggregation degree
	Before sonication	After sonication	
MCC1	190.1±0.22	40.0±0.14	4.75
MCC2	49.4±0.06	33.5±0.67	1.47
MCC3	56.4±0.09	29.9±0.06	1.89
MCC4	54.6±0.04	50.2±0.12	1.09
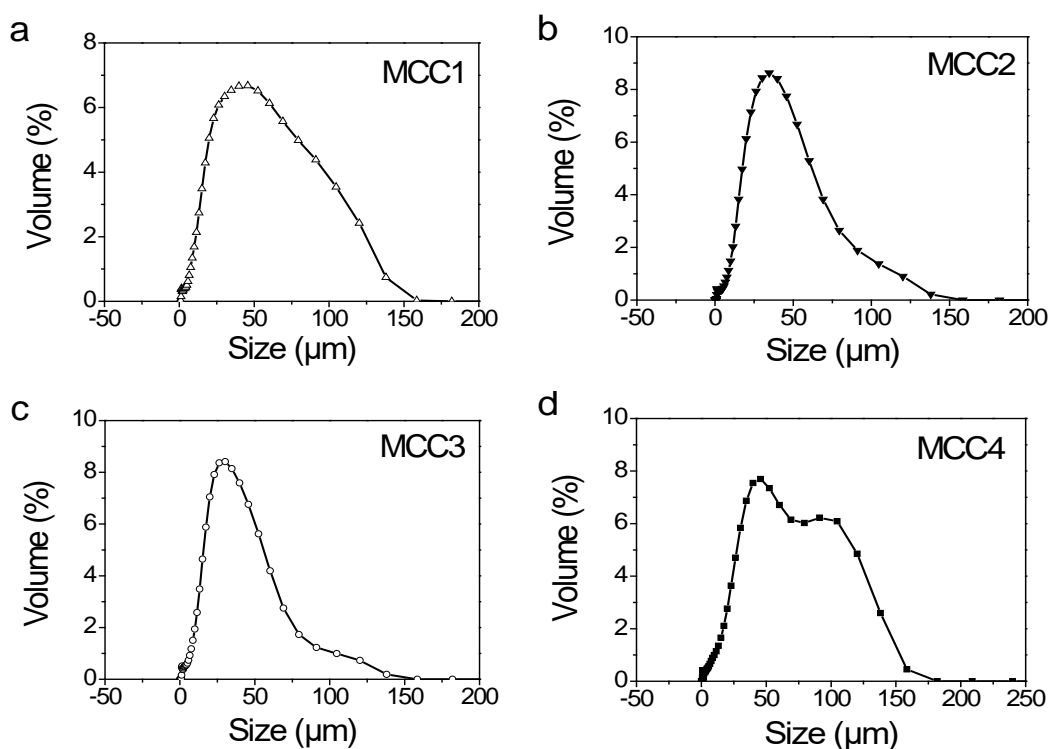
Figure 4 Particle size distribution of the MCCs: (a) MCC1, (b) MCC2, (c) MCC3, and (d) MCC4.

Figure 4 presents the particle size distributions of the four MCCs. The size distribution of the samples after sonication showed that the mean volume diameters were 40.0, 33.5, 29.9, and 50.2 μm, which is in accordance with the results shown in SEM micrographs. As shown in Figure 4 (b) and (c), MCC2 and MCC3 showed a main simple peak with a slight tail. However, the original particle distributions of MCC1 and MCC4 shown in Figure 4 (a) and (d) present two or even more peaks. For MCC1, this result was mainly caused by the high aggregation degree of the original particles. MCC4 showed two main peaks at around 35 and 100 μm, which may be due to the raw material species or the preparation technology.

3.3 Morphology and size of CNCs

3.3.1 TEM

Figure 5 shows TEM micrographs of all nanoparticles prepared by sulfuric acid hydrolysis of the four commercial MCCs. The nanoscale particles isolated from MCCs all present an elongated rod shape. The CNCs were approximately 100 nm to 250 nm long and 10 nm to 30 nm wide. CNC4 showed the thinnest width at around 10 nm, whereas the other three all ranged from 20 nm to 25 nm. An evident whisker fraction was observed in Figure 5(b), which is possibly caused by localized damage created during the process of sonication treatment. Elazzouzi-Hafraoui et al.[18] also found this phenomenon in their study of acid hydrolysis of tunicin whiskers. Each image of the samples clearly revealed by negative staining that most particles were composed of several parallel elongated rods. Given the significant electrostatic repulsion because of the negative charge of sulfate groups present on the nanocrystal surface after sulfuric acid hydrolysis[18], this association was attributed to an artificial aggregation during staining and/or drying of the specimens. Among the four micrographs of the CNCs, CNC4 agglomerated to form larger particles in the micron range compared with CNC1, CNC2, and CNC3. This result presents evidence that thinner particles are easier to assemble together.
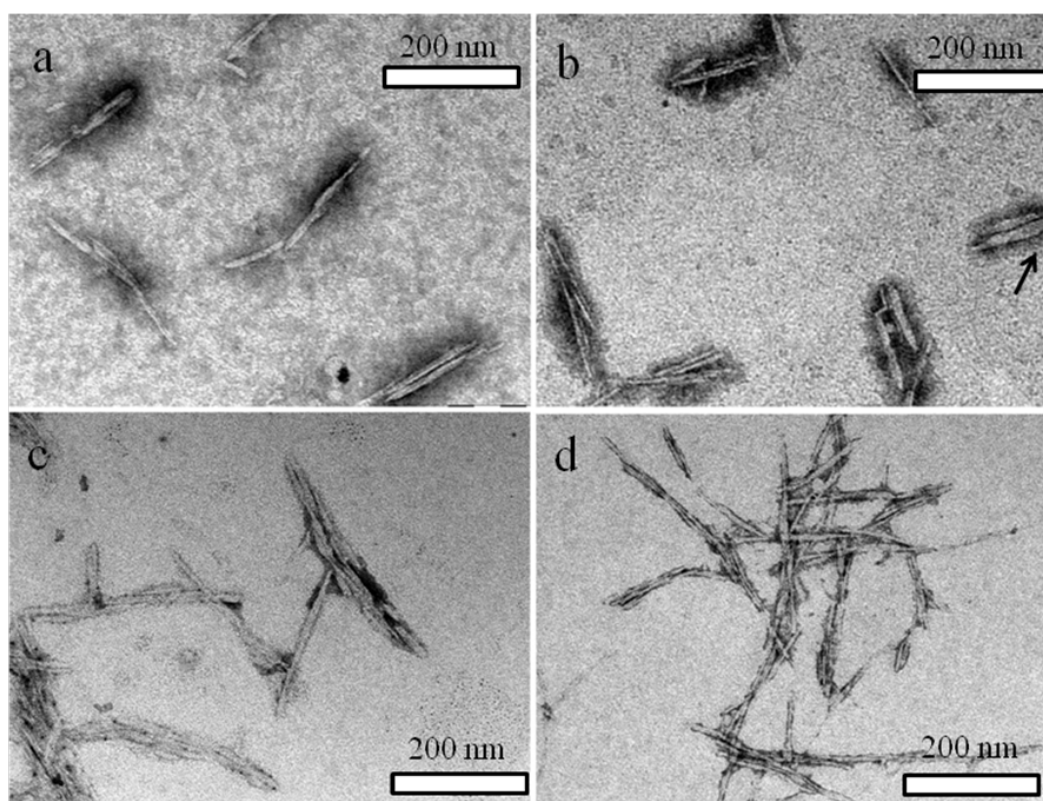
Figure 5. TEM micrographs of the CNCs separated from the MCCs: (a) CNC1, (b) CNC2, (c) CNC3, and (d) CNC4.

3.3.2 AFM

Several recent reports have discussed the morphology and crystal structure of nanocrystalline

cellulose using AFM. Elazzouzi-Hafraoui et al.[18] used AFM to study the cellulose surface and determine the nanoparticle thickness by topography measurements of cellulose particles isolated from cotton and tunicin. Images generated in this study using AFM illustrated the morphology and height distribution of CNCs isolated from the four MCCs. The four left-hand images are height images that represent surface topography, and the right-hand images show the particle height from the section analysis in the height image. The height images of Figure 6 show AFM images from CNC1 to CNC4 particles deposited onto freshly cleaved mica surfaces. Despite sonication of the suspensions performed before spreading on mica, some aggregation was observed on certain parts of the surface. Statistical analysis of the section in terms of height distribution could lead to inconclusive results, which are most probably due to particle superimposition during drying[18]. The height images showed that the particle height distribution from the section analysis was calculated with a number of better-isolated particles. The height peaks of CNC1 to CNC4 were about 25.8, 19.6, 23.7, and 11.5 nm, respectively. CNC3 showed the highest peak among the four images, indicating that this sample had the most uniform particle size distribution. The height images of CNCs showed that height could typically range from 10 nm to 30 nm, which is consistent with the results shown in TEM images. The order of particle height of CNCs resulted in the following trend: CNC1 > CNC3 > CNC2 > CNC4, which is consistent with the order of aggregation degree of MCCs instead of the original particle size. This result indicates that MCCs with lower aggregation degrees tend to produce narrower CNC particles during acid hydrolysis.
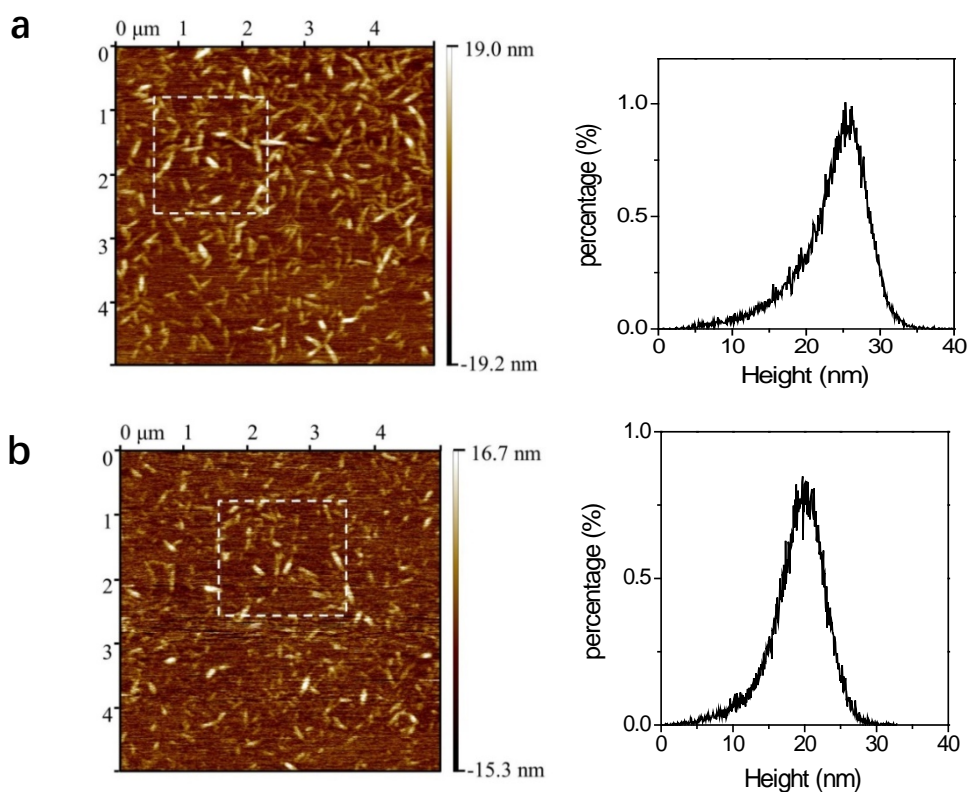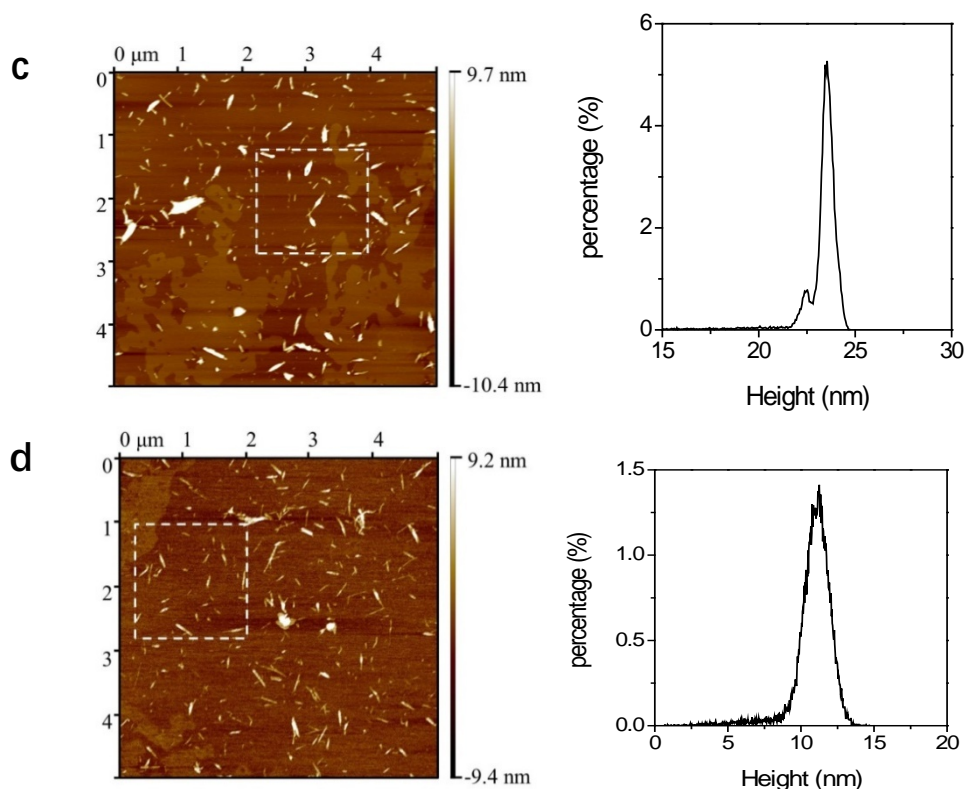
Figure 6. AFM images and particle height distribution of CNCs: (a) CNC1, (b) CNC2, (c) CNC3, and (d) CNC4.

3.4 FTIR spectra

The structure change of the polymer materials are generally determined by FTIR technology [25, 26]. The four MCCs and the corresponding CNCs were analyzed using FTIR to determine the various chemical changes present during hydrolysis. The FTIR spectrum of each sample is shown in Figure 7 The FTIR spectra of the four MCCs and the corresponding CNCs were highly similar to each other. The band at 1640 cm^{-1} was assigned to the absorbed water. The spectra of the samples were dominated by the peaks at 3430 to 3478 and 1059 cm^{-1}, reflecting the stretching vibrations of O—H and C—O, respectively. The bands at 1061 and 897 cm^{-1} are associated with C—O stretching and C—H deformation of glucose rings[8]. The absorption peaks at 1642, 1429, 1376, 1163, and 1038 cm^{-1} are normalized with regard to the cellulose peak at 897 cm^{-1} [27]. The peaks at around 3400 cm^{-1} in the spectra represent hydroxy stretching. The similar intensity of the aforementioned cellulose peaks in both of MCCs and CNCs indicated that the basic structure did not change during nanocrystallization. However, certain imperceptible changes could be observed by comparing the spectra of each MCC and CNC. Amorphous regions are "dissolved" by acid attack, and the absorption peak at 897 cm^{-1} of glucose rings decreased slightly in the CNC spectra. The shape change of the stretching peak that represents the hydroxy group was also found in the FTIR spectra. The peaks of O—H at 3430 cm^{-1} to 3478 cm^{-1} in the spectra of four MCCs were wider and bigger than those of

CNCs. After acid hydrolysis, the bands shifted to a higher frequency area, indicating the decrease of hydrogen bond during this treatment process.
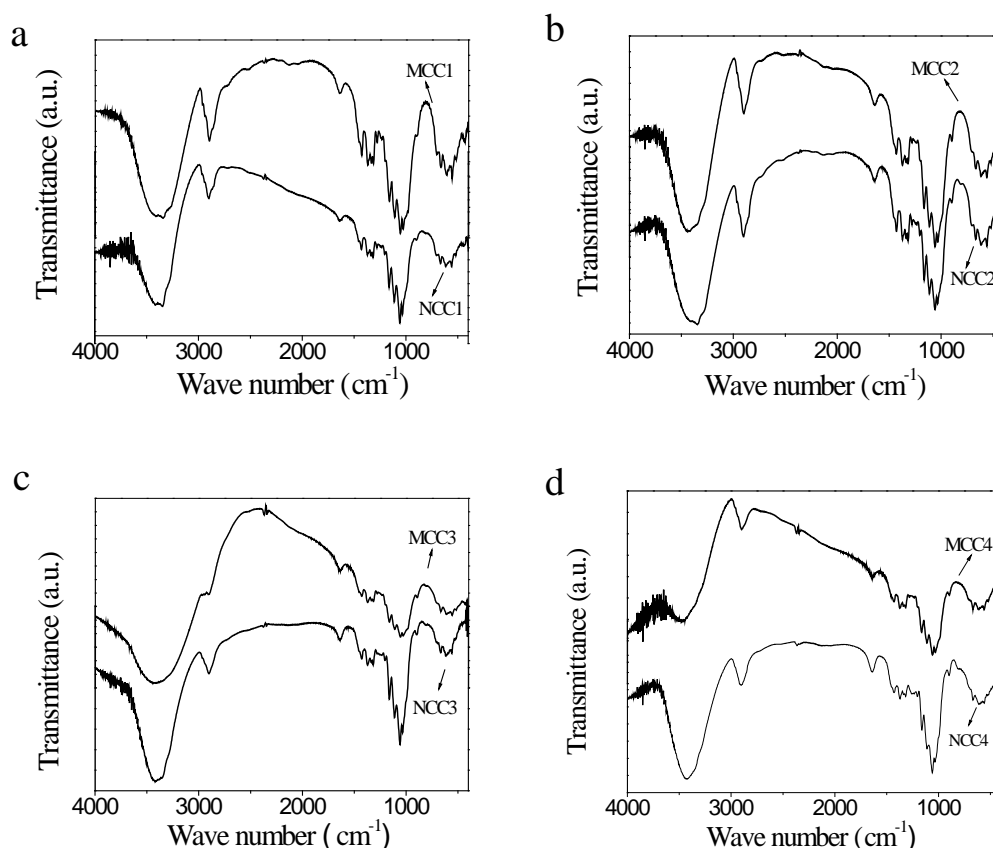
Figure 7 FTIR spectra of MCCs and CNCs: (a) MCC1 and CNC1, (b) MCC2 and CNC2, (c) MCC3 and CNC3, and (d) MCC4 and CNC4.

3.5 X-ray analysis

XRD studies of the MCC and CNC fibers were performed to investigate the crystalline feature of each cellulose sample. Figure 8 and Table 5 show the XRD patterns and the crystallinity of each MCC and CNC sample. Five diffraction rings or arcs, namely, ($1\bar{1}0$), (110), (102/012), (200), and (040), were recognized in all samples. These rings or arcs are characteristics of cellulose I that are based on the monoclinic indexation by Sugiyama *et al.*[28] All patterns of the CNC samples showed peaks around $2\theta = 16.5°$ and $22.5°$, which were speculated to represent the typical cellulose I structure[29], thus indicating that the crystal properties were not altered during hydrolysis. The crystallinities in the original four MCC fibers were 85.3%, 78.4%, 75.8%, and 76.9%. However, an evident decrease in crystallinity was observed in the CNC patterns. This reduction of crystallinity was caused by the high concentration of sulfuric acid during nanocrystallization. The breakdown of the cellulose chains, as well as their entanglement and agglomeration, has been proven to be significantly dependent on the acid concentration used[30]. The crystallinities of CNCs reduced by 18.5%, 17.2%, 68.7%, and 37.6%,

respectively, compared with those of relevant MCCs. The MCC3 sample was destroyed most seriously, which may be because the smallest original particles of the sample provide the highest superficial area for sulfuric attack.
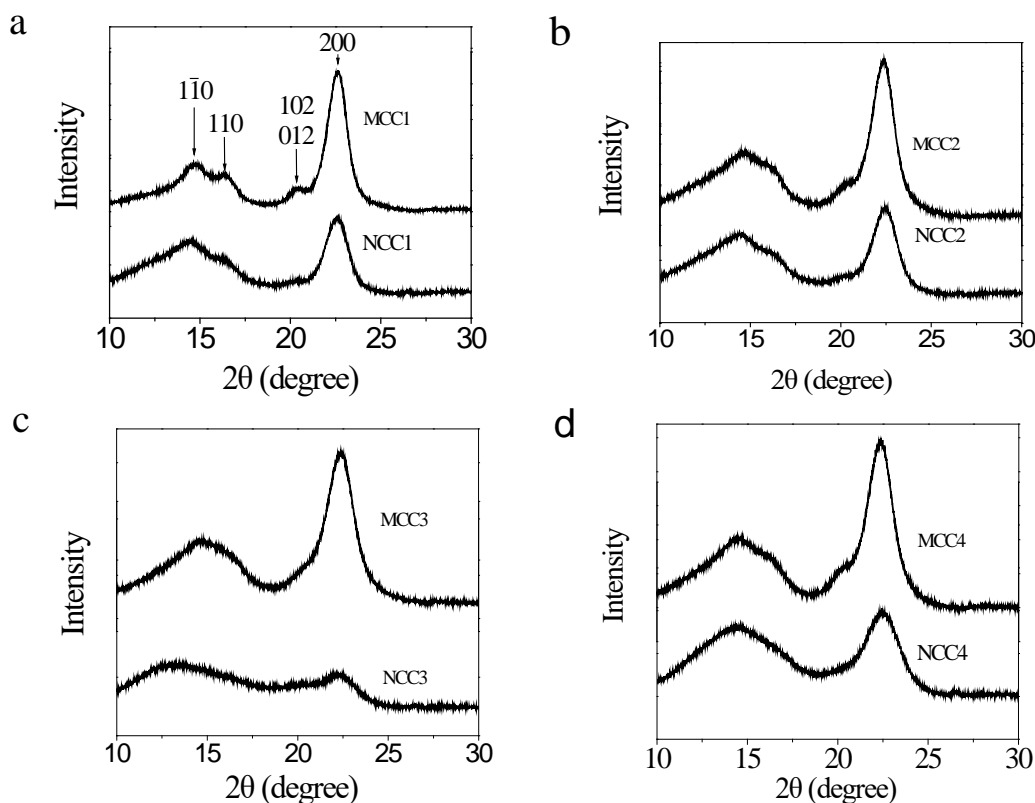
Figure 8. XRD pattern of MCCs and CNCs: (a) MCC1 and CNC1, (b) MCC2 and CNC2, (c) MCC3 and CNC3, and (d) MCC4 and CNC4.

Table 4. Crystallinities of the MCCs and CNCs

	Relative crystallinity (%)			
	1	2	3	4
MCCs	85.3	78.4	75.8	76.9
CNCs	69.5	64.9	23.7	48.0
Reduced percentage (%)	18.5	17.2	68.7	37.6

3.6 TGA

Although the thermal properties could be studied through computational and theoretical chemistry [31, 32], TGA is widely used to test the thermal stability. Investigation on the thermal properties of the fibers is important to estimate their applicability for biocomposite processing, in which the processing temperature for thermoplastic polymers rises above 200 °C[8]. Figure 9 shows the TGA curves of all MCCs and CNCs. All TGA curves showed an initial small drop between 50 °C and 150 °C, which corresponded to a mass loss of approximately 5% absorbed moisture. The dominant decomposition peak of MCCs, which was observed at around 330 °C, accounted for the pyrolysis of cellulose. In contrast to the MCC samples, we observed that the

four CNCs all exhibited two stages of degradation. These results clearly illustrate that the thermal stability of the fibers decreased after hydrolysis and sonication treatments. Sonication treatment had slight effect on the thermal decomposition of nanofibers[33]; thus, the decrease in thermal stability was caused by the severe condition of sulfuric acid hydrolysis. Hydrolysis of fibers by H_2SO_4 is a heterogeneous reaction[34]. This reaction is influenced by reaction conditions, such as acid concentration, temperature, time, and mechanical agitation, as well as the physical state of the cellulose. Among all these factors, acid concentration is one of the key parameters that determine the resulting nature of the fibers[35]. The results are highly consistent with those obtained from FTIR and XRD measurements. Compared with the other three CNCs, CNC3 showed the highest degradation temperature, which was approximately 230 °C. The high thermal properties of CNC3 may broaden the fields of application of cellulose fibers, especially at temperatures higher than 200 °C for biocomposites processing.
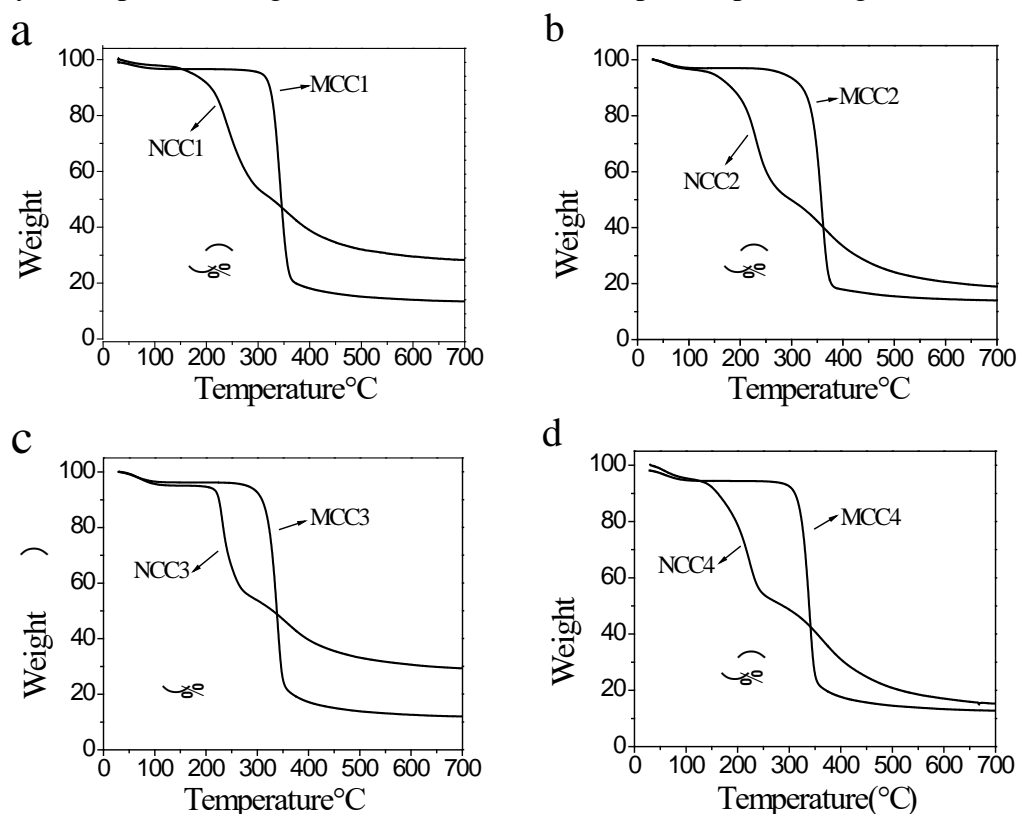
Figure 9. TGA curves of MCCs and CNCs: (a) MCC1 and CNC1, (b) MCC2 and CNC2, (c) MCC3 and CNC3, and (d) MCC4 and CNC4.

4. Conclusion

CNCs were separated from four commercial MCCs by sulfuric acid hydrolysis and then sonicated. The morphology and particle size of MCCs were characterized through SEM and laser particle size analyzer. The results showed different shapes and sizes, and the aggregation degree followed the order MCC1 > MCC3 > MCC2 > MCC4. The resulting CNCs were composed of elongated rods with 100 nm to 250 nm in length and 10 nm to 30 nm in width. The same order of CNC height as the aggregation degree of MCCs indicates that MCCs with

lower aggregation degree tend to produce narrower CNC particles during acid hydrolysis process, which were easier to assemble together. Besides the morphology and particle size of CNCs characterized by TEM and AFM, the molecular structure, crystallinity, and thermal properties of the nano-sized particles were also investigated. The FTIR and XRD results showed that the basic structure and crystal properties of MCCs did not change during the preparation process. However, the harsh hydrolysis condition reduced their crystallinity and decreased the thermal stability to varying degrees. MCC3, which presented the lowest original particle size and good dispersity, produced the most uniform and thermally stable CNC. This result suggests that both particle size and dispersity are key parameters that influence the separation of CNCs.

Acknowledgments

References

1. M. Deng, Q. Zhou, A. Du *et al.*, *Mater. Lett.* **63**, 1851 (2009).
2. E. M. Teixeira, D. Pasquini , A. A. S. Curvelo *et al.*, *Carbohydr. Polym.* **78**, 422 (2009).
3. K. Das, D. Ray, N. R. Bandyopadhyay *et al.*, *Cellulose* **16**, 783 (2009).
4. T. Virtanen, K. Svedström, S.Andersson *et al.*, *Cellulose* **19**, 219 (2012).
5. M. S. Jahan, A. Saeed, Z. He *et al.*, *Cellulose* **18**, 451 (2011).
6. R. L. de Oliveira, H. da Silva Barud, R. M. de Assunção *et al.*, *J. Therm. Anal. Calorim.* **106**, 703 (2011).
7. F. F. Morehead, *Text. Res. J.* **20**, 549 (1950).
8. A. Alemdar and M. Sain, *Bioresour. Technol.* **99**,1664 (2008).
9. W. Chen, H. Yu, Y. Liu *et al.*, *Cellulose* **18**, 433 (2011).
10. R. H. Marchessault, F. F. MMorehead and M. J. Koch, *J. Colloid. Sci.* **16**, 327 (1961).
11. S. M. Mukherjee and H. J. Woods, *Biochim. Biophys. Acta* **10**, 499 (1953).
12. M. A. Herrera, A. P. Mathew and K. Oksman, *Mater. Lett.* **71**, 28 (2012).
13. D. Bondeson, A. Mathew and K. Oksman, *Cellulose* **13**,171 (2006).
14. X. M. Dong, J. F. Revol and G. D. Gray, *Cellulose* **5**, 19 (1998).
15. J. Araki and S. Kuga, *Langmuir* **17**, 4493 (2001).
16. E. Belamie, P. Davidson and M. M. Giraud-Guille, *J. Phys. Chem. B* **108**, 14991 (2004).
17. J. F. Revol, H. Bradford, J. Giasson *et al.*, *Int. J. Biol. Macromol.* **14**, 170 (1992).
18. S. Elazzouzi-Hafraoui, Y. Nishiyama, J. L. Putaux *et al.*, *Biomacromolecules* **9**, 57 (2007).
19. D. Bhattacharya, L. T. Germinario and W. T.Winter, *Carbohydr. Polym.* **73**, 371 (2008).
20. L. G. J. M. A. Segal, J. J. Creely, A. E. Martin *et al.*, *Text. Res. J.* **29**, 786 (1959).

21. X. Chen, K. Ding and N. Ayres, *Polym. Chem.* **2**, 2635 (2011).

22. X. Chen and N. Ayres, *Macromolecules*, **43***, 1341 (2010).

23. X. Chen and N. Ayres, *J. Polym. Sci., Part A: Polym. Chem.* **49**, 3030 (2011).

24. K. Abe and H. Yano, *Cellulose* **17**, 271 (2010).

25. Y. Huang, L. Taylor, X. Chen, et al., *J. Polym. Sci., Part A: Polym. Chem.* **51**, 5230 (2013).

26. L. Taylor, X. Chen and N. Ayres, *Polym. Int.* **63**, 127 (2014).

27. M. F. Rosa, E. S. Medeiros, J. A. Malmonge *et al.*, *Carbohydr. Polym.* **81**, 83 (2010).

28. J. Sugiyama, R. Vuong and H. Chanzy, *Macromolecules* **24**, 4168 (1991).

29. Y. Nishiyama, P. Langan and H. Chanzy, *J. Am. Chem. Soc.* **124**, 9074 (2002).

30. K. Das, D. Ray, N. R. Bandyopadhyay *et al.*, *Cellulose* **16**, 783 (2009).

31. G. W. Wang, X. P. Chen, and X. Cheng, *Chem.- Eur. J.* **12**, 7246 (2006).

32. P. Wu, X. Chen, J. Li, et al., *Comput. Theor. Chem.* **1030**, 67 (2014).

33. D. Klemm, B. Philipp, T. Heinze et al., *Comprehensive Cellulose Chemistry, Vol. 1: Fundamentals and Analytical Methods* (Wiley-VCH publication, Weinheim, 1998)

34. Q. Xiang, Y. Y. Lee , P. O. Pettersson *et al.*, *Appl. Biochem. Biotechnol.* **105**, 505 (2003).

35. M. A. Saïd Azizi Samir, F. Alloin, M. Paillet *et al.*, *Macromolecules* **37**, 4313 (2004).

Chapter III Cellulose and cellulose nanofiber isolation from wheat straw.
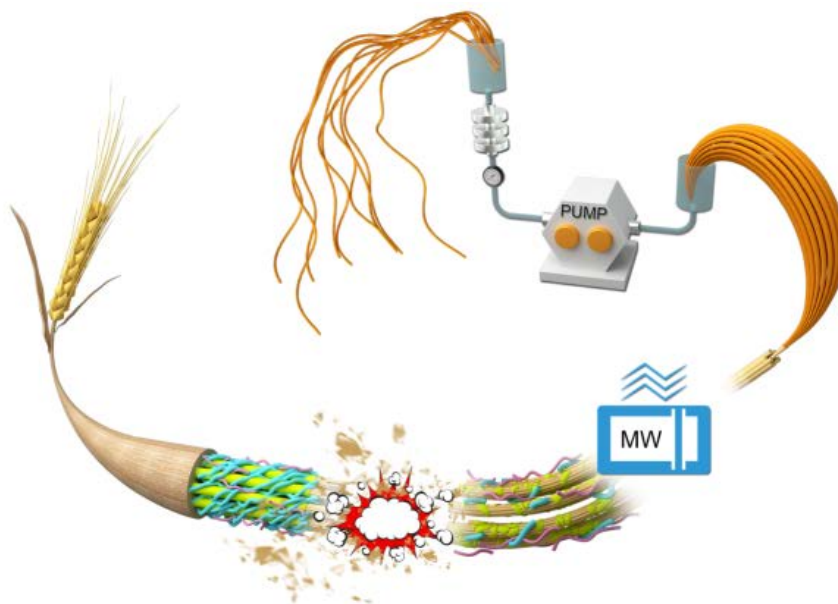
Introduction to Chapter III

We have discussed about the CNC isolation in *Chapter II (Article 2)* focusing on the effect of MCC itself on the morphology, structure and properties of the resulting CNC. Compared with the research history of CNC isolation, CNF isolation was not so long as that. However, more various kinds of techniques about "How to obtain CNF from the cellulose and natural materials" appeared, from chemical treatment to physical ways. Most of these isolations combined two or more methods, which firstly abstract the cellulose from the raw materials and then treat them into CNF. Like the paper pulping process, cellulose isolation from the raw fibers has a significant impact on the environment because of abundant chemicals used in the manufacture. Therefore, it's very important to search for a more "green" way to isolate cellulose for the environmental purpose.

Microwave (MW) technique is widely used in chemistry. In organic reaction, compared with conventional method, microwave irradiation has some advantages such as quick velocity, simply operation, less outgrowth, high purity, clean process and saving energy. As summarized in the *Chapter I (Article 2)*, there were several studies on MW-assisted isolation of cellulose. However, few works have systemically studied cellulose isolation from natural biomass via MW-assisted alkali treatment. The non-thermal effect of MW on the resulting fibers has also been rarely investigated, which could well reveal the catalytic mechanism of it. Therefore, *Article 3* focused on revealing the effects of reaction temperature, reaction time, and alkali concentration on cellulose purity and lignin removal. The non-thermal effect, catalytic mechanism, of the microwave to cellulose isolation reactions were also discussed.

The next research work based on the main target of using as less chemical as possible during the CNF isolation process, meanwhile to obtain CNF with high purity. In *Article 4*, CNF were isolated from wheat straw through an environmentally friendly, multi-step treatment process that combined steam explosion, microwave-assisted hydrolysis, and microfluidization. The chemical analysis and characterization were carried out to study the effect of each treatment step, as well as to investigate the potential utilization of the CNFs in nanocomposites. This work presented an environmentally friendly method yielded CNFs with high purity from agricultural waste.

Article 3 Microwave-assisted alkali hydrolysis for cellulose isolation from wheat straw: influence of reaction conditions and non-thermal effects of microwave

Qi Liu[†,‡,§], Mario Aguedo[§], Yun Lu[ǁ], Canbin Ouyang[⊥], Wenqing He[†], Changrong Yan[†], Xu Xia[†], Rui Guo[†], Aurore Richel*[,§], Jiqing Song*[,†], Dorothée Goffin*[,‡,§]

[†]National Engineering Laboratory for Crop Efficient Water Use and Disaster Mitigation, Key Laboratory of Dryland Agriculture, Ministry of Agriculture and Key Laboratory for Prevention and Control of Residual Pollution in Agricultural Film, Ministry of Agriculture, Institute of Environment and Sustainable Development in Agriculture, Chinese Academy of Agricultural Sciences, No.12 Zhongguancun South Street, Beijing 100081, China
[‡]TERRA Research Center and Laboratory of Gastronomical Science, Gembloux Agro-Bio Tech-University of Liège, Passage des Déportés 2B-5030 Gembloux, Belgium
[§]Unit of Biomass and Green Technologies, Gembloux Agro-Bio Tech-University of Liège, Passage des Déportés 2B-5030 Gembloux, Belgium
[ǁ]Research Institute of Wood Industry, Chinese Academy of Forestry, No.1 Dongxiaofu, Xiangshan Road, Beijing 100091, China
[⊥]Department of Pesticides, Institute of Plant Protection, Chinese Academy of Agricultural Sciences, Ministry of Agriculture, and State Key Laboratory for Biology of Plant Diseases and Insect Pests, No.2 Yuanmingyuan West Road, Beijing 100193, China

Abstract: The influences of reaction conditions and the non-thermal effects of microwave on cellulose isolation from wheat straw in microwave-assisted alkali hydrolysis process were investigated. Fiber contents, Klason lignin and individual neutral sugars were determined to reveal the components change with various reaction conditions. Temperature exerted the most positive effect on cellulose isolation. At 140 °C, about 90.66% cellulose remained in the processed fibers. Characterizations including scanning electron microscopy, atomic force microscopy, Fourier transform infrared spectroscopy, X-ray diffraction, and thermogravimetric analysis were employed to analyze the morphology, surface roughness, structure, crystallinity, and thermal stability of the raw and treated fibers. Results showed that fibers with higher cellulose content, smoother surfaces, higher crystallinity and improved thermal stability were obtained after microwave assisted alkali hydrolysis. Characterization comparison between treatments with and without microwave revealed that the cementing materials, including hemicelluloses, lignin, and pectin, around the fiber bundles dissolved more readily with than without microwave treatment, which confirming the non-thermal effect of microwave on improving the cellulose isolation efficiency. Microwave can save abundant reaction time or chemical use in this isolation process. This efficient, environment-friendly microwave treatment is believed to possess broad application prospects in the field of biomass treatment.

Key words: Wheat straw; Cellulose isolation; Microwave-assisted hydrolysis; Reaction conditions; Non-thermal effect

1. Introduction

Cellulose is the most abundant, clean, and renewable resource in the world and is found in various plants.[1–3] High proportions of cellulose are obtained from agricultural residues.[4] China produces large amounts of agricultural residues especially from straw. In 1.35×106 hm^2 farmlands, crops, such as wheat, maize, and rice, can generate more than 7×10^8 tons of straw each year. Proper management of straw waste remains challenging. Burning of straw is the simplest and fastest method used by farmers. However, this method produces not only environmental pollutants, such as smog,[5] but also wastes, such as cellulose resources. Indeed, cellulose materials are widely used in different fields, such as in manufacturing, agriculture, medicine, food, and environmental protection.[6] These are due to its features of biodegradability, non-toxicity, excellent mechanical properties,[7, 8] adsorption performances,[9] ultra-light properties,[10] and easy functionalization.[11, 12] Therefore, reasonable utilization of straw will yield economic benefits and prevent environmental pollution.

Cellulose can be separated through physical, chemical, physicochemical, and biological methods.[13, 14] Chemical treatments or pretreatments (PTs) include acid or alkaline pulping, solvents, ozone treatment, or peroxide bleaching. Hydrolysis using acids or alkalis is a popular method for separating cellulose because of its high yield, high purity, and ease of handling. For example, Sun et al. found the optimal condition for wheat straw (WS) degradation comprised the hydrolysis using 1.5% NaOH for 144 hours at 20 °C; the process released 60% and 80% lignin and hemicellulose, respectively. [15] Using high alkali concentration and temperature can increase the cellulose purity and shorten the reaction period. Sánchez et al. obtained 91.8% and 60.7% cellulose contents through Kraft process (170 °C, 16% alkalinity, 25% sulfidity, 40 min) and soda process (100 °C, 7% NaOH, 150 min), respectively.[16] Brodeur et al. reported that treatment with 0.2%–2.5% acids after alkali treatment can remove most hemicellulose and lignin to produce relatively pure cellulose.[17] Alemdar and Sain performed a chemical treatment involving the successive addition of 17.5% w/w NaOH, 1 M HCl, and 2% w/w NaOH solution to obtain 84.6% pure cellulose from WS.[18] Accordingly, fiber treatment requires high alkali concentrations, which may add considerable stress to the environment. Therefore, chemical treatment for isolating cellulose must be improved.

Microwave (MW) is an effective assistive technology used in chemical synthesis and chemical reactions, such as organic synthesis, solid-state chemistry, nanotechnology, and nanomaterial synthesis.[19–22] By directly converting electromagnetic energy into heat at the molecular level, MW can reduce the energy consumption and shorten the reaction time compared with conventional heating.[23, 24] MW can also help synthesize N-heterocycles and heating in aqueous medium for C–C coupling reactions.[25–28] Sathvika et al. reported that baker's yeast (*Saccharomyces cerevisiae*) immobilized in glutaraldehyde cross-linked cellulose could be a novel and green adsorbent for removing toxic Cr(VI) with MW assistance.[29] Lu et al. observed that MW can increase the temperature to 55 °C–75 °C from room temperature within 2 min; the synergistic effect between MW and ultrasonic wave could reduce the reaction temperature, acidity, and time, thereby enhancing the acid hydrolysis of cellulose.[30] MW can also be used to improve the reaction conditions and increase the yield of alkali hydrolysis of plants. Zhu et al.

examined the effects of MW PT on the alkali hydrolysis of rice straw. Results showed that MW shortened the treatment time, increased the hydrolysis rate, and removed larger amounts of lignin and hemicellulose compared with alkali-only PT.[31, 32] Hu and Wen found that MW elevated the sugar yield from switchgrass with respect to that in conventional heating; the optimal alkali concentration was 0.1 g/g, which lead to the highest sugar yield of 0.05–0.3 g alkali/g biomass. Moreover, MW technology is also employed in biomass treatment.[33] Chowdhury and Hamid pretreated jute stalk powder with sodium hydroxide under MW irradiation to remove lignin and prepare crude cellulose.[34] Long et al. isolated lignin from softwood by high-temperature microwave treatment at 160−210 °C for 10 min with dilute sulfuric acid.[35] In our previous research, we found that MW could enhance the isolation of cellulose from natural biomass materials by removing lignin from the fibers with less alkali and a shorter duration.[36]

Despite there were several studies on MW-assisted isolation of cellulose from WS, only few works have systemically studied cellulose isolation from natural biomass via MW-assisted alkali treatment. The non-thermal effect of MW on the resulting fibers has also been rarely investigated. Therefore, the present investigation focused on revealing the effects of reaction temperature, reaction time, and alkali concentration on cellulose purity and lignin removal. Various characterization methods, including scanning electron microscopy (SEM), atomic force microscopy (AFM), Fourier transform infrared (FTIR) spectroscopy, X-ray diffraction (XRD), and thermogravimetric analysis (TGA), were conducted to analyze the morphology, structure, crystallinity, and thermal stability of the fibers. The effects of the reaction conditions of MW-assisted hydrolysis and the non-thermal effect of MW during treatment were also elucidated.

2. Experimental section

2.1 Materials. Wheat straw (WS) was obtained from the Huantai experimental fields in Shandong Province, China. The straw was air dried after collection and milled into powder of <1 mm size. The sodium hydroxide and concentrated hydrochloric acid used were analytically pure and supplied by Sigma–Aldrich Co. Ltd. Distilled water was employed in all experiments.

2.2 Pretreatment (PT) of WS

Dried and milled WS powder was combined with 1 M HCl under stirring at 80 ± 1 °C for 2 h. Next, the mixture was washed with distilled water until neutral pH. The pretreated WS (PT-WS) was obtained after lyophilizing through a Labconco freeze-dry system (Freezone 4.5; Labconco Corporation, Kansas City, USA).

2.3 MW-assisted alkali hydrolysis

MW-assisted alkali hydrolysis was conducted using a Start Synth microwave digestion system (Milestone Srl, Sorisole, Italy). For all the MW treatments, 1.5 g dry weight of each fiber was mixed with 30 mL each of various NaOH concentrations (C_{NaOH} = 1%, 2%, 3%, 4%, 5%) in a 50-mL sealed vessel.[36, 37] The mixtures were then continuously stirred under homogeneous

heating during reaction. The temperature rose to the target value within 3 min and maintained for another few minutes. A changeable power (maximum of 1200 W) and a temperature monitor were used to achieve precise temperatures. The reactions were stopped by placing the vessels in the ice water. Then, distilled water was used to wash the samples filtrate reached pH 7. The obtained treated fiber slurries were stored at 4 °C for later use.

To determine the effect of the MW, we treated PT-WS in the same 50 mL sealed vessel with 3% NaOH at 100 °C for 20 min but without MW. Raw WS fibers without PT were also exposed to MW at 100 °C for 20 min along with 3% NaOH to ascertain the influence of the PT. All the samples and corresponding treatments are listed in Table 1.

2.4 Chemical composition analysis of WS

Whole chemical compositions were determined using different methods. All the data were expressed as percent dry weight. Water content was determined by continuous heating at 105 °C overnight. The fiber contents were analyzed on the basis of the Van Soest method.[38, 39] The total nitrogen (TN) content was determined using the Kjeldahl method.[40, 41] The protein contents were calculated from TN × 6.25. The fat content was determined by extracting with chloroform/methanol (2/1, v/v) and then 0.58% NaCl. The ash content was obtained by heating to 525 °C for 2 h and maintaining the temperature for 3 h in a muffle furnace. The starch content was determined from 100 mg samples through the α-amylase method by using the Megazyme Total Starch Assay Kit (Megazyme Ltd, Bray, Ireland).

2.5 Fiber determination

The cellulose, hemicellulose, lignin, and ash contents were obtained through the Van Soest method.[38, 39] Meanwhile, the amount of neutral detergent fiber (NDF), which was the insoluble portion of a neutral detergent solution, was determined via the Van Soest gravimetric method.[38] Acid detergent fiber (ADF) refers to the fraction of insoluble components in the acid detergent solution, whereas acid detergent lignin (ADL) is the weight of the acid detergent lignin residue regarded as the lignin content. These parameters were also determined using the Van Soest gravimetric method.[39] The cellulose content was computed as the difference between ADF and ADL values, whereas the hemicellulose content was determined by subtracting the ADF amount from the NDF amount. The cellulose, hemicellulose, and lignin contents were calculated from NDF, ADF, and ADL as shown below:

$$\text{Hemicellulose} = \text{NDF} - \text{ADF} \tag{1}$$

$$\text{Cellulose} = \text{ADF} - \text{ADL} \tag{2}$$

$$\text{Lignin} = \text{ADL} \tag{3}$$

To thoroughly elucidate the effect on lignin removal, the amounts of soluble and insoluble lignin were determined with the Klason method.[42, 43] Through this method, soluble and insoluble lignin was separated by depolymerizing cellulose and hemicellulose in 72% sulfuric acid at 30 °C for 60 min, followed by hydrolyzing dissolved polysaccharides with boiling 4% sulfuric acid in an autoclave (121 °C) for 60 min. The soluble lignin was then obtained by UV spectroscopy (at 205 nm), and the insoluble lignin was determined as the difference in weight

of the residue before and after ashing at 450 °C for 6 h.

2.6 Sugar determination

From each fiber, individual neutral sugars were released by acid hydrolysis, and the corresponding contents were determined by gas chromatography as described by Blakeney et al.[44] To release the cellulosic sugar, samples were initially treated with 72% H_2SO_4 for 1 h at 30 °C. Then, we adjusted the acid concentration to 1 M and maintained the temperature at 100 °C for 3 h. Next, the sugar content was measured by a Hewlett-Packard HP6890 gas chromatograph (Agilent, Palo Alto, CA, USA) equipped with a flame ionization detector and a high-performance capillary column HP1-methylsiloxane (30 cm × 320 μm, 0.25 μm, Scientific Glass Engineering, SGE Pty. Ltd., Melbourne, Australia). 2-Deoxyglucose (internal standard), glucose, xylose, arabinose, mannose, and galactose solutions (Sigma–Aldrich, St. Louis, USA), were used as standards. The measurements were conducted at least twice, and the data were examined using ChemHP software.

2.7 Characterization of the fibers

The following six typical fibers were characterized with SEM, FTIR, XRD, and TG: WS, PT-WS, T100-t20-3% (fibers obtained after MW treatment with 3% NaOH at 100 °C for 20 min), T140-t20-3% (fibers obtained after MW treatment with 3% NaOH at 140 °C for 20 min), (T100-t20-3%)$_{NO-MW}$ (fibers obtained without MW with 3% NaOH at 100 °C for 20 min) and (T100-t20-3%)$_{NO-PT}$ (fibers obtained after MW treatment with 3% NaOH but without PT at 100 °C for 20 min).

Fiber morphology was then visualized by SEM (Hitachi S-4800, Hitachi High Technologies America, Inc., USA). The samples were coated with gold by an ion sputter coater and observed under SEM at 15 kV.

FTIR spectroscopy was adopted to examine changes in fiber structure among the treatments. The spectrum of each sample was then recorded with a Thermo Scientific Nicolet iN10 (Thermo Electron Corp., USA). Fibers were ground and blended with KBr. Afterward, the mixture was pressed into thin, transparent pellets. The FTIR spectrum of each sample was obtained at 4000–400 cm^{-1} with a resolution of 4 cm^{-1}.

The fiber XRD patterns were attained using a Bruker AXS D8 Focus (Bruker AXS Inc., Madison, WI, USA) equipped with a high-power point focus Cu–kα target, a graphite monochromator to eliminate Cu–kβ lines, and a Hi-Star General Area Diffraction Detection System area detector for 2D images. High-resolution frames were recorded to accurately integrate the diffraction images. Scattered radiation was sensed at $2\theta = 10°–40°$ at a scan rate of 4°/min.

The crystallinity index (C_I) was calculated from the height of the 200 peak (I_{200}, $2\theta = 21.7°$), as well as the minimum intensity between the 200 and 110 peaks (I_{am}, $2\theta = 18°$), in accordance with Segal's method (Eq. 4):[45]

$$C_I(\%) = \left(1 - \frac{I_{am}}{I_{200}}\right) \times 100 \qquad (4)$$

Where I_{200} represents both crystalline and amorphous material and I_{am} represents the

amorphous material.

Thermal analysis was conducted to compare the degradation characteristics and thermal behavior of the fibers. Samples were examined by a TGA/DSC 1 thermogravimetric analyzer (Mettler Toledo Corporation, Switzerland). Then, the samples were heated from room temperature to 700 °C under a nitrogen atmosphere at a heating rate of 10 °C/min.

To obtain the dimensions and homogeneity of WS and treated fibers, WS and T140-t20-3% were characterized by AFM. AFM was performed with a Bruker Multimode 8 (Bruker Corporation, Billerica, MA, USA) AFM in tapping mode with constant oscillation frequency. The images were scanned in tapping mode and in air via silicon cantilevers at a scan rate of 1 Hz.

3. Result and discussion

3.1 Chemical composition of the WS

The chemical composition, including the contents of cellulose, hemicellulos, lignin, water, protein, fat, ash, and starch, was calculated and displayed in Figure 10. The 44.8% ± 0.7% cellulose content was the highest proportion in the composition and indicated the abundant cellulose resource in the raw materials. However, the 33.1% ± 0.8% hemicellulose and 8.46% ± 0.31% lignin contents, as well as the contents of the other non-cellulosic components, also suggested the need and challenge in the cellulose isolation processes.
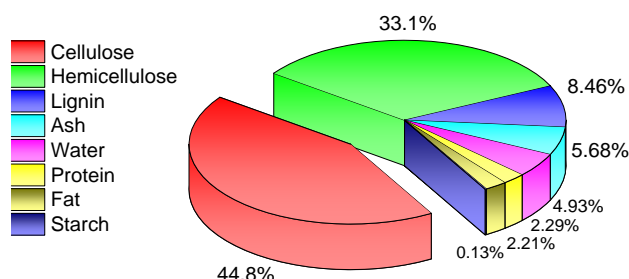
Figure 10. Chemical composition of the wheat straw (WS)

3.2 Process treatments and fiber yield

All the treatments and the corresponding fiber and cellulose yields are listed in Table 6. The PT-WS achieved a fiber yield of 44.13% and a cellulose yield of 65.92%. Three treatment groups with various reaction temperatures, durations, and C_{NaOH} were adopted. The treatments that involved MW-assisted hydrolysis for 20 min in 3% NaOH at various temperatures were named as T60-t20-3%, T80-t20-3%, T100-t20-3%, T120-t20-3%, and T140-t20-3%. In these treatments, the fiber and cellulose yields decreased with rising temperature. Meanwhile, the treatments hydrolyzed with MW at 100 °C in 3% NaOH for varying reaction times were designated as T100-t5-3%, T100-t10-3%, T100-t20-3%, T100-t40-3%, and T100-t80-3%. In this group, reaction time negatively correlated with the two yields. Finally, the treatments hydrolyzed with MW at 100 °C for 20 min in assorted C_{NaOH} solutions were assigned as T100-t20-1%, T100-t20-2%, T100-t20-3%, T100-t20-4%, and T100-t20-5%. In these treatments, the fiber and cellulose yields exhibited a declining trend. To thoroughly illuminate

the effect of MW, a treatment with the same conditions as those of T100-t20-3% but without MW was carried out and designated as (T100-t20-3%)$_{NO-MW}$, which showed similar yields to that of T100-t20-3%. Meanwhile, to demonstrate the influence of the PT, we obtained a sample from the WS treated with the same conditions as those of T100-t20-3% but without PT. The yields were of the highest among all treated fiber.

Table 5. Treatments and yields.

| Samples | Treatments | | | | | Yields of fibers (%) | Yields of cellulose (%) |
| | PT[a] | Hydrolysis Conditions | | | MW[b] | | |
		Temperature (°C)	Time (min)	C_{NaOH} (%)			
WS	—	—	—	—	—	—	—
PT-WS	+	—	—	—	—	44.13±1.15	65.92±1.71
T60-t20-3%	+	60	20	3	+	37.67±1.24	60.13±1.98
T80-t20-3%	+	80	20	3	+	35.11±0.02	58.66±0.03
T100-t20-3%	+	100	20	3	+	29.46±1.07	52.08±1.90
T120-t20-3%	+	120	20	3	+	23.32±0.51	43.96±0.96
T140-t20-3%	+	140	20	3	+	20.09±0.20	40.64±0.41
T100-t5-3%	+	100	5	3	+	34.10±0.13	55.89±0.21
T100-t10-3%	+	100	10	3	+	32.48±0.11	55.67±0.19
T100-t40-3%	+	100	40	3	+	27.35±0.90	48.93±1.62
T100-t80-3%	+	100	80	3	+	25.52±0.64	45.84±1.15
T100-t20-1%	+	140	20	1	+	33.79±0.48	55.53±0.79
T100-t20-2%	+	100	20	2	+	30.08±0.49	51.34±0.84
T100-t20-4%	+	100	20	4	+	29.40±0.81	53.30±1.48
T100-t20-5%	+	100	20	5	+	29.04±0.45	53.11±0.83
(T100-t20-3%)$_{NO-MW}$	+	100	20	3	−	29.83±0.39	48.31±0.63
(T100-t20-3%)$_{NO-PT}$	−	100	20	3	+	52.61±0.60	68.34±0.78

PT [a]: Pretreatment
MW [b]: MW treatment
+: positive (with treatment)
−: negative (without treatment)

3.3 Effects of treatments on fiber contents

NDF, ADF, and ADL were determined, and the three main fibers were calculated. The results of the NDF, ADF, and ADL of all the fibers are listed in Table S1 (Supporting Information). Meanwhile, the fiber content calculations are shown in Figure 11. The raw fiber contained the highest percentage of hemicellulose and lignin contents (Figure 11a). After acid hydrolysis PT, the hemicellulose content diminished drastically, whereas the cellulose content rose. Hence, during the acid hydrolysis, the hemicellulose fraction was mainly hydrolyzed. The cellulose content further increased after MW-assisted alkali hydrolysis. The 58.21% cellulose achieved in (T100-t20-3%)$_{NO-MW}$ was much lower that of T100-t20-3% and revealed the promotive effect of MW on the hydrolysis. Meanwhile, in (T100-t20-3%)$_{NO-PT}$, only limited cellulose and lignin was removed from the raw materials. Thus, acid hydrolysis PT not only removed most of the hemicellulose but also helped the chemicals access the peripheral portion of the fibers' cellulose. Figure 11b–d reveal that the fiber contents changed in the processed fibers with varying temperature, reaction duration, and alkali concentration. The fibers' cellulose content obviously increased with rising reaction temperature (Figure 11b). Moreover, up to 90.66% cellulose was obtained in the resulting fibers at 140 °C. Meanwhile, the hemicellulose and

lignin contents in T140-t20-3% reached as low as 6.76% and 3.82%, respectively. However, reaction time and alkali concentration did not considerably influence the isolation reaction. With prolonging reaction time, the cellulose content in the obtained fibers rose quickly within the first 20 min. When the duration lasted for 20 min, the cellulose content reached 79.22%. No change in the components of the resultant fiber was noted thereafter. A similar variation trend in fiber content with alkali concentration was recorded. In Figure 11d, the cellulose content increased, whereas the hemicellulose and lignin contents diminished with rising C_{NaOH}. However, when $C_{NaOH} > 3\%$, the cellulose content did not change considerably. Therefore, the temperature played a greater role in cellulose isolation than those of the other two factors. In terms of time and energy conservation or a green viewpoint, reaction with 3% NaOH for 20 min achieved sufficient results. Furthermore, the cellulose content in $(T100-t20-3\%)_{NO-MW}$ was similar to those in T100-t5-3% and T100-t20-1%. This observation indicating that the MW can reduce approximately three-fourths of the reaction time or two-thirds of the chemical use in the cellulose isolation process with respect to those in normal hydrolysis without MW.
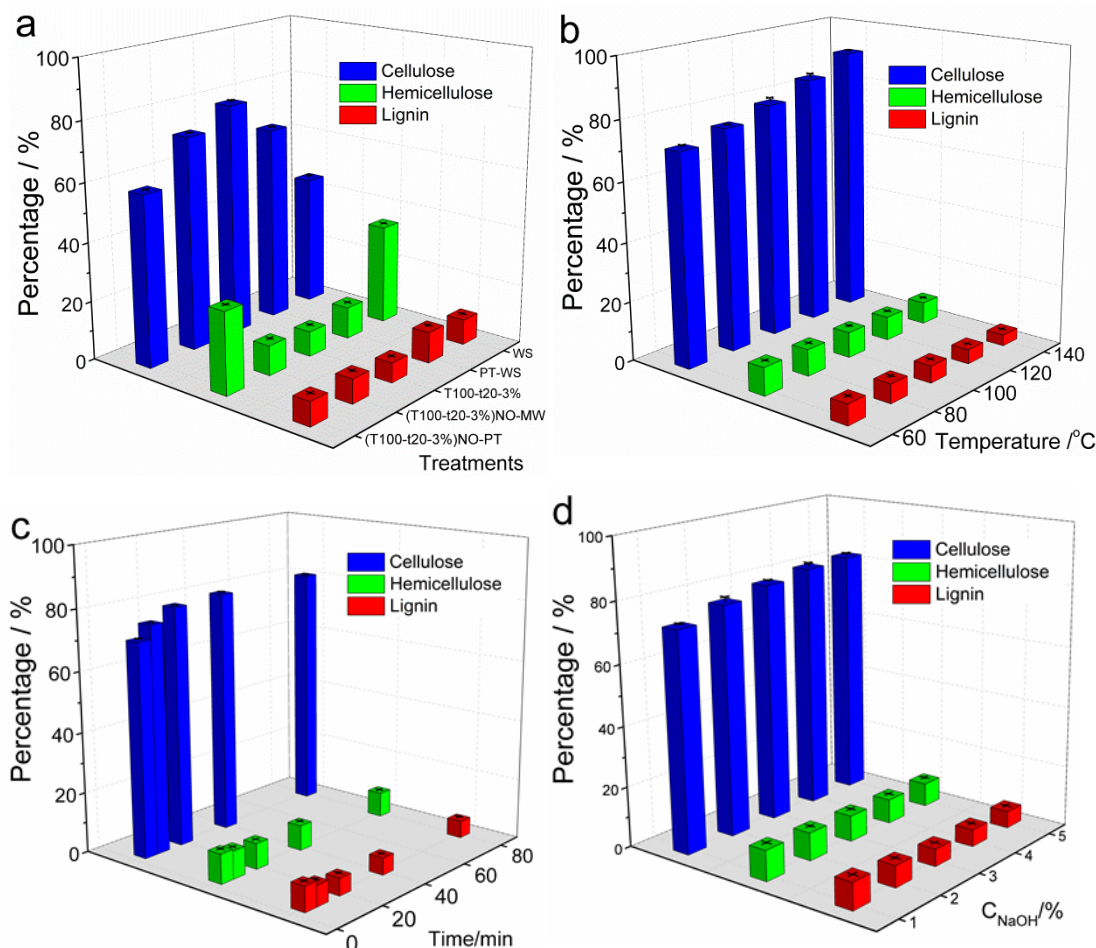
Figure 11. Changes in fiber content with various treatments (a), temperature (b), reaction time (c), and NaOH concentration (CNaoH) (d).

3.4 Effects of treatments on sugar content change

Although the changes in fiber content can indicate the effects of the treatments, sugar

determination can provide more detailed information on the decomposition and destruction effects on a specific area of fibers. The individual neutral sugar compositions of the raw and treated fibers are shown in Table 7. Xylose and glucose were of the highest content in WS, followed by arabinose, rhamnose, mannose, and galactose, ranging from 1.77% to 5.46%. Glucose mainly resulted from cellulose hydrolysis. Xylose was the major sugar in the hemicellulosic fractions with arabinose, glucose, and galactose as minor constituents. These proportions were consistent with the results of Lawther's research.[46] After PT, almost all the rhamnose, mannose and more than half of the arabinose was decreased in amount drastically in the PT-WS through the decomposition of the pectin. From T60-t20-3% to T140-t20-3%, with increasing reaction temperature, all sugars, except glucose, diminished in content. The glucose content increased gradually until 92.99% in T140-t20-3%, which gave the highest value among all the treatments. In the T120-t20-3% and T140-t20-3% fibers, rhamnose and galactose were not detected, and arabinose and mannose were found only in trace amounts. When the effect of the reaction duration was compared, similar results were obtained from T100-t5-3% to T100-t80-3%. The monosaccharide contents decreased, given that the non-cellulosic components were further hydrolyzed. The glucose content grew with increasing reaction time, but no longer changed substantially beyond 20 min. A similar relationship was found among the T100-t20-1% to T100-t20-5% fibers. Xylose decreased obviously with the rising C_{NaoH} and revealed the decomposition effect of the alkali concentration on hemicellulose. Meanwhile, the cellulose content was 6.77% lower in (T100-t20-3%)$_{NO-MW}$ than in T100-t20-3% and indicated the lower cellulose content in the obtained fibers treated without MW. Compared with T100-t20-3%, (T100-t20-3%)$_{NO-PT}$ contained much more sugar content, except that of glucose. The sugars were even higher than those of the PT-WS. This result clarified the important effect of acid hydrolysis PT on cellulose isolation. Among all the treated fibers, the xylose content considerably decreased, which signified the successful removal of hemicellulose during the treatments. These findings are consistent with those of fiber determination.

Table 6. Sugar compositions of the raw and treated fibers (Rha: rhamnose; Ara: arabinose; Xyl: xylose; Man: mannose; Glu: glucose; Gal: galactose; TS: total sugars).

Samples	Sugars contents (%)						
	Rha	Ara	Xyl	Man	Glu	Gal	TS
WS	5.36±2.98	5.46±1.02	28.27±0.89	2.38±0.95	28.02±0.73	1.77±0.57	71.3±7.14
PT-WS	0.25±0.01	2.56±0.06	13.27±1.96	0.41±0.01	68.85±0.14	0.41±0.10	85.7±2.28
T60-t20-3%	0.23±0.03	0.15±0.01	3.49±0.03	0.38±0.05	72.11±0.06	0.30±0.03	76.7±0.73
T80-t20-3%	0.21±0.03	0.14±0.00	3.39±0.21	0.35±0.01	75.86±0.57	0.17±0.04	80.1±0.86
T100-t20-3% **	0.15±0.01	0.14±0.02	3.25±0.42	0.23±0.02	80.40±0.57	0.20±0.01	84.4±1.06
T120-t20-3%	ND*	0.09±0.01	2.94±0.13	0.20±0.03	86.28±0.37	ND*	89.5±0.55
T140-t20-3%	ND*	0.10±0.00	2.68±0.08	0.18±0.00	92.99±0.16	ND*	96.9±0.24
T100-t5-3%	0.24±0.01	0.18±0.01	3.88±0.35	0.24±0.02	74.76±0.09	0.21±0.03	79.5±0.51
T100-t10-3%	0.22±0.03	0.18±0.02	3.74±0.32	0.26±0.01	77.45±0.64	0.17±0.01	82.0±1.03
T100-t20-3% **	0.15±0.01	0.14±0.02	3.25±0.42	0.23±0.02	80.40±0.57	0.20±0.01	84.4±1.06
T100-t40-3%	0.12±0.01	0.13±0.01	2.88±0.16	0.21±0.04	80.66±0.51	0.09±0.03	84.1±0.76
T100-t80-3%	0.10±0.00	0.09±0.01	2.65±0.07	0.19±0.03	80.87±0.06	ND*	83.9±0.17

T100-t20-1%	0.17±0.04	0.15±0.01	4.40±0.00	0.28±0.01	74.49±0.13	0.21±0.03	79.7±0.21
T100-t20-2%	0.18±0.01	0.14±0.00	3.83±0.26	0.22±0.01	77.26±0.42	0.18±0.03	81.8±0.73
T100-t20-3%**	0.15±0.01	0.14±0.02	3.25±0.42	0.23±0.02	80.40±0.57	0.20±0.01	84.4±1.06
T100-t20-4%	ND*	0.09±0.01	2.54±0.30	0.24±0.04	80.80±1.06	0.09±0.01	83.8±1.42
T100-t20-5%	ND*	0.08±0.01	1.76±0.10	0.23±0.01	81.09±0.37	0.09±0.01	83.2±0.49
(T100-t20-3%)$_{NO-MW}$	0.16±0.01	0.15±0.01	3.54±0.31	0.29±0.04	73.63±1.21	0.21±0.00	78.0±1.58
(T100-t20-3%)$_{NO-PT}$	0.46±0.02	2.21±0.05	15.09±0.10	0.53±0.07	52.93±1.13	0.52±0.04	71.7±1.41

ND*: not determined

T100-t20-3%**: The same sample was adopted three times in three groups for thorough analysis and visualization of the variation trend.

3.5 Effects of treatments on lignin removal

The contents of insoluble lignin, soluble lignin, and total lignin in all the fibers subjected to the Klason method are summarized in Figure 12 Similar to those in the studies of Ronald et al. and Kondo et al., the Klason values were about 30%–50% higher than the ADL values[47, 48]. These higher values were due to the solubilization of lignin components by the ADL treatment. Hence, Klason values may more accurately quantify the contents of insoluble lignin and total lignin in forage plants.[47] In the WS fibers, 15.66% insoluble lignin and 2.89% soluble lignin were found. After PT, these contents decreased to 13.85% and 2.21%, respectively. Less lignin residue was obtained in the T100-t20-3% fibers than in the (T100-t20-3%)$_{NO-MW}$ fibers and indicated a more efficient removal of lignin under MW (Figure 13a). Meanwhile, Figure 12b showed a sharply decreasing insoluble lignin with increasing reaction temperature. When the lignin reached 140 °C, the contents of insoluble and soluble lignin were only 3.30% and 1.81%, respectively, and demonstrated the obvious effect of reaction temperature on lignin hydrolysis. Figure 12c revealed the effect of reaction time on lignin removal. The amount of residual lignin declined when the reaction time was increased from 5 min to 20 min and then barely changed beyond 20 mins. To investigate the effect of C_{NaOH} on cellulose isolation 1% to 5% NaOH was added to the reactions, and the results are given in Figure 12d. The lignin contents in the fibers obtained after 1% NaOH treatments was similar to that in the PT-WS and indicated the limited effect of such low C_{NaOH}. The lignin contents continued decreasing with increasing C_{NaOH}. However, the lignin contents of the fibers did not basically change beyond the C_{NaOH} of 3%. These results suggest the enhancement of lignin removal from the fibers as well as the significant effect of temperature on the process.
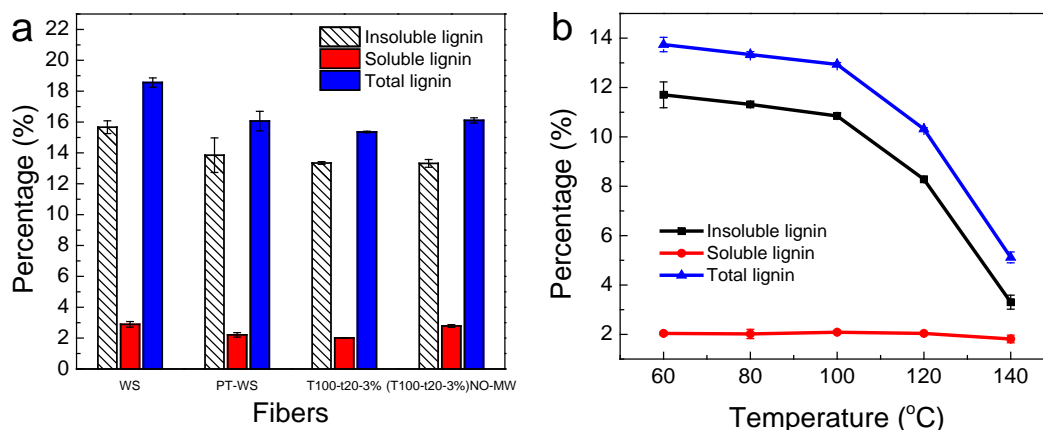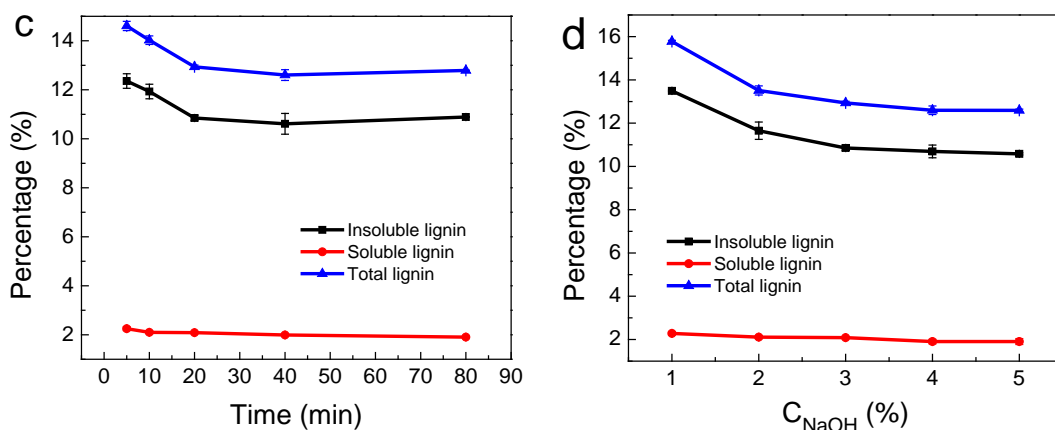
Figure 12. Effects of pretreatment (PT) and microwave (MW) (a), reaction temperature (b), reaction time (c), and CNaoH (d).

3.6 Morphology and Microstructure comparison of WS and treated fibers

The microstructures of WS and T140-t20-3% fibers were investigated using SEM and AFM (Figure 13). The 3D simulation schemes of the two fibers were also employed to determine the effects of the treatment on fiber microstructure. SEM imaging (Figure 13a) shows that the raw WS fibers were regularly arranged in bundles with various widths. After treatment, the T140-t20-3% fibers changed into approximately 10–20 μm-diameter individual fibrils, which were considerably narrower than the raw fiber bundles (Figure 13b). Through this process, hemicellulose, lignin, pectin, and other cementing materials were lost to a great extent. The AFM topographies, 3D images, and height profiles of WS and T140-t20-3% are shown in Figure 14c and 14d. NanoScope Analysis software was then employed to analyze the surface roughness (R_a/R_q) and measure three typical heights of both fibers. For each sample, the values of R_a and R_q were calculated within a selected area size in 50.0 μm × 50.0 μm. Three highest peaks in the 3D image were measured. The results of the roughness (R_a/R_q) and heights of the two fibers are shown in Table 8. As shown, the raw fibers exhibited a rough topography with a high R_a/R_q value of 0.712, which were due to the complex components in the raw fibers. The highest peak of WS was more than 200 nm, which indicated the large particles as well as the complex structure in WS. After treating with alkali along with MW (Figure 13d and Table 8), abundant sharp peaks were observed. The T140-t20-3% fibers exhibited much smoother surfaces, a lower R_a/R_q of 0.578, and decreased peak height, which implied that the surfaces of the isolated cellulose fibers were cleaner and smoother.
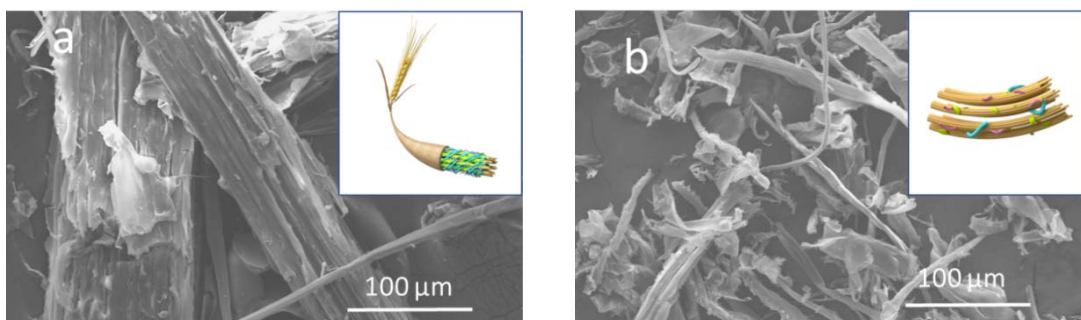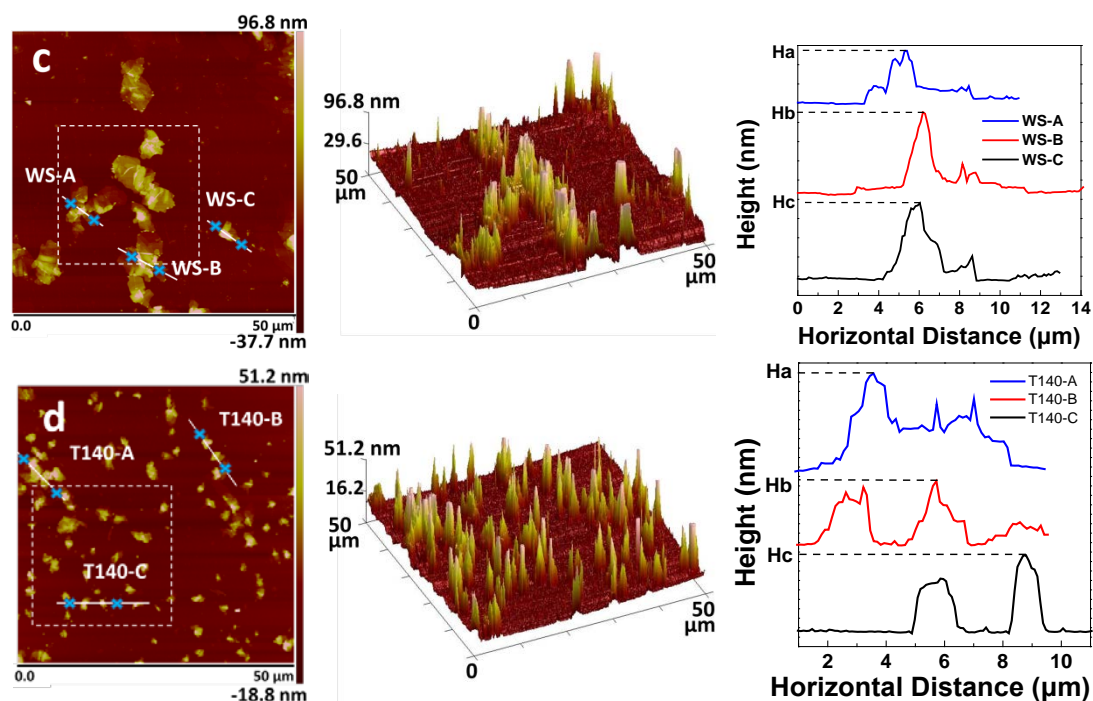
Figure 13. SEM images of WS (a) and T140-t20-3% (b). AFM topographies, 3D images, and height profiles of WS(c) and T140-t20-3% (d).

Table 7. Roughness (Ra/Rq) and heights of WS and T140-t20-3%.

Fibers	Ra (nm)	Rq (nm)	Ra/Rq	Height (nm)		
				Ha	Hb	Hc
WS	16.6	23.3	0.712	118.88	200.18	190.05
T140-t20-3%	5.20	9.00	0.578	96.99	53.32	76.63

3.7 Structure, crystallinity, and stability of WS and treated fibers

The FTIR spectra, XRD patterns, thermogravimetry (TG) curves, and derivative TG (DTG) curves of WS and T140-t20-3% are shown in Figure 14 to comprehensively present the effects of the treatment. The FTIR spectra of the raw and T140-t20-3% fibers are shown in Figure 14a. The peaks at 1254, 1509, and 1734 cm^{-1} are almost absent in the spectrum of T140-t20-3%, indicating the removal of hemicellulose and lignin. Specifically, the peaks at 1253 and 1509 cm^{-1} corresponded to the aromatic skeletal vibrations of lignin[49], whereas the peak at 1734 cm^{-1} was attributed to the acetic and uronic ester groups in the hemicelluloses and the ester linkages of the carboxylic group of ferulic and *p*-coumaric acids in lignin or the hemicelluloses.[50, 51] The XRD patterns of the raw and T140-t20-3% fibers are presented in Figure 14b. The peaks at $2\theta = 15.4°$, $21.7°$ suggested that only cellulose I was present in the raw WS fibers. However, approximately half of cellulose I was converted to cellulose II after the treatments, as indicated by $I_{21.7}/I_{20.0}$, which represents the ratio of cellulose I to cellulose II, with a value of 1.016 for T140-t20-3% (Table 9). Moreover, the crystallinity index increased from 42.50% to 60.56% (Table 9). The TG (Figure 14c) and DTG (Figure 14d) results clearly illustrated that the thermal stability of the fibers increased after the treatments. The maximum

decomposition rate was obtained at the peak temperature T_p, which was determined by the DTG peak. The residue weight percentage Rtp corresponded to the peak temperature. At 700 °C, the residual content decreased from 23.96% of the raw fibers to 16.18% of T140-t20-3%. The T_p of the treated fibers increased from 327.6 °C (Rtp of 51.32%) to 351.9 °C (Rtp of 42.23%) because the non-cellulosic materials were mostly removed. Therefore, the higher thermal stability and fewer residual of the T140-t20-3% fibers than those of the raw fibers were caused by the removal of hemicelluloses and lignin. These results are highly consistent with the results of FTIR spectroscopy and crystallinity measurements.

The SEM images, FTIR spectra, XRD patterns, TG curves, and DTG curves of PT-WS (compared with WS) and (T100-t20-3%)$_{NO-PT}$ (compared with T100-t20-3%) are shown in Figure S1–S5 (Supporting Information). These data revealed the important effect of PT on hemicellulose removal from WS and its effect for access of chemical during the MW-assisted treatment. Furthermore, the acid hydrolysis not only substantially helped in removing non-cellulosic components in the PT but also improved the efficiency of the MW-assisted alkali hydrolysis.
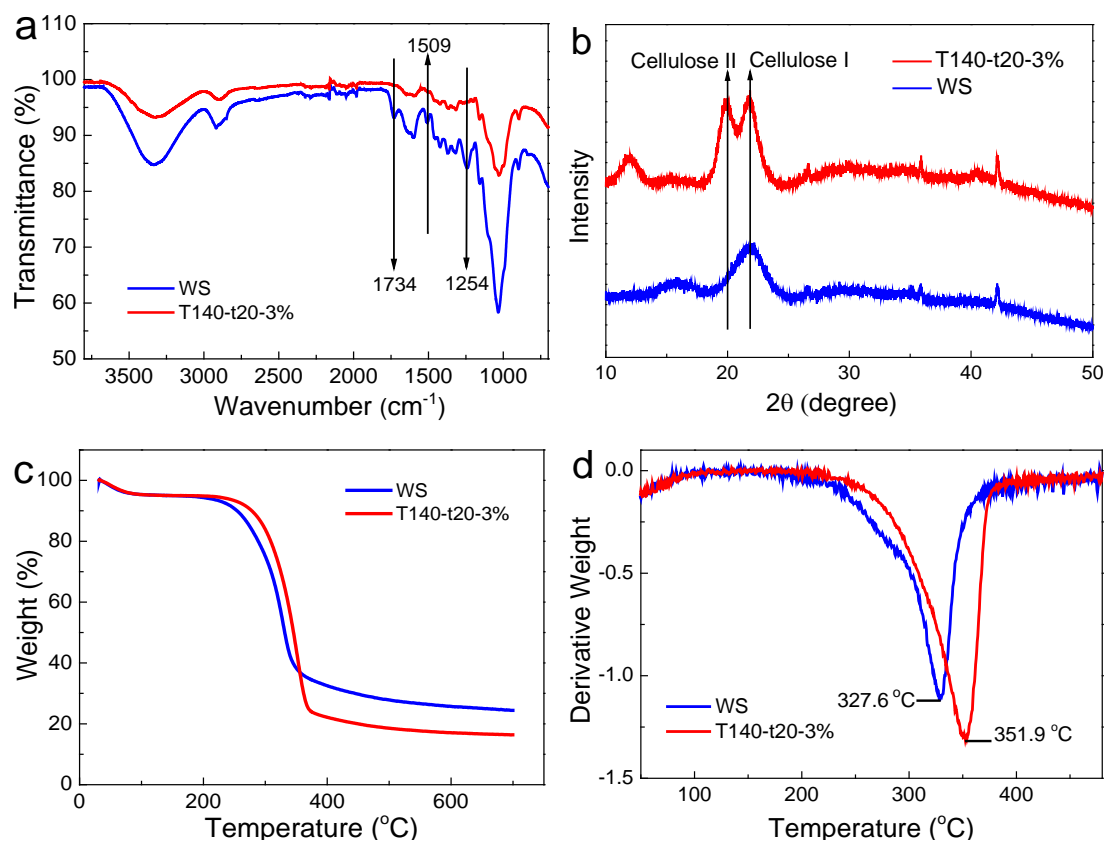
Figure 14. FTIR spectra (a), XRD patterns (b), TG curves (c), and DTG curves (d) of WS and T140-t20-3% fibers.

Table 8. Crystallinity index and thermal behaviors of WS, PT-WS, T100-t2-3%, (T100-t2-3%)NO-MW, T140-t2-3%, and (T100-t2-3%)NO-PT.

Fibers	Crystallinity index (Cellulose I, %)	$I_{21.7}/I_{20.0}$	Tp (°C)	Rtp (%)	Residue at 700 °C (%)
WS	42.50	—	327.6	51.32	23.96

PT-WS	49.93	1.131	358.8	45.97	13.82
T100-t20-3%	57.21	1.037	335.3	45.85	11.92
(T100-t20-3%)$_{NO-MW}$	53.02	1.072	336.7	50.52	19.48
T140-t20-3%	60.56	1.016	351.9	42.23	16.18
(T100-t20-3%)$_{NO-PT}$	51.98	—	350.2	42.21	13.72

3.8 Non-thermal effect of MW

To further elucidate the effect of MW on cellulose isolation, the fiber composition, morphology, structure, crystallinity, and thermal properties of T100-t20-3% and (T100-t20-3%)$_{NO-MW}$ were compared. SEM, FTIR, XRD, and TGA were used for characterization (Figure 15). As shown in the SEM images (Figure 15a and 15b), the T100-t20-3% fibers exhibited cleaner cellulose bundles and more individual fibrils with an average diameter of approximately 10 μm than those of the (T100-t20-3%)$_{NO-MW}$ fibers. Figure 15a also displays the differences in fiber content between the two samples. The 6.64% higher cellulose content of T100-t20-3% confirmed that MW not only helped control the reaction temperature but also promoted the degree of reaction through its non-thermal effect. Meanwhile, the FTIR spectra (Figure 15d), XRD patterns (Figure 15e), TG (Figure 15f), and DTG curves (Figure S5, Supporting Information) of the two fibers were fairly similar because of the comparable compositions. However, subtle distinctions caused by reaction extension and component differences during processing were noted in the presence and absence of MW. In Figure 15d, the FTIR spectra were almost the same for both fibers. By contrast, the peaks at 1265 and 1507 cm^{-1} corresponding to the aromatic skeletal vibrations of lignin differed in strength. This result semi-quantitatively signified the presence of less lignin content in the T100-t20-3% fiber.[51] XRD results (Figure 15e and Table 9) showed the transformation of crystalline state during MW-assisted alkali treatment and the difference in crystallinity index between the two fibers. A polymorphic modification of the crystalline state of the samples from cellulose I to cellulose II was observed, as similarly reported by other works.[51, 52] The ratios of cellulose I to cellulose II were 1.037 and 1.072 for T100-t20-3% and (T100-t20-3%)$_{NO-MW}$, respectively, which revealed that more cellulose I were transformed to cellulose II with MW than without MW. The TG (Figure 15f) and derivative thermogravimetry (DTG) curves (Figure S5, Supporting Information) of the T100-t20-3% fibers showed larger absolute values for the slope than those of the (T100-t20-3%)$_{NO-MW}$ fibers. The residue weight percentage corresponding to the peak temperature was designated as Rtp. At 700 °C, the residual content of T100-t20-3% and (T100-t20-3%)$_{NO-MW}$ decreased from 23.96% of the raw material to 11.92% and 19.82% for the fibers, respectively. The T_p of the two fibers were almost the same, but (T100-t20-3%)$_{NO-MW}$ achieved a higher Rtp, which signified the greater contents of non-cellulosic components. The thermal determination results were consistent with the results of SEM, fiber, crystallinity, and FTIR measurements. All these results suggested that the cementing materials, including hemicelluloses, lignin, and pectin, around the fiber bundles dissolved more readily with than without MW treatment. This finding further confirmed the non-thermal effect of MW on improving the cellulose isolation efficiency. The specific

mechanism of this non-thermal effect and its relationship with the consumed energy will be further explored in future work.
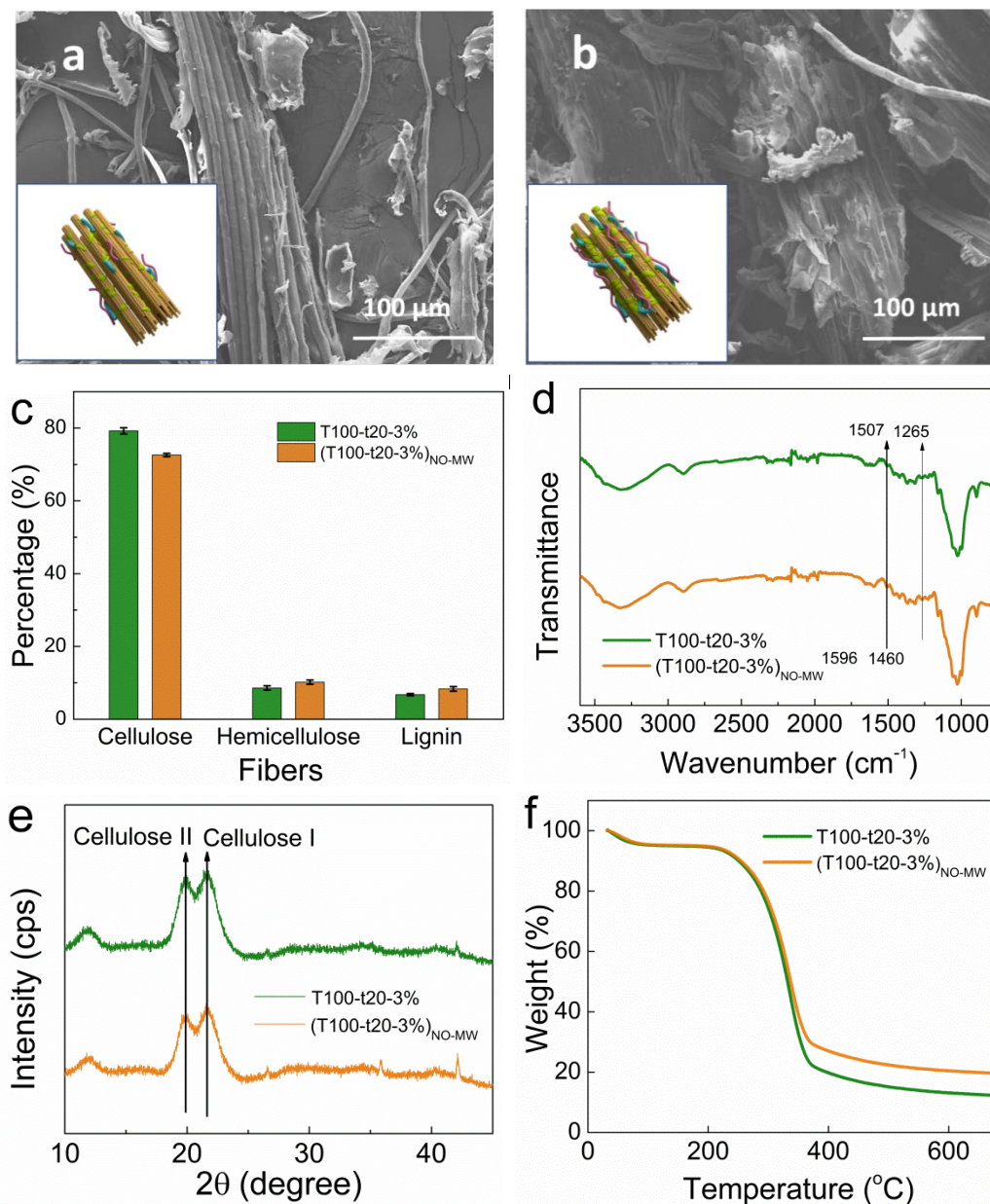
Figure 15. Comparison of SEM images (a & b), fiber contents (c), FTIR spectra (d), XRD patterns (e), and TG curves (f) between T100-t20-3% and (T100-t20-3%)NO-MW.

4. Conclusions

This work focused on the cellulose isolation from WS with MW-assisted alkali hydrolysis, especially on the influences of the reaction conditions and the non-thermal effect of MW. The cellulose contents in the treated fibers increased with rising temperature, reaction time, and alkali concentration. Meanwhile, the lignin contents decreased correspondingly mainly due to the decomposition of the insoluble lignin under Klason method. Temperature exerted the most efficient effect on the cellulose isolation. 90.66% cellulose was obtained in the resulting fibers under heating at 140 °C. The sugar determination results were consistent with those of the fiber tests. After the PT and MW-assisted hydrolysis at 140 °C with 3% NaOH for 20 min, AFM

results revealed that the surface roughness R_a/R_q of the raw fibers diminished from 0.712 to 0.578, and the dramatic decrease in peak height confirmed the removal of non-cellulosic components. Comparison of morphology, structure, crystallinity, and thermal properties between T100-t20-3% and (T100-t20-3%)$_{NO-MW}$ showed the non-thermal effect of MW on promoting the isolation. The cellulose content in (T100-t20-3%)$_{NO-MW}$ was similar to those in T100-t5-3% and T100-t20-1%. This observation indicating that the MW can reduce three-fourths of the reaction time or two-thirds of the chemical use in this MW-assisted alkali hydrolysis process with respect to those in normal one without MW.

The experimental results showed that MW may either conserve energy or exert a green effect on cellulose isolation from raw materials; MW may also be utilized to meet the requirements of high-purity cellulose isolation from natural biomass. The results of this work should further stimulate research interest in developing green methods for isolating cellulose from natural fibers.

Acknowledgement

References

(1) Urruzola, I. A.; Robles, E.; Serrano, L.; Labidi, J. Nanopaper from almond (Prunus dulcis) shell. *Cellulose* **2014**, *21* (3), 1619−1629.

(2) Colmenares, J. C.; Varma, R. S.; Lisowski, P. Sustainable hybrid photocatalysts: titania immobilized on carbon materials derived from renewable and biodegradable resources. *Green Chem.* **2016**, *47* (51), 5737−5750.

(3) Siró, I.; Plackett, D. Microfibrillated cellulose and new nanocomposite materials: a review. *Cellulose* **2010**, *17* (3), 459–494.

(4) Jonoobi, M.; Oladi, R.; Davoudpour, Y.; Oksman, K.; Dufresne, A.; Hamzeh, Y.; Davoodi, R. Different preparation methods and properties of nanostructured cellulose from various natural resources and residues: a review. *Cellulose* **2015**, *22* (2), 935−969.

(5) Zhang, L.; Liu, Y.; Hao, L., Contributions of open crop straw burning emissions to PM2.5 concentrations in China. *Environ. Res. Lett.* **2016**, *11* (1).

(6) Klemm, D.; Heublein, B.; Fink, H. P.; Bohn, A. Cellulose: fascinating biopolymer and

sustainable raw material. *Angew. Chem.* **2005**, *44* (22), 3358–3393.

(7) Wu, C. N.; Yang, Q.; Takeuchi, M.; Saito, T.; Isogai, A. Highly tough and transparent layered composites of nanocellulose and synthetic silicate. *Nanoscale* **2014**, *6* (1), 392–399.

(8) Wen, Y.; Wei, B.; Cheng, D.; An, X.; Ni, Y. Stability enhancement of nanofibrillated cellulose in electrolytes through grafting of 2-acrylamido-2-methylpropane sulfonic acid. *Cellulose* **2016**, *24* (2),731–738.

(9) Sehaqui, H.; Michen, B.; Marty, E.; Schaufelberger, L.; Zimmermann, T. Functional cellulose nanofiber filters with enhanced flux for the removal of humic acid by adsorption. *ACS Sustain. Chem. Eng.* **2016** *4*(9), 4582-4590.

(10) Wang, Y.; Yadav, S.; Heinlein, T.; Konjik, V.; Breitzke, H.; Buntkowsky, G.; Schneider, J.; Zhang, K. Ultra-light nanocomposite aerogels of bacterial cellulose and reduced graphene oxide for specific absorption and separation of organic liquids. *RSC Adv.* **2014**, *4* (41), 21553–21558.

(11) Wan, C.; Jiao, Y.; Li, J. Cellulose fibers-supported hierarchical forest-like cuprous oxide/copper array architecture as flexible and free-standing electrodes for symmetric supercapacitors. *J. Mater. Chem. A* **2017**. DOI: 10.1039/C7TA04994C.

(12) Grigoray, O.; Wondraczek, H.; Pfeifer, A.; Fardim, P.; Heinze, T. Fluorescent Multifunctional Polysaccharides for Sustainable Supramolecular Functionalization of Fibers in Water. *ACS Sustain. Chem. Eng.* **2017** *5*(2), 1794–1803.

(13) Mosier, N.; Wyman, C.; Dale, B.; Elander, R.; Lee, Y. Y.; Holtzapple, M.; Ladisch, M. Features of promising technologies for pretreatment of lignocellulosic biomass. *Bioresource technol.* **2005**, *96* (6), 673–686.

(14) Zhang, M.; Wei, Q.; Rui, L.; Su, R.; Wu, S.; He, Z. Fractionating lignocellulose by formic acid: Characterization of major components. *Biomass Bioenerg.* **2010**, *34* (4), 525–532.

(15) Sun, R.; Lawther, J. M.; Banks, W. B. Influence of alkaline pre-treatments on the cell wall components of wheat straw. *Ind. Crop Prod.* **1995**, *4* (2), 127–145.

(16) Sánchez, R.; Espinosa, E.; Domínguez-Robles, J.; Loaiza, J. M.; Rodríguez, A. Isolation and characterization of lignocellulose nanofibers from different wheat straw pulps. *Int. J. Biol. Macromol.* **2016**, *92*, 1025–1033.

(17) Brodeur, G.; Yau, E.; Badal, K.; Collier, J.; Ramachandran, K. B.; Ramakrishnan, S. Chemical and Physicochemical Pretreatment of Lignocellulosic Biomass: A Review. *Enzyme Research* **2011**, *2011*.

(18) Alemdar, A.; Sain, M. Isolation and characterization of nanofibers from agricultural residues: wheat straw and soy hulls. *Bioresource Technol.* **2008**, *99* (6), 1664–1671.

(19) Domini, C.; Vidal, L.; Cravotto, G.; Canals, A. A simultaneous, direct microwave/ultrasound-assisted digestion procedure for the determination of total Kjeldahl nitrogen. *Ultrason. Sonochem.* **2009**, *16* (4), 564–569.

(20) Gawande, M. B.; Shelke, S. N.; Zboril, R.; Varma, R. S. Microwave-Assisted Chemistry: Synthetic Applications for Rapid Assembly of Nanomaterials and Organics. *Accounts*

Chem. Res. **2014**, *47* (4), 1338−1348.

(21) Bayazit, M. K.; Yue, J.; Cao, E.; Gavriilidis, A.; Tang, J. Controllable synthesis of gold nanoparticles in aqueous solution by microwave assisted flow chemistry. *ACS Sustain. Chem. Eng.* **2016** *4*(12), 6435−6442.

(22) Zelong, L.; Lianfu, Z. Optimization and comparison of ultrasound/microwave assisted extraction (UMAE) and ultrasonic assisted extraction (UAE) of lycopene from tomatoes. *Ultrason. Sonochem.* **2008**, *15* (5), 731−737.

(23) Cravotto, G.; Cintas, P. The Combined Use of Microwaves and Ultrasound: Improved Tools in Process Chemistry and Organic Synthesis. *Chem-Eur. J.* **2007**, *38* (23), 1902−1909.

(24) Moretti, M. M. D. S.; Bocchini-Martins, D. A.; Villena, M. A.; Perrone, O. M.; Silva, R. D.; Boscolo, M.; Gomes, E. Pretreatment of sugarcane bagasse with microwaves irradiation and its effects on the structure and on enzymatic hydrolysis. *Appl. Energ.* **2014**, *122* (6), 189−195.

(25) Polshettiwar, V.; Varma, R. S. ChemInform Abstract: Nano-Organocatalyst: Magnetically Retrievable Ferrite-Anchored Glutathione for Microwave-Assisted Paal—Knorr Reaction, aza-Michael Addition, and Pyrazole Synthesis. *Tetrahedron* **2010**, *66* (5), 1091−1097.

(26) Shi, F.; Li, C.; Xia, M.; Miao, K.; Zhao, Y.; Tu, S.; Zheng, W.; Zhang, G.; Ma, N. ChemInform Abstract: Green Chemoselective Synthesis of Thiazolo[3,2-a]pyridine Derivatives and Evaluation of Their Antioxidant and Cytotoxic Activities. *Bioorg. Med. Chem. Lett.* **2009**, *19* (19), 5565−5568.

(27) Sedelmeier, J.; Ley, S. V.; Lange, H.; Baxendale, I. R. ChemInform Abstract: Pd-EnCat TPP30 as a Catalyst for the Generation of Highly Functionalized Aryl- and Alkenyl-Substituted Acetylenes via Microwave-Assisted Sonogashira Type Reactions. *Eur. J. Org. Chem.* **2010**, *41* (3), 4412−4420.

(28) Qu, G. R.; Xin, P. Y.; Niu, H. Y.; Jin, X.; Guo, X. T.; Yang, X. N.; Guo, H. M. Microwave promoted palladium-catalyzed Suzuki-Miyaura cross-coupling reactions of 6-chloropurines with sodium tetraarylborate in water, *Tetrahedron* **2011**, *67* (47), 9099−9103.

(29) Sathvika, T.; Manasi; Rajesh, V.; Rajesh, N. Microwave assisted immobilization of yeast in cellulose biopolymer as a green adsorbent for the sequestration of chromium. *Chem. Eng. J.* **2015**, *279*, 38−46.

(30) Z, Lu.; L, Fan.; H, Zheng.; Q, Lu.; Y, Liao.; B, Huang. Preparation, characterization and optimization of nanocellulose whiskers by simultaneously ultrasonic wave and microwave assisted. *Bioresource Technol.* **2013**, *146* (10), 82−88.

(31) Zhu, S.; Wu, Y.; Yu, Z.; Liao, J.; Zhang, Y. Pretreatment by microwave/alkali of rice straw and its enzymic hydrolysis. *Process Biochem.* **2005**, *40* (9), 3082−3086.

(32) Zhu, S.; Wu, Y.; Yu, Z.; Wang, C.; Yu, F.; Jin, S.; Ding, Y.; Chi, R. A.; Liao, J.; Zhang, Y. Comparison of Three Microwave/Chemical Pretreatment Processes for Enzymatic

Hydrolysis of Rice Straw. *Biosyst. Eng.* **2006**, *93* (3), 279–283.

(33) Hu, Z.; Wen, Z. Enhancing enzymatic digestibility of switchgrass by microwave-assisted alkali pretreatment. *Biochem. Eng. J.* **2008**, *38* (3), 369–378.

(34) Chowdhury, Z. Z.; Sharifa Bee, A. H. Preparation and characterization of nanocrystalline cellulose using ultrasonication combined with a microwave-assisted pretreatment process. *BioResources* **2016**, *11*, 3397–3415.

(35) Zhou, L.; Budarin, V.; Fan, J.; Sloan, R.; Macquarrie, D. Efficient Method of Lignin Isolation Using Microwave-Assisted Acidolysis and Characterization of the Residual Lignin. *ACS Sustain. Chem. Eng.* **2017** *5*(5), 3768–3774.

(36) Liu, Q.; Lu, Y.; Aguedo, M.; Jacquet, N.; Ouyang, C.; He, W.; Yan, C.; Bai, W.; Guo, R.; Goffin, D.; Song, J.; Richel, A. Isolation of high-purity cellulose nanofibers from wheat straw through the combined environmentally friendly methods of steam explosion, microwave-assisted hydrolysis, and microfluidization. *ACS Sustain. Chem. Eng.* **2017**, *5*(7), 6183–6191.

(37) Aguedo, M.; Ruiz, H. A.; Richel, A. Non-alkaline solubilization of arabinoxylans from destarched wheat bran using hydrothermal microwave processing and comparison with the hydrolysis by an endoxylanase. *Chem. Eng. Process.: Process. Chem. Eng. Process* **2015**, *96*, 72–82.

(38) Soest, V.; P., J. Use of detergents in the analysis of fibrous feeds. 2. A rapid method for the determination of fiber and lignin. *J. Assoc. Official Agri. Chemist.* **1963**, *49*, 546–551.

(39) Bradstreet, R. B. Kjeldahl method for organic nitrogen. *Anal. Chem.* **1954**, *26* (1), 169–234.

(40) Van Soest, P. J.; Wine, R. N. Use of detergents in analysis of fibrous feeds. IV. Determinations of plant cell-wall constituents. *J. Assoc. Official Agri. Chemist.* **1967**, 50–55.

(41) Bremner, J. M. Determination of nitrogen in soil by the Kjeldahl method. *J. Agr. Sci.* **1960**, *55*, 11–33.

(42) Hatfield, R. D.; Hjg, J.; Ralph, J.; Buxton, D. R.; Weimer, P. J. A comparison of the insoluble residues produced by the Klason lignin and acid detergent lignin procedures. *J. Sci. Food Agr.* **1994**, *65* (1), 51–58.

(43) Yasuda, S.; Fukushima, K.; Kakehi, A. Formation and chemical structures of acid-soluble lignin I: sulfuric acid treatment time and acid-soluble lignin content of hardwood. *J. Wood Sci.* **2001**, *47* (1), 69–72.

(44) Blakeney, A. B.; Harris, P. J.; Henry, R. J.; Stone, B. A. A simple and rapid preparation of alditol acetates for monosaccharide analysis. *Carbohyd. Res.* **1983**, *113* (2), 291–299.

(45) Segal, L. C.; Creely, J.; Martin, A. E. J.; Conrad, C. M. An Empirical Method for Estimating the Degree of Crystallinity of Native Cellulose Using the X-Ray Diffractometer. *Text. Res. J.* **1959**, *29* (10), 786–794.

(46) Lawther, J. M.; Sun, R.; Banks, W. B. Extraction, fractionation, and characterization of structural polysaccharides from wheat straw. *J. Agr. Food Chem.* **1995**, *43* (3), 667–675.

(47) Hatfield, R. D.; Hjg, J.; Ralph, J.; Buxton, D. R.; Weimer, P. J. A comparison of the insoluble residues produced by the Klason lignin and acid detergent lignin procedures. *J. Sci. Food Agr.* **1994**, *65* (1), 51−58.

(48) Kondo, T.; Mizuno, K.; Kato, T. Some Characteristics of Forage Plant Lignin. *JARQ.* **1987**, *5* (4), 341−356.(48) Mandal, A.; Chakrabarty, D. Isolation of nanocellulose from waste sugarcane bagasse (SCB) and its characterization. *Carbohydr. Polym.* **2011**, *86* (3), 1291−1299.

(49) Mandal, A.; Chakrabarty, D. Isolation of nanocellulose from waste sugarcane bagasse (SCB) and its characterization. *Carbohydr. Polym.* **2011** *86*(3), 1291-1299.

(50) Kaushik, A.; Singh, M. Isolation and characterization of cellulose nanofibrils from wheat straw using steam explosion coupled with high shear homogenization. *Carbohyd. Res.* **2011**, *346* (1), 76−85.

(51) Cherian, B. M.; Leão, A. L.; Souza, S. F. D.; Thomas, S.; Pothan, L. A.; Kottaisamy, M. Isolation of nanocellulose from pineapple leaf fibres by steam explosion. *Carbohyd. Polym.* **2010**, *81*, (3), 720−725.

(52) Kim, N. H.; Imai, T.; Wada, M.; Sugiyama, J. Molecular directionality in cellulose polymorphs. *Biomacromolecules* **2006**, *7* (1), 274.

Supporting information
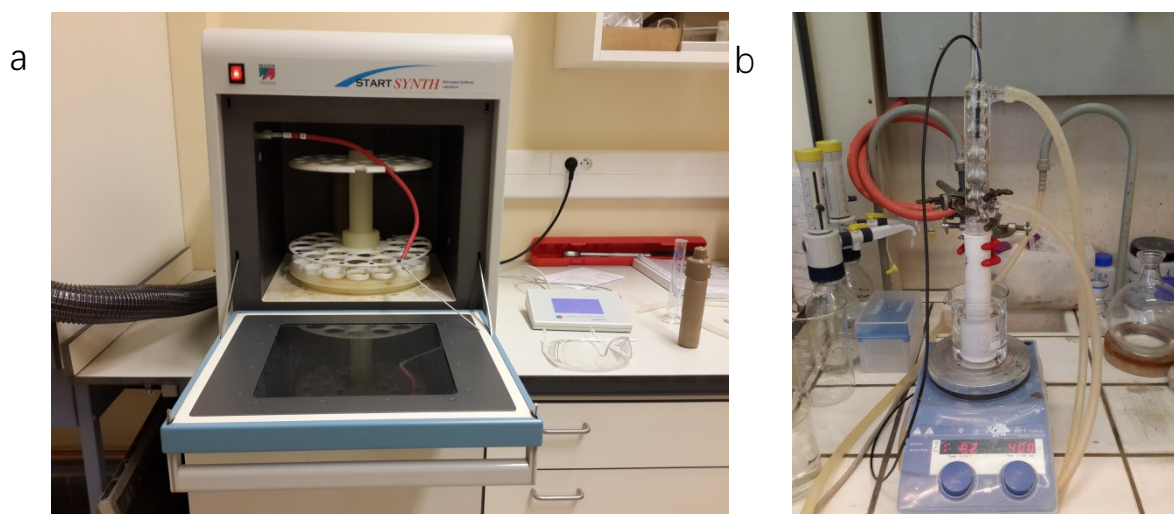
Figure S1. Microwave apparatus used (a) and experimental installation of (T100-t20-3%)$_{\text{NO-MW}}$ (b).

Table S1. Neutral detergent fiber (NDF), acid detergent fiber (ADF) and acid detergent lignin (ADL) of all fibers.

Fibers	NDF (%)	ADF (%)	ADL (%)
WS	87.67±0.62	53.56±0.49	8.75±0.31
PT-WS	88.40±0.37	78.52±0.28	10.58±0.64
T60-t20-3%	87.89±0.88	78.46±0.54	6.93±0.43
T80-t20-3%	90.56±0.67	81.59±0.35	6.42±0.63
T100-t20-3%	93.54±2.51	84.96±1.93	5.74±0.29
T120-t20-3%	97.29±2.31	89.28±1.87	4.88±0.06
T140-t20-3%	101.90±0.47	94.48±0.70	3.82±0.19
T100-t5-3%	88.93±0.34	79.06±0.08	8.32±0.20
T100-t10-3%	91.39±0.96	82.17±1.07	6.88±0.51
T100-t40-3%	94.24±0.33	85.82±0.72	5.67±0.13
T100-t80-3%	94.49±0.66	86.20±0.81	5.71±0.44
T100-t20-1%	91.69±0.45	81.56±0.92	8.93±0.18
T100-t20-2%	92.85±1.62	83.64±1.22	7.16±0.39
T100-t20-4%	94.98±1.23	86.91±1.53	5.68±0.23
T100-t20-5%	95.46±1.15	87.61±0.60	5.65±0.17
(T100-t20-3%)$_{\text{NO-MW}}$	80.90±1.10	70.73±0.50	8.32±0.64
(T100-t20-3%)$_{\text{NO-PT}}$	66.41±0.76	38.50±0.37	8.21±0.47
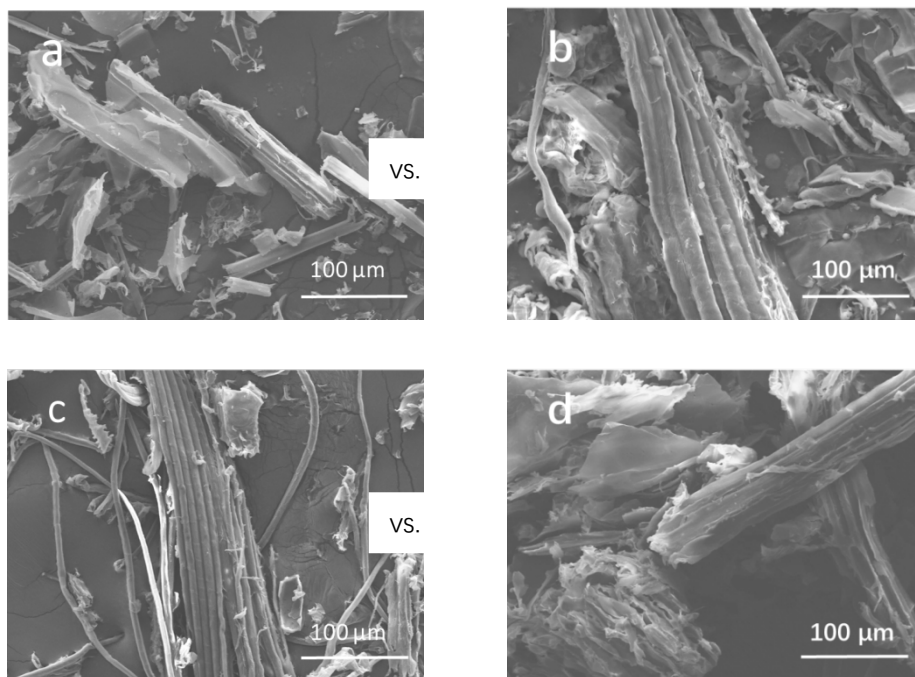
Figure S2. Comparison of SEM images of WS (a) and PT-WS (b), T100-t20-3% (c) and (T100-t20-3%)ₙₒ₋ₚₜ (d).
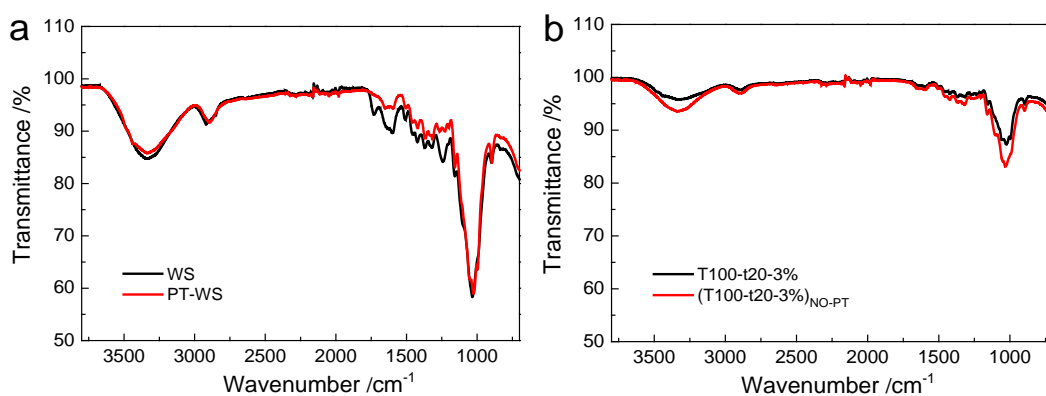
Figure S3. FTIR spectra of WS and PT-WS (a), T100-t20-3% and (T100-t20-3%)ₙₒ₋ₚₜ (b).
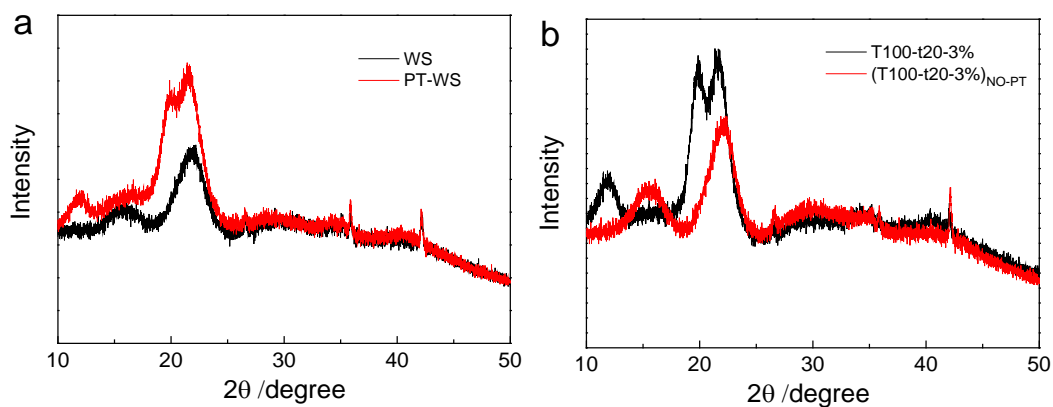
Figure S4. XRD patterns of WS and PT-WS (a), T100-t20-3% and (T100-t20-3%)_{NO-PT}
(b).
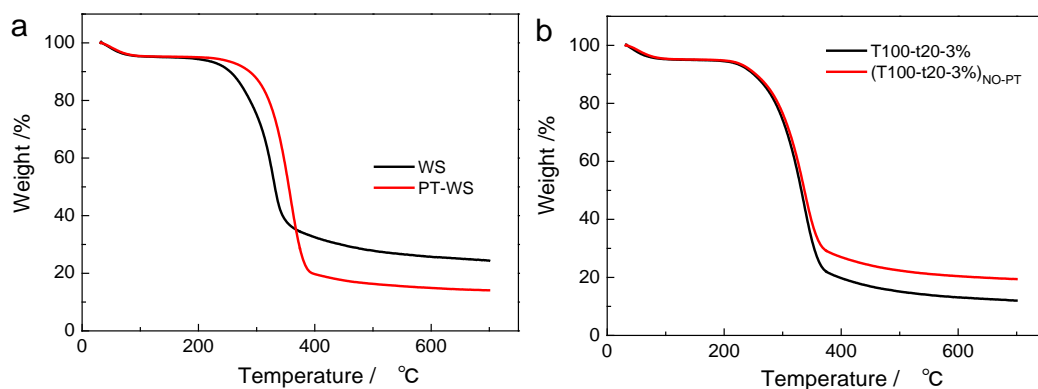
Figure S5. TG curves of WS and PT-WS (a), T100-t20-3% and (T100-t20-3%)_{NO-PT} **(b).**
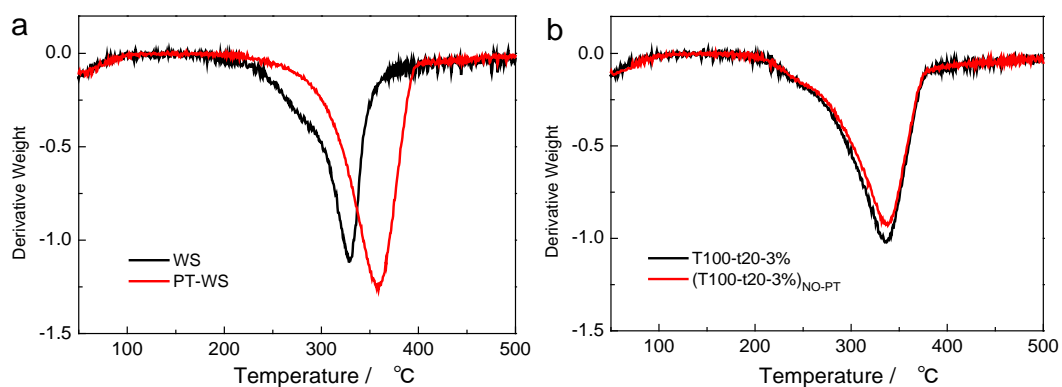
Figure S6. DTG curves of WS and PT-WS (a), T100-t20-3% and (T100-t20-3%)_{NO-PT} **(b).**

Article 4 Isolation of high-purity cellulose nanofibers from wheat straw through the combined environmentally friendly methods of steam explosion, microwave-assisted hydrolysis, and microfluidization

Qi Liu,[†,‡,§] Yun Lu,[∥] Mario Aguedo,[§] Nicolas Jacquet,[§] Canbin Ouyang,[⊥] Wenqing He,[†] Changrong Yan,[†] Wenbo Bai,[†] Rui Guo,[†] Dorothée Goffin,*[,‡,§] Jiqing Song,*[,†] Aurore Richel*[,§]

[†]National Engineering Laboratory for Crop Efficient Water Use and Disaster Mitigation, Key Laboratory of Dryland Agriculture, Ministry of Agriculture and Key Laboratory for Prevention and Control of Residual Pollution in Agricultural Film, Ministry of Agriculture, Institute of Environment and Sustainable Development in Agriculture, Chinese Academy of Agricultural Sciences, No.12 Zhongguancun South Street, Beijing 100081, China

[‡]TERRA Research Center and Laboratory of Gastronomical Science, Gembloux Agro-Bio Tech-University of Liège, Passage des Déportés 2B-5030 Gembloux, Belgium

[§]Unit of Biomass and Green Technologies, Gembloux Agro-Bio Tech-University of Liège, Passage des Déportés 2B-5030 Gembloux, Belgium

[∥]Research Institute of Wood Industry, Chinese Academy of Forestry, No.1 Dongxiaofu, Xiangshan Road, Beijing 100091, China

[⊥]Department of Pesticides, Institute of Plant Protection, Chinese Academy of Agricultural Sciences, Ministry of Agriculture, and State Key Laboratory for Biology of Plant Diseases and Insect Pests, No.2 Yuanmingyuan West Road, Beijing 100193, China

Abstract: High-purity cellulose nanofibers were isolated from wheat straw through an environmentally friendly, multi-step treatment process that combined steam explosion, microwave-assisted hydrolysis, and microfluidization. The cellulose content of the processed nanofibers increased from 44.81% to 94.23%, whereas the hemicellulose and lignin contents significantly decreased. Scanning electron microscopy revealed the effects of the isolation treatments on fiber morphology and width. Atomic force microscopy was used to observe the changes in the components, surface roughness, and crystallinity of the fibers. Transmission electron microscope showed long, loose nanofiber bundles that were 10–40 nm wide with an average individual diameter of 5.42 nm. Fourier transform infrared spectroscopy showed that non-cellulosic components were effectively removed. X-ray diffraction analysis revealed the improved crystallinity of the processed fibers, as well as the partial crystalline transformation of cellulose I to cellulose II. Thermogravimetric analysis and derivative thermogravimetric results showed the enhanced thermal properties of the nanofibers. The removal of hemicellulose and lignin increased the crystallinity of the fibers, thus enhancing the thermal properties of the processed fibers. Results indicated that the efficient, environmentally friendly multi-step treatment process yields nanofibers with potential advanced applications.

Key words: wheat straw; cellulose nanofibers; high purity; steam explosion; microwave-assisted hydrolysis; microfluidization

1. Introduction

Cellulose is one of the most ancient and abundant natural polymers on earth. Cellulose nanofibers (CNFs) exist in plant cell walls as highly crystalline microfibrils that are several nanometers in width and are formed when hydrogen bonding causes long cellulose molecules to become laterally packed.[1] CNFs exhibit outstanding mechanical properties, such as a high strength (2–6 GPa),[2] high Young's modulus (30–150 GPa),[3] high thermal stability (T_m > T_d~300 °C), and large surface areas (100–1000 m^2g^{-1}).[4] Given these properties, CNFs have potential uses as reinforcement materials in nanocomposites,[5,6,7] contaminant adsorbents,[8,9] hydrogels or superabsorbent polymers,[10–13] flexible conductive composites,[4,14] transparent composites,[15] ultra-light and high-porosity aerogels,[16–18], and flexible supercapacitors.[19]

Wheat, one of the most common crops in the world, is the main agricultural plant of the Yangtze River and Huanghuaihai Plains in China. More than 120 million tons of wheat is harvested annually in China. Wheat residue accounts for 15.7% of all the post-harvest crop residues left in the field.[20] Farmers prefer to burn crop residues directly in the field because this is the quickest and cheapest approach to prepare fields for the upcoming cropping season. However, this approach not only wastes biomass but also contributes to air pollution: In China, open straw burning produces an estimated 1.036 million tons of PM$_{2.5}$ emissions per year.[21] By contrast, the utilization of straw as a bioenergy or biomass source remains insufficient. Each year, only a limited percentage of WS is used as feedstock or in energy production. Similar to wood, WS mainly contains cellulose, hemicellulose, and lignin[22,23] and is therefore a low-cost and renewable source of CNFs. Moreover, the use of agricultural residues in biocomposites is a prospective commercial application that can unlock the potential of these underutilized renewable materials and provide a non-food based market for the agricultural industry.[24]

Numerous studies have been conducted to isolate and utilize CNFs from WS.[5,24–28] Similar to wood CNFs, wheat straw CNFs have been isolated through a combination of chemical and mechanical treatments. Alemdar et al. used a chemi–mechanical method to isolate wheat straw CNFs. In their method, the chemical treatment step involved the successive use of 17.5% w/w NaOH, 1 M HCl, and 2% w/w NaOH solution, which was then followed by a mechanical step. This multi-step method yielded homogeneous CNFs with 10–80 nm diameters and 84.6% purity.[24] To isolate CNFs from four different materials, including WS, Chen et al. adopted a chemical–ultrasonic method that combined benzene/ethanol, acidified NaClO, 2% w/w KOH, acidified NaClO, and 5% w/w KOH chemical treatments. Nanofibers with diameters of 15 nm to 35 nm with 84.1% cellulose content were successfully isolated through this method.[25] Kaushik and Singh isolated CNFs from WS by using a steam explosion approach with 10%–12% NaOH solution, followed by a high shear homogenization treatment. This treatment method yielded CNFs diameters of 10 nm to 50 nm and 86.38% purity.[26] Singh et al. used a propionylation process under different conditions to isolate CNFs from WS fibers. They then performed homogenization to obtain surface-modified CNFs.[27] Sánchez et al. prepared CNFs from WS through different pulping processes followed by mechanical processing and 2,2,6,6-tetramethylpiperidine-1-oxyl radical (TEMPO)-mediated oxidation. Fibers with 91.8% cellulose content were obtained via the Kraft process (170 °C, 16% alkalinity, 25% sulfidity, 40

min). This purity is higher than those of fibers obtained via the soda (100 °C, 7% NaOH, 150 min) and Organosolv processes (210 °C, 60% ethanol, 60 min). Nanofibers obtained from mechanical processing and TEMPO-mediated oxidation with soda-processed pulp exhibit a minimum diameter of 6.81 nm.[28] Nuruddin et al. extracted cellulose via an initial formic acid/peroxyformic acid/H_2O_2 treatment followed by ball milling and acid hydrolysis. They obtained CNFs with diameters of 10 nm to 25 nm.[29] Shamsabadi et al. isolated CNFs from WS via acid hydrolysis, alkali treatment, and bleaching, followed by ultrasonic treatment. The final nanofibers possessed an average diameter of 45 nm and cellulose content of 85.5%.[30]

Despite the availability of several acclaimed studies on the isolation of CNFs from WS, the research for environmentally friendly treatment processes for the isolation of high-purity CNFs remains limited. The pretreatment effects of steam explosion have been certified by numerous results for cellulose isolation.[26, 31, 32] This method treats the fibers with high pressure steam for a short period of time, followed by a rapid release of pressure, which results in the hydrolysis of significant amounts of hemicellulose and some lignin in the raw materials. For lignin removal, alkali hydrolysis is an efficient way. However, the use of large amounts of chemicals is not regarded as environmentally friendly. Likewise, microwave could be employed to both accelerate the reaction process and reduce the use of alkali. Most hemicellulose and lignin would be removed using a combination of steam explosion and microwave-assisted hydrolysis. Nechyporchuk et al. summarized the mechanical ways for delamination of fiber cell walls and CNFs isolation considering that microfluidization was one of the most efficient method.[33] Therefore, high purity could be attained through the combination of steam explosion, microwave-assisted hydrolysis, and microfluidization.

The main goal of this study is to use as less chemical as possible during the CNFs isolation process, meanwhile to obtain nanofiber with high purity. In this work, CNFs were isolated from WS through an environmentally friendly, multi-step treatment process that combined steam explosion, microwave-assisted hydrolysis, and microfluidization. The morphological, structural, thermal, and mechanical properties of the isolated fibers were evaluated via chemical analysis and characterization to demonstrate the potential utilization of the CNFs in biocomposites, as well as to investigate the effect of each treatment step. The morphology, size, and surface roughness of the raw materials, processed fibers, and final CNFs were investigated by using scanning electron microscopy (SEM), transmission electron microscope (TEM), and atomic force microscopy (AFM). The cellulose, hemicellulose, lignin, and sugar contents of the fibers were determined with chemical analysis. Fourier transform infrared (FTIR) spectroscopy, X-ray diffraction (XRD), and thermogravimetric analysis (TGA) were conducted to characterize the structure, crystallinity, and thermal stability of the fibers. To the best of our knowledge, the present environmentally friendly method yielded CNFs with the highest purity from WS.

2. Experimental section

2.1 Materials

WS was collected from Huantai experimental fields in 2015 in Shandong Province, China. Chemical composition, including cellulose, hemicellulos, lignin, water, protein, fat, ash and starch contents, was determined (Supporting Information, Table S2). The contents of cellulose, hemicellulose, and lignin, the three main polymer components of WS, were 44.81 ± 0.67%, 34.11 ± 0.75% and 8.75 ± 0.31%, respectively. The collected straw was dried before use and milled into powder with a particle size of less than 1 mm. NaOH (ACS reagent grade, 98%) and HCl (ACS reagent grade, 37% HCl) were procured from Sigma-Aldrich. Only distilled water was used in the experiments.

2.2 Steam explosion

CNFs were prepared via a multi-step treatment process, as shown in Scheme S1. First, steam explosion was employed as a pre-treatment process. WS was pre-treated in steam explosion equipment that was designed by the Unit of Biomass and Green Technologies at Gembloux Agro-Bio Tech - University of Liège.[34, 35] First, 500 g (dry weight) WS was placed in the reactor. Then, the reactor was preheated to 100 °C. The reaction was run under a pressure of 3.0 MPa for 2 min. After treatment, the steam-exploded fibers (SEFs) were washed several times with distilled water and dried via lyophilization using a Labconco freeze-dry system (Freezone 4.5; Labconco Corporation, Kansas City, USA).

2.3 Microwave-assisted alkali hydrolysis treatment

SEFs were treated with acid hydrolysis prior to microwave-assisted alkali hydrolysis treatment. The dried SEFs were soaked in 1 M HCl solution with a solid-liquid ratio 1：20 stirring at 80 ± 1 °C for 2 h and then washed with distilled water until neutral. A Start Synth microwave digestion system (Milestone Srl, Sorisole, Italy) was used for microwave-assisted alkali hydrolysis treatment. A total of 1.5 g (dry weight) sample was suspended in 30 mL of 2% NaOH aqueous solution in a 50-mL sealed vessel. A magnetic stirring bar was employed to evenly heat the vessel. Temperature was increased to 140 ± 2 °C within 3 min and maintained for 20 min. A changeable power source (maximum setting at 1200 W) and a temperature monitor (inserted inside the vessel) were introduced to precisely achieve the process temperature.[36] Then, the samples were washed with distilled water until the pH of the filtrate reached 7. The obtained microwave-assisted alkali-hydrolyzed fibers (MWFs) slurry was stored at 4 °C for later use.

2.4 Microfluidization treatment

A high-pressure microfluidizer (Microfluidizer M-110 P, Microfluidics Corp., Newton, Massachusetts, USA) was used to isolate CNFs under pressures of 150 MPa (21,750 psi) to 159 MPa (23,000 psi). The fiber slurry was diluted to 0.1% solid consistency and passed five times through the microfluidizer chamber. The CNFs suspension was partially freeze-dried and stored at 4 °C until further characterization.

2.5 Fiber analysis

Cellulose, hemicellulose, and lignin contents were determined in accordance with the Van

Soest method.[37, 38] The amounts of neutral detergent fiber (NDF), acid detergent fiber (ADF), and acid detergent lignin (ADL) were determined by using a Fibertec apparatus (Foss Tecator AB, Höganäs, Sweden) with a measuring range of 0.1% to 100% with a repeatability of ±1%. For details of the analysis, refer to the Supporting Information. Cellulose, hemicellulose, and lignin contents were calculated as follows:

$$Hemicellulose = NDF - ADF \tag{1}$$
$$Cellulose = ADF - ADL \tag{2}$$
$$Lignin = ADL \tag{3}$$

2.6 Sugar determination

Individual neutral sugars were released from each fiber via acid hydrolysis and were then determined by gas chromatography in accordance with the procedure described by Blakeney et al.[39] Samples were first treated with 72% H_2SO_4 for 1 h at 30 °C. Then, acid concentration was adjusted to 1 M and maintained at 100 °C for 3 h. Sugar content was determined using a Hewlett-Packard HP6890 gas chromatograph (Agilent, Palo Alto, CA, USA) equipped with a flame ionization detector and a high-performance capillary column HP1-methylsiloxane (30 cm × 320 μm, 0.25 μm, SGE Pty. Ltd., Melbourne, Australia). 2-Deoxyglucose (internal standard), glucose, xylose, arabinose, mannose, and galactose solutions (Sigma-Aldrich, St. Louis, USA), were used as standards. Measurements were taken at least twice.

2.7 Morphology Observation

The morphology of the raw materials and treated fibers was observed using Hitachi S-4800 SEM (Hitachi High Technologies America, Inc., USA). The samples were coated with gold by an ion sputter coater and observed under SEM at 15 kV. Morphological changes in all fibers during treatment were characterized using AFM, which was conducted with a Bruker Multimode 8 (Bruker Corporation, Billerica, MA, USA) AFM in tapping mode at constant oscillation frequency. Images were scanned in tapping mode and in air using silicon cantilevers and a scan rate of 1 Hz. The results of the images were calculated using NanoScope Analysis software. The diameter of individual CNFs was examined by JEOL JEM- 1200EX TEM (JEOL Inc., Tokyo, Japan). A drop of diluted nanofiber suspension was deposited on a carbon-coated grid and allowed to dry at room temperature. Images were taken at 120 kV. Fiber diameters were estimated by Nano Measure software. At least 300 measurements were taken to obtain the distribution of individual fiber diameters.

2.8 Structure Characterization

FTIR spectroscopy was used to examine changes in fiber structure during treatments. The spectrum of each sample was recorded with a Thermo Scientific Nicolet iN10 (Thermo Electron Corp., USA). Fibers were ground and blended with KBr. Then, the mixture was pressed into thin, transparent pellets. The FTIR spectrum of each sample was obtained at 4000–400 cm^{-1} with a resolution of 4 cm^{-1}. The XRD patterns of the fibers at different stages were obtained using Bruker AXS D8 Focus (Bruker AXS Inc., Madison, WI, USA) that was

equipped with a high-power point focus Cu–kα target and a graphite monochromator to eliminate Cu–kβ lines. Scattered radiation was detected at $2\theta = 10°–40°$ at a scan rate of 4°/min.

The crystallinity index (C_I) was calculated from the height of the 200 peak (I_{200}, $2\theta = 22.6°$) and the minimum intensity between the 200 and 110 peaks (I_{am}, $2\theta = 18°$) in accordance with Segal's method,[40] as shown in Eq.4:

$$C_I(\%) = \left(1 - \frac{I_{am}}{I_{200}}\right) \times 100 \tag{4}$$

Where I_{200} represents both crystalline and amorphous material and I_{am} represents amorphous material.

2.9 Thermal testing

Thermal analysis was conducted to compare the degradation characteristics and thermal behavior of the fibers during processing. Samples were analyzed using a TGA/DSC 1 thermogravimetric analyzer (Mettler Toledo Corporation, Switzerland). Samples were heated from room temperature to 700 °C under a nitrogen atmosphere at a heating rate of 10 °C/min.

3. Result and discussion

3.1 Change in the chemical composition of the fibers during treatments

WS fibers were subjected to steam explosion, acid treatment, microwave-assisted hydrolysis, and microfluidization. The chemical composition of the fibers was determined after each treatment. The NDF, ADF, and ADL determination results are shown in Table S3 (Supporting Information). The calculation results for the three main fiber components and the content of ash are presented in Figure 16. Among all the tested fibers, raw fiber contained the highest percentage of hemicellulose, lignin, ash and the lowest percentage of cellulose. Hemicellulose, lignin and ash contents decreased, and cellulose content increased after steam explosion. This finding indicated that during steam explosion, the lignocellulosic fraction was degraded, the hemicellulosic fraction was partially hydrolyzed, and the lignin fraction was depolymerized.[41] Hemicellulose and lignin contents further decreased and cellulose content further increased after microwave-assisted hydrolysis. The high solubility of lignin and hemicelluloses was attributed to the cleavage of α-ether linkages between these polymers.[42] Fibers and ash contents did not change during microfluidization. Cellulose content increased from 44.81% in the raw fiber to 94.04% in the final CNFs. Correspondingly, hemicellulose content decreased from 33.41% to 5.54%, lignin content decreased from 8.75% to 1.68% and ash content decreased from 5.87% to 0.15%. Yields of fibers and cellulose were calculated for each treated sample showed in Table S4 (Supporting Information). In the final CNFs fibers, cellulose yield was 23.97±2.03%. The final fibers are expected to possess higher strength than other fibers with lower cellulose content.
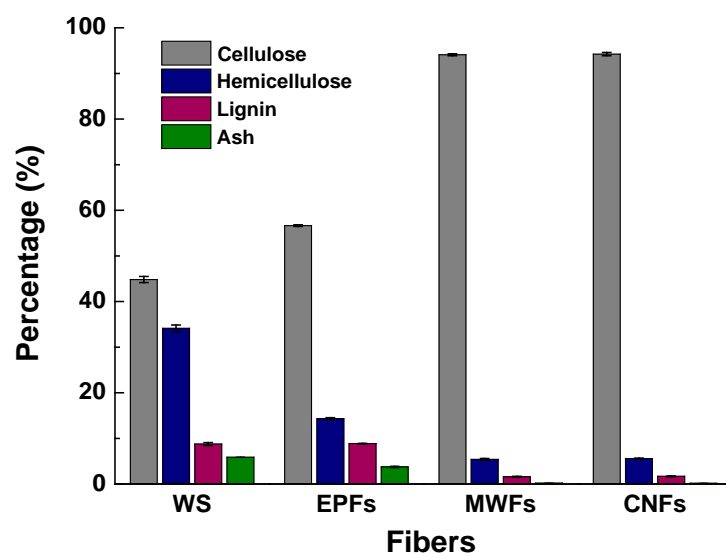
Figure 16. Fiber and ash content of wheat straw (WS), steam-exploded fibers (SEFs), microwave-assisted alkali-hydrolyzed fibers (MWFs), and cellulose nanofibers (CNFs).

3.2 Sugar contents of the fibers

The sugar contents of the fibers after each treatment step are shown in Table 10. Xylose and glucose were identified as the main sugars in the raw materials. Rhamnose, arabinose, mannose, and galactose contents varied from 1.77% to 5.46%. Monosaccharide content decreased because non-cellulosic components were hydrolyzed during the explosion treatment. The content of rhamnose decreased more markedly than those of other sugars. This result indicated that higher proportions of rhamnogalacturonic regions were hydrolyzed during the explosion treatment. The glucose content of MWFs was 98.47%. The contents of other sugars further decreased and ranged from 0.06% to 1.18%. Xylose content considerably decreased, which indicated the successful removal of hemicellulose during microwave-assisted hydrolysis. Moreover, rhamnose disappeared. Sugar contents did not change during microfluidization treatment. These results were consistent with those of fiber determination.

Table 9. Sugar composition of wheat straw (WS), steam-exploded fibers (SEFs), microwave-assisted alkali-hydrolyzed fibers (MWFs), and cellulose nanofibers (CNFs). (Rha: rhamnose; Ara: arabinose; Xyl: xylose; Man: mannose; Glu: glucose; Gal: galactose; TS: total sugars).

Fibers	Rha	Ara	Xyl	Man	Glu	Gal	TS
WS	5.36±2.98	5.46±1.02	28.27±0.89	2.38±0.95	28.02±0.73	1.77±0.57	71.3±7.14
EPFs	0.30±0.30	1.08±0.13	14.66±0.34	0.53±0.16	45.95±2.08	0.48±0.07	63.0±3.08
MWFs	ND[*]	0.25±0.05	1.18±0.13	0.21±0.03	98.47±0.99	0.06±0.01	100.2±1.02
CNFs	ND[*]	0.24±0.03	1.21±0.12	0.20±0.01	97.58±3.30	0.06±0.01	99.3±3.49

ND[*]: not determined.

3.3 Effects of treatments on fiber morphology and CNF dimension

The structures of the treated and untreated WS fibers were investigated using SEM. The 3D simulation schemes of the fibers were also constructed to better reveal the effects of the

treatments on fiber microstructure. Similar to other plant fibers, the raw WS fibers were regularly arranged and clustered together in bundles (Figure 17 (a)). Steam explosion destroyed the structure of the raw fibers, as shown in Figure 17 (b). The fiber bundles were loosened after steam explosion. The damage and the decomposition of hemicellulose and other non-cellulosic components loosened the fiber bundles, thus enabling chemicals to access the peripheral portions and cementing materials of the raw fibers. Microwave-assisted hydrolysis caused superficial, structural, and chemical changes in the fibers (Figure17(c)). The fibers separated into individual fibrils with an average diameter of approximately 10 μm, which was considerably lower than the average diameters of the fiber bundles prior to chemical treatment. Hemicelluloses, lignin, and pectin, the cementing materials around the fiber bundles, were dissolved. SEM micrographs revealed that the fibers shortened during chemical processing. Figure 17(d) presents the SEM image of the WS CNFs after microfluidization. The mechanical treatment resulted in the defibrillation of the CNFs from the cellulose fiber. Moreover, SEM images showed that the fibers aggregated. The diameters of the nanofiber bundles were 10–40 nm.

Figures 17(e) and 17(f) show the TEM images and diameter distribution of the prepared CNFs. The TEM images also revealed that the individual CNF bundles possessed widths of 10–40 nm and that individual fibers possessed widths of approximately 5 nm. Agglomeration has been reported in nanofibers that were obtained via different treatment methods and from various materials.[26, 43] As measured from the enlarged TEM images shown in Figure 17(f), the average fiber width was 5.42 nm. Approximately 76.4% of the individual fibers were 4.75 nm to 6.25 nm in width.
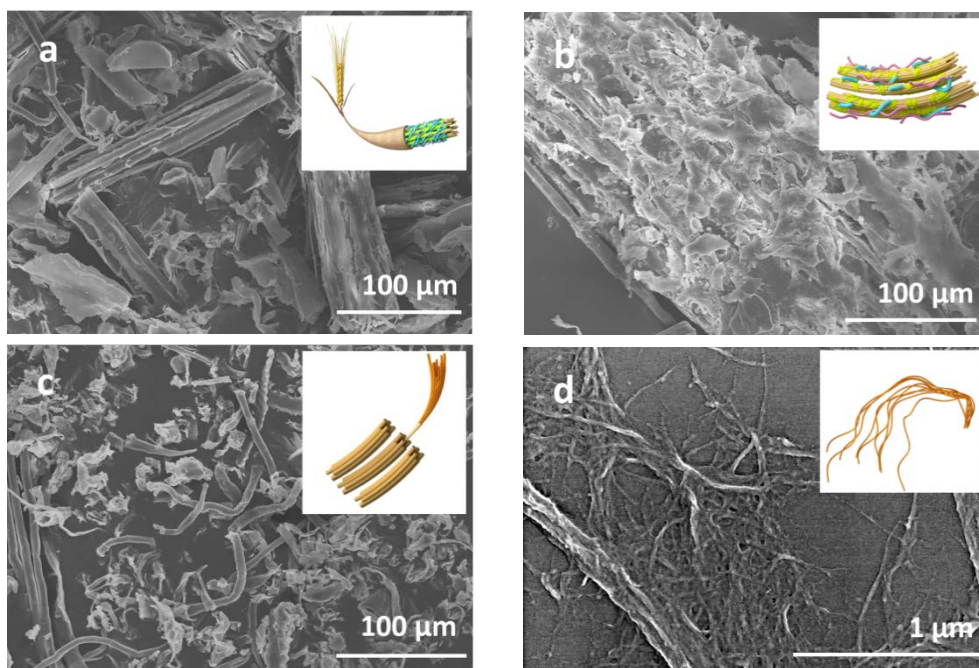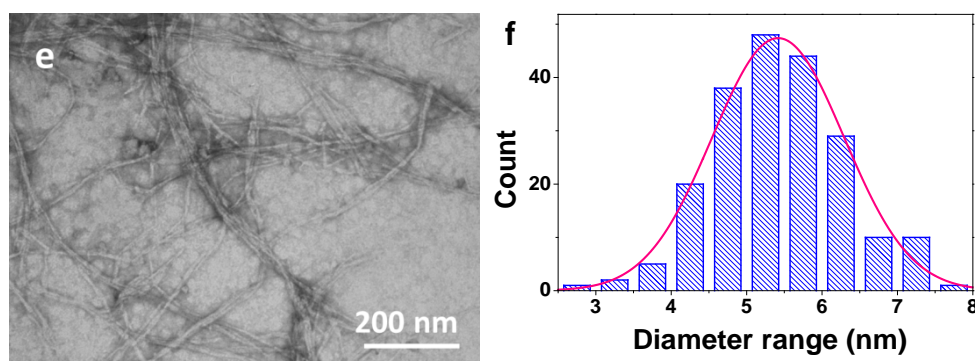
Figure 17. SEM image and simulation scheme of (a) wheat straw (WS), (b) steam-exploded fibers (SEFs), (c) microwave-assisted alkali-hydrolyzed fibers (MWFs), and (d) cellulose nanofibers (CNFs); TEM images (e) and (f) diameter range of cellulose nanofibers.

3.4 Microstructure of fibers

NanoScope Analysis software with AFM topography was employed to analyze the surface roughness (R_a/R_q) and to measure the heights from three sites of each fiber sample. The AFM topography, 3D image, and height profile of WS, SEFs, MWFs, and CNFs are shown in Figures 19(a) to 19(d). And the roughness (R_a/R_q) and heights of the fibers are listed in Table 2. As shown in Figure 19(a) and Table 2, the raw fibers exhibited a rough topography with a high R_a/R_q value of 0.695. These characteristics resulted from the complex structures of hemicellulose, lignin, pectin, and other components of the raw materials. The height of WS was as high as 169.5 nm, indicating large particles. After steam explosion, the R_a/R_q value negligibly decreased but height drastically decreased. As shown in Figure 19(b) and Table 11, the3D image presented numerous sharp instead of wide peaks. These changes indicated that non-cellulosic material was removed as a result of considerable breakage during this process. SEM profiles also confirmed this result. After microwave-assisted hydrolysis (Figure 19(c) and Table 11), the fibers exhibited notably smoother surfaces and a lower R_a/R_q of 0.548, which indicated that the surfaces of the isolated cellulose fibers were cleaner and smoother. The obtained CNFs had considerably sharper and wider peaks, which reflected the fine crystalline cellulose components of the fiber structure (Figure 19(d) and Table 11). Kaushik and Singh et al. obtained similar results after subjecting nanofibers to acid treatment. [31] In this study, the high R_a/R_q value (0.738) indicated the presence of an increasing number of pits on the surfaces of the fibers, which provided evidence for the isolation of nanoscale fibers. The height profile provided more information on CNF width. Individual fibers had widths of less than 10 nm, whereas those of aggregated CNF bundles reached dozens of nanometers.
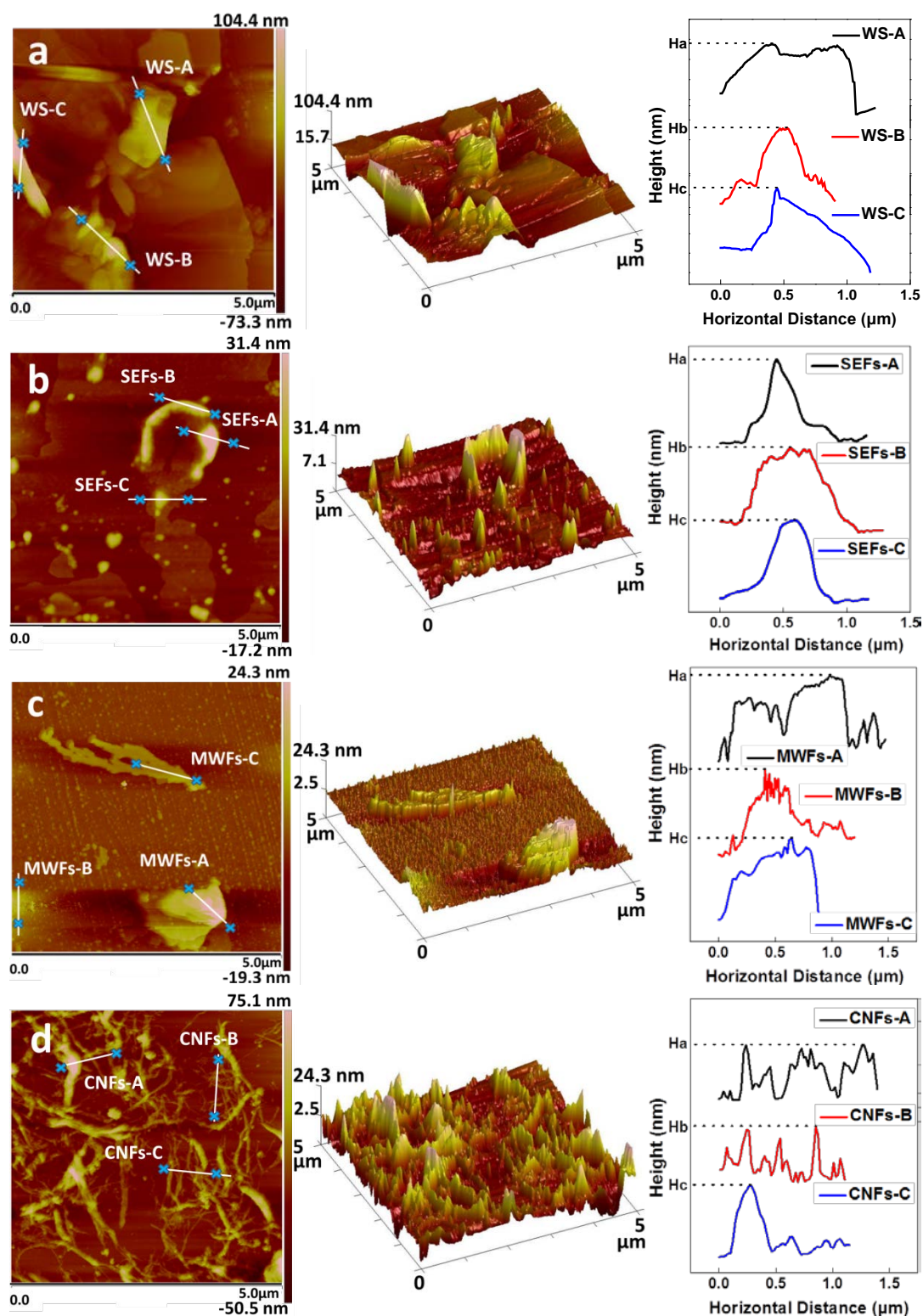
Figure 18. AFM topography, 3D image, and height profile of (a) wheat straw (WS), (b) steam-exploded fibers (SEFs), (c) microwave-assisted alkali-hydrolyzed fibers (MWFs), and (d) cellulose nanofibers (CNFs).

Table 10. Roughness (Ra/Rq) and heights of wheat straw (WS), steam-exploded fibers (SEFs), microwave-assisted hydrolyzed fibers (MWFs), and cellulose nanofibers (CNFs).

Fibers	Ra (nm)	Rq (nm)	Ra/Rq	Height (nm)		
				Ha	Hb	Hc

WS	14.6	21.0	0.695	70.21	83.66	169.5
SEFs	3.27	5.43	0.602	25.40	29.74	48.14
MWFs	2.34	4.27	0.548	8.12	17.42	31.53
CNFs	12.1	16.4	0.738	21.75	21.83	97.52

3.5 Change in components and structure based on FTIR results

FTIR was carried out to illustrate the changes in the chemical constituents of the fibers before and after each treatment. The FTIR spectra of the untreated and treated WS fibers are shown in Figure 20. Similar to the results of other works,[26, 44-46] two main absorption regions were observed for all fibers: one in a low wavelength region from 550 cm^{-1} to 1750 cm^{-1}, and the other situated at a higher wavelength region between 2900 cm^{-1} and 3450 cm^{-1}. The peaks in the 3429 cm^{-1}–3442 cm^{-1} region corresponded to the O–H stretching band. The absorption band at 2927 cm^{-1} was attributed to C–H stretching vibrations in cellulose and hemicellulose.[26] Furthermore, the increasing importance of peaks at 992 and 897 cm^{-1} that corresponded to the C–H glycosidic deformation of cellulose was consistent with increasing cellulosic content.[47] The peaks at 1253 and 1509 cm^{-1} in the spectrum of raw fiber corresponded to the aromatic skeletal vibrations of lignin.[48] The peak at 1734 cm^{-1} in the spectra of both untreated and exploded WS was attributed to the acetic and uronic ester groups in hemicelluloses and the ester linkages of the carboxylic group of ferulic and *p*-coumaric acids in lignin or hemicelluloses, as previously reported.[26,44] As seen from Figure 19, peaks at 1254, 1509, and 1734 cm^{-1} were virtually absent from the spectra of fibers subjected to microwave-assisted hydrolysis and microfluidization. The absence of these peaks indicated the nearly complete cleavage of both hemicellulose and lignin. Therefore, cellulose could be isolated via explosion treatment and microwave-assisted alkali hydrolysis. Moreover, the chemical components of the fibers did not change during mechanical treatment.
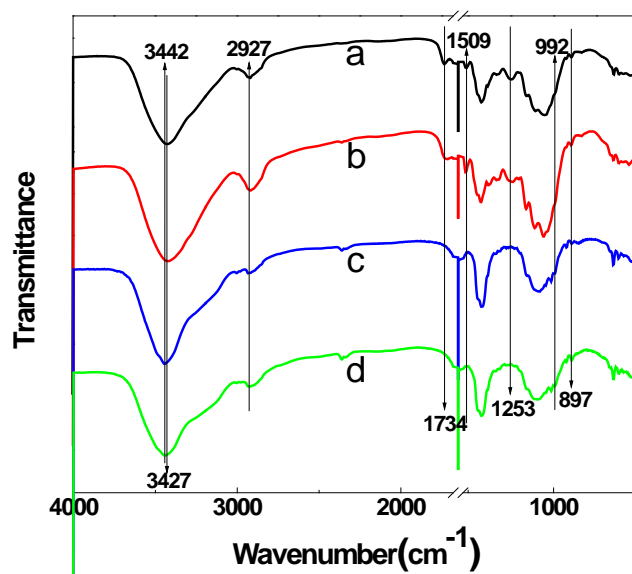

Figure 19. FTIR spectra of (a) wheat straw (WS), (b) steam-exploded fibers (SEFs), (c) microwave-assisted alkali-hydrolyzed fibers (MWFs), and (d) cellulose nanofibers (CNFs).

3.6 Crystal structure and crystallinity of the fibers

The XRD patterns of both raw and treated fibers are presented in Figure 20. XRD analysis was conducted to investigate the crystalline features of the fibers and the relationship between fiber structures and properties. Peaks at $2\theta = 15.4°$ and $21.7°$ provided confirmation that only cellulose I was present in the native WS cellulose, as shown in Figure 20. Low crystallinity was observed for the fibers given that crystalline domains were embedded in a matrix of amorphous components, such as hemicelluloses, lignin, and pectin. As shown in Table 12, crystallinity increased after steam explosion and drastically increased after microwave-assisted alkali hydrolysis. The crystallinity index increased from 45.85% to 48.72% and was 62.15% after microwave-assisted alkali hydrolysis (Table 12). This result was attributed to the effective removal of non-crystalline components. However, the crystallinity index slightly decreased after microfluidization because of the severe mechanical force that was used during this process.

Moreover, a slight plateau at the scattering angle of $21.7°$ was observed. This plateau turned into two peaks after microwave-assisted alkali hydrolysis (Figure 21), which indicated the crystalline transformation of cellulose fibers. Comparative $21.7°/20.0°$ scans of the raw materials and acid-treated fibers revealed differences in cellulose I/cellulose II content.[32] After microwave-assisted alkali treatment, the polymorphic modification of the crystalline state of the samples from cellulose I to cellulose II was observed, similar to that previously reported in other works.[32, 49] For example, Cherian et al. reported the crystalline transformation of pineapple leaf fibers after the first treatment step of alkali steam explosion with 2% NaOH.[32] They reported cellulose I/cellulose II ratios of 0.43 for fibers after alkali steam explosion and 0.93 for the final processed nanofibers. A similar cellulose I/cellulose II content was obtained in this work. Approximately half of cellulose I was converted to cellulose II during the 20-min microwave-assisted alkali treatment. This finding may be attributed to the previous steam explosion treatment, which improved the accessibility of cellulose to chemicals, or to the effectiveness of the microwave treatment. Further investigation will be conducted in later works.
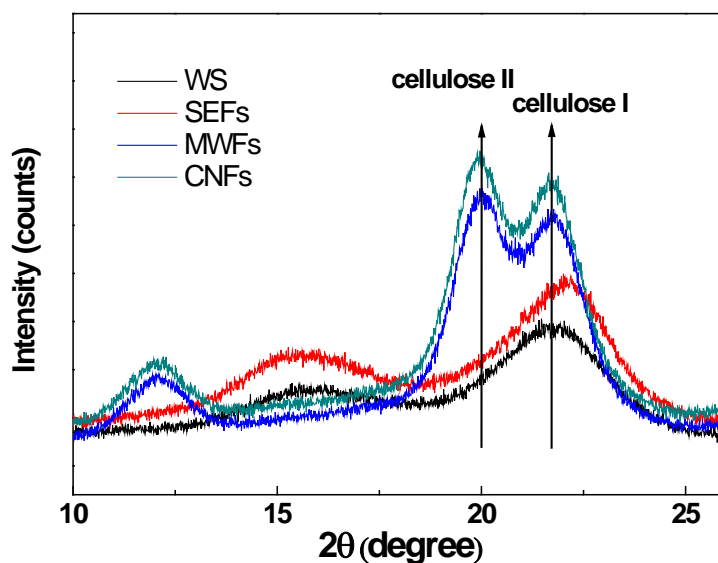
Figure 20. XRD patterns of wheat straw (WS), steam-exploded fibers (SEFs),

microwave-assisted alkali-hydrolyzed fibers (MWFs), and cellulose nanofibers (CNFs).

Table 11. Crystallinity index and thermal behaviors of wheat straw (WS), steam-exploded fibers (SEFs), microwave-assisted alkali-hydrolyzed fibers (MWFs), and cellulose nanofibers (CNFs).

| Fibers	Crystallinity index (Cellulose I) (%)	I21.7/I20.0	Tp (°C)	Rtp (%)	Residue at 700 °C (%)
WS	45.85	—	327.6	51.32	22.96
SEFs	48.72	—	372.4	44.60	16.83
MWFs	62.15	0.936	351.4	42.20	16.44
CNFs	58.62	0.928	367.2	37.88	7.24

3.7 Thermal properties of the fibers

The thermal properties of the CNFs are crucial to their intended use in biocomposites. TGA was conducted to study the thermal stability and degradation characteristics of the fibers at various stages of treatment. The TG and derivative thermogravimetric (DTG) curves of the raw, exploded, microwave-assisted alkali-hydrolyzed, and microfluidized fibers are shown in Figure 21 (a) and (b). The results clearly illustrated that the thermal stability of the fibers increased after the series of treatments. The increase in thermal stability likely resulted from the removal of non-cellulosic material and the increased degree of structural order. A higher crystalline structure requires higher degradation temperatures.[50]

The thermal behaviors of raw and treated WS fibers are presented in Table 12. The peak temperature T_p was determined from the DTG peak at which the maximum decomposition rate was obtained. The residue weight percentage that corresponded to the peak temperature was symbolized by Rtp. At 700 °C, residual content decreased from 22.96% of the raw material to 7.24% of the resulting nanofibers. The T_p of exploded fibers increased from 327.6 °C (Rtp of 51.32%) to 372.4 °C (Rtp of 44.60%) given the decomposition of non-cellulosic materials. The temperature with the maximum degradation rate of microwave-assisted hydrolyzed fibers decreased to 351.4 °C (Rtp 42.20%) because of cellulose decomposition. This result is consistent with that reported in Chandra's study.[44] The DTG of microfluidized fibers showed a sharp peak at 367.2 °C, which indicated the decomposition of crystalline cellulose.

Therefore, the higher temperature of thermal decomposition and lower residual mass of the final fibers are related to the partial removal of hemicellulose and lignin from the fibers, as well as the higher crystallinity of cellulose. These results are consistent with the results for crystallinity and FTIR measurements.
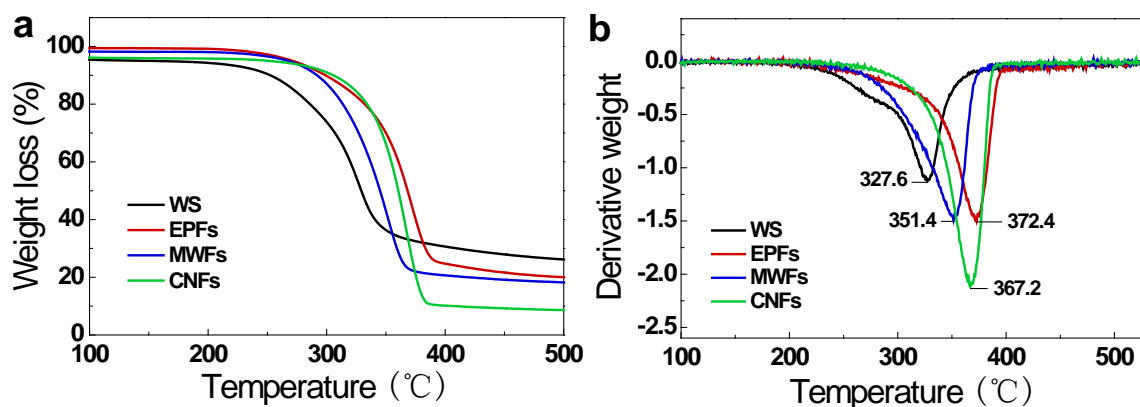
Figure 21. (a) TG curve and (b) DTG curve of wheat straw (WS), steam-exploded fibers (SEFs), microwave-assisted alkali-hydrolyzed fibers (MWFs), and cellulose nanofibers (CNFs).

4. Conclusions

Cellulose nanofibers were extracted from wheat straw through an environmentally friendly, multi-step process that combined steam explosion, microwave-assisted hydrolysis, and microfluidization. The raw materials and processed fibers were analyzed to better understand the effect of each treatment step; to assess the chemical composition, morphology, structural features, and thermal behavior of the obtained fibers; and to evaluate the potential applications of the processed nanofibers in biocomposites. Chemical analysis showed that cellulose content increased from 44.81% to 94.23%, whereas hemicellulose and lignin contents significantly decreased from 33.41% and 8.75% to 5.54% and 1.68% respectively. These results were validated by the increased glucose content that was determined via sugar analysis. SEM revealed the loosening effect of steam explosion, the purifying effect of microwave-assisted hydrolysis, and the decreases in fiber diameter during treatment. Surface roughness and height profile changes of the fibers analyzed with the AFM results also confirmed the changes both in the chemical components and structure. TEM images revealed long, loose nanofiber bundles with widths of 10 nm to 40 nm, as well as an entangled network of cellulose fibers with an average individual diameter of 5.42 nm. FTIR measurements indicated that the treatment process partially removed non-cellulosic materials from the raw fibers. The crystallinity index increased from 45.85% to 58.62% and nearly half of cellulose I was converted to cellulose II during the process. The T_p of the raw fibers increased from 327.6 °C to 367.2 °C after the treatments caused by the decomposition of non-cellulosic materials, which showing the enhanced thermal properties of the processed nanofibers. The increased thermal stability of the nanofibers was related to the higher crystallinity of cellulose after the removal of hemicellulose and lignin components from the raw fiber.

The experimental results showed that thermally stable CNFs with high aspect ratio and high purity could be prepared from WS using the environmentally friendly methods of steam explosion, microwave-assisted hydrolysis, and microfluidization. The results of this multi-step isolation method should further stimulate research interest in the development of

environmentally friendly methods for nanofiber isolation from natural fibers. Given their high purity, high aspect ratio, thermal stability, and strength, the CNFs obtained in this study have potential applications in the auto industry, chemical industry, agriculture, environmental protection, and medical biocomposites.

Acknowledgments

References

(1) Abe, K.; Yano, H. Comparison of the characteristics of cellulose microfibril aggregates of wood, rice straw and potato tuber. *Cellulose* **2009**, *16* (6), 1017−1023.

(2) Wu, C. N.; Yang, Q.; Takeuchi, M.; Saito, T.; Isogai, A. Highly tough and transparent layered composites of nanocellulose and synthetic silicate. *Nanoscale* **2014**, *6* (1), 392−399.

(3) Sakurada, I.; Nukushina, Y.; Ito, T. Experimental determination of the elastic modulus of crystalline regions in oriented polymers. *J. Polym. Sci*. **1962**, *57* (165), 651−660.

(4) Koga, H.; Nogi, M.; Komoda, N.; Nge, T. T.; Sugahara, T.; Suganuma, K. Uniformly connected conductive networks on cellulose nanofiber paper for transparent paper electronics. *NPG Asia Mater*. **2014**, *6* (3), e93.

(5) Kaushik, A.; Singh, M.; Verma, G. Green nanocomposites based on thermoplastic starch and steam exploded cellulose nanofibrils from wheat straw. *Carbohydr. Polym.* **2010**, *82* (2), 337−345.

(6) Fatah, I. Y. A.; Khalil, H. P. S.; Hossain, M. S.; Aziz, A. A.; Davoudpour, Y.; Dungani, R.; Bhat, A. Exploration of a chemo-mechanical technique for the isolation of nanofibrillated cellulosic fiber from oil palm empty fruit bunch as a reinforcing agent in composites materials. *Polymer*s **2014**, *6* (10), 2611−2624.

(7) Lu, B.; Lin, F.; Jiang, X.; Cheng, J.; Lu, Q.; Song, J.; Chen, C.; Huang, B. One-pot assembly of microfibrillated cellulose reinforced PVA–borax hydrogels with self-healing and pH-responsive properties. *ACS Sustainable Chem. Eng.* **2016**, *5* (1), 948−956.

(8) Wan, C.; Li, J. Facile synthesis of well-dispersed superparamagnetic γ-Fe2O3 nanoparticles encapsulated in three-dimensional architectures of cellulose aerogels and their applications for Cr (VI) removal from contaminated water. *ACS Sustainable Chem. Eng.* **2015**, *3* (9), 2142−2152.

(9) Sehaqui, H.; Michen, B.; Marty, E.; Schaufelberger, L.; Zimmermann, T. Functional cellulose nanofiber filters with enhanced flux for the removal of humic acid by adsorption. *ACS Sustainable Chem. Eng.* **2016**, *4* (9), 4582–4590.

(10) Wen, Y.; Zhu, X.; Gauthier, D. E.; An, X.; Cheng, D.; Ni, Y.; et al. Development of poly (acrylic acid)/nanofibrillated cellulose superabsorbent composites by ultraviolet light induced polymerization. *Cellulose* **2015**, *22* (4), 2499–2506.

(11) Abe, K.; Yano, H. Formation of hydrogels from cellulose nanofibers. *Carbohydr. Polym.* **2011**, *85* (4), 733–737.

(12) Rodrigues, F. H. A.; Spagnol, C.; Pereira, A. G. B.; Martins, A. F.; Fajardo, A. R.; Rubira, A. F.; Muniz, E. C. Superabsorbent hydrogel composites with a focus on hydrogels containing nanofibers or nanowhiskers of cellulose and chitin. *J. Appl. Polym. Sci.* **2014**, 131 (2), 39725–39737.

(13) Wen, Y.; Zhu, X.; Gauthier, D. E.; An, X.; Cheng, D.; Ni, Y.; et al. Development of poly (acrylic acid)/nanofibrillated cellulose superabsorbent composites by ultraviolet light induced polymerization. *Cellulose* **2015**, *22* (4), 2499–2506.

(14) Wang, Z.; Tammela, P.; Strømme, M.; Nyholm, L. Nanocellulose coupled flexible polypyrrole@ graphene oxide composite paper electrodes with high volumetric capacitance. *Nanoscale* **2015**, *7* (8), 3418–3423.

(15) Jin, J.; Lee, D.; Im, H. G.; Han, Y. C.; Jeong, E. G.; Rolandi, M.; Choi, K. C.; Bae, B. S. Chitin nanofiber transparent paper for flexible green electronics. *Adv. Mater.* **2016**, *28* (26), 5169–5175.

(16) Sehaqui, H.; Salajková, M.; Zhou, Q.; Berglund, L. A. Mechanical performance tailoring of tough ultra-high porosity foams prepared from cellulose I nanofiber suspensions. *Soft Matter* **2010**, *6* (8), 1824–1832.

(17) Chin, S. F.; Romainor, A. N. B.; Pang, S. C. Fabrication of hydrophobic and magnetic cellulose aerogel with high oil absorption capacity. *Mater. Lett.* **2014**, *115*, 241–243.

(18) Feng, J.; Nguyen, S. T.; Fan, Z.; Hai, M. D. Advanced fabrication and oil absorption properties of super-hydrophobic recycled cellulose aerogels. *Chem. Eng. J.* **2015**, *270*, 168–175.

(19) Gao, K.; Shao, Z.; Li, J.; Wang, X.; Peng, X.; Wang, W. Cellulose nanofiber-graphene all solid-state flexible supercapacitors. *J. Mater. Chem. A* **2011**, *1* (1), 63–67.

(20) Jiang, D.; Zhuang, D.; Fu, J.; Huang, Y.; Ken, K. Bioenergy potential from crop residues in China: Availability and distribution. *Renew. Sus. Energ. Rev.* **2012**, *16* (3), 1377–1382.

(21) Zhang, L.; Liu, Y.; Hao, L. Contributions of open crop straw burning emissions to PM2. 5 concentrations in China. *Environ. Res. Lett.* **2016**, *11* (1), 014014.

(22) Ferguson, W. S. The digestibility of wheat straw and wheat-straw pulp. *Biochem. J.* **1942**, *36*, 786.

(23) Sharma, B.; Agrawal, R.; Singhania, R. R.; Satlewal, A.; Mathur, A.; Tuli, D.; Adsul, M. Untreated wheat straw: Potential source for diverse cellulolytic enzyme secretion by Penicillium janthinellum EMS-UV-8 mutant. *Bioresour. Technol.* **2015**, *196*, 518–524.

(24) Alemdar, A.; Sain, M. Isolation and characterization of nanofibers from agricultural residues–Wheat straw and soy hulls. *Bioresour. Technol*. **2008**, *99* (6), 1664–1671.

(25) Chen, W.; Yu, H.; Liu, Y.; Hai, Y.; Zhang, M.; Chen, P. Isolation and characterization of cellulose nanofibers from four plant cellulose fibers using a chemical-ultrasonic process. *Cellulose* **2011**, *18*(2), 433-442.

(26) Kaushik, A.; Singh, M. Isolation and characterization of cellulose nanofibrils from wheat straw using steam explosion coupled with high shear homogenization. *Carbohydr. Res.* **2011**, *346* (1), 76–85.

(27) Singh, M.; Kaushik, A.; Ahuja, D. Surface functionalization of nanofibrillated cellulose extracted from wheat straw: Effect of process parameters. *Carbohydr. Polym.* **2016**, *150*, 48–56.

(28) Sánchez, R.; Espinosa, E.; Domínguez-Robles, J.; Loaiza, J. M.; Rodriguez, A. Isolation and characterization of lignocellulose nanofibers from different wheat straw pulps. *Int. J. Biol. Macromol.* **2016**, *92*, 1025–1033.

(29) Nuruddin, M.; Hosur, M.; Triggs, E.; et al. Comparative study of properties of cellulose nanofibers from wheat straw obtained by chemical and chemi-mechanical treatments. ASME 2014 International Mechanical Engineering Congress and Exposition. American Society of Mechanical Engineers, **2014**, V014T11A042–V014T11A042.

(30) Shamsabadi, M. A.; Behzad, T.; Bagheri, R. Optimization of acid hydrolysis conditions to improve cellulose nanofibers extraction from wheat straw. *Fiber. Polym.* **2015**, *16* (3), 579–584.

(31) Deepa, B.; Abraham, E.; Cherian, B. M.; Bismarck, A.; Blaker, J. J.; Pothan, L. A.; Leao, A. l.; Souza, S. F.; Kottaisamy, M. Structure, morphology and thermal characteristics of banana nano fibers obtained by steam explosion. *Bioresour. Technol*. **2011**, *102* (2), 1988–1997.

(32) Cherian, B. M.; Leão, A. L.; Souza, S. F.; Thomas, S.; Pothan, L.A.; Kottaisamy, M. Isolation of nanocellulose from pineapple leaf fibres by steam explosion. *Carbohydr. Polym.* **2010**, *81* (3), 720–725.

(33) Nechyporchuk, O.; Belgacem, M. N; Bras, J. Production of cellulose nanofibrils: a review of recent advances. *Ind. Crop. Prod.* **2016**, *93*, 2-25.

(34) Jacquet, N.; Quievy, N.; Vanderghem, C.; Janas, S.; Blecker, C.; Wathelet, B.; Devaux, J.; Paquot, M. Influence of steam explosion on the thermal stability of cellulose fibres. *Polym. Degrad. Stabil.* **2011**, *96* (9), 1582–1588.

(35) Jacquet, N.; Vanderghem, C.; Danthine, S.; Quievy, N.; Blecker, C.; Devaux, J.; Paquot, M. Influence of steam explosion on physicochemical properties and hydrolysis rate of pure cellulose fibers. *Bioresour. Technol.* **2012**, *121*, 221–227.

(36) Aguedo, M.; Ruiz, H. A.; Richel, A. Non-alkaline solubilization of arabinoxylans from destarched wheat bran using hydrothermal microwave processing and comparison with the hydrolysis by an endoxylanase. *Chem. Eng. Proc.: Proc. Int.* **2015**, *96*, 72–82.

(37) Soest V, P. J. Use of detergents in the analysis of fibrous feeds. 2. A rapid method for the determination of fiber and lignin. *J. Assoc. Official Agri. Chemist.* **1963**, *46*, 829–835.

(38) Soest V, P. J.; Wine, R. H. Use of detergents in the analysis of fibrous feeds. IV. Determination of plant cell-wall constituents. *J. Assoc. Off. Anal. Chem.* **1967**, *50* (1), 50–55.

(39) Blakeney, A. B.; Harris, P. J.; Henry, R. J.; Stone, B. A. A simple and rapid preparation of alditol acetates for monosaccharide analysis. *Carbohydr. Res.* **1983**, *113* (2), 291–299.

(40) Segal, L.; Creely, J. J.; Martin, A. E.; Conrad, C. M. An empirical method for estimating the degree of crystallinity of native cellulose using the X-ray diffractometer. *Textile. Res. J.* **1959**, *29* (10),786–794.

(41) Cherian, B. M.; Pothan, L. A.; Nguyen-Chung, T.; Menning, G.; kottaisamy, M.; Thomas, S. A novel method for the synthesis of cellulose nanofibril whiskers from banana fibers and characterization. *J. Agr. Food Chem.* **2008**, *56* (14), 5617–5627.

(42) Xiao, B.; Sun, X. F.; Sun, R. C. Chemical, structural, and thermal characterizations of alkali-soluble lignins and hemicelluloses, and cellulose from maize stems, rye straw, and rice straw. *Polym. Degrad. Stabil.* **2001**, *74* (2), 307–319.

(43) Zuluaga, R.; Putaux, J. L.; Cruz, J.; Vélez, J.; Mondragon, I.; Gañán, P. Cellulose microfibrils from banana rachis: Effect of alkaline treatments on structural and morphological features. *Carbohydr. Polym.* **2009**, *76* (1), 51–59.

(44) Chandra, J.; George, N.; Narayanankutty, S. K. Isolation and characterization of cellulose nanofibrils from arecanut husk fibre. *Carbohydr. Polym.* **2016**, 142: 158–166.

(45) Velásquez-Cock, J.; Gañán, P.; Posada, P.; Castro, C.; Serpa, A.; et al. Influence of combined mechanical treatments on the morphology and structure of cellulose nanofibrils: Thermal and mechanical properties of the resulting films. *Ind. Crop. Prod.* **2016**, *85*, 1–10.

(46) Xu, C.; Zhu, S.; Xing, C.; Xing, C.; Li, D.; Zhu, N.; Zhou, H. Isolation and properties of cellulose nanofibrils from coconut palm petioles by different mechanical process. *Plos One* **2015**, *10* (4), e0122123.

(47) Avolio, R.; Bonadies, I.; Capitani, D.; Errico, M. E.; Gentile, G.; Avella, M. A multitechnique approach to assess the effect of ball milling on cellulose. *Carbohydr. Polym.* **2012**, *87* (1), 265–273.

(48) Mandal, A.; Chakrabarty, D. Isolation of nanocellulose from waste sugarcane bagasse (SCB) and its characterization. *Carbohydr. Polym.* **2011**, *86* (3), 1291–1299.

(49) Kim, N. H.; Imai, T.; Wada, M.; Sugiyama, J. Molecular directionality in cellulose polymorphs. *Biomacromolecules* **2006**, *7* (1), 274-280.

(50) Yang, P.; Kokot, S. Thermal analysis of different cellulosic fabrics. *J. Appl. Polym. Sci.* **1996**, *60* (8), 1137–1146.

Supporting information

Determination of total chemical composition of WS.

Fibers were determined in accordance with the Van Soest method.[1,2]

The determination of protein, fat, ash, starch, and water contents were performed as follows:

Protein content: The total nitrogen (TN) content of starch was determined with the Kjeldahl method. Protein contents were calculated as TN × 6.25. Data were expressed as percent of dry weight.

Fat content: First, 5 g of sample was mixed with 50 mL chloroform/methanol (2/1, v/v) and shacked overnight. Then, the sample was filtered and then extracted with 0.58% NaCl. The organic phase was collected, dried, and weighed.

Ash content: Crucibles were first dried at 105 °C for 1 hour and weighed (W_C). Then, 1 g sample (dry matter, W_S) was added to each crucible, which was then heated to 525 °C in 2h and maintained for 3h in a muffle furnace. Finally, the crucibles were weighed (W_{ash}).

$$\omega_{ash} = \frac{W_{ash} - W_C}{W_S} \times 100\% \tag{S1}$$

Starch content: Total starch content was determined from 100-mg samples via the α-amylase method using the Megazyme Total Starch Assay Kit (Megazyme Ltd, Bray, Ireland).

Water content: One gram of sample (Ww) was kept overnight at 105 °C. The dry matter (Wd) was then obtained.

$$\omega_{water} = \frac{(W_w - W_d)}{W_d} \times 100 \tag{S3}$$

Table S2. Chemical composition of wheat straw (WS).

Composition of WS (%)		
Fibers	Cellulose	44.81±0.67
	Hemicellulose	34.11±0.75
	Lignin	8.75±0.31
Others	Protein	2.38±0.05
	Fat	2.29±0.18
	Ash	5.87±0.01
	Starch	0.13±0.01
	Water	5.10±0.02

Treatment processes and fiber morphology after each treatment

Scheme S1 shows that CNFs were prepared from WS via an environmentally friendly, multi-step process that combined steam explosion, microwave-assisted hydrolysis, and microfluidization. First, WS was pretreated at 100 °C and 3.0 MPa for 2 min to obtain SEFs. Then, the SEFs were further pretreated with acid hydrolysis. The dried fibers were soaked in 1

M HCl solution with stirring at 80 ± 1 °C for 2 h. A total of 1.5 g sample (dry weight) was suspended in 30 mL of 2% NaOH solution with magnetic stirring at 140 ± 2 °C for 20 min under microwave. Finally, the MWFs were treated in a high-pressure microfluidizer under 150–159 MPa (21,750–23,000 psi). The fiber slurries were diluted to 0.1% solid consistency and passed five times through the microfluidizer chamber to obtain CNFs.
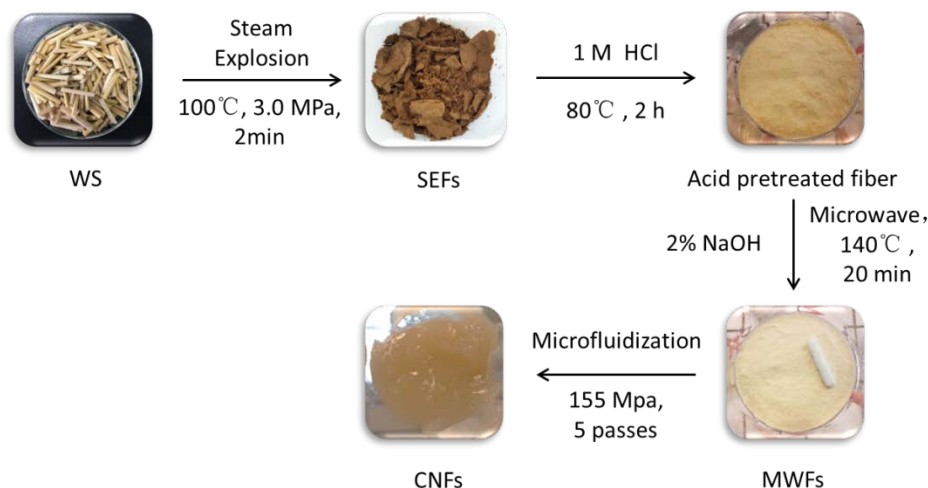
Scheme S1. Process of cellulose nanofiber (CNFs) isolation and digital image of fibers after each treatment.

Determination of NDF, ADF, and ADL

Solution for determination. NDF extraction solution: 93.05 g EDTA, 34.05 g Sodium borate decahydrate, 50 ml triethylene glycol, 22.8 g disodium hydrogen phosphate, and 150 g sodium lauryl sulfate/5L. ADF extraction solution: 140 ml 98% H_2SO_4 and 100 g cetyl trimethylammanium bromide/5L. ADL extraction Solution: 72% H_2SO_4.

Determination of NDF. Crucibles containing 1 g celite were placed in the oven at 105 °C for 1 h and then weighed. A total of 1 g sample (m_0) was added to the corresponding crucible and inserted into the Fibertec® apparatus. Approximately 100 mL preheated NDF extraction solution (~99 °C) and 3 to 4 drops of octanol were added to the sample. The apparatus was then heated and kept boiling for 1 h. Then, the samples were filtered and successively rinsed with preheated distilled water (~99 °C) and acetone thrice. The samples were placed at room temperature to allow the acetone to evaporate. Finally, the crucibles were placed in an oven at 105 °C overnight. The final samples were weighed and designated as m_{NDF}.

Determination of ADF. The process was the same as NDF determination except for the use of ADF extraction solution. The final weight after overnight processing in a 105 °C oven was designated as m_{ADF}.

Determination of ADL. A total of 25 mL of ADL extraction solution was added to each crucible and mixed thoroughly. The reaction was allowed to proceed for 3h. Then, the samples were filtered and rinsed with preheated distilled water (~90 °C) at least five times. The crucibles were then placed in an oven at 105 °C overnight. The samples were weighed and designated as m_{ADL}. To obtain ash content, the crucibles were heated to 525 °C in 2h and then

kept for 3 h in a muffle furnace. Finally, the crucibles were weighed and designated as m_{Ash}.

NDF, ADF, and ADL fiber contents were calculated as follows and are listed in Table S2:

$$NDF = \frac{(m_{NDF} - m_{Ash})}{m_0} \times 100\% \tag{S3}$$

$$ADF = \frac{(m_{ADF} - m_{Ash})}{m_0} \times 100\% \tag{S4}$$

$$ADL = \frac{(m_{ADL} - m_{Ash})}{m_0} \times 100\% \tag{S5}$$

Table S3. Neutral detergent fiber (NDF), acid detergent fiber (ADF), and acid detergent lignin (ADL) of wheat straw (WS), steam-exploded fibers (SEFs), microwave-assisted alkali-hydrolyzed fibers (MWFs), and cellulose nanofibers (CNFs).

Fibers	NDF	ADF	ADL
WS	87.67±0.62	53.56±0.49	8.75±0.31
EPFs	79.79±0.18	65.49±0.13	8.86±0.06
MWFs	102.01±0.13	95.35±0.05	1.57±0.11
CNFs	101.06±0.18	95.66±0.17	1.68±0.08

Table S4. Yields of fibers and cellulose during steam explosion, acid hydrolysis, microwave-assisted alkali hydrolysis and microfluidization.

Fibers	Yield of fibers (%)	Cellulose content (%)	Yield of cellulose (%)
WS	——	44.81±0.67	——
EPFs	32.3±4.56%	56.63±0.19	40.98±3.37
MWFs	13.92±3.21%	94.09±0.22	28.97±2.28
CNFs	11.25±1.44%	94.23±0.35	23.97±2.03

REFERENCE

(1) Soest V, P. J. Use of detergents in the analysis of fibrous feeds. 2. A rapid method for the determination of fiber and lignin. *J. Assoc. Official Agri. Chemist.* **1963**, *46*, 829-835.

(2) Soest V, P. J.; Wine, R. H. Use of detergents in the analysis of fibrous feeds. IV. Determination of plant cell-wall constituents. *J. Assoc. Off. Anal. Chem.* **1967**, *50*, 50-55.

Chapter IV Nanocellulose application in agricultural water-saving materials.
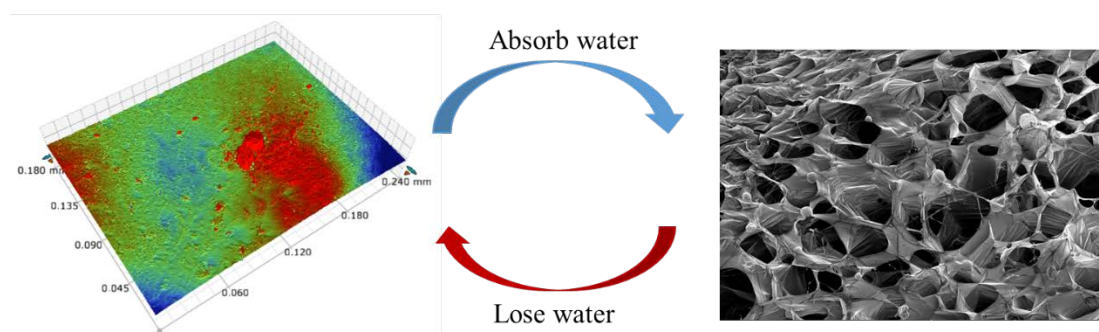
Introduction to Chapter IV

China is a country with huge agricultural production and is also a country being short of water, especially in the north China where water scarcities are more serious. The shortage of water resources in China has badly hindered the sustaining development of economy, society as well as agriculture. Therefore, many water-saving agricultural measurements were put forward according to water resource, distribution characters, and farming system in different areas. Among these agricultural water-saving techniques, the water-saving materials, such as mulching film and superabsorbent polymers (SAPs), have been widely used and extensively popularized in the north and west. While both these water-saving materials have their limitation when applicated in agriculture. As CNC and CNF isolation were discussed in *(Article 2)* and *Chapter III (Article 3* and *Article 4).* The following contents of the thesis (*Chapter IV*) focused on the effects of adding nanocellulose on the properties of the materials.

SAPs are normally used in soil to preserve soil moisture therefore the it's necessary to improve the biodegradablity. Meanwhile, their application in agriculture also requires higher mechanical properties and high performance of water reserving. In *Article 5*, SAPs of acrylamide–acrylate (AA-AM) copolymer and CNF, CNC and MCC were synthesized respectively. The swelling capacities in pure water, in KCl, $CaCl_2$, $FeCl_3$ and 0.9% NaCl solutions were investigated. The abilities of repeated water-absorbing, water retaining capacity in the soil and the mechanical properties of the hydrogels were compared.

Agricultural mulching film in China have always set fresh records for crop production every year since its initial application three decades ago. People are increasingly aware of the disadvantage of the Polyethylene film for environment, so that degradable film became more and more important both in the research and actual production. As one of the most popular degradable materials for agricultural mulching film, poly (butylene-adipate-co-terephtalate) (PBAT) is usually produced blending with PLA. However, the mechanical and barrier properties of the blended materials are not so satisfied. In *Article 6*, CNC was introduced into the film of PBAT/PLA composites. The PBAT/PLA/CNC films with various contents of CNC were prepared, characterized and performed properties testing. Tensile properties and puncture performance were tested to evaluate the effect of CNC on the mechanical properties of the films. The water vapor barrier properties were also investigated.

Article 5 Comparison of absorption behavior and mechanical performance of superabsorbent polymers reinforced with cellulose nanocrystalline, nanofibers and microcrystalline

Qi Liu[a,b,c], Dorothée Goffin[b,c], Min Wu[d], Aurore Richel[b], Wenqing He[a], Changrong Yan[a], Wenbo Bai[a], Xu Xia[a], Lili Mao[a], Haoru Li[a], Jiqing Song[a,*]

[a] National Engineering Laboratory for Crop Efficient Water Use and Disaster Mitigation, Key Laboratory of Dryland Agriculture, Ministry of Agriculture and Key Laboratory for Prevention and Control of Residual Pollution in Agricultural Film, Ministry of Agriculture, Institute of Environment and Sustainable Development in Agriculture, Chinese Academy of Agricultural Sciences, Beijing 100081, China
[b] Unit of Biomass and Green Technologies, Gembloux Agro-Bio Tech-University of Liège, Passage des Déportés 2B-5030 Gembloux, Belgium
[c] TERRA Research Center and Laboratory of Gastronomical Science, Gembloux Agro-Bio Tech-University of Liège, Passage des Déportés 2B-5030 Gembloux, Belgium
[d] College of Engineering, China Agricultural University, Beijing 100083, China

Abstract: To compare effects of CNF, CNC and MCC on the properties of SAPs, superabsorbent polymers of acrylamide–acrylate copolymer and CNF, CNC and MCC were synthesized respectively. SEM results revealed the compact and coarse surface of the dry SAPs and the irregular and numerous sizes porous morphology of hydrogels. All the FTIR results verified that CNF, CNC and MCC were successfully grafted onto the P(AA-co-AM) chains respectively. The effect of CNF, CNC and MCC on the swelling abilities, water retention capacity and mechanical properties of the SAPs hydrogels were investigated. The SAPs synthesized with CNF or CNC were with lower swelling capacities in distilled water. However, they could achieve equilibrium faster and have similar swelling abilities in the KCl, $CaCl_2$, $FeCl_3$ and 0.9% NaCl solutions. AA-AM behaved better water retention abilities than AA-AM-CNF, AA-AM-CNC and AA-AM-MCC especially at higher temperature. For the abilities of repeated water-absorbing, a similar water-absorbing ability of the first and second round for AA-AM-CNF and AA-AM-CNC was found. AA-AM-CNC showed the most remarkable water retaining capacity among the four SAPs in the soil and the results indicated the positive correlation between the addition amount of SAPs and the water retention ability of soil. When the mulching was employed, SAPs helped the soil keep more moisture when the Biodegradable PBAT based film was employed. AA-AM-CNF and AA-AM-CNC showed higher G' which is attributed to the reinforcement effect of the CNC, CNF and MCC. G'' of the SAPs in the measured frequency range were similar or a little bit lower than the G' plots. AA-AM-CNC and AA-AM-CNF showed better mechanical properties than the other two SAPs.

Key words: Superabsorbent polymers; wheat straw; cellulose nanocrystalline; cellulose nanofiber; absorption behavior; mechanical performance

1. Introduction

Superabsorbent polymers (SAPs) are three-dimensional crosslinked hydrophilic polymers with high-performance water absorbent and retention abilities compared to ordinary absorbing materials [1,2]. Due to this advantage, SAPs are widely used in various fields, such as food, absorbent core for hygiene products, pharmaceutical industries and soil water retention, particularly, in arid regions [3]. However, the swollen SAPs normally are of poor mechanical

performance and thus easy to fracture. This disadvantage could be explained by the low resistance to crack propagation and lack of an efficient energy dissipation mechanism in the network [4]. Another disadvantage of most of the SAPs are synthetic polymers based on petrochemical monomer, such as acrylic acid (AA) or acrylamide (AM), which are ungradable and environmentally unfriendly [5]. Furthermore, with the growing environmental pollution awareness and the gradual depletion of petroleum resources, natural biodegradable materials attract more and more attention [6-8].

Cellulose is one of most abundant biopolymers on earth, found in wood and other plant-based materials and serving as the dominant reinforcing phase in plant structures. Cellulose is the basic structural element of cell wall. It is a kind of natural polysaccharide formed by cellobiose (D-glucopyranosyl-β-1,4-D-glucopyranose) chains. Via strong intermolecular hydrogen bonds between hydroxyl groups of adjacent macromolecules, highly ordered cellobiose form cellobiose microfibrils [9]. Nowadays, cellulose materials are widely used in different fields including industry, agriculture, medicine, food, environmental protection, etc. Cellulose nanofibers (CNFs) and cellulose crystalline (CNC) are the two types of nanostructured cellulose with very similar chemical compositions but different morphologies due to their different isolation methods [10]. The CNCs are short, rod-like pure cellulose crystals and the CNFs are long, 5-20 nm wide fibrils. Both CNCs and CNFs own excellent reinforcing effect in polymer nanocomposites [11-14].

Both of CNCs and CNFs have been employed to synthesis and reinforce SAPs [15-20]. Mahfoudhi and Boufi studied the effect of CNFs content on the swelling properties, mechanical compression and water holding capacity of the hydrogel nanocomposites based on cellulose nanofibrils and poly(acrylic acid-co-acrylamide) [15]. Wen et al. synthesized poly-(acylic acid)/CNF composites via UV-induced polymerization and found that 1 wt% CNF addition increased both of the water absorbency as well as the swelling rate in deionized water and 0.9 % NaCl solution [16]. Dash et al. prepared a renewable and biocompatible co-cross-linked nanocomposite hydrogel from poly(methyl vinyl ether-co-maleic acid), poly(ethylene glycol) and CNF; the nanocomposite exhibited a superior mechanical properties [17]. CNCs are also used for reinforcing SAPs. Spagnol et al. synthesized superabsorbent hydrogels, based on poly(acrylamide-co-acrylate) filled with varying percentage of CNC which exhibited a pH-responsiveness and cation-sensitivity character [18]. Bary et al. reported a novel superabsorbent membrane consisting of polyvinyl alcohol, CNCs, glutaraldehyde and glycerin which showed great equilibrium swelling capacity, pH-dependent swelling reversibility, water retention capability, biodegradability and antimicrobial activities [19]. Zhang et al. reported a nanocomposite network of poly(acrylic acid-co-acrylamide) (PAAAM) sequentially cross-linked by quaternized tunicate CNCs; the toughness of dual cross-linked hydrogel was found 340 times of mono-cross-linked hydrogel, which was 10 times that of PAAAM hydrogel [20].

Though there are some researches to study the reinforcement of CNF or CNC in SAPs, there is little research about comparison between CNF and CNC or comparison among CNF, CNC and MCC. In this work, superabsorbent composites of acrylamide–acrylate copolymer and CNF,

CNC and MCC were synthesized respectively. Scanning electronic microscopy (SEM) and Fourier transform infrared spectroscopy (FTIR) were used to characterize the morphology and structure of the SAPs. The effect of CNF, CNC and MCC on the swelling abilities, water retention capacity and mechanical properties of the SAPs hydrogels was also investigated.

2. Methods

2.1. Materials

WS was collected from Huantai experimental fields in 2015 in Shandong Province, China. The collected straw was dried before use and milled into powder with a particle size of less than 1 mm. MCC were obtained from Sigma-Aldrich Co., Ltd., USA. AA and AM (analytical grade) were bought from Aladdin Chemistry Co., Ltd., China. $K_2S_2O_8$ (Xilong Chemical Co., Ltd., China), N,N′-(dimethylene)acrylamide (NMBA) (Amresco, USA) and Acylamide (Amresco, USA), acrylic acid (Aladdin Chemistry Co. , Ltd., China) were all analytical grade. Poly (lactic acid) (PLA) (4032D, Nature works, USA) and poly (butylene-adipate-co-terephtalate) (PBAT) (Ecoflex-F-Blend-C1200, BASF, Germany) were dried before use. And the PBAT/PLA film (12μm) was prepared with a laboratory blow-film extruder (SJ35-MF360, Zedao Co., Ltd., China). Polyethylene (PE) film (8 μm) was obtained from Huanxin plastic company. Distilled water and ultra-pure water were used in this experiment.

2.2. Preparation of CNCs and CNFs

CNCs preparation: WS was pretreated with 17.5% NaOH (room temperature for 2 h), 2 M HCl (80 °C for 2 h) and 2% NaOH (80 °C for 2 h) to obtain the MCC. Then the CNCs were prepared from MCC with the method stated in the previous work [21]. CNFs were prepared with the method according to the previous work [22].

2.3. Preparation of SAPs

The SAPs were prepared with AA, AM with or without cellulose in aqueous solution. They were synthesized by graft copolymerization. 0.2 g CNFs suspension was transferred in a three-neck flask equipped with a magnetic stirrer, reflux condenser, and nitrogen line. The oil bath was maintained at 25 °C at the beginning. 2.0 g AM and 8.0 g AA with neutralization degree of 70% were successively added. After bubbling for 20 min, solutions of 1.0 ml $K_2S_2O_8$ (0.03 g/mL) and 1.0 ml (0.005 g/mL) NMBA were added into the flask. Nitrogen gas was bubbled into the suspension for 30 min before adding the monomer. Then the oil bath was heated and maintained at 70 °C for 4 h to complete the polymerization reaction to obtain CNF-g-poly (acrylic acid-co-acrylamide) superabsorbent (named as AA-AM-CNF). CNC-g-poly (acrylic acid-co-acrylamide (AA-AM-CNC) and MCC-g-poly (acrylic acid-co-acrylamide (AA-AM-MCC) and poly (acrylic acid-co-acrylamide (AA-AM) were prepared by the same method with adding CNC or MCC. After that, the SAPs were washed

with distilled water oven dried at 60 °C until to reach constant weight. The four products were milled through a 40-60 mesh screen.

2.4 Characterization

2.4.1 SEM
The morphology of the SAPs before and after swelling in distilled water were observed using SEM, Hitachi SU8010 SEM (Hitachi Ltd., Chiyoda-ku, Japan). The samples were coated with gold by an ion sputter coater and observed under SEM at 5-10 kV.

2.4.2 FTIR
FTIR spectroscopy was used to examine the differences among the structure of SAPs. The spectrum of each sample was recorded with a Thermo Scientific Nicolet iN10 (Thermo Electron Corp., USA). SAPs particles were ground and blended with KBr. Then, the mixture was pressed into thin, transparent pellets. The FTIR spectrum of each sample was obtained at 4000–400 cm^{-1} with a resolution of 4 cm^{-1}.

2.5. Swelling measurements

2.5.1 Measurement of water absorbency
Accurately weighed SAPs polymer powder (0.1 ± 0.0001 g) were added into the tea bags (100 mesh nylon screen) and then immersed in 500 mL of ultra-pure water, at room temperature to reach the swelling equilibrium (about 1 h) [23]. The tea bag was hung for 5 min to remove the excess solution before weighing at certain duration. The equilibrium swelling Q_{eq} was calculated using the following equation:

$$Q_{eq} = \frac{m_2 - m_1}{m_1} \tag{1}$$

where m_1 and m_2 are the weights of the dry and swollen samples (g), respectively and Q_{eq} represents the water absorbency per gram of dried sample (g/g). All samples were carried out at least two times and the averages were reported in this paper.

2.5.2 Absorbency in various solutions
The measurement method was the same as described in Section 2.4.1, except that different salt solutions (KCl, $CaCl_2$, $FeCl_3$, 0.9% NaCl and city water) were used instead of the ultra-pure water. Only Q_{eq} of the SAPs in various solutions were recorded.

2.6 Measurement of water residue content at various temperatures
A certain gram of the SAPs was immersed in ultra-pure water at room temperature to reach swelling equilibrium [23]. The swollen gels were hung for 5 min in a tea bag to remove excess water, weighed (W_1), and placed in an oven at 30 and 60 °C respectively. The samples were weighed every hour (W_i) for 12 h. The water residue content of the SAPs at various temperatures was calculated with the following equation:

$$R_{iT} = \frac{W_i - W_0}{W_1 - W_0} \times 100 \tag{2}$$

where W_0 is the weight of the dry SAPs. Three measurements were taken for each.

2.7 Repeated water absorption

The measurement method was the same as described in Section 2.4.1. And the SAPs were oven dried at 60 °C until to reach constant weight. Then the measurement described in 2.4.1 was repeated. Three rounds of experiments were taken and recorded.

2.7.1 Soil surface exposed

Soil was collected from the Shunyi experimental fields in Beijing, China. It was dried in a constant temperature oven at 105 °C for 24 h, and sieved through 10 mesh nylon. 0.1g of the resulting SAPs was mixed with 100 g soil in 300 ml glass beakers. Approximately 150 g water was added to each beaker slowly to make the soil water content reach saturation but no water accumulation on the soil surface. A control experiment without the superabsorbent was also carried out. The beakers were maintained at room temperature and weighed every day for 10 days. The water retention in the soil (R_{is}%) was calculated by the following equation:

$$R_{is} = \frac{m_i}{m_0} \times 100 \qquad (3)$$

Where m_0 is the total weight of the saturated water absorbency sample and soil. Three duplicates were carried out.

2.7.2 Plastic film mulching on the soil surface

The measurement method was the same as described in Section 2.4.1, except that the treated soil was mulched with PBAT/PLA film and ordinary PE film (0.8 μm). Three duplicates were carried out.

2.8 Rheological studies

Rheological studies were carried out with an AR 2000 rheometer (TA Instruments, New Castle, DE). The gel sample was gently loaded onto the rheometer Peltier Plate carefully to avoid shearing [24]. For oscillatory stress sweep, the oscillation stress sweep studies to scan the material were conducted among 0.01–100 Pa (log mode), and at a frequency of 1 Hz unless specified otherwise. For frequency sweep, samples were subjected to a frequency ranging from 0.1 to 10 Hz（angular frequency 0.6283 -62.83 rad/s）at a controlled variable of 2% strain. All rheology studies were done at 25 °C.

3. Result and discussion

3.1 SEM

Structural changes on the SAPs due to addition of CNF, CNC and MCC into the matrix were evaluated through SEM images. The SEM images of dry and swollen SAPs hydrogels in distilled water are also shown in Fig. 22. The surface of dry samples are quite compact and coarse (Fig. 22a, c, e and g). This structure provided huge surface area which made the composite absorb water and swollen immediately when immersed in water. The images of the swollen hydrogels (Fig. 22b, d, f and h) showed the irregular and numerous sizes porous morphology. These pores were the regions of water permeation, where water easily diffused into. The main reason for the formation of pores in the composite was due to the dehydration

with ethanol [23]. The pores are heterogeneous in size and distribution on the hydrogel composite network. AA-AM and AA-AM-MCC shows bigger pores but collapsed structure. However, with the incorporation of CNF and CNC into the hydrogel matrix, the 3D structure of AA-AM-CNF and AA-AM-CNC were stronger.
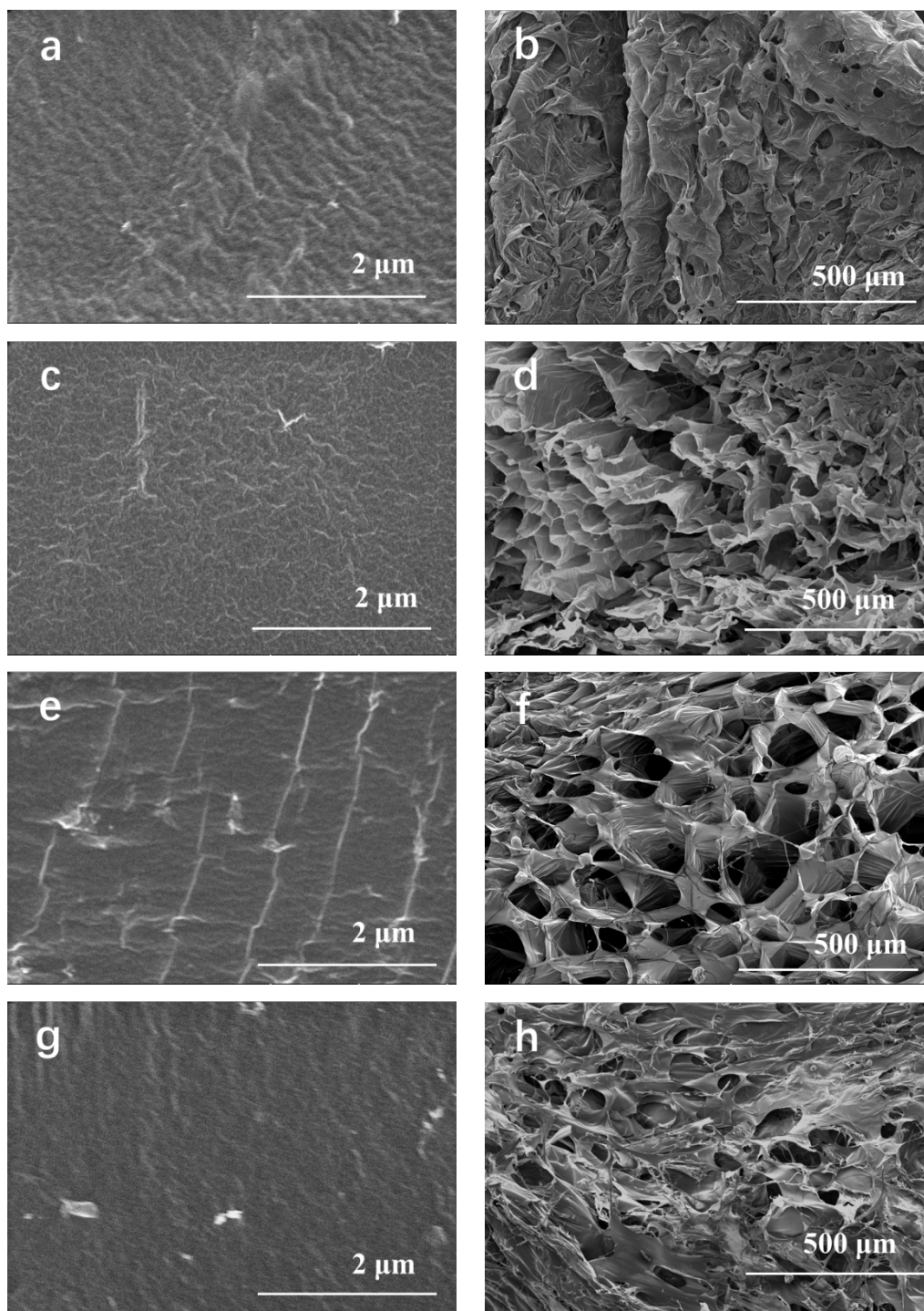
Figure 22. SEM images of AA-AM (dry (a) and hydrogel (b)), AA-AM-CNF (dry (c) and hydrogel (d)), AA-AM-CNC (dry (e) and hydrogel (f)), AA-AM-MCC (dry (g) and hydrogel (h)).

3.2 FTIR studies

Figure 23 shows the FTIR spectra of AA-AM, AA-AM-CNF, AA-AM-CNC and AA-AM-MCC, respectively. The peak at 1558 cm^{-1} appeared in all samples corresponded to the asymmetric –COO− stretching reflecting the basic structure of P (AA-co-AM) in the four composites. The band at 3428 cm^{-1} for all samples was attributed to the –NH stretching vibration of the AM unit, which overlapped with the –OH groups of the acrylate units and cellulose. However, the wider peak at 3200-3500 cm^{-1} of AA-AM-CNF, AA-AM-CNC and AA-AM-MCC could be attributed to the hydrogen bond association indicating the grafted cellulose to the SAPs. The C=O stretching vibration at 1720 cm^{-1} in –COO– was strengthened in AA-AM-CNF, AA-AM-CNC and AA-AM-MCC corresponding to carbonyl stretching of ester group. The C=O stretching vibration at 1673 cm^{-1} was also strengthened in these three SAPs. Among the three samples with grafted cellulose, the two peaks enlarged most obviously in AA-AM-CNC, which may due to the Nano-size effect of the CNC. The two peaks strengthened at 1720 cm^{-1} and 1673 cm^{-1} manifested the existence of cellulose in the AA-AM-CNF, AA-AM-CNC and AA-AM-MCC composites. All these FTIR results verified that the three kinds of cellulose fibers were successfully grafted onto the P(AA-co-AM) chains.
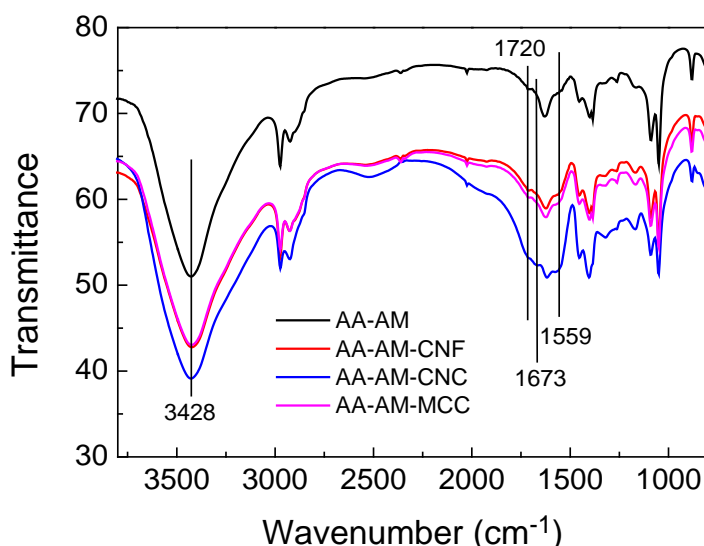
Figure 23. FTIR spectra of AA-AM, AA-AM-CNF, AA-AM-CNC and AA-AM-MCC.

3.3 behaviors of SAPs

3.3.1 Swelling in distilled water

A determination was conducted on the swelling capacities of the SAPs in distilled water. Figure 24 shows the relationship between time soaking in water and swelling ratio of four kinds of superabsorbent polymer synthesized with different cellulose. All samples exerted very similar and significant water absorption behavior as the rate of swelling sharply increased initially. The absorption rate of the SAPs was quite fast. However, the swelling equilibrium achieved in various duration for different polymers. AA-AM-CNC and AA-AM-CNF achieved equilibrium less than 40 mins, which were more rapidly than the other two. AA-AM and AA-AM-MCC could only reach swelling equilibrium after 2 h. This result indicated that though the SAPs synthesized with CNF or CNC were with lower swelling capacities in distilled water, they could achieve equilibrium faster. Furthermore, all the swelling kinetics of

the SAPs was consistent with the research of the others. The swelling processes of all the SAPs fit the processes of the first dynamics [25,26].
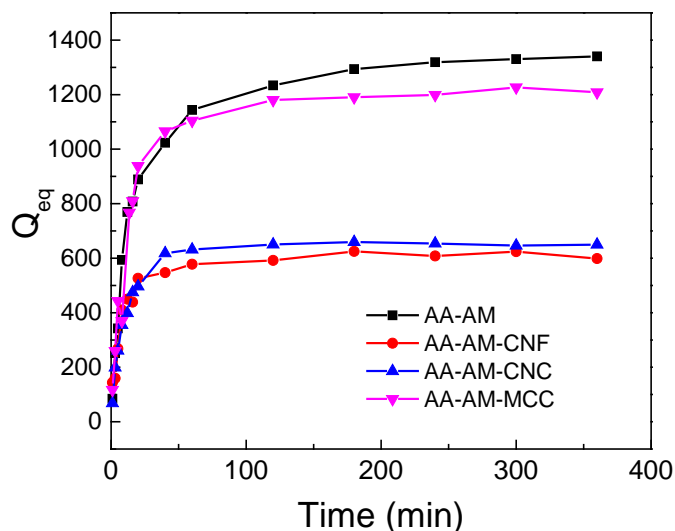
Figure 24. Water-swelling kinetics for the SAPs in distilled water.

3.3.2 Swelling in various solutions

Because the applications of SAPs are usually not in pure water, it is very important to investigate the swelling capacity of the SAPs in salt solution. This is particularly essential in its practical applications in many fields. Fig. 25 shows the Q_{eq} of the samples in KCl, $CaCl_2$, $FeCl_3$, 0.9% NaCl and city water. Because the condition of the medium plays a very important role on the swelling behavior of a superabsorbent polymer such as ionic strength and cationic charge, to better investigate the effect of the cationic charge, the same ionic strength (I=0.1 mol/L) solutions of the KCl, $CaCl_2$ and $FeCl_3$ were employed. Compared with the Q_{eq} in KCl, the swelling capacity were considerably decreased in the $CaCl_2$ and $FeCl_3$ ($Na^+ > Ca^{2+} \approx Fe^{3+}$). This result may be ascribed to the reduced osmotic pressure difference between the polymer network and the external solution, which were caused by the cationic charge and cationic radius. In the city water, the SAPs showed the similar order of the swelling capacity: AA-AM > AA-AM-MCC > AA-AM-CNC > AA-AM-CNF. However, though the swelling capacity of AA-AM-CNC and AA-AM-CNF in distilled water and city water were not so satisfying, their similar manifestation as AA-AM and AA-AM-MCC in the KCl, $CaCl_2$, $FeCl_3$ and 0.9% NaCl solutions also made their broader utilization potentiality in many practical application areas.
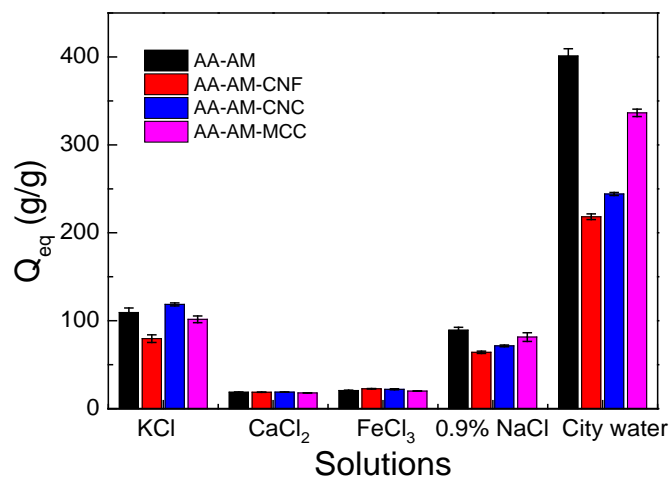
Figure 25. Water absorbency of the SAPs in various solutions.

3.4 Water residue content at various temperatures

Ambient temperature played an important role in the water reserve capacity of the superabsorbent composite. Therefore, the water residue content curve of the four SAPs were determined at 30 ℃ and 60 ℃. Figure 26 (a) and (b) shows these results. As the time increased, the water content of all samples under both temperatures decreased significantly. When the SAPs were taken for dehydration at 30 ℃, there were very similar results among the four composites with AA-AM a little bit higher than the other (Figure 26 (a)). The samples retained 38.44%, 34.61%, 35.52% and 33.75% of water absorbency after being kept at 30 ℃ for 12 h, respectively. However, though similar regular was found with the test under 60 ℃, AA-AM decreased with a slower speed compared with the others (Fig.26 (b)). For instance, the water content of the four samples was 38.51%, 21.79%, 15.00% and 13.98% after kept at 60 ℃ for 6 h. And all the samples became dry after 12 h heating. It is the interaction of H-bonding and Vander Waals force between water molecules and the SAPs which decided this dehydration process. Because AA-AM-CNF, AA-AM-CNC and AA-AM-MCC which contended cellulose had less –COO$^-$, their water residue content was less than the AA-AM especially at higher temperature. This feature made the SAPs contented cellulose some special application prospect somewhere need dehydration with increasing temperature.
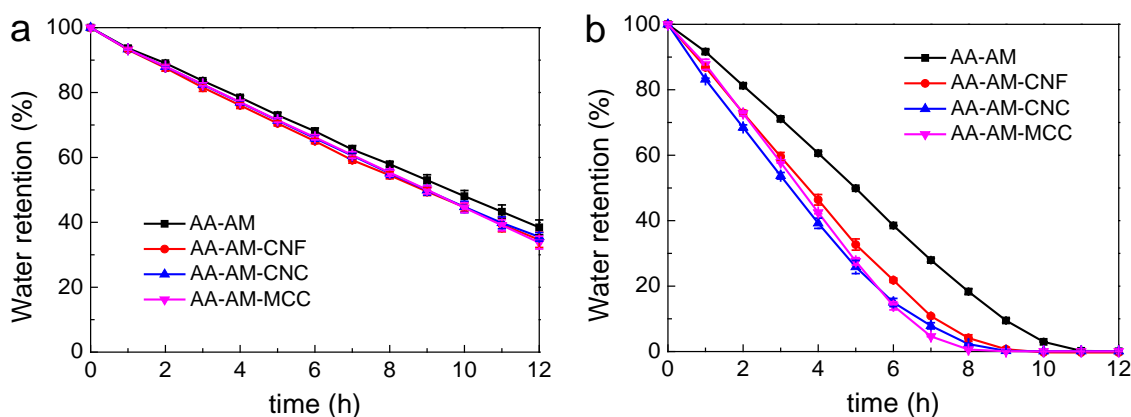
Figure 26. Water residue content of SAPs at 30 ℃ (a) and 60 ℃ (b).

135

3.5 Repeated water-absorbing capacity of SAPs in distilled water

Repeated water-absorbing capacity is an important property of SAPs in various applications especially for agriculture. The repeat water absorbencies of the four SAPs were determined through an absorption-dehydration-absorption-dehydration process. Repeated water absorbency capacities of the SAPs for 3 times in distilled water are listed in Table13. The water absorbencies of AA-AM, AA-AM-CNF, AA-AM-CNC and AA-AM-MCC were found decreasing over time. However, the repeat water absorbency of the four SAPs samples appeared different changing tendency. After the second water-absorbing process, the water absorbencies of the four SAPs reduced by 12.7%, -2.4%, -1.6% and 16.7%.24.3% in distilled water. A pretty interesting founding was that the WA ability of AA-AM-CNF and AA-AM-CNC of the second-time absorbing was almost the same as those of the first time. Furthermore, the water absorbencies of SAPs reduced further in the third-time absorbing. And the reduction of each (σ2-3) were more thanσ1-2. Though the primarily absorbing abilities of AA-AM-CNF and AA-AM-CNC were much lower than those of AA-AM and AA-AM-MCC, there were comparative less decreasing in WA after three times absorbing. The totally reduction of WA of the four SAPs were 30.9%, 18.2%, 17.8%, 37.4% of each. The feature that the similar water-absorbing ability of the first and second round for AA-AM-CNF and AA-AM-CNC made these two SAPs more potential applications in some fields.

Table 12. Repeated water absorbency capacities of SAPs in distilled water.

SAPs	Water Absorbency (g·g⁻¹) of each repeat			Reduction of WA		
	1	2	3	σ1-2 (%)	σ2-3 (%)	σ1-3 (%)
AA-AM	789.6±9.7	688.7±1.0	535.8±10.0	12.7±1.9	22.9±2.4	30.9±1.8
AA-AM-CNF	434.7±5.2	447.1±1.2	355.6±0.8	-2.4±1.1	19.6±0.2	18.2±1.2
AA-AM-CNC	475.3±10.1	483.1±8.3	390.6±2.8	-1.6±0.4	18.6±1.4	17.8±2.3
AA-AM-MCC	785.7±14.3	652.3±3.9	492.0±3.9	16.7±0.7	24.1±0.6	37.4±1.6

3.6.1 Water retention ability in soil without mulching

Because of the influential role of SAPs on improving the soil moisture content, seedling survival rates and promoting crop growth in agriculture, it is very essential to study the water retention capacity of the SAPs in soil. The water retention abilities of the soil mixed with various SAPs in dosage of 0.1% and 0.3% are showed in Figure 27 (a) and (b). Compared with the soil without SAPs (CK), water retention of the soil with 0.1% and 0.3% both increased significantly. Water contents of the soil at day 4 with 0.1% AA-AM, AA-AM-CNF, AA-AM-CNC and AA-AM-MCC were 32.64%, 39.94%, 43.82% and 37.28% respectively. The water transpiration ratio of the soil without SAPs was more than 90% at 6 d. However, the water contents of the soil at this time with 0.1 g of the four SAPs were 5.97%, 13.73%, 20.17% and 11.34%. This intriguing result indicated that AA-AM-CNC owned the most remarkable water retaining capacity among the samples in the soil. A similar relationship was found among the soil with 0.3% SAPs (Figure 27 (b)). 39.89%, 47.22%, 50.74% and 43.15% of water was reserved in the soil respectively at day 4, which was approximately 6-8% higher than the soli with 0.1% SAPs. This indicated the positive correlation between the addition amount of

SAPs and the water retention ability of soil. Fang et al. [23] found the similar result with cellulose-g-poly(acrylic acid-co-acrylamide) composite based on flax yarn waste. The soil with 0.3% AA-AM-CNC could help to extend the humidification maintaining from 6 days to 10 days under this experiment condition.
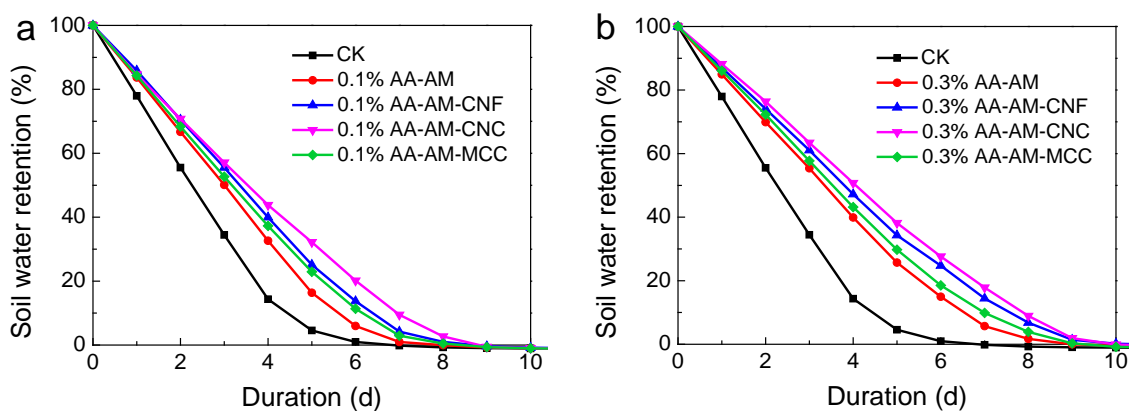
Figure 27. Soil water retention abilities adding 0.1% SAPs (a) and 0.3% SAPs (b) of the soil.

3.6.2 Water retention ability in soil with mulching

Plastic mulching is a globally agricultural practice because of its outstanding effects on improving product quality and yield, optimizing growth conditions and extending the growing season [27]. Therefore, effects of mulching on soil water retention ability with various SAPs were tested. The soil water retention abilities adding 0.1% SAPs with PBAT mulching and PE mulching are shown in Figure 28 (a) and (b). Because the PBAT based film has at least 3 times higher water vapor permeability than that of PE [28], the water retention of the soil covered by PBAT based film decreased significantly compared with that of soil mulching PE film. As shown in Figure 28 (a), under the PBAT film, water contents of the soil samples with 0.1% AA-AM, AA-AM-CNF, AA-AM-CNC and AA-AM-MCC were 7.75%, 10.85%, 15.37% and 10.71% respectively at 30 days. At the same time, the water contents of the soil without SAPs were only 1.96% indicating that the SAPs helped the soil keep more moisture when the Biodegradable PBAT based film was employed. However, the corresponding values in the soil samples covered by PE film were 92.66%, 92.96%, 94.21%, 94.34 and 93.47% respectively at 30 days. This indicated that in the first month, SAPs had limited promoting effect on soil water content with covering PE film. Furthermore, under the PE film, when the time lasted as long as 65 days, water contents of soil with AA-AM-CNC and without SAPs were 85.80% and 79.66%. This indicated the possible application of soil water promoting potential in the long run.
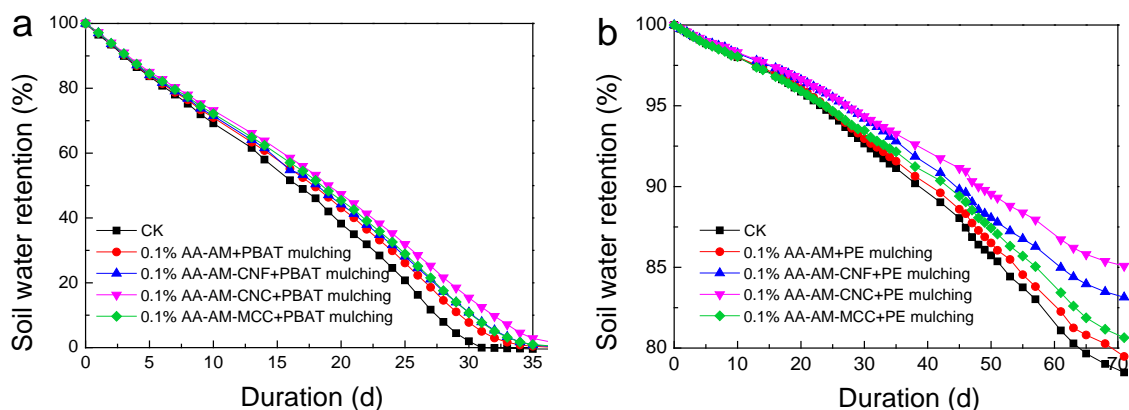
Figure 28. Soil water retention abilities adding 0.1% SAPs with PBAT mulching (a) and PE mulching (b).

3.7 Rheology studies

3.7.1 Oscillatory stress sweep

All the four SAPs hydrogels were subjected to dynamic oscillation stress ramping and the results are presented in Figure 29 Linear viscoelastic (LVR) region refers to the stress range over which G' is independent with the increasing applied stress. The material structure was not broken within the LVR as shown in Fig.8 where the applied stress is in phase with the resulting strain ($\delta=0$). The end of linear region of LVR is called the critical stress, σC. Once beyond the σC, the structure of the material was disturbed in the subset where applied stress is not in phase with the responding strain ($\delta>0$). As shown in Fig.30, the hydrogels of AA-AM-CNF and AA-AM-CNC exhibited significantly higher G' values and longer linear viscoelastic regions compared to that of AA-AM-MCC and AA-AM. The G', the length of LVR and the σC is: AA-AM-CNC $\approx$ AA-AM-CNF > AA-AM-MCC > AA-AM. This is attributed to the reinforcement effect of the CNC, CNF and MCC. At stresses below the critical stress, the sample behaves as a viscoelastic solid. At higher stresses, the material starts to flow. The critical stress has a significant use in developing stable products, and this aspect will be investigated further in other studies.
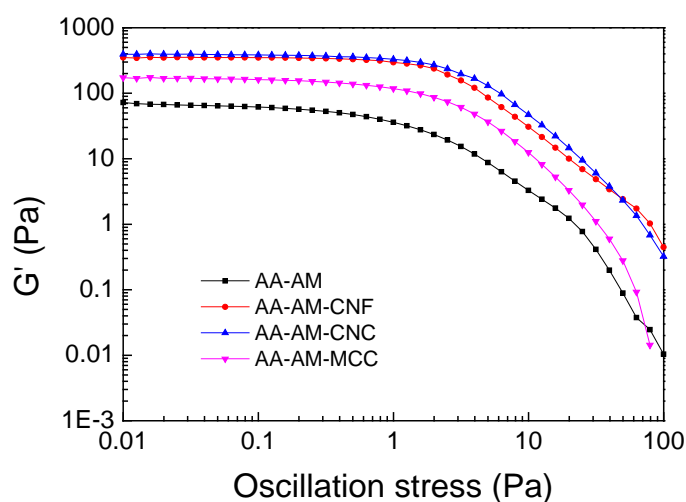
Figure 29. Effect of oscillation shear stress on the elastic modulus (G') of SAPs hydrogels.

3.8.2 Frequency stress sweep

The interpretation of data from oscillatory studies on viscoelastic materials can be conveniently visualized by considering a number of elastic elements or springs coupled in series with a number of viscous dashpots or pistons [29, 30]. The variation of G' and G'' with frequency changing for the four hydrogels is shown in Figure 30. The plots of G' versus frequency for all samples were in similar pattern. G' plots show a very small but gradual increase with an increase in frequency. This indicates a largely elastic behavior with comparatively small energy dissipation. AA-AM-CNC, AA-AM-CNF and AA-AM-MCC behaved better than AA-AM. G'' of the SAPs in the measured frequency range were similar or a little bit lower than the G' plots. The four SAPs showed the similar trend with various G'' level. The loss tangent (tan δ) is a dimensionless parameter that measure the ratio of energy lost to the energy stored in a cyclic deformation. The curves of tan δ versus frequency (Figure 30 c) provide a comparative measure of both the elastic and viscous contributions. The AA-AM hydrogel showed the biggest shift in tan δ over the frequency among the four SAPs. This could be indicative of the predominantly viscous nature of the material [24].
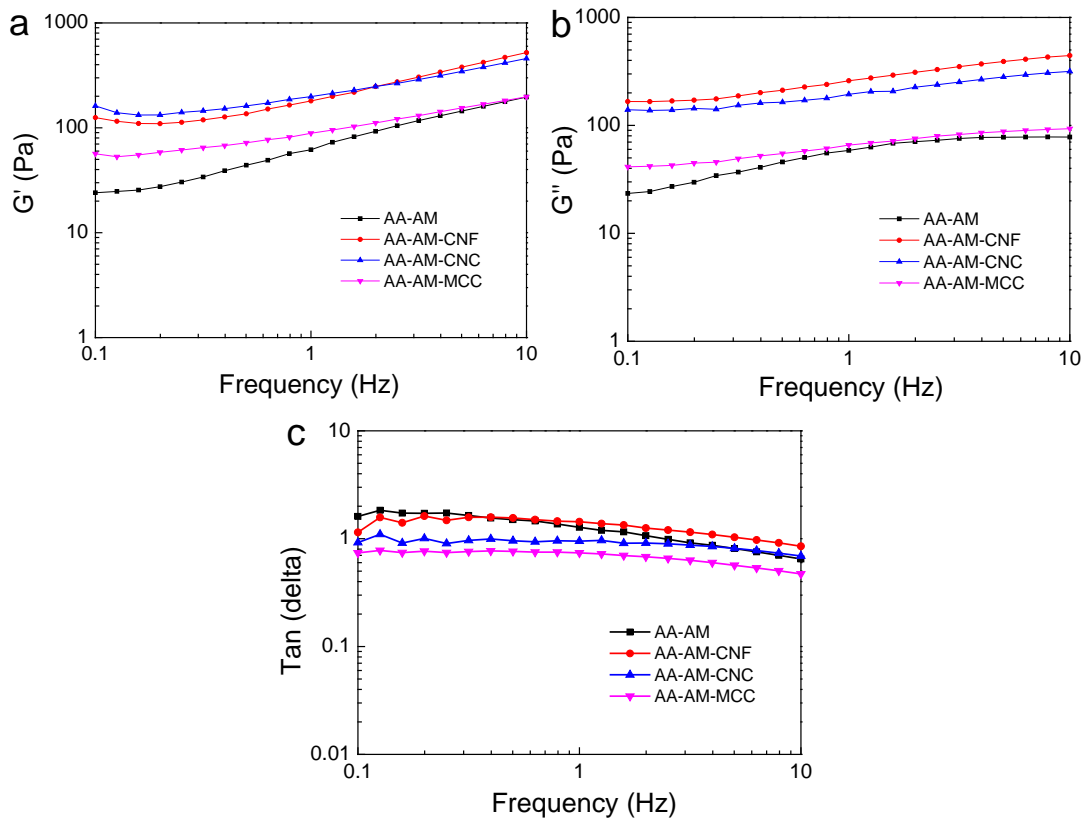
Figure 30. Effect of Frequency on the elastic modulus (G') (a), viscous modulus (G'') (b) and tanδ(c) of SAPs hydrogels.

4. Conclusions

To compare effects of CNF, CNC and MCC on the properties of SAPs, superabsorbent polymers of acrylamide–acrylate copolymer and CNF, CNC and MCC were synthesized

respectively. SEM results revealed the compact and coarse surface of the dry SAPs and the irregular and numerous sizes porous morphology of hydrogels. And, the 3D structure of AA-AM-CNF and AA-AM-CNC were strengthened with the incorporation of CNF and CNC. All the FTIR results verified that CNF, CNC and MCC were successfully grafted onto the P(AA-co-AM) chains respectively. The effect of CNF, CNC and MCC on the swelling abilities, water retention capacity and mechanical properties of the SAPs hydrogels were investigated. The SAPs synthesized with CNF or CNC were with lower swelling capacities in distilled water. However, they could achieve equilibrium faster and have similar swelling abilities in the KCl, CaCl$_2$, FeCl$_3$ and 0.9% NaCl solutions. AA-AM behaved better water retention abilities than AA-AM-CNF, AA-AM-CNC and AA-AM-MCC especially at higher temperature. For the abilities of repeated water-absorbing, the water absorbencies of the four SAPs reduced by 12.7%, -2.4%, -1.6% and 16.7%.24.3% in distilled water after the second water-absorbing round indicating the similar water-absorbing ability of the first and second round for AA-AM-CNF and AA-AM-CNC. AA-AM-CNC showed the most remarkable water retaining capacity among the four SAPs in the soil and the results indicated the positive correlation between the addition amount of SAPs and the water retention ability of soil. When the mulching was employed, SAPs helped the soil keep more moisture when the Biodegradable PBAT based film was employed. SAPs had limited promoting effect on soil water content with covering PE film at 30 days but better later. The G', the length of LVR and the σC is: AA-AM-CNC ≈ AA-AM-CNF > AA-AM-MCC > AA-AM. This is attributed to the reinforcement effect of the CNC, CNF and MCC. G'' of the SAPs in the measured frequency range were similar or a little bit lower than the G' plots. AA-AM-CNC and AA-AM-CNF showed better mechanical properties.

Acknowledgements

Reference

[1] Buchholz F L, Graham A T. Modern superabsorbent polymer technology [J]. John Wiley & Sons, Inc, 605 Third Ave, New York, NY 10016, USA, 1998. 279, 1998.

[2] Superabsorbent polymers: science and technology [M]. American Chemical Society, 1994.

[3] Ahmed E M. Hydrogel: Preparation, characterization, and applications: A review [J]. Journal of advanced research, 2015, 6(2): 105-121.

[4] Rose S, Dizeux A, Narita T, et al. Time dependence of dissipative and recovery processes in nanohybrid hydrogels [J]. Macromolecules, 2013, 46(10): 4095-4104.

[5] Zohuriaan-Mehr M J, Kabiri K. Superabsorbent polymer materials: a review [J]. Iranian Polymer Journal, 2008, 17(6): 451.

[6] Qiao D, Liu H, Yu L, et al. Preparation and characterization of slow-release fertilizer encapsulated by starch-based superabsorbent polymer[J]. Carbohydrate polymers, 2016, 147: 146-154.

[7] Essawy H A, Ghazy M B M, El-Hai F A, et al. Superabsorbent hydrogels via graft polymerization of acrylic acid from chitosan-cellulose hybrid and their potential in controlled release of soil nutrients [J]. International journal of biological macromolecules, 2016, 89: 144-151.

[8] Demitri C, Scalera F, Madaghiele M, et al. Potential of cellulose-based superabsorbent hydrogels as water reservoir in agriculture [J]. International Journal of Polymer Science, 2013, 2013.

[9] García, A., Gandini, A., Labidi, J., Belgacem, N., & Bras, J. (2016). Industrial and crop wastes: A new source for nanocellulose biorefinery. Industrial Crops and Products, 93, 26-38.

[10] Jonoobi M, Oladi R, Davoudpour Y, et al. Different preparation methods and properties of nanostructured cellulose from various natural resources and residues: a review [J]. Cellulose, 2015, 22(2): 935-969.

[11] Xu X, Wang H, Jiang L, et al. Comparison between cellulose nanocrystal and cellulose nanofibril reinforced poly (ethylene oxide) nanofibers and their novel shish-kebab-like crystalline structures [J]. Macromolecules, 2014, 47(10): 3409-3416.

[12] Jiang L, Xu X. Crystallization Behavior of Cellulose Nanocomposites and Cellulose Nanofibril-Reinforced Polymer Nanocomposites [J]. Handbook of Nanocellulose and Cellulose Nanocomposites, 2017: 553-580.

[13] Spinella S, Re G L, Liu B, et al. Polylactide/cellulose nanocrystal nanocomposites: Efficient routes for nanofiber modification and effects of nanofiber chemistry on PLA reinforcement [J]. Polymer, 2015, 65: 9-17.

[14] Grygiel K, Wicklein B, Zhao Q, et al. Omnidispersible poly (ionic liquid)-functionalized cellulose nanofibrils: surface grafting and polymer membrane reinforcement [J]. Chemical Communications, 2014, 50(83): 12486-12489.

[15] Mahfoudhi N, Boufi S. Poly (acrylic acid-co-acrylamide)/cellulose nanofibrils nanocomposite hydrogels: effects of CNFs content on the hydrogel properties [J]. Cellulose, 2016, 23(6): 3691-3701.

[16] Wen Y, Zhu X, Gauthier D E, et al. Development of poly (acrylic acid)/nanofibrillated cellulose superabsorbent composites by ultraviolet light induced polymerization [J]. Cellulose, 2015, 22(4): 2499-2506.

[17] Dash R, Cateto C A, Ragauskas A J. Synthesis of a co-cross-linked nanocomposite hydrogels from poly (methyl vinyl ether-co-maleic acid)-polyethylene glycol and nanofibrillated cellulose [J]. Cellulose, 2014, 21(1): 529-534.

[18] Spagnol C, Rodrigues F H A, Neto A G V C, et al. Nanocomposites based on poly (acrylamide-co-acrylate) and cellulose nanowhiskers[J]. European Polymer Journal, 2012, 48(3): 454-463.

[19] Bary E A, Fekri A, Solomon Y, et al. Novel Superabsorbent Membranes Made of PVA and

Ziziphus Spina-Christi cellulose for Agricultural and Horticultural Applications[J]. New Journal of Chemistry, 2017.

[20] Zhang T, Zuo T, Hu D, et al. Dual Physically Crosslinked Nanocomposite Hydrogels Reinforced by Tunicate Cellulose Nanocrystals with High Toughness and Good Self-recoverability [J]. ACS Applied Materials & Interfaces, 2017.

[21] Liu Q, Hao W, Yang Y, et al. Effects of size and dispersity of microcrystalline celluloses on size, structure and stability of nanocrystalline celluloses extracted by acid hydrolysis [J]. Nano Life, 2014, 4(04): 1441014.

[22] Liu Q, Lu Y, Aguedo M, et al. Isolation of high-purity cellulose nanofibers from wheat straw through the combined environmentally friendly methods of steam explosion, microwave-assisted hydrolysis, and microfluidization [J]. ACS Sustainable Chemistry & Engineering, 2017.

[23] Wu F, Zhang Y, Liu L, et al. Synthesis and characterization of a novel cellulose-g-poly (acrylic acid-co-acrylamide) superabsorbent composite based on flax yarn waste [J]. Carbohydrate Polymers, 2012, 87(4): 2519-2525.

[24] Rudraraju V S, Wyandt C M. Rheology of microcrystalline cellulose and sodiumcarboxymethyl cellulose hydrogels using a controlled stress rheometer: part II [J]. International journal of pharmaceutics, 2005, 292(1): 63-73.

[25] Chen Y, Tan H. Crosslinked carboxymethylchitosan-g-poly (acrylic acid) copolymer as a novel superabsorbent polymer [J]. Carbohydrate Research, 2006, 341(7): 887-896.

[26] Liu M, Cheng R, Qian R. Investigation of swelling property of poly (vinyl alcohol) hydrogel [J]. Acta Polymerica Sinica, 1996: 234-239.

[27] Steinmetz Z, Wollmann C, Schaefer M, et al. Plastic mulching in agriculture. Trading short-term agronomic benefits for long-term soil degradation [J]. Science of the Total Environment, 2016, 550: 690-705.

[28] Touchaleaume F, Martin-Closas L, Angellier-Coussy H, et al. Performance and environmental impact of biodegradable polymers as agricultural mulching films [J]. Chemosphere, 2016, 144: 433-439.

[29] Davis S S, Khanderia M S. Rheological characterization of plastibases and the effect of formulation variables on the consistency of these vehicles [J]. Int. J. Pharm. Tech. Prod. Manuf, 1980, 1(11).

[30] Barry B W, Meyer M C. The rheological properties of carbopol gels II. Oscillatory properties of carbopol gels [J]. International Journal of Pharmaceutics, 1979, 2(1): 27-40.

Article 6 PBAT/PLA/cellulose nanocrystalline film: Preparation, characterization, mechanical properties and barrier properties

Qi Liu, [†,‡,§] Changrong Yan,[†] Lincan Liu,[†] Xu Xia,[†] Jiqing Song,[†] Dorothée Goffin,[‡,§]Aurore Richel[§] Wenqing He,[*,†]

[†]National Engineering Laboratory for Crop Efficient Water Use and Disaster Mitigation and Key Laboratory of Dryland Agriculture, Ministry of Agriculture, Institute of Environment and Sustainable Development in Agriculture, Chinese Academy of Agricultural Sciences, Beijing 100081, China

[‡]TERRA Research Center and Laboratory of Gastronomical Science, Gembloux Agro-Bio Tech-University of Liège, Passage des Déportés 2B-5030 Gembloux, Belgium

[§]Unit of Industrial and Biological Chemistry, Gembloux Agro-Bio Tech-University of Liège, Passage des Déportés 2B-5030 Gembloux, Belgium

Abstract: The PBAT/PLA/CNC films with various contents of CNC were prepared and characterized, mechanical and barrier properties of which were tested. Fourier transform infrared spectroscopy and X-ray diffraction results confirmed the embedding of CNC into the PLA/PBAT polymer matrix. PLA/PBAT/3% CNC film showed 188.80% deformation among the films in the tensile testing. With the increasing the CNC content, the puncture force and the puncture strength increased. Barrier testing indicated that CNC improved the barrier performance of the PLA/PBAT films. After 30 days mulching, water contents of the soil mulched with PLA/PBAT, PLA/PBAT/1% CNC, PLA/PBAT/3% CNC and PLA/PBAT/5% CNC films were56.16%, 67.50%, 74.21% and 80.83% respectively. Therefore, CNC behaved improving effect on barrier property and deformation ability of the PLA/PBAT films, which made PLA/PBAT/CNC an applicable prospect in agricultural planting production.

Key words: PBAT/PLA/CNC, nanocomposites, characterization, mechanical properties and barrier properties

1. Introduction

China is an agricultural country and is also a country with severe water scarcity[1]. Plastic film mulching in China is a common agricultural planting technology[2], the main application of which is polyethylene (PE) film. The main effect of plastic film mulching is soil moisture preservation[3], soil temperature[4] and weeds controlling[5]. However, the use of PE plastic film has brought serious white pollution problems, resulting in a huge burden on the environment[6].

For the outstanding degradation performance, biodegradable plastic mulching film is a strategic substitute for PE plastic film[7]. Biodegradable film can be fully degraded in farmland to avoid recycling and environmental pollution[8]. Therefore, biodegradable plastic mulching film may replace PE film in the long run. However, biodegradable plastic film also has many disadvantages, such as high price[9], poor mechanical properties[10], unsatisfactory barrier[11] and so on. Among them, the price can be reduced by expanding production or using more affordable materials. And better mechanical properties and barrier properties can be achieved through the raw materials seeking or blending modification[12].

Cellulose is one of the most ancient and abundant natural polymers on earth. Cellulose possess highly advantageous properties, such as low cost, biodegradability, renewability, high strength and modulus, low density, easy processability and relatively reactive surface for grafting specific groups [13]. CNC is a rod-shaped nanofiber crystal separated from cellulose. CNC exhibit outstanding mechanical properties, such as a high strength [14], high Young's modulus [15], high thermal stability [16], and large surface areas [17].

Given these properties, CNC have potential uses as reinforcement materials in nanocomposites. Arrieta et al. reported the preparation of nanocomposite films based on poly(lactic acid)-poly(hydroxybutyrate) (PLA-PHB) blends and synthesized CNC as bio-based reinforcement; the obtained PLA-PHB-CNCs formulations showed enhanced mechanical performance, improved water resistance, reduced oxygen and UV-light transmission [18]. Sapkota et al. found that the materials of mixed poly (vinyl acetate) with CNC were much stiffer than the neat matrix [19]. Morelli et al. improved mechanical properties of the polybutyrate adipate terephthalate (PBAT) with CNC treated, an increase by 120% and 40% in the elastic modulus and the tensile strength were reached respectively [20]. In addition, Mariano et al. revealed that more elastic behavior of the PBAT matrix was observed as CNC content increases through the small-amplitude oscillary shear experiments. Because of the shear stresses involved during processing, the composites presented stronger anisotropic character than the neat PBAT matrix [21].

In addition, CNC has been studied for enhancing barrier property of polymer (or plastic) films in recent years. Matuana et al. examined the effect of CNC addition on the water vapor and oxygen transmission rates of extrusion-blown poly (lactic) acid (PLA)/CNC nanocomposite films and found that the addition of only 1% CNC into PLA matrix improved the water vapor and oxygen barrier performance of nanocomposite films by 33% and 62% respectively [22]. Fortunati et al. obtained PLA/CNC nanocomposites prepared by the solvent casting method, which showed 34% reductions of water permeability for film containing 1 % of surfactant-modified cellulose nanocrystals and good oxygen barrier properties were detected for films with both 1 % and 5 % of modified and un-modified cellulose nanocrystals [23]. Fortunati et al. also used surfactant modified cellulose nanocrystals and silver nanoparticles as the matrix modifiers in the PLA nano-biocomposites which increased the barrier effect of the produced films [24]. Nassima et al. develop bio-nanocomposite films of carboxymethyl cellulose /starch polysaccharide matrix reinforced with CNC using the solution casting method. The water vapor permeability was significantly reduced, and the elastic modulus and tensile strength were increased gradually with the addition of CNC [25].

As one of the most popular degradable materials of agricultural mulching film, PBAT is usually used to produce mulching film blending with PLA [26,27]. However, the mechanical and barrier properties of the blended materials are not so satisfied. In this work, CNC was introduced into the film of PBAT/PLA composites. The PBAT/PLA/CNC films with various contents of CNC were prepared, characterized and performed properties testing. Scanning electronic microscopy (SEM), Fourier transform infrared spectroscopy (FTIR), X-ray diffraction (XRD) and thermogravimetric analysis (TGA) were used to characterize the

morphology and structure of the SAPs. Tensile properties test (TPT) and puncture performance test (PPT) were carried out to evaluate the mechanical properties of the films. The water vapor barrier properties were also investigated.

2. Materials and methods

2.1 Materials

WS was collected from Huantai experimental fields in 2015 in Shandong Province, China. Poly (lactic acid) (PLA 2002D, Mn= 98,000 g mol^{-1},4 wt% d-isomer) was supplied by Nature Works (USA). PBAT was bought from BASF Company (Germany). Microcrystalline cellulose (MCC, dimensions of 20 μm) was purchased from Sigma–Aldrich. Trichloromethane was supplied by Beijing Chemical Company (China). The other chemicals were all analytical pure. Only distilled water was used in the experiments.

2.2 Preparation of CNC

CNCs preparation: WS was pretreated with 17.5% NaOH (room temperature for 2 h), 2 M HCl (80 °C for 2 h) and 2% NaOH (80 °C for 2 h) to obtain the MCC. Then the CNCs were prepared from MCC with the method stated in the previous work [28].

2.3 Preparation of PLA/PBAT/CNC film

PLA and PBAT were dissolved in trichloromethane with string at room temperature and 5% PLA solution and 5% PBAT solution were obtained respectively.

For film without CNC, 30g PLA solution and 30g PBAT solution were mixed well with stirring. Then the mixture was poured into a Teflon mold (450×300×30 mm inside). The mold was placed in a fume hood for 12h. Then the film was removed from the mold to obtain PLA/PBAT film, which was named as PLA/PBAT/0% CNC film.

For film with CNC, 30g PLA solution, 30g PBAT solution and 240g trichloromethane were mixed well with certain quantity of CNC with stirring. The contents of CNC added varied in 0, 0.03 g, 0.09 g and 0.15g. The process was the same as that of PLA/PBAT film. And the resulting products were named as PLA/PBAT/1% CNC film, PLA/PBAT/3% CNC film, and PLA/PBAT/5% CNC film respectively.

2.4 Characterization

2.4.1 FTIR

FTIR spectroscopy was used to examine changes in fiber structure during the treatments. The spectrum of each sample was recorded with a Thermo Scientific Nicolet iN10 (Thermo Electron Corp., USA). Fibers were ground and blended with KBr. Then, the mixture was pressed into thin, transparent pellets. The FTIR spectrum of each sample was obtained at 4000–400 cm^{-1} with a resolution of 4 cm^{-1}. The XRD patterns of the fibers at different stages

were obtained using Bruker AXS D8 Focus (Bruker AXS Inc., Madison, WI, USA) that was equipped with a high-power point focus Cu–kα target and a graphite monochromator to eliminate Cu–kβ lines. Scattered radiation was detected at $2\theta = 10°–40°$ at a scan rate of 4°/min.

2.4.2 TG

Thermal analysis was conducted to compare the degradation characteristics and thermal behavior of the films with different CNC contents. Samples were analyzed using a TGA/DSC 1 thermogravimetric analyzer (Mettler Toledo Corporation, Switzerland). Samples were heated from room temperature to 700 °C under a nitrogen atmosphere at a heating rate of 10 °C/min.

2.5 Properties

2.5.1 Tensile test

Tensile properties such as tensile strength (TS) and elongation at break (E) of each film were evaluated with a XLW(B) Intelligent electronic testing machine (Labthink Corporation, jinan, China). Three 150mm long and 15mm wide samples were cut out from the Initial grip separation was set at 80 mm and cross-head speed at 250 mm/min.

2.5.2 Puncture performance test

The puncture test measurements were performed with a XLW(B) Intelligent electronic testing machine (Labthink Corporation, jinan, China). Five round samples (diameter=100mm) were cut out from the prepared films. The samples were fixed down on perforated heavy-duty platform. The films were punctured in the center with a 2mm wide probe at cross-head speed 50 mm/min. The initial distance was set to be 5mm. Puncture tension was calculated by dividing the maximum force by the initial cross-sectional area of the sample.

2.5.3 Barrier test

Approximately 70g dry soil and 30g distilled water was added into an 80ml beaker, which was covered by the PLA/PBAT film, PLA/PBAT/1% CNC film, PLA/PBAT/3% CNC film, and PLA/PBAT/5% CNC film respectively. The beakers are then weighed every two or three days. Three duplicates were done. The data were recorded and analyzed.

3. Result and discussion

3.1 FTIR

Interfacial interaction between the CNC and the polymer in composites can be identified by FTIR determination. The FTIR spectra of four PLA/PBAT/CNC film films are shown in Figure 31. In the FTIR spectra of all the four samples, a characteristic peak could be observed at 1749cm^{-1}, which referring to the band of C=O stretching existing in both of PLA and PBAT in all the films. The band at 2855 cm^{-1} and 2926 cm^{-1} related to =CH$_2$ symmetric and asymmetric stretch decreased in spectra where CNC was added into the films. This means that the CNC contents increased because there is no =CH$_2$ in CNC molecular. No other significant changes

or shifts in the characteristic peaks of PLA/PBAT film with the addition of CNC are observed, indicating little chemical interaction between CNC and the polymer matrix.
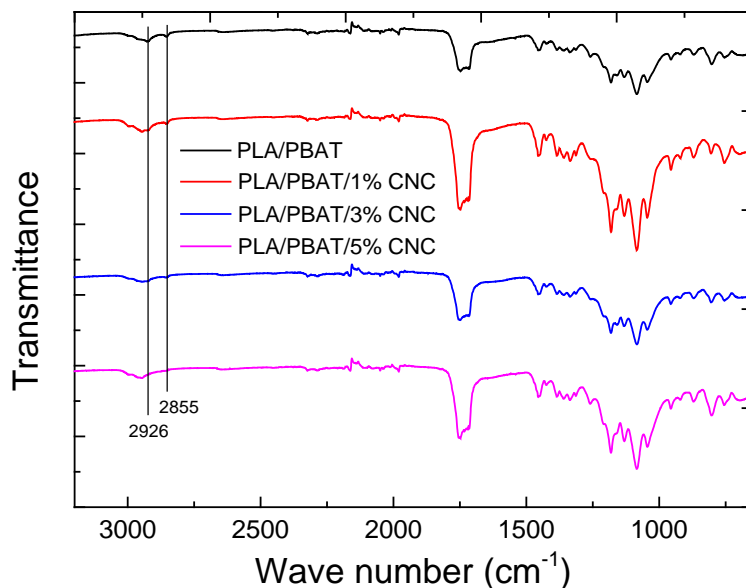
Figure 31. FTIR spectra of PLA/PBAT (a), PLA/PBAT/1% CNC (b), PLA/PBAT/3% CNC (c) and PLA/PBAT/5% CNC (d) films.

3.2 TG and DTG

The effect of CNC and CNCs on the thermal properties of the PLA/PBAT composites was investigated by thermogravimetric analysis. All the four PLA/PBAT/CNC films degraded in two-steps (Figure 32 a) with the first peak related to the PBAT decomposition, and the second peak due to the PLA degradation. This result was similar to that of PLA–PHB blends based on the study of Arrieta et al [29]. The addition of CNC shifted the onset of the PLA/PBAT films degradation process toward lower temperatures (Figure 32b). The changes were due to CNC introduction leaded to enhance the interface interaction between PLA and PBAT. No significant changes in the temperature corresponding to the maximum degradation rate of the second stage process were observed. For all the samples, there was no degradation at temperatures below 200 ◦C, which provide a wider producing possibility. These results are consistent with the results for crystallinity and FTIR measurements.
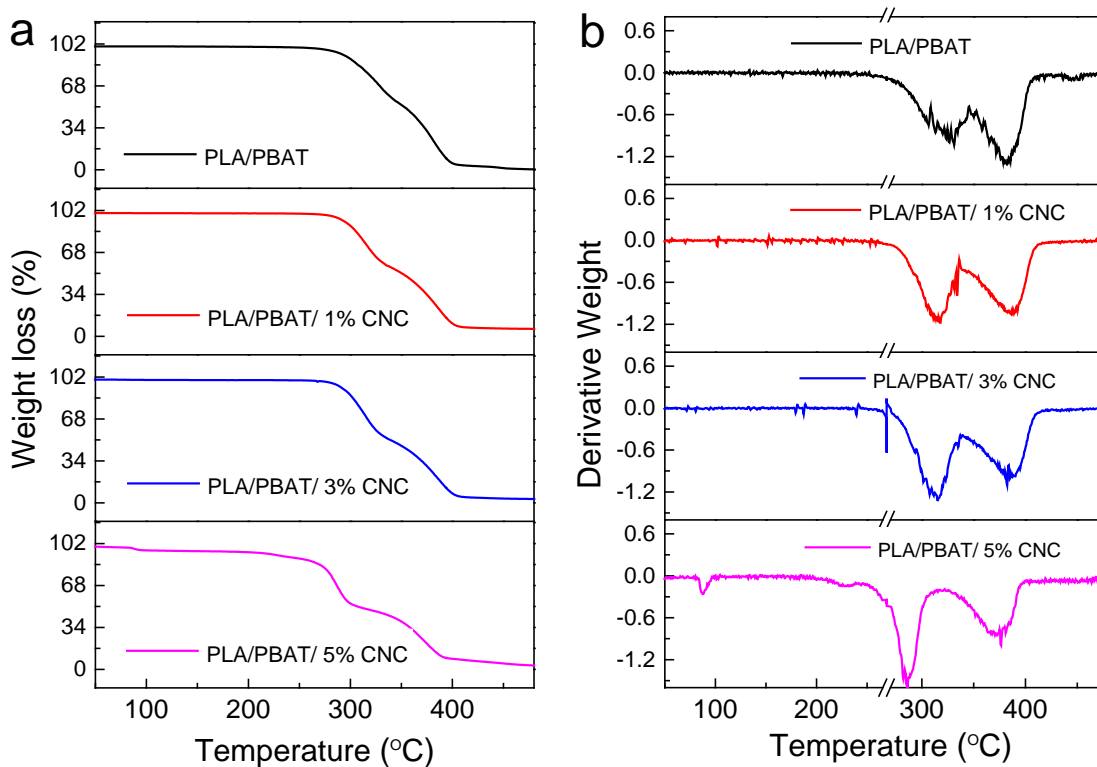
Figure 32. TG (a) and DTG (b) curves of PLA/PBAT, PLA/PBAT/1% CNC, PLA/PBAT/3% CNC and PLA/PBAT/5% CNC films.

3.3 Tensile testing

Effect of content of CNC on tensile properties of PLA/PBAT, PLA/PBAT/1% CNC, PLA/PBAT/3% CNC and PLA/PBAT/5% CNC films compounded are shown in Figure 33 and Table 14. Usually, a well-developed nanocomposite polymer results in highly increased mechanical strength compared to the pure polymer matrix since uniform dispersion of the nano-sized particles produces an ultra-high interfacial area and ionic bonds between the nanoparticles and host polymer [30, 31]. However, compounding the CNC reduced the TS in the PLA/PBAT in this study, indicating that the CNC are not well dispersed in the polymer matrix. CNC produced a decrease on the tensile strength (TS) of PLA/PBAT, the combination of PLA/PBAT and 1% or 3% CNC produce a nanocomposite with comparable TS with respect to PLA. However, the TS of PLA/PBAT/5% CNC film decreased dramatically. Moreover, the PLA/PBAT/3% CNC film revealed the highest deformation at break, showing an increase of 188.80% with respect to the neat PLA/PBAT film. Films for agricultural mulching are required to maintain their integrity in order to keep the water content and temperature of the soil during application on farmland. Therefore, PLA/PBAT/3% is more stretchable than pure PLA/PBAT and could be defined as a better formulation for agricultural mulching applications.
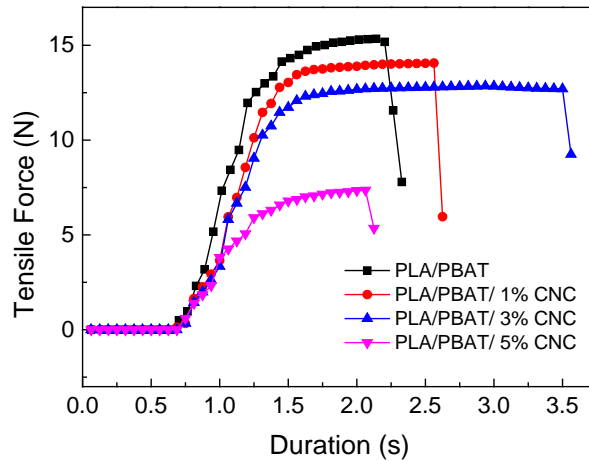
Figure 33. Tensile curves of PLA/PBAT, PLA/PBAT/1% CNC, PLA/PBAT/3% CNC and PLA/PBAT/5% CNC films.

3.4 Puncture performance test

From the puncture test measurements (Table 14) it could be noted that the load necessary to puncture the polymer film has highest value for pure PLA/PBAT film, which was 3.89 N. With increasing the content of CNC nanoparticles, the puncture force as well as the puncture strength showed an increasing tendency. The force of puncture (FP) of PLA/PBAT/1% CNC, PLA/PBAT/3% CNC and PLA/PBAT/5% CNC films are 2.24, 2.77 and 3.16 N respectively. This indicate that CNC nanoparticles immobilized PLA/PBAT macromolecules would absorbs fracture energy which forbid growth of plastic deformation.

Table 13. Results obtained from the tensile and puncture measurements.

Samples	Tensile measurement			Puncture measurement	
	F_T (N)	Elongation at break (%)	Tensile strength (MPa)	F_P (N)	Puncture strength (MPa)
PLA/PBAT	15.12±0.32	114.32±5.16	0.0126±0.0003	3.89±0.07	0.00062±1.15E-5
PLA/PBAT/1% CNC	13.87±0.28	135.08±2.32	0.0116±0.0002	2.24±0.10	0.000352±1.61 E-5
PLA/PBAT/3% CNC	12.60±0.35	188.80±9.21	0.0105±0.0003	2.77±0.13	0.000435±2.12E-5
PLA/PBAT/5% CNC	7.06±0.42	112.32±6.89	0.0059±0.0003	3.16±0.12	0.000496±1.92E-5

3.5 Barrier performance for soil moisture keeping

Plastic mulching is a globally agricultural practice which is much more important in China because of its outstanding effects on soil water and temperature keeping and product quality and yield improving. Therefore, barrier performance of the films was tested. The change of soil water contents mulching with the four films are shown in Figure 34. Water content of the soil covered by PLA/PBAT film decreased significantly compared with others. As shown in Figure 34, under the PLA/PBAT film, water contents of the soil was only 56.16% at 30 days. However, the water contents of the soil mulching with PLA/PBAT/1% CNC, PLA/PBAT/3% CNC and PLA/PBAT/5% CNC films were 67.50%, 74.21% and 80.83% respectively. This result

indicated that the CNC improved the barrier performance of the PLA/PBAT films which decreased the water vapor transmission rate. Furthermore, the barrier performance of the films was strengthened by increasing the CNC content into the PLA/PBAT composites. This result reveal that the CNC could improve the barrier of PLA/PBAT which is a main problem that the degradable film is facing to.
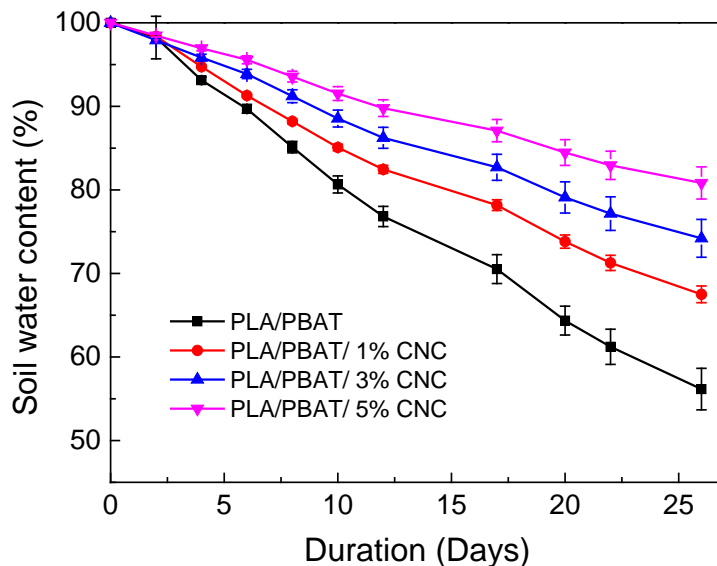
Figure 34. Change of soil water contents mulching with PLA/PBAT, PLA/PBAT/1% CNC, PLA/PBAT/3% CNC and PLA/PBAT/5% CNC films.

4. Conclusions

PBAT/PLA and PLA/PBAT/CNC with various CNC content composite films were prepared. The results of FTIR confirmed the mixing of CNC into the polymer matrix but without much chemical interaction. TG and DTG results revealed the addition of CNC shifted the onset of the PLA/PBAT films degradation process toward lower temperatures. Tensile testing showed that CNC produced a decreasing on the tensile strength of PLA/PBAT film, especially for PLA/PBAT/5% CNC. The PLA/PBAT/3% CNC film showed an increase of 188.80% deformation compared to the PLA/PBAT film. Puncture test measurements showed that CNC decreased the load necessary to puncture the polymer film while with the increasing the CNC content, the puncture force and the puncture strength increased. Barrier testing indicated that CNC improved the barrier performance of the PLA/PBAT films. At 30 days, water contents of the soil mulched with PLA/PBAT, PLA/PBAT/1% CNC, PLA/PBAT/3% CNC and PLA/PBAT/5% CNC films were56.16%, 67.50%, 74.21% and 80.83% respectively. Therefore, appropriate proportion of the CNC content in the films would improve the barrier property and deformation ability which is very useful in agricultural application.

The results of this research suggest that the novel combination of PLA/PBAT blends and CNC provide a new perspective for their agricultural application as mulching film.

Acknowledgements

Reference

[1] Yang H, Zhang X, Zehnder A J B. Water scarcity, pricing mechanism and institutional reform in northern China irrigated agriculture [J]. Agricultural Water Management, 2003, 61(2): 143-161.

[2] Li F M, Song Q H, Jjemba P K, et al. Dynamics of soil microbial biomass C and soil fertility in cropland mulched with plastic film in a semiarid agro-ecosystem [J]. Soil Biology and Biochemistry, 2004, 36(11): 1893-1902.

[3] Youzhen W, Xianjiang Y, Hu X, et al. Effects of Plastic Film Mulching on Temperature Increase and Preservation of Soil Moisture and Its Responses to Growth Character of Rice with Dry-land Cultivation [J]. Transactions of The Chinese Society of Agricultural Engineering, 2002, 2: 007.

[4] Wu Y, Huang F, Jia Z, et al. Response of soil water, temperature, and maize (Zea may L.) production to different plastic film mulching patterns in semi-arid areas of northwest China [J]. Soil and Tillage Research, 2017, 166: 113-121.

[5] Mahajan G, Sharda R, Kumar A, et al. Effect of plastic mulch on economizing irrigation water and weed control in baby corn sown by different methods[J]. African Journal of Agricultural Research, 2007, 2(1): 19-26.

[6] Changrong Y, Wenqing H, Neil C. Plastic-film mulch in Chinese agriculture: Importance and problems [J]. World Agriculture, 2014, 4(2): 32-36.

[7] Sintim H Y, Flury M. Is Biodegradable Plastic Mulch the Solution to Agriculture's Plastic Problem [J]. 2017.

[8] Gu X B, Li Y N, Du Y D. Biodegradable film mulching improves soil temperature, moisture and seed yield of winter oilseed rape (Brassica napus L.) [J]. Soil and Tillage Research, 2017, 171: 42-50.

[9] Shah A A, Hasan F, Hameed A, et al. Biological degradation of plastics: a comprehensive review [J]. Biotechnology advances, 2008, 26(3): 246-265.

[10] Ikada Y, Tsuji H. Biodegradable polyesters for medical and ecological applications [J]. Macromolecular rapid communications, 2000, 21(3): 117-132.

[11] Sorrentino A, Gorrasi G, Vittoria V. Potential perspectives of bio-nanocomposites for food packaging applications [J]. Trends in Food Science & Technology, 2007, 18(2): 84-95.

[12] Briassoulis D. An overview on the mechanical behaviour of biodegradable agricultural films [J]. Journal of Polymers and the Environment, 2004, 12(2): 65-81.

[13] Teixeira E M, Pasquini D, Curvelo A A S, et al. Cassava bagasse cellulose nanofibrils reinforced thermoplastic cassava starch[J]. Carbohydrate polymers, 2009, 78(3): 422-431.

[14] Fox J, Wie J J, Greenland B W, et al. High-strength, healable, supramolecular polymer nanocomposites [J]. Journal of the American Chemical Society, 2012, 134(11): 5362-5368.

[15] Wei L, Stark N M, Sabo R C, et al. Modification of cellulose nanocrystals (CNCs) for use in poly (lactic acid) (PLA)-CNC composite packaging products [J]. Review Process: Informally Refereed (Peer-Reviewed), 2016.

[16] Lizundia E, Urruchi A, Vilas J L, et al. Increased functional properties and thermal stability of flexible cellulose nanocrystal/ZnO films [J]. Carbohydrate polymers, 2016, 136: 250-258.

[17] Lizundia E, Fortunati E, Dominici F, et al. PLLA-grafted cellulose nanocrystals: Role of the CNC content and grafting on the PLA bionanocomposite film properties [J]. Carbohydrate polymers, 2016, 142: 105-113.

[18] Arrieta M P, Castro-López M M, Rayón E, et al. Plasticized poly (lactic acid)–poly (hydroxybutyrate)(PLA–PHB) blends incorporated with catechin intended for active food-packaging applications [J]. Journal of agricultural and food chemistry, 2014, 62(41): 10170-10180.

[19] Morelli C L, Belgacem M N, Branciforti M C, et al. Supramolecular aromatic interactions to enhance biodegradable film properties through incorporation of functionalized cellulose nanocrystals [J]. Composites Part A: Applied Science and Manufacturing, 2016, 83: 80-88.

[20] Mariano M, El Kissi N, Dufresne A. Structural Reorganization of CNC in Injection-Molded CNC/PBAT Materials under Thermal Annealing [J]. Langmuir, 2016, 32(39): 10093-10103.

[21] Arrieta M P, Peltzer M A, López J, et al. PLA-Based Nanocomposites Reinforced with CNC for Food Packaging Applications: From Synthesis to Biodegradation [M]//Industrial Applications of Renewable Biomass Products. Springer, Cham, 2017: 265-300.

[22] Matuana L M, Karkhanis S S, Stark N, et al. Cellulose nanocrystals as barrier performance enhancer of extrusion-blown PLA films for food applications [J]. Review Process: Non-Refereed (Other), 2016.

[23] Fortunati E, Peltzer M, Armentano I, et al. Effects of modified cellulose nanocrystals on the barrier and migration properties of PLA nano-biocomposites [J]. Carbohydrate polymers, 2012, 90(2): 948-956.

[24] Fortunati E, Peltzer M, Armentano I, et al. Combined effects of cellulose nanocrystals and silver nanoparticles on the barrier and migration properties of PLA nano-biocomposites [J]. Journal of Food Engineering, 2013, 118(1): 117-124.

[25] El Miri N, Abdelouahdi K, Barakat A, et al. Bio-nanocomposite films reinforced with cellulose nanocrystals: Rheology of film-forming solutions, transparency, water vapor barrier and tensile properties of films [J]. Carbohydrate polymers, 2015, 129: 156-167.

[26] Weng Y X, Jin Y J, Meng Q Y, et al. Biodegradation behavior of poly (butylene adipate-co-terephthalate) (PBAT), poly (lactic acid) (PLA), and their blend under soil conditions [J]. Polymer Testing, 2013, 32(5): 918-926.

[27] Arruda L C, Magaton M, Bretas R E S, et al. Influence of chain extender on mechanical, thermal and morphological properties of blown films of PLA/PBAT blends [J]. Polymer Testing, 2015, 43: 27-37.

[28] Liu Q, Hao W, Yang Y, et al. Effects of size and dispersity of microcrystalline celluloses

on size, structure and stability of nanocrystalline celluloses extracted by acid hydrolysis [J]. Nano Life, 2014, 4(04): 1441014.

[29] Arrieta M P, Fortunati E, Dominici F, et al. Multifunctional PLA–PHB/cellulose nanocrystal films: processing, structural and thermal properties [J]. Carbohydrate polymers, 2014, 107: 16-24.

[30] Vollick B, Kuo P Y, Thérien-Aubin H, et al. Composite Cholesteric Nanocellulose Films with Enhanced Mechanical Properties [J]. Chemistry of Materials, 2017, 29(2): 789-795.

[31] De France K J, Chan K J W, Cranston E D, et al. Enhanced mechanical properties in cellulose nanocrystal–poly (oligoethylene glycol methacrylate) injectable nanocomposite hydrogels through control of physical and chemical cross-linking [J]. Biomacromolecules, 2016, 17(2): 649-660.

Chapter V General conclusions and perspectives

This thesis focused on cellulose and nanocellulose isolation from wheat straw and their application in polymers used for water-saving practices in agriculture. After a review of the existing literature (Chapter I), the first set of experiments (Chapter II) aimed to isolate the CNC through acid hydrolysis, focusing on the effects of MCCs size and disparity on the size, structure, and stability of CNCs. The second set of experiments (Chapter II) focused on the microwave-assisted cellulose purification process (Article 2), and the CNF isolation from wheat straw through a combined environmental friendly method (Article 3). The third set of experiments (Chapter III) targeted the applications of CNC and CNF, especially their effects on the structure and properties of two kinds of agricultural water-saving materials (i.e., SAPs and mulching plastic films).

1. General discussion

1.1 CNC isolation and the effect of the size and dispersity of MCC on the size, structure, and stability of CNC during the acid hydrolysis process

CNC could be prepared through various methods. Among these methods, the most important step is almost always the sulfuric acid hydrolysis, which is typically performed at the end of the isolation process. In Article 2, CNCs were isolated from four kinds of commercial MCCs through sulfuric acid hydrolysis and ultrasonic treatment. The morphology and particle size of MCCs were characterized through scanning electron microscopy (SEM) and laser particle size analysis. The results showed the different shapes, sizes, and aggregation degrees of the resulting CNCs, which were composed of elongated rods that were 100–250 nm long and 10–30 nm in wide. The same order of CNC height as the aggregation degree of MCCs indicated that MCCs with lower aggregation degree tend to produce narrower CNCs, which were easier to assemble. Fourier transform infrared spectroscopy results and X-ray diffraction revealed that the structure and crystal properties of MCCs did not change during the preparation process. However, the harsh hydrolysis conditions reduced their crystallinity and thermal stability to varying degrees. The MCC that presented a smaller original particle size and a good disparity produced more uniform and thermally stable CNCs. This result suggested that both particle size and disparity were key parameters for CNCs isolation.

1.2 Important role of microwave and the reaction conditions on wheat straw cellulose purification

Microwaves (MW) were used for cellulose purification because of its accelerating effect on promoting chemical reactions. Article 3 described the cellulose isolation from wheat straw through MW-assisted alkali hydrolysis, and particularly the influence of the reaction conditions and the non-thermal effect of MW. The cellulose contents in the treated fibers increased with increased temperature, reaction time, and alkali concentration. In comparison, the lignin contents decreased correspondingly because of the insoluble lignin decomposition. Temperature exerted the most efficient effect on cellulose isolation. Cellulose with purity

higher than 90% was obtained in the resulting fibers under a 140 °C heat treatment. The non-thermal effect of MW on promoting the isolation of cellulose was revealed by comparing the morphology, the structure, the crystallinity, and the thermal properties of the samples that were treated with or without MW (T100-t20-3% and (T100-t20-3%)NO-MW). Comparison of the samples cellulose contents indicated that the MW can reduce three-fourths of the reaction time or two-thirds of the amount of chemicals used in the MW-assisted alkali hydrolysis process. The experimental results revealed that MW may either conserve energy or reduce chemical use during the cellulose isolation from raw materials. MW may also be utilized to meet the requirements of high-purity cellulose isolation from natural biomass.

1.3 The combinaition of isolation methods, steam explosion, microwave-assisted hydrolysis, and microfluidization, for CNF is useful and environmentally friendly

As mentioned in Chapter I, dozens of methods are available for CNF isolation. However, only a few techniques can efficiently isolate CNF from agricultural waste. In Article 4, CNFs were extracted from wheat straw by using an environmentally friendly, multi-step process which combined steam explosion, microwave-assisted hydrolysis, and microfluidization. Chemical analysis showed that the cellulose content increased from 44.81% to 94.23%, whereas the hemicellulose and lignin contents significantly decreased after all treatments. These results were validated by the increased glucose content determined by sugar analysis. SEM revealed the loosening effect of steam explosion, the purifying effect of microwave-assisted hydrolysis, as well as the reduction of the fibers diameter during treatment. In addition, AFM analysis confirmed the changes in the chemical components and surface roughness of the fibers. Transmission electron microscopy images revealed long and loose nanofiber bundles with widths in the range between of 10–40 nm and an entangled network of cellulose fibers with an average individual diameter of 5.42 nm. The results suggested that thermally stable CNFs with high aspect ratios and high purities can be prepared from wheat straw with the combined method.

1.4 Both CNC and CNF displayed their distinct effects on the properties of the polymer composites used in agriculture

As summarized in Chapter I, both CNCs and CNFs present excellent reinforcing effects on polymer nanocomposites. In this thesis, they were introduced into SAPs and mulching film to investigate their effects on the mechanical as well as other properties.

In Article 5, SAPs of acrylamide–acrylate (AA-AM) copolymer were synthesized with CNF, CNC, and MCC. SEM results revealed that the 3D structure of AA-AM-CNF and AA-AM-CNC were strengthened by the incorporation of CNF and CNC. The SAPs synthesized with CNF or CNC displayed lower swelling capacities in distilled water. However, they could achieve equilibrium faster and exhibit similar swelling abilities to that of AA-AM in KCl, CaCl2, FeCl3, and 0.9% NaCl solutions. For the repeated water-absorption capacities, the water absorbencies of the four SAPs were reduced by 12.7%, −2.4%, −1.6%, and 16.7%. The

reduction by 24.3% observed for distilled water after the second water-absorption round indicated similar water-absorbing ability for the first and second rounds for AA-AM-CNF and AA-AM-CNC. In addition, AA-AM-CNC demonstrated the most remarkable water-retaining capacity among the four SAPs in the soil. When mulching was employed, SAPs helped the soil to retain more moisture when the biodegradable PBAT film was employed. Moreover, AA-AM-CNC and AA-AM-CNF displayed better mechanical properties than AA-AM-MCC and AA-AM.

In Article 6, PBAT/PLA and PLA/PBAT/CNC composite films with various CNC contents were prepared. Tensile testing showed that CNC decreased the tensile strength of PLA/PBAT films and particularly in the case of PLA/PBAT/5% CNC. The PLA/PBAT/3% CNC film showed an increased deformation by 188.80% compared with that of the PLA/PBAT film. Barrier testing indicated that CNC improved the barrier performance of the PLA/PBAT films. After 30 days, the water contents of the soil mulched with PLA/PBAT, PLA/PBAT/1% CNC, PLA/PBAT/3% CNC, and PLA/PBAT/5% CNC films were 56.16%, 67.50%, 74.21%, and 80.83% respectively. Therefore, the appropriate proportions of the CNC content in the films would improve the barrier property and deformation ability, which are very useful in agricultural application.

2. Conclusions

Agricultural biomass can be considered as an alternative resource of environmentally friendly and renewable materials that can be potentially used for different applications. Wheat straw has been successfully recognized as a great potential resource for the production of composite materials. Given their excellent specific properties, natural fibers can serve as outstanding reinforcing fillers in the polymers. In this thesis, CNCs and CNFs were successfully isolated and then introduced into two typical water-saving materials in agriculture to improve their properties. CNFs were obtained through an environmentally friendly process that reduced the use of chemicals. The two types of nanocelluloses improved the mechanical properties and water-saving performance of both SAP and PBAT/PLA films. The results provided a new perspective for their agricultural application.

3. Perspectives and future developments

Cellulose account for half of the dry weight of plant biomass and even approximately half of the dry weight of secondary sources of waste biomass. This study focused on cellulose fibers mainly because of its renewable and degradable properties. At the end of their lifetime, cellulose fibers do not induce any pollution. Moreover, the application of cellulose fibers could meet the goal of using lignocellulosic residues produced from agricultural and industrial activities. In this way, high value-added products, such as nanocellulose, can be obtained from renewable sources and nanocellulose-based materials as the environmental impact of these wastes are reduced, together with an economic benefit. Based on the evaluation of the wheat straw nanocellulose isolation and its application studied in this study, four points of attention

and suggestions for prospective research directions are summarized.

The main purpose of nanocellulose application, especially those form natural fibers, is for environmental protection purpose as well as to satisfy the demand for "green" development. Consequently, nanocellulose isolation process should also be conducted with a "green chemistry" or an "eco-friendly" approache. In our work, microwave was introduced into the chemical treatment process to reduce the use chemicals. In future studies, additional green treatment processes must be developed. Fortunately, our continuous investigation has highlighted a number of effective and green treatment methods. For example, the application of ionic liquids, provides a greener and simpler isolation process because of the easy product separation, the catalyst recycling, and the lack of volatile and harmful organic solvents. Physical technologies have also been developed for a green process that exhibits broad application prospects in industrial production.

Nanocellulose enhances the mechanical properties of composite materials through the reinforcement of the matrix interfacial interaction. Due to the presence of hydroxyl groups in the cellulose fibers, the moisture regain is high, leading to a poor organic wettability with the matrix material and ultimately resulting in a weak interfacial bonding between the nanocellulose and the hydrophobic matrices. Therefore, to further improve the mechanical properties and environmental performance of composites, the hydrophobicity of the nanocellulose must be enhanced to improve its compatibility with the matrix. Thus, further studies must be conducted to improve the compatibility between nanocellulose fibers and hydrophobic polymer matrices. Various greener methods, such as plasma treatment and treatments using fungi, enzymes, and bacteria, have been explored.

At present, the applications of nanocellulose are limited by its cost. Nonetheless, this situation may be improved, as companies and researchers are increasingly looking for solutions to the existing challenges faced for these materials. Agricultural wastes are a globally available, cheap, and unexploited source of cellulose that could be used for the large-scale production of nanocellulose products. In addition, the literature posited that this kind of cellulosic materials generally provides higher nanocellulose yields than other materials. However, their seasonality makes them inadequate as constant and homogeneous feed-stock. Therefore, lignocellulosic residues from agricultural waste and processed agricultural waste activities have become the most ideal resource with respect to cost/energy savings and economic development. This approach should lead to significant cost savings for industries and the development of new nanocellulose-based materials. The cost of nanocellulose also depend partly on the amount of consumption in industrial production. Therefore, the increased enthusiasm for its application may lead to the production of new nanocellulose-based materials which will reduce the costs of production.

In our study, we discussed environmentally friendly isolation methods for nanocellulose from wheat straw and the mechanical properties and water-saving performance of agricultural-biomass-based polymer composite materials. Future studies on natural-fiber-based

composites should not be limited only to its applications in such polymers but also to its application in many other fields, such as automotive industry, construction industry, ceilings and partition boards, aerospace, sports, boats, office products, machinery, etc.

4. Closing words

New materials, including polymer composites, nanocomposites, and biocomposites materials have become available in recent years. This field has observed rapid advancements, so that studies on nanocelluloses have become more extensive than four years ago when we began the study. Eco-friendly materials are becoming the preferred choice. The rapid industrial growth and improvements in science and technology have led to the continuous deterioration in our living environmental conditions. However, the disposal or burning of agricultural waste results in the emission of toxic gases and dust into the air, and the poisoning of soil due to non-biodegradable plastics or other polymers disposed in the soil. Therefore, researchers all over the world are focusing on eco-friendly materials. To realize this goal, raw natural materials and green technologies must be adopted. Our work is beneficial to agricultural waste use, particularly the isolation process based on green chemistry and the applications of nanocelluloses on improving water-saving polymers. From the perspective of sustainability, we believe that green technologies for isolating and the use of natural cellulose fibers are now required to reduce the pollution and conserve resources.

Appendix -Publications and communications

1. Publications included in the thesis

Liu, Q., Hao, W., Yang, Y., Richel, A., Ouyang, C., Liu, H., ... & Goffin, D. (2014). Effects of size and dispersity of microcrystalline celluloses on size, structure and stability of nanocrystalline celluloses extracted by acid hydrolysis. *Nano Life*, *4*(04), 1441014.

Liu, Q., Lu, Y., Aguedo, M., Jacquet, N., Ouyang, C., He, W., ... & Song, J. (2017). Isolation of high-purity cellulose nanofibers from wheat straw through the combined environmentally friendly methods of steam explosion, microwave-assisted hydrolysis, and microfluidization. *ACS Sustainable Chemistry & Engineering*.

Liu, Q., Aguedo, M., Lu, Y., Ouyang, C., He, W., Yan, C.,…& Goffin,D. (2017). Microwave-assisted Alkali Hydrolysis for Cellulose Isolation from Wheat Straw: Influence of Reaction Conditions and Non-thermal Effects of Microwave. Submitted to *ACS Sustainable Chemistry & Engineering*.

Yun Lu, Ru-Nan Gao, Shaoliang Xiao, Yafang Yin, **Qi Liu**, Jian Li. Native, Modified and Cellulose-Based Aerogels: Processing and Morphology [M]. *Royal society of chemistry*. [Accepted book chapter]

Liu, Q., He, W., Yan, C., Guo, R., Song, J., Richel, A., Goffin, D. Isolation and Application of Nanocelluloses from Agricultural Biomass: A review. [to be submitted]

Liu, Q., Goffin, D., Wu, M., Richel, A., He.W., Yan, C., …& Song, J. Comparison of absorption behavior and mechanical performance of superabsorbent polymers reinforced with cellulose nanocrystalline, nanofibers and microcrystalline. [to be submitted]

Liu, Q., Yan, C., Liu, L., Xia, X., Song, J., Goffin, D., Richel, A., He, W. PBAT/PLA/cellulose nanocrystalline film: Preparation, characterization, mechanical properties and barrier properties. [to be submitted]

2. Publications not included in the thesis

Ouyang, C., Liu, J., **Liu, Q.**, Li, Y., Yan, D., Wang, Q., ... & Cao, A. (2017). Preparation of Main-Chain Polymers Based on Novel Monomers with D− π–A Structure for Application in Organic Second-Order Nonlinear Optical Materials with Good Long-Term Stability. *ACS Applied Materials & Interfaces*, *9*(12), 10366-10370.

Li, J. H., Lv, G. H., Bai, W. B., **Liu, Q.**, Zhang, Y. C., & Song, J. Q. (2016). Modification and use of biochar from wheat straw (Triticum aestivum L.) for nitrate and phosphate removal from water. *Desalination and Water Treatment*, *57*(10), 4681-4693.

Ouyang, C. B., Liu, X. M., **Liu, Q.**, Bai, J., Li, H. Y., Li, Y., ... & Guo, M. X. (2015). Toxicity assessment of cadinene sesquiterpenes from Eupatorium adenophorum in mice. *Natural products and bioprospecting*, *5*(1), 29-36.

Guo, R., Zhou, J., Hao, W., Gu, F., **Liu, Q.**, Li, H., ... & Mao, L. (2014). Germination, Growth, Chlorophyll Fluorescence and Ionic Balance in Linseed Seedlings Subjected to Saline and Alkaline Stresses. *Plant Production Science*, *17*(1), 20-31.

3. Patents

LIU Q., SONG J., HAO W., et al. A Synthetic Method of Cellulose Grafted Cyclodextrin based superabsorbent polymers. 2016.08.17，China，Patent，ZL201410323542.2

LIU Q., SONG J., HE W., et al. A method for preparing cellulose nanofibers. China， Patent，under review

4. Oral communications internationally and nationally

LIU Q. Cellulose separation and cellulose nanofibers (CNFs) preparation from wheat straw. Gembloux (Belgium), 11/12/2015.

LIU Q. Nanocellulsoes and their application in polymers. Suzhou (China), 14/06/2017.

5. Posters in international conferences

LIU Q., Jacquet N., Aguedo M., et al. (2016) Cellulose nanofibers derived from wheat straw with a multi-step method: Effect of the treatments on composition, structure, morphology and properties. *IUFRO Regional Congress for Asia and Oceania 2016*, October 24-27, 2016, Beijing, China